Master of Science Thesis

The Effect of Multiple Storms on the Stability of Near-Bed Structures

ing. H.P.A. van den Heuvel

September 26, 2013

Boskalis

TUDelft

The Effect of Multiple Storms on the Stability of Near-Bed Structures

MASTER OF SCIENCE THESIS

For obtaining the degree of Master of Science in Civil Engineering at Delft University of Technology

Hans Peter Alexander van den Heuvel

September 26, 2013

Faculty of Civil Engineering and Geosciences · Delft University of Technology

Photo cover image:

Heavy sea with clouds. Online image.
Retrieved February 2013 from: http://wallpaperscraft.com/

Note: This document has been designed for full colour double-sided printing

DELFT UNIVERSITY OF TECHNOLOGY
DEPARTMENT OF
Civil Engineering and Geosciences

In cooperation with

ROYAL BOSKALIS WESTMINSTER
DEPARTMENT OF
Hydronamic

September 26, 2013

Graduation committee:

Prof. dr. ir. W.S.J. Uijttewaal
        Delft, University of Technology
        Hydraulic Engineering, Environmental Fluid Mechanics

Ir. J.P. van den Bos
        Delft, University of Technology
        Hydraulic Engineering, Coastal Engineering

Dr. ir. M. Zijlema
        Delft, University of Technology
        Hydraulic Engineering, Environmental Fluid Mechanics

Ir. P.F.J. van Baaren
        Royal Boskalis Westminster

Dr. ir. B. Hofland
        Deltares

"I did tests on small stones before collecting and committing myself to the larger ones"

Andy Goldsworthy (1956)

Abstract

Pipeline covers on the seabed are called near-bed structures which are generally made of rip rap. The crest height of a near-bed structure is such that waves do not break over it. Near-bed structures are used to protect pipelines against fishing equipment, ship anchors, dropped objects and preventing destabilizing of the pipeline. There are two ways of designing a near-bed structure. The first is to design a stable construction given the design conditions present in the lifetime of the structure. The second approach is to allow some damage during the lifetime of the structure, and is the approach which this research focuses on.

Presently the Rock Manual advises to use a formula from Wallast and Van Gent [2002] to describe the damage development during a storm. In this formula the damage development in time is forced to a dependency found by Van der Meer [1988]. It is unknown if this time dependency based on the number of waves is valid for damage development with near-bed structures. Besides this, the way to include cumulative damage for several subsequent storm conditions is presently calculated as a first approximation with a method from Van der Meer [1999] designed for breakwaters. It is not verified that this method can also be applied for near-bed structures.

The goal of this research is to determine the actual relation between damage and time, and to investigate the cumulative damage development for near-bed structures in multiple storm events. To answer the research questions which have been made from these goals, an investigation is performed which makes use of physical scale model testing. Tests are performed in the Environmental Fluid Mechanic Laboratory at Delft University of Technology.

After the execution of the model tests, an extensive analysis is performed based on the results of the scale model tests and results of previous research from Lomónaco [1994], Wallast and Van Gent [2002], Saers [2005], Van den Bos [2006] and Tørum et al. [2008].

The analysis concluded that there is not 'one' parameter as assumed so far to describe the relation between damage to near-bed structures and the number of waves. This parameter is thought to be depended on wave height, water depth, stone size and actual damage that occurs after a certain time. Besides this, the damage development did not reach an equilibrium in time with a large number of waves, which was assumed to be the case in other research. The average value for the exponent which describes the relation between the number of waves and damage is used in this thesis. With this relation and more data a new and improved damage prediction formula is investigated. The new prediction found in this thesis calculates the damage to a higher degree of accuracy with less variation present. It includes more parameters than the current prediction formula from Wallast and Van Gent. The extra parameters in this formula are the relative width, structure slope and Keulegan-Carpenter number.

The method to include cumulative damage for multiple storm events from Van der Meer was proven to be usable by using the formulas found in this research. An important conclusion from these tests is that damage development stops or reduces to a large degree when a low wave condition passes the near-bed structure when a high condition is already imposed to the near-bed structure.

Summary

Pipeline covers on the seabed are called near-bed structures which are generally made of rip rap. The crest height of a near-bed structure is such that waves do not break over it. Near-bed structures are used to protect pipelines against fishing equipment, ship anchors, dropped objects and preventing destabilizing of the pipeline. There are two ways of designing a near-bed structure. The first is to design a stable construction given the design conditions present in the lifetime of the structure. The second approach is to allow some damage during the lifetime of the structure, and is the approach which this research focusses on.

Presently the Rock Manual advises to use a formula from Wallast and Van Gent [2002] to describe the damage development during a storm. In this formula the damage development in time is forced to a dependency found by Van der Meer [1988]. It is unknown if this time dependency based on the number of waves is valid for damage development with near-bed structures. Besides this, the way to include cumulative damage for several subsequent storm events is presently calculated as a first approximation with a method from Van der Meer [1999] designed for breakwaters. It is not verified that this method can also be applied for near-bed structures.

This research is split up in two parts:

- To determine the actual relation between damage and time.
- To investigate the cumulative damage development for near-bed structures in multiple storm events.

To answer the research questions which have been made from these goals, an investigation is performed which makes use of physical scale model testing. Tests are performed in the Environmental Fluid Mechanic Laboratory at Delft University of Technology. After the execution of the model tests, an extensive analysis is performed based on the results of the scale model tests and results of previous research from Lomónaco [1994], Wallast and Van Gent [2002], Saers [2005], Van den Bos [2006] and Tørum et al. [2008].

The first part of the analysis deals with the relation between damage (S) and time. Time is in most damage development formulas expressed as the number of waves N. Several parameters exist in previous research such as $S/\sqrt{N}$, $S/\log{(N)}$ and $S/N^{0.3}$ to express the relation between damage and time. This research concluded that the exponent of the number of waves is not 'one' parameter as assumed in previous research. This parameter is thought to be depended on wave height, water depth, stone size and actual damage that occurs after a few thousand waves. A prediction formula of this parameter was never found and the average exponent is used in this thesis.

In this thesis a distinction is made between a large and small mobility of stones which can be indicated by the velocity parameter. This is done because in reality mostly a structure is designed with low velocity parameters and consequently low damage. The velocity parameter was proven by several researchers to be the best stability parameter to describe the damage development in near-bed structures. In Table 1 the best fit found in this thesis for the relation between damage

and time (S/N^{β}) is shown. The average β factor is shown for a large and small velocity parameter. The velocity parameter $\theta_{hc1\%}$ is calculated with linear wave theory with the use of wave height $H_{1\%}$, peak period T_p and depth above the near-bed structure h_c and can be seen in Equation 1.

$\theta_{hc1\%,max} > 7$	$\theta_{hc1\%,max} < 7$
0.436	0.369

Table 1: The average exponent β from the relation between damage and time.

$$\theta_{hc\ 1\%} = \frac{(\hat{u}_{hc\ 1\%})^2}{g\Delta D_{n50}} \tag{1}$$

In previous research it was assumed that the construction would armour itself against damage after a few thousand waves. This research shows that with a very large number of waves this is not the case. After more than 25,000 waves still damage development was visible in every tests although it was reduced in comparison with earlier stages of the test. A new damage development formula was obtained in this thesis which includes parameters such as the relative width of the structure, the slope of the structure and the Keulegan-Carpenter number. All these parameters were proven to be of importance in the physical scale model tests. The formula is split up in two parts again, where the main form can be seen in Equation 2. In this equation α and c_1 until c_3 are coefficients calculated for for a high and low velocity parameter shown in Table 2.

$$\frac{S^*}{N^{\beta}} = \alpha \cdot \theta_{hc1\%}^{c_1} \cdot \left(\frac{B_c}{D_{n50}}\right)^{c_2} \cdot (m_0 \cdot Kc)^{c_3} \tag{2}$$

	β	α	c_1	c_2	c_3
$\theta_{hc1\%,max} > 7$	0.44	0.134	2.96	-0.39	-1.05
$\theta_{hc1\%,max} < 7$	0.37	0.238	2.69	-0.40	-0.90

Table 2: Parameters from Equation 2.

These new damage development equations calculate the damage to a higher degree of accuracy in relation to previous damage development formulas and have less variation present in the formula. The 90% confidence interval for this formula can be calculated by including these values for parameter α. These values for the α parameters can be seen in Table 3.

Confidence bounds α	5%	50%	95%
$\theta_{hc1\%,max} > 7$	0.0524	0.1340	0.1962
$\theta_{hc1\%,max} < 7$	0.0908	0.2376	0.3582

Table 3: Confidence bounds for parameter α.

It is observed in these scale model tests that in the first thousand waves a lot of randomness in damage development was present. Because of this, damage calculations for a limited number of waves is uncertain. Processes that could influence the randomness in the damage development are irregularities in the structure profile, compaction and how the stones are mixed.

The second part of this thesis concerns cumulative damage in multiple storm events. It was observed that the method of Van der Meer is very usable, together with the formulas found in this thesis to calculate damage during multiple storm events. In the first few storm events the damage is underestimated but after this the calculated damage is very accurate. After a very large number of waves the calculated damage starts to deviate from the measured damage where, in

these tests, it was still within the 90% confidence interval. Because of this it can be concluded that the method of Van der Meer to include multiple storm events can be used for near-bed structures.

An important conclusion from the physical scale model tests is that when a large storm has been imposed to the near-bed structure, a smaller storm event creates none or very few damage. If the large storm returns again, damage development continues.

Preface

This thesis is the final report of a research project undertaken in order to obtain the degree of Master of Science at Delft University of Technology[1]. This research was undertaken for Hydronamic, which is the engineering department for Royal Boskalis Westminster. The scale model tests were executed in the Environmental Fluid Mechanic Laboratory in Delft while most of the report was written at Hydronamic in Papendrecht.

This thesis is about experimental research in order to obtain a better insight in the stability of near-bed structures in multiple storm conditions. This research could not be achieved without the assistance of many people who I would like to thank.

First of all I would like to thank my graduation committee prof. dr. ir. W.S.J. Uijttewaal, ir. J.P. van den Bos, dr. ir. M. Zijlema, ir. P.F.J. van Baaren and dr. ir. B. Hofland for their guidance and feedback during the project. Additionally to my committee I would like to thank ir. H.J. Verhagen for his feedback and help during the tests and analysis of the physical scale model.

Secondly I would like to thank all colleagues from Hydronamic who helped me from time to time with difficulties in the process and with their input and support. Also greatly acknowledged are my fellow students and roommates who often shed new light on important matters. Special thanks goes towards A.C. Biesheuvel and G.D. Eigenraam for their help during this thesis.

In addition to this I would like to thank all staff members from the Environmental Fluid Mechanic Laboratory for their help and support. Special thanks goes towards S. de Vree who helped me set-up the scale model tests.

Last, but not least, I would like to thank my friends and parents for their support throughout this graduation. Especially I would like to thank my brother, M.P.C. van den Heuvel, for correcting and checking my whole thesis.

Papendrecht, September 2013
Hans-Peter van den Heuvel[2]

---

[1]Faculty CiTG; Section of Hydraulic Engineering; specialisation Coastal Engineering
[2]Contact information: hanspeter.vdh@gmail.com, telephone: +31 6 12622852

Table of Contents

List of Figures

List of Tables

List of symbols

Symbol	What	Unit
A_e	Erosion area (area of displaced stones in cross section)	$[\text{m}^2]$
a	Amplitude defined as $H/2$	$[\text{m}]$
$\hat{a}_0$	Maximum horizontal excursion orbital motion at the bottom	$[\text{m}]$
B_c	Crest width	$[\text{m}]$
C	Chézy coefficient	$[\text{m}^{1/2}/\text{s}]$
C_B	Bulk coefficient, combines effects of C_D and C_L	$[\text{-}]$
C_D	Drag force coefficient	$[\text{-}]$
C_L	Lift force coefficient	$[\text{-}]$
C_M	Inertia coefficient; added mass coefficient	$[\text{-}]$
C_r	Reflection coefficient	$[\text{-}]$
c_f	friction factor	$[\text{-}]$
D	Stone diameter	$[\text{m}]$
D	Diameter of transducer or pile	$[\text{m}]$
D_{n50}	Nominal stone diameter, defined as $D_{n50} = \sqrt[3]{W_{50} g \cdot \rho_s}$	$[\text{m}]$
E	Spectrum variance density	$[\text{m}^2\text{s}]$
$E_{JONSWAP}$	Spectrum shape defined by JONSWAP	$[\text{m}^2\text{s}]$
F	Frequency of echo-sounder	$[\text{cycles/s}]$
F_D	Drag force	$[\text{N}]$
F_L	Lift force	$[\text{N}]$
F_M	Inertia force	$[\text{N}]$
F_R	Resultant force (of drag and lift forces)	$[\text{N}]$
Fr	Froude number	$[\text{-}]$
f	Wave frequency, defined as $(1/T)$	$[\text{s}^{-1}]$
G	Gravity force (underwater weight)	$[\text{N}]$
g	Acceleration of gravity, $g = 9.81$	$[\text{m/s}^2]$
H	Wave height in a regular wave field	$[\text{m}]$
H_b	Wave height when breaking occurs	$[\text{m}]$
h_c	Water depth over crest of near-bed structure	$[\text{m}]$
H_s	Significant wave height in an irregular wave field	$[\text{m}]$
$H_{1\%}$	Wave height that is exceeded by 1% of the waves in an irregular wave field	$[\text{m}]$
H_{m0}	Significant wave height for a wave spectrum	$[\text{m}]$
h	Water depth	$[\text{m}]$
Kc	Keulegan Carpenter number, defined as $(u_m T)/D$	$[\text{-}]$
k	Wave number, defined as $(2\pi/L)$	$[\text{m}^{-1}]$
k_s	Bed roughness for a horizontal bed, defined as $2 \cdot D_{n50}$	$[\text{m}]$
L	Wave length	$[\text{m}]$
M_p	Mobility parameter	$[\text{-}]$

Symbol	What	Unit
m_0	Area beneath the energy spectrum	[m^2]
m_0	Slope of a near-bed structure 1:$m0$.	[-]
N	Number of waves	[-]
N_s	Stability number of Hudson number, defined as $N_s = H_s/(\Delta D_{n50})$	[-]
P	Perimeter	[m]
p	Pressure	[Pa]
R	Hydraulic radius, defined as $R = A/P$	[m]
Re	Flow Reynolds number, defined as $Re = \left(\bar{\bar{u}}h\right)/\nu$	[-]
Re_*	Particle Reynolds number, defined as $Re_* = (u_* d)/\nu$	[-]
Re_w	Wave Reynolds number, defined as $Re = \left(\bar{\bar{u_0}}a_0\right)/\nu$	[-]
S	Damage number (dimensionless erosion area), defined as $S = A_e/D_{n50}^2$	[-]
Sa	Sears number, defined as $Sa = z_c m_0/\hat{a}_0$	[-]
S_N	Damage after N waves	[-]
S^*	Damage number (dimensionless erosion area), defined as $S = A_e/(D_{n50} \cdot B_c)$	[-]
s	Wave steepness, defined as $s = H_s/L$	[-]
s_f	Shape factor	[-]
s_m	Wave steepness based on mean period, defined as $s_m = 2\pi/g \cdot H_s/T_m^2$	[-]
T	Wave period (with frequency $f = 1/T$)	[s]
T_m	Mean wave period from a time domain	[s]
T_p	Peak wave period from a time domain	[s]
t	Time	[s]
u	Flow velocity	[m/s]
u_*	Shear velocity, defined as $u_* = \sqrt{\tau_0/\rho}$	[m/s]
$\hat{u}$	Maximum near-bed horizontal velocity	[m/s]
V	Volume	[m^3]
V	Velocity of sound in water	[m/s]
W_{50}	Mean stone weight (mass)	[N]
x	Horizontal coordinate	[m]
z	Vertical coordinate. $z = 0$ represents still water level, $z = -h$ represents bottom	[m]
z_c	Crest height of a near-bed structure	[m]
z_d	Crest height of a pipeline cover after damage	[m]

Greek Letters

Symbol	What	Unit
α	JONSWAP scale parameter	[-]
γ	JONSWAP peak enhancement function	[-]
Δ	Specific density, defined as $\Delta = (\rho_s - \rho_w)/\rho_w$	[-]
δ	Boundary layer thickness	[m]
ϵ	Dissipation rate of turbulent kinetic energy	[m^2/s^3]
ζ	Coefficient that includes the drag, shear and lift coefficient	[-]
η	Surface elevation	[m]
Θ	Stability parameter based on velocity and acceleration (Morison)	[-]
θ	Stability parameter based on wave orbital velocity, defined as $\theta = u^2/(g \cdot D_{n50})$	[-]
κ	Von Kàrmàn constant	[-]
λ	Scale factor	[-]
ν	Kinematic viscosity of the fluid (water)	[m^2/s]

Symbol	What	Unit
ξ	Breaker parameter, defined as $\xi = \tan(\alpha)/\left(\sqrt{H_s/L_0}\right)$	[-]
π	The ratio of a circles circumference to its diameter, $\pi = 3.141$	[-]
ρ_s	Density of stone material	[kg/m^3]
ρ_w	Density of water	[kg/m^3]
σ	Standard deviation	[-]
σ_a	Shape parameter with an average value in JONSWAP of 0.07	[-]
σ_b	Shape parameter with an average value in JONSWAP of 0.09	[-]
τ	Shear stress	[Pa]
τ	Viscous stress tensor	[Pa]
τ_0	Bed shear stress	[Pa]
ϕ	Angle of repose	[°]
Ψ	Shields parameter, stability parameter based on bed shear stress. Called a mobility parameter in this thesis.	[-]
ω	Angular frequency of the wave ($2\pi/T$)	[s^{-1}]

Frequently used subscripts	
w	Waves
$\hat{at}$	Maximum value
0	Based on undisturbed velocity at bed
hc	Based on enhanced velocity at crest
1%	Based on $H_{1\%}$

In this thesis a coordinate system is used in which:

x	The horizontal coordinate in the wave direction.
y	The horizontal coordinate perpendicular to the waves.
z	The vertical coordinate.
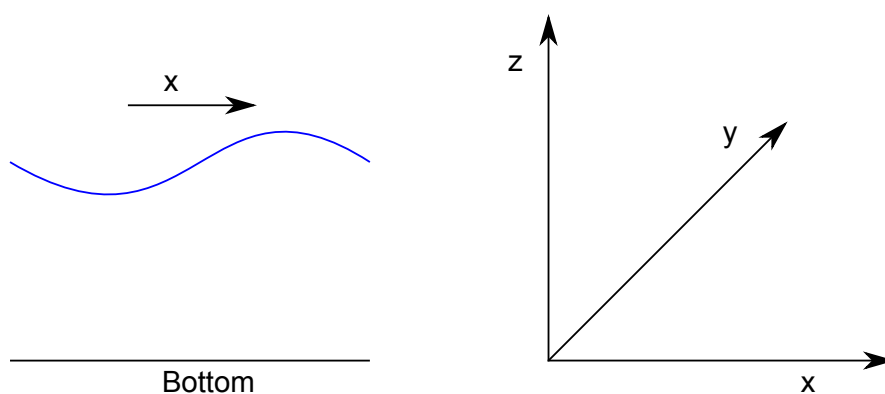
Chapter 1

Introduction

Around the world, a near-bed structure is a common type within the hydraulic structures. There are several types of near-bed structures, such as bed protections or pipeline covers in the offshore industry. This thesis studies pipeline covers which are generally made of riprap and used to protect pipelines against fishing equipment, ship anchors, ship wreckage, illegally dumped objects and hydraulic loads. The depth in which a near-bed structure is constructed can vary from several meters to over a hundred meters. An artist impression of a near-bed structure is shown in Figure 1.1. The crest height of a near-bed structure is such that waves do not break over the near-bed structure so that this does not influence the stability of the rocks [Van Gent and Wallast, 2001].
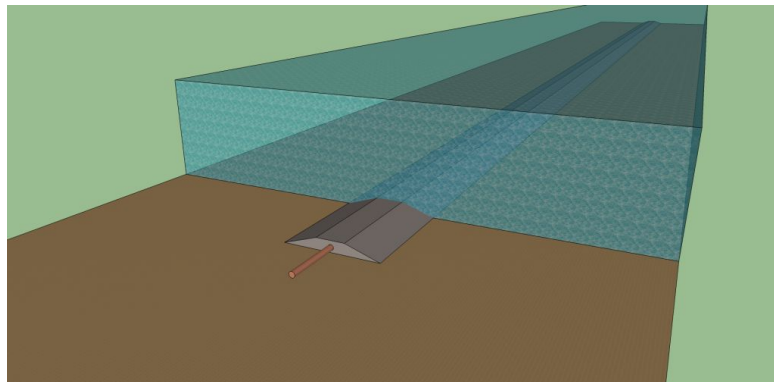
Figure 1.1: An artist impression of a near-bed structure. Here a small stretch of sea can be seen with on the bottom a near-bed structure with a pipeline inside.

In this chapter an introduction is given for this master thesis, the problem is described, the goal of this thesis is explained, how this is reached and the current design method will be introduced.

The riprap structures for protecting pipelines can be designed in several ways. There are two design methodologies for near-bed structures which are a statically stable design and a dynamically stable design. A statically stable design means that a stable construction is designed, whereas a dynamically stable design focusses on a structure that allows a certain amount of damage during its lifetime. The dynamically stable design methodology, which is also called a damage approach, is the subject of this thesis.

Sometimes a dynamically stable structure may lead to a more cost efficient design. The design conditions for a near-bed structure are the hydrodynamic forces acting on the near-bed structure

with a certain probability of occurrence. It is important that the near-bed structure is not wiped away in a storm. Therefore, stability is the most important concept in designing such a structure. The reaction of the near-bed structure to the design conditions or the governing loads (waves and flow currents) can be seen in terms of damage to the structure profile. Damage occurs when the loads are too high compared to the stability of the near-bed structure. This damage can be defined as an erosion area or as a certain amount of stones displaced. The stability of a near-bed structure can actually be seen as the stones in the structure trying to overcome the load forces with, for instance, their weight and interlocking between each other.

This study is carried out for Hydronamic which is the engineering company of Royal Boskalis Westminster to obtain the degree Master of Science at Delft University of Technology. Boskalis is one of the main contractors on the offshore market. They design and construct pipeline covers on a regular basis. Therefore it is important for Boskalis to have the proper design tools to design a near-bed structure in an optimal way.

1.1   Dynamically stable design approach and shortcomings

The Rock Manual [CIRIA, 2007] advises to design a dynamically stable near-bed structure according to the method of Van Gent and Wallast [2001]. In the formulas they propose there are hydraulic, load and strength parameters which are applicable in a certain range. Without going into too much detail, one of these parameters is the number of waves (N). The formula is only validated between 1000 and 3000 waves, which is comparable with one storm. However, it is unlikely that a near-bed structure is exposed to only one storm. During a lifetime, for example 25 years, it has to endure many storms. This means that the near-bed structure is exposed to many waves while the design formula is only validated for a limited number. After being exposed to all these waves, the near-bed structure must still have an amount of safety left to protect the pipeline. Therefore it is important to know the damage development due to a large number of waves. So far it has been assumed that the construction will 'armour' itself and no more damage will develop after a large number of waves (say $N = 3000$).

Currently the way to incorporate multiple subsequent storms into the design of near-bed structures is unknown. 'Multiple storms' refers to several storms conditions with different wave heights or return periods (for example a 1:100 year storm) that occur in the lifetime of the structure. There are no design methods available to assess the damage during multiple storms for near-bed structures. Presently a method that is developed for breakwaters is applied to incorporate damage during multiple storms [Van der Meer, 1999]. It is not proven that this method can also be applied for near-bed structures.

In summary, the problems in designing a near-bed structure are currently that the influence of a large number of waves has not been tested, and it is not known if the current design formulas give representative results for this. Besides this, the current way to incorporate multiple storms is designed for breakwaters and it is not known if the method is also valid for near-bed structures. To investigate both problems use is made of physical scale model testing because of the complexity and lack of knowledge on this subject.

1.2   Research objective and outline thesis

Because of the limitations of the present design method, which was pointed out in Paragraph 1.1, the following main objective has been formulated:

> *To investigate the effect of multiple storms and a large number of waves on the stability of near-bed structures and to develop a design method to include this effect.*

A secondary objective has been formulated at the start of this thesis for the computer model IH-2VOF, which is a side step in this thesis:

> *To investigate to which extend the IH-2VOF numerical model can be used to calculate the flow velocities ot the bottom by a near-bed structure and if this flow velocity can be used to predict the damage from the physical scale model tests.*

During the physical scale model tests the wave generator broke down for several weeks. Because of this breakdown, the tests for validating the numerical model could not be performed. It was therefore decided that the secondary objective had to be abandoned in this thesis. The work done on the numerical model until that point can be found in Appendix A so that it can be included in further studies.

To reach the remaining objective, three steps are undertaken. In the first step a literature review is performed in which the current design methods and research about damage development methods are investigated. In the second part the physical scale model tests are explained and the initial results are presented. In the third part the analysis is done on the scale model tests where the results are compared to results found in the literature study an includes evaluations, conclusions and recommendations about the investigation done with the physical scale model tests.

1.2.1 Part I: Literature review

In Chapter 2 the literature study which is performed for this thesis is presented. In the past a lot of research has been done on the stability of near-bed structures. Several researchers and MSc-students have tested the influence of waves or currents on near-bed structures. Some researchers have done tests while others have looked at different methods to design bottom protections or near-bed structures.

In the first part of the literature study it is explained what a near-bed structure is, how it is designed and how it can be build. Subsequently the forces that play a role on near-bed structures are explained. Generally, the most important force that causes damage to near-bed structures is a flow that is caused by waves. This chapter explains in detail how these forces are generated and how they can be calculated. Subsequently the two ways to design a near-bed structure are explained. The first method follows Shields [1936] steps and tries to link the bottom shear stress caused by a combination of currents and waves to the stability of the near-bed structure. Because this thesis focuses on damage development, this way to design a near-bed structure can be found in Appendix B. The second method describes damage development formulas and damage parameters. In these damage development formulas the way to include multiple storms can be included, which is explained here as well.

Because the dynamic stability or damage development formulas are the most important part in this thesis, the present formulas are compared in the literature study. Comparisons between several parameters of these formulas and an example of a real situation can be found in this chapter. Subsequently, conclusions are drawn and the most important concepts that are described in the rest of the thesis are summarized.

1.2.2 Part II: Physical scale model tests

In Chapter 3 the second part of this thesis deals with the physical scale model testing. The scale model tests are executed at the wave flume of the TU Delft. In these scale model tests several tests with a large number of waves and tests with multiple storms are investigated. This chapter deals with how the scale model tests are built-up, what the boundary conditions are, what the tests are, what is measured and why certain tests are executed.

In Chapter 4 the results of the physical scale model tests are shown which were explained in Chapter 3. Besides the results, observations from the physical scale model tests are reported and linked to physical processes in the wave flume. The results from these scale model tests are presented in such a way that they can be compared and conclusions can be drawn.

1.2.3 Part III: Analysis and Conclusions

Chapter 5 describes the analysis of the physical scale model test. From the results presented in Chapter 4, calculations are performed and analysed. This part focusses on how the damage compared to the number of waves and the damage due to several storms can be calculated. A comparison is made to damage development formulas found in the literature study and a new and improved damage prediction formula is investigated.

After the analysis evaluations, conclusions and recommendations on the work done in previous chapters are presented in Chapter 6. The results are combined and with these results the research question is answered. From this conclusions are drawn, and in the last part recommendations for further research are made.

1.3 Objective and limitations of study

This study aims for understanding the effect of multiple storms on the stability of a near-bed structure. The complexity and lack of knowledge on this subject requires the use of physical model testing. During the model testing it is tried to find answers to the problems imposed in Paragraph 1.1. This thesis follows the design approach from a designers point of view, which means relations and formulations are given which can be understand and calculated easily.

The following limitations apply to this thesis:

- Other near-bed structures such as bed protections are not taken into account.

- Van Gent and Wallast [2001] found that the erosion caused by added currents did not result in more erosion compared to waves alone. This is why the scale model tests are not performed with added currents but for waves only.

- The near-bed structure that is tested, consists only of one type of rock grading and no filter layers are present. In reality near-bed structures are often made of one type of rock grading as well.

- A near-bed structure is normally placed on a sandy bottom. In the scale model tests a sandy bottom is not present. It is expected that this does not influence the tests. In reality sand will be flushed away by large waves present in a storm and the near-bed structure has to coop with the forces present because of these waves.

Part I

Literature Review

Chapter 2

Present design and literature

Near-bed structures are mostly designed to be stable under a given design storm. This approach can be expensive and sometimes not possible. It might for instance require too large stones which cannot be dropped through the fall pipe of a fall-pipe vessel. Designers might in these cases be in favour of a 'dynamically stable' design. These solutions may be more cost-effective than stable solutions. In this approach some movement of stones is allowed in combination with an appropriate maintenance program. This chapter describes only the dynamically stable method while the statically stable method is described in Appendix B. Besides the dynamically stable design method this chapter describes the forces that are present on the near bed structure, how these forces act and how the stability of a near-bed structure can be calculated.

2.1   A rock berm

The main function of a near-bed structure investigated in this thesis is a pipeline protection. The purpose of the protection is to protect the pipeline against fishing equipment, ship anchors, dropped objects and preventing destabilizing of the pipeline. These hazards usually have a negative economic impact, which is of course undesired. Besides this, maintenance or repair on a pipeline is very difficult. A rubble mound cover layer over the near-bed structure can provide cover and protection for the pipeline. A detailed overview of a near-bed structure is shown in Figure 2.1. A near bed structure can be defined by the crest width (B_c), height (z_c) and side slopes ($1 : m_0$) of the structure. The forces on a near-bed structure can be characterised by the local water depth (h), the water depth above the structure (h_c), the wave height and wave period (H_s and T_m) and the currents (u) to which the structure is exposed. This section deals with the characteristics of near-bed structures: how it looks and how it is built.

2.1.1   Rubble

Rubble (rock) is a natural product which is won in a quarry. A common size for a rock in a near-bed structure to protect a pipeline has a D_{n50} in the order of 0.15 m [Hendrickx, 2013]. The D_{n50} is the median stone diameter where 50% of the stones have a smaller mass. A characteristic parameter for a rock grading is the median stone weight W_{50}. This parameter is defined as the stone weight where 50% of the individual stones have a lower mass. From this the D_{n50} can be derived. The D_{n50} is the nominal stone diameter which is the size from a rib of a cube with the same volume as the W_{50}. The relation between both parameters can be described with Equation 2.1. In this equation g is the gravitational constant (9.81 m/s^2) and ρ_s is the specific density of stone.
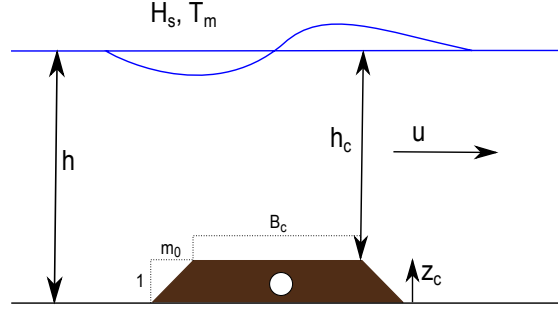
Figure 2.1: Near-bed structure detail.

$$D_{n50} = \sqrt[3]{\frac{W_{50}}{g \cdot \rho_s}} \tag{2.1}$$

Different gradings of rocks can be used to create near-bed structures. A way to characterize these gradings can be done using by the W_{85}/W_{15} ratio, its cube root or the D_{85}/D_{15} ratio. The D_{50} is used for smaller sand and represents the characteristic sieve diameter for which 50% of the sand falls through. The relation between the D_{n50} and the D_{50} can be calculated using a shape factor which can be seen in Equation 2.2. The shape factor s_f depends on the shape of the stone. For rock the shape factor is approximately 0.84.

$$D_n = \sqrt[3]{s_f} \cdot D \approx 0.84 \cdot D \tag{2.2}$$

In near-bed structures the grading is normally 'wide'. The very wide gradation could result in de-mixing during installation or transport and is therefore not often applied in near-bed structures. The grading classification is shown in Table 2.1.

Grading width	D_{85}/D_{15}			W_{85}/W_{15}		
Narrow or single-size gradation	<1.5			1.7	-	2.7
Wide gradation	1.5	-	2.5	2.7	-	16
Very wide or quarry run gradation	2.5	-	5	16	-	125+

Table 2.1: Armourstone gradation related to uniformity. Taken from CIRIA [2007].

2.1.2   Execution and maintenance

A near-bed structure can be installed in several ways. The execution method mainly depends on the water depth where the near-bed structure has to be constructed. Generally, when a near-bed structure has to be constructed in more than 20 m water depth, a fall-pipe vessel is used. A fall-pipe vessel has a pipe which can extend towards the bottom where the rocks fall through. On the end of this pipe mostly a Remote Operated Vehicle (ROV) maintains a position directly above the pipeline. Rock with a maximum size (D_{100}) of around 300 mm can be installed very precisely on the pipeline through the fall-pipe [Hendrickx, 2013]. An artist impression is shown in Figure 2.2.

For more shallow water a side stone dumping vessel, crane ship or split barge can be used. The accuracy between all the construction methods differ greatly. This, and the construction methods are not described any further in this thesis.
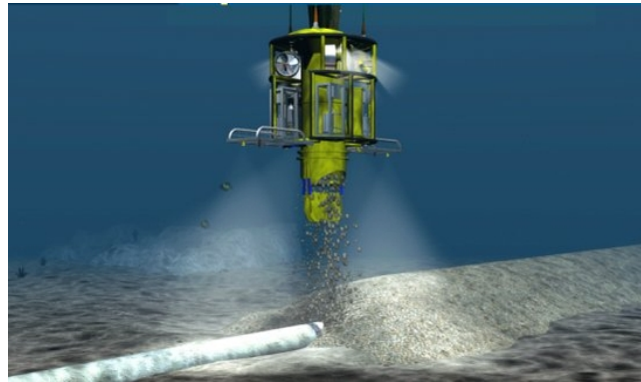
Figure 2.2: Artist impression of rock dump with a fall-pipe vessel. Taken from Van de Velde [2013].

Construction and maintenance cannot be separated from each other. If a certain structure is constructed, maintenance is always necessary. Maintenance is for instance important when a certain amount of transport of stones is accepted and thus damage occurs to the near-bed structure. Most of the time this is a cost optimization. When too large stones have to be used, it might become very expensive and it might sometimes be economically better to install smaller stones with an appropriate maintenance program on the near-bed structure. Maintenance can be done for instance on a regular time bases, after high storms or as a preventive measure before storms. Maintenance is therefore a very important concept in the design of a near-bed structure. Because in this thesis the focus is on damage development and stability in time, a maintenance program can be designed according to the expected damage development. In this way designers can calculate the expected damage and design an appropriate maintenance program. A designer can also choose to install extra stones in order to avoid unnecessary maintenance and allow a certain amount of damage.

2.2 Forces

In this paragraph the forces that affect a near-bed structure are described. The stone motion follows from the hydrodynamic forces caused by the velocity of water around a stone. This is a complex phenomenon and depends on depth and flow conditions. Besides the velocity, also acceleration of the flow can be a force for destabilizing a stone. Accelerations create pressure gradients that can cause this destabilizing force. The flow velocities and accelerations are caused by the waves (wave height H, period T) and velocity of the water from for instance a tidal current. The wave height influences the velocity near the bottom and the period determines how fast the velocity changes in time.

Generally the most important deformation force of a near-bed structure are the wave induced currents and not the added currents to which the structure is exposed. This is because wave generated currents in storm conditions are more severe than normal currents. In other words, in wave dominated situations wave induced currents are the main deformation force. This is why a detailed research is carried out for waves and in a lesser extent on currents.

2.2.1 Linear wave theory

Linear wave theory is a theoretical theory to describe waves in a simple and understandable manner. In this theory there are several assumptions that might not be the case in reality. Linear wave theory assumes that the water is an ideal fluid with only the earth's gravitation force acting on the water particles. As an ideal fluid, water is assumed to be incompressible, to have a constant

density and to have no viscosity. Of course, water is not an ideal fluid but this is ignored in linear wave theory. Although water is not an ideal fluid, it can be seen as incompressible and over a few wavelengths the water has a constant density and viscosity. The vertical variations of this are usually ignored as well. In this theory the water is subject to only one external force. Both wind induced pressures and surface tension are excluded from linear wave theory as well. This implies that waves in linear wave theory are longer than a few centimetres so no capillary waves are included. Because the Coriolis force is not part of this theory as well, the wavelength must be smaller than a few kilometres. Bottom friction is also excluded from the linear theory. This is not a big limitation because this is a local effect. However, in shallow water this can be of big importance. Another important implication is that the wave kinematics (motions) and wave forces need to be neglected. For this, the wave amplitude must be small relative to the wave length and water depth.

Based on all these limitations and assumptions a simplified momentum balance equation and continuity equation can be derived [Holthuijsen, 2007]. These equations describe the kinematic and dynamic aspect of waves. With boundary conditions these equations can be solved and two results are obtained. One of these is a long-crested harmonic wave propagating in the positive x-direction. This answer is shown in Equation 2.3. In this Equation η is the surface elevation, a is the amplitude which is defined as $H/2$, ω is the angular frequency of the wave which is defined as 2π divided by the wave period T and k is the wave number which is defined as 2π divided by the wave length L.

$$\eta(x,t) = a\sin(\omega t - kx) = \frac{H}{2}\sin\left(\frac{2\pi}{T}t - \frac{2\pi}{L}x\right) \tag{2.3}$$

The second result from solving the momentum balance and continuity equation gives a velocity potential function which can be seen in Equation 2.4. In this formula z is the vertical coordinate where $z = 0$ represents still water level and $z = -h$ the bottom.

$$\phi(x,z,t) = \hat{\phi}\cos(\omega t - kx) \quad \text{in which} \quad \hat{\phi} = \frac{\omega a}{k}\frac{\cosh[k(h+z)]}{\sinh(kh)} \tag{2.4}$$

This velocity potential function applies to both free and forced waves as long as the surface wave is the harmonic wave of Equation 2.3 [Holthuijsen, 2007]. A free wave is only subject to gravity and a forced wave can be affected by other external forces, for instance a metal sheet moving in the water. Water particle velocities can be obtained from the velocity potential function. The spatial derivative of the velocity potential function are the velocity components in that direction. For example, for the flow in the x direction this gives $\partial\phi/\partial x = u_x$. The answer for this derivative is given in Equation 2.5. This can be done in the same way for the z direction. The velocity in the y-direction is zero since the long crested harmonic wave is propagating in the positive x-direction. These velocities are called orbital velocities and correspond to the motion of the particles in closed, circular or elliptical orbits.

$$u_x = \omega a\frac{\cosh[k(h+z)]}{\sinh(kh)}\sin(\omega t - kx) \tag{2.5}$$

The water particles describe an elliptical orbit. From the water surface to the bottom, the vertical displacement of the water particles reduces to zero while the horizontal displacement remains almost constant. In deep water $kh \to \infty$ and in shallow water $kh \to 0$. For these two situations these equations reduce to a shorter and easier form. In a deep water case the waves do not 'feel' the bottom and thus no velocity on the bottom is present due to waves. In intermediate and shallow water the waves feel the bottom and a velocity is present. In shallow water $h/L < 1/20$ and in deep water $h/L > 1/2$. In Figure 2.3 the process that the waves feel the bottom is visualised.
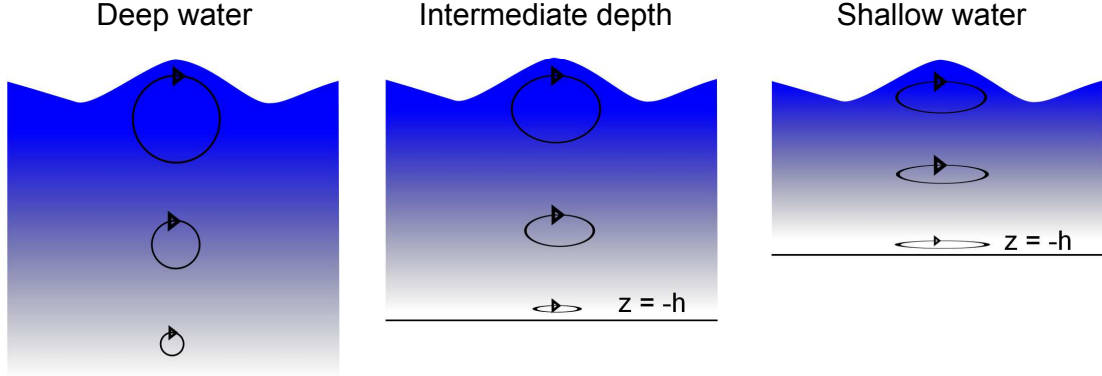
Figure 2.3: The orbital motion in deep, intermediate and shallow water.

Equation 2.6 gives the maximum horizontal velocity at the bottom $\hat{u}_0$ and the maximum horizontal displacement amplitude at the bottom $\hat{a}_0$. The maximum horizontal velocity on the bottom is an important parameter because it can be seen as the maximum flow velocity responsible for damage to a near-bed structure. This is described further on in this thesis.

$$\hat{u}_0 = \frac{\pi H_s}{T_m} \frac{1}{\sinh(kh)}$$
$$\hat{a}_0 = \frac{H}{2} \frac{1}{\sinh(kh)} = \frac{\hat{u}_0 T_m}{2\pi} \tag{2.6}$$

This linear theory of surface gravity waves matches the description of ocean waves perfectly because it is based on the assumption that wave components are harmonic and independent. In other words, the waves behave as linear harmonic waves. Unfortunately this also implies that this theory has only a limited range for which it can be applied. When waves are too steep or the water is too shallow, the linear wave theory is no longer valid. By using Equation 2.7 and the mean wave period T_m the wave steepness s_m can be calculated. If the non-linear effects are weak, or only occur intermittently, the waves can be treated on large scale as linear waves. When this cannot be applied higher order wave theories have to be used. In these theories each wave is assumed to be one wave in a train of periodic waves, with a constant shape, amplitude and length [Holthuijsen, 2007]. An overview of which theory should be used is shown in Figure 2.4. The horizontal axis represents the water depth which is made dimensionless with the acceleration of gravity and the square of the period, which is a measure of the wavelength. The vertical axis represents the wave height, which is also made dimensionless with the wave length. The vertical axis represents in this way the wave steepness. The upper limit of the graph is limited by wave breaking due to steepness or water depth.

$$s_m = \frac{2\pi}{g} \frac{H_s}{T_m^2} \tag{2.7}$$

The upper limit, due to wave breaking in Figure 2.4, is described by the Miche wave breaking theory. This theory is given by Equation 2.8 [Schiereck, 2001]. In this Equation H_b is the wave height at which the wave starts to break.

$$H_b = 0.142 L \tanh\left(\frac{2\pi}{L} h\right) \tag{2.8}$$

The boundary conditions to solve the balance equations assume that the velocity on the bottom is zero. However, a boundary layer is present where this assumption is not valid. In Appendix B
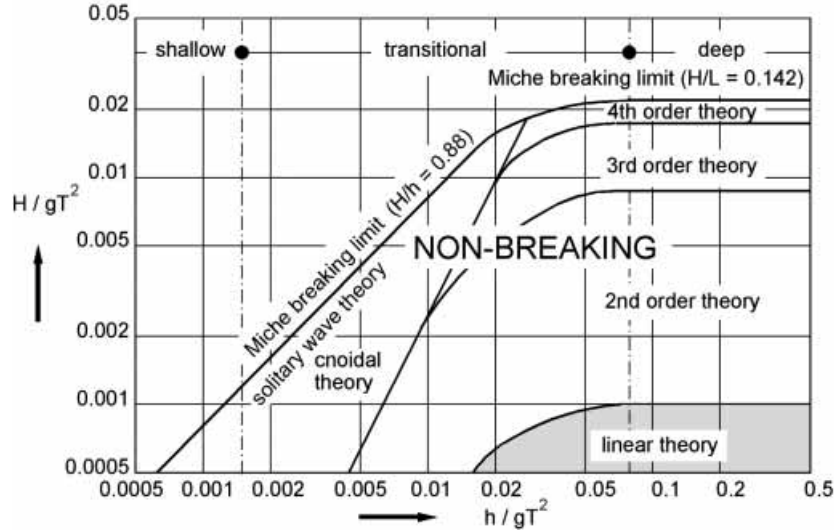
Figure 2.4: Validity of wave theories [LeMéhauté, 1976 cf. Schiereck, 2001]

the boundary layer is described in more detail. However, a general conclusion is that there is an increase in velocity just above the boundary layer which could be important. This increase in velocity might be responsible for the earlier movement of stones in near-bed structures and thus more damage would occur. In this thesis the bottom velocity is calculated using linear wave theory where in fact a second or third order theory should be used. However, the velocity calculated using linear wave theory is considered as a good approximation for the destabilizing flow force on the near-bed structure.

2.2.2 Irregular waves

Irregular waves are caused by wind. Each wind speed, in relation with other parameters as for instance the water depth, can create its own wave period and wave height. All the wind components together can make a very irregular water surface profile. To describe all of these waves a spectrum is used. This spectrum does not describe in detail one wave observation but describes the sea surface as a stochastic process. This is to characterise all possible observations that could have been made under the condition of the actual observation. There are two ways get a wave spectrum.

The first uses wave height versus time measurements from a sea state and is called the random-phase/amplitude model. From wave height versus time measurements, wave height and wave period can be calculated. With the use of spectral analysis (Fourier-Transform) the surface elevation or amplitude and phase for each wave frequency can be determined which is called the amplitude and phase spectrum. The phases have a value between 0 and 2π and no preference for any value can be determined. With only the amplitude spectrum left, the previous step to get the amplitude spectrum with Fourier-Transform is repeated many times for the same record. Because the time record would be different, the amplitude spectrum is also different and an average over all amplitudes is taken. This is denoted by an over-line. Subsequently the variance of each wave component must be taken and with this the variance spectrum is obtained. Dividing this by the frequency and taking the limit towards zero, a continuous line is found which represents an amplitude with a certain frequency f. This spectrum is called the variance density spectrum and is represented in Equation 2.9 [Holthuijsen, 2007].

$$E(f) = \lim_{\Delta f \to 0} \frac{1}{\Delta f} \frac{1}{2} \overline{a^2} \tag{2.9}$$

The second way to obtain a spectrum is with many random phases and amplitudes. The same spectrum is obtained but now the expected value of the amplitude is taken, $E\{\frac{1}{2}\underline{a}^2\}$ (See also Equation 2.10). The under-line represents that the variable is treated as a random variable. In this way the same spectrum can be obtained as showed in Equation 2.9. The integral over all positive values of f, equals the variance of the surface elevation. Multiplying this variance amplitude spectrum by $\frac{1}{2}\rho_w g$ gives the total average energy in this wave observation. The variance density spectrum gives a complete description of the surface elevation of ocean waves in a statistical sense. This implies that all statistical characteristics of the wave field can be expressed in terms of this spectrum [Holthuijsen, 2007]. In Equation 2.10 the variance density spectrum is shown. The variance density spectrum gives a complete description of the surface elevation of ocean waves in a statistical sense. For each frequency the variance density spectrum gives the expected amplitude to that frequency.

$$E(f) = \lim_{\Delta f \to 0} \frac{1}{\Delta f} E\{\frac{1}{2}\underline{a}^2\} \tag{2.10}$$

The overall appearance of the wave can be inferred from the shape of the spectrum. The narrower the spectrum, the more regular the waves are. This is visualised in Figure 2.5. The wave period where the spectrum $(E(f))$ has its maximum value such as in Figure 2.5, is called the peak period (T_p). Besides the wave period, the characteristic wave height can be calculated from a spectrum by Equation 2.11. In this Equation m_0 is defined as the area beneath the energy spectrum $E_{energy}(f) = \rho g E_{variance}(f)$.
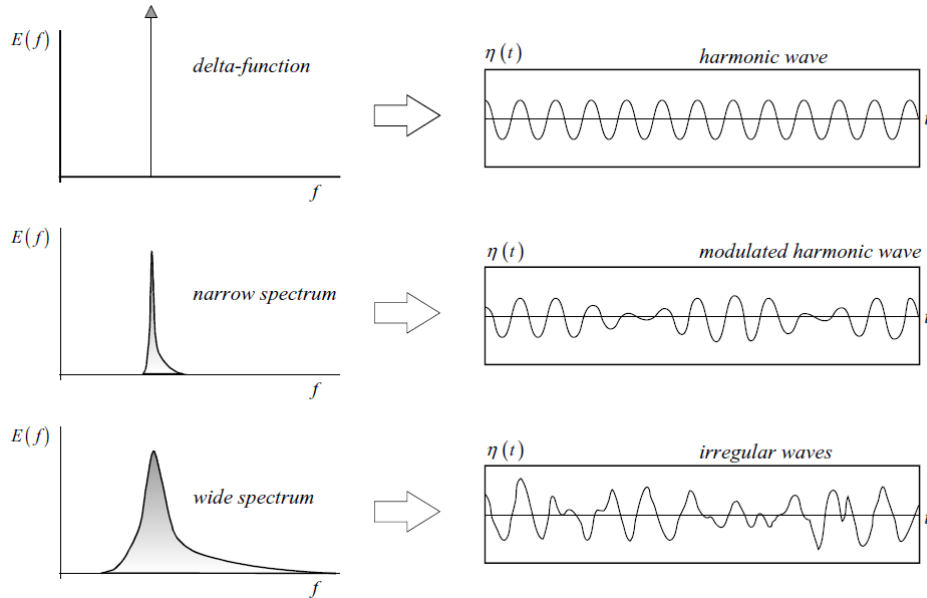
Figure 2.5: Wave character for different widths of the spectrum. Taken from Holthuijsen [2007].

$$H_s \equiv H_{1/3} \approx 4\sqrt{m_0} \tag{2.11}$$

There are two important 'standard' spectra which are used a lot. The first is the Pierson and Moskowitz [1964 cf. Holthuijsen, 2007] spectrum $E_{pm}(f)$. This spectrum is based on 'fully developed' wind waves on relatively deep water. However, because these waves are fully developed it is likely that this method overestimates, on for instance the North-Sea, the real wave conditions which are present in reality. The second important spectrum is the JONSWAP (JOint North Sea WAve Project) spectrum [Hasselman et al., 1973 cf. Holthuijsen, 2007]. The JONSWAP spectrum

is based on the Pierson and Moskowitz spectrum but with a sharper peak. Besides this, the JON-SWAP spectrum is not fully developed. The JONSWAP spectrum and the Pierson Moskowitz spectrum are shown in Equation 2.12. In this equation γ is a peak-enhancement factor for the JONSWAP spectrum, σ is a peak-width parameter ($\sigma = \sigma_a$ for $f \leq f_{peak}$ and $\sigma = \sigma_b$ for $f > f_{peak}$) and α is the energy scale parameter. It can be seen that the JONSWAP spectrum is the Pierson Moskowitz spectrum multiplied by a factor γ. From the JONSWAP and Pierson Moskowitz also a significant wave height can be obtained. This is called the significant wave height from a wave spectrum H_{m0}.

$$
E_{JONSWAP}(f) = \underbrace{\alpha g^2 \left(2\pi\right)^{-4} f^{-5} \exp\left[-\frac{5}{4}\left(\frac{f}{f_{peak}}\right)^{-4}\right]}_{\text{Pierson-Moskowitz shape: } E_{PM}(f)} \overbrace{\gamma^{\exp\left[-\frac{1}{2}\left(\frac{f - f_{peak}}{\sigma f_{peak}}\right)^2\right]}}^{\text{JONSWAP}} \tag{2.12}
$$

Because the JONSWAP spectrum is designed for undeveloped waves which is more representative for a real sea state where near-bed structures are build, the JONSWAP spectrum is used in this thesis.

2.3   Design approaches

In this section one of the two design approaches for a near-bed structure is explained. The first one is to design a stable construction under the design conditions present in the lifetime of the structure. For this design approach and the forces present on a single stone reference is made to Appendix B. The second approach is to allow some damage during the lifetime of the structure and design the near-bed structure accordingly to this which is described in this chapter. In this way some movement and reshaping of stones is allowed. In time the developed damage can be calculated and it can be seen if enough stones are present on top of the near-bed structure.

2.3.1   Damage research

Van der Meer.
Thompson and Shuttler [1975] did a large number of tests with waves on a riprap breakwater. This is of course not the same as near-bed structures but formed a bases still used today. Later reanalysis by Van der Meer [1988] and with additional tests, Van der Meer concluded that the number of waves and the damage could be described using the $S/\sqrt{N}$ ratio. Here S is a dimensionless damage parameter which is explained further on in this chapter. He uses this ratio in most of his famous formulations. Further on in this thesis it is explained that several researchers have used this ratio for breakwaters to described damage to near-bed structures.

Van der Meer states that from $N = 0 - 1000$ the damage function actually should be linear and that after a large number of waves ($N > 15000$) a stable equilibrium should be reached. A function found by Van der Meer to describe this process is shown in Equation 2.13. In this formula he limited the damage to 1.3 times the damage he found after $N = 5000$.

$$
\frac{S(N)}{S(5000)} = 1.3 \left[1 - \exp(-3 \cdot 10^{-4})\right] \tag{2.13}
$$

Besides this relationship Van der Meer gives another important relationship for $N < 8,500$. This relationship can be seen in Equation 2.14. He states that the influence of the number of waves can simply be described by $S/\sqrt{N}$.

$$S = 0.014\sqrt{N} \tag{2.14}$$

Lomónaco.
Lomónaco [1994] was one of the first researchers who did physical scale model testing for near-bed structures. He did physical scale model tests in order to understand the stability of near-bed structures in waves and currents. Lomónaco used a JONSWAP spectrum and in some tests a small current. He observed that after approximately 1000 waves almost no damage or transport occurs and each near-bed structure became relatively stable. Lomónaco tried several ways to describe the damage to near-bed structures. He included present formulas for reef breakwaters but concluded these were not applicable. He concluded that the damage to a pipeline cover could be described by the stability parameter θ. In this thesis this symbol is used to describe a stability parameter based on the orbital velocity. To avoid confusion this stability parameter is called the velocity parameter in this thesis. The velocity parameter is defined in Equation 2.15.

$$\theta = \frac{\hat{u}^2}{g\Delta D_{n50}} \tag{2.15}$$

In this formula the maximum bottom velocity on top of the near-bed structure should be used. This velocity should be calculated using linear wave theory with the use of H_s, T_m and height h_c. Height h_c is the water depth above the near-bed structure. Later it was confirmed by a case study that height h_c would be the best height for calculating the stability of near-bed structures [Lomonaco et al., 2005]. The formulas to calculate the bottom velocity can be seen in Equation 2.16 where iteration for the wave number k on height h_c is necessary which can be done with Equation 2.17 [Holthuijsen, 2007].

$$\hat{u} = \frac{\pi H_s}{T_m} \frac{1}{\sinh(k_c h_c)} \tag{2.16}$$

$$\frac{2\pi}{T_m} = \sqrt{gk_c \tanh(k_c h_c)} \qquad \text{Local dispersion relation} \tag{2.17}$$

Because of the dependency between the damage level S and the velocity parameter Lomónaco mentions that this must be in some sort of power function like $S = a\theta^b$. Though, because of the lack of data and tests he does not provide an actual design formula. He concludes that the structure slope also influences the damage. However, the number of waves are not included in this formula. The damage number S is defined as Equation 2.18 [Broderick, 1983]. In this formula A_e is the erosion area.

$$S = \frac{A_e}{D_{n50}^2} \tag{2.18}$$

The test ranges for Lomónaco's scale model tests using irregular waves are shown in Table 2.2.

Klomp and Lomónaco.
Klomp and Lomónaco [1995] studied the stability of pipeline covers under combined action of waves (JONSWAP spectrum) and currents. This research was based on the M.Sc. thesis of Lomónaco [1994]. In this paper more detail is given about ways to predict damage to near-bed structures. Here the formula $S = a \cdot \theta^b$ is used again to predict damage. The factor a is thought to be related to the slope of the structure by the formula $a = 21.4 \tan(\alpha)$. Note that α is not the same as m_0. α can be defined as $\tan(\alpha) = 1/m_0$. This relation was only the case for two of the designs he tested. For these two structures the damage prediction formula after 1000 waves is shown in Equation 2.19. In this formula the number of waves is again not present.

Parameter [unit]	Symbol	Range		
Stone diameter [mm]	D_{n50}	3.65	–	8.33
Crest width [m]	B_c	0.06	–	0.25
Front side slope [-]	m_0	1	–	5
Relative buoyant density [-]	Δ	1.46	–	1.71
Number of waves [-]	N	898	–	2897
Fictitious wave steepness [-]	s_m	0.028	–	0.07
Velocity parameter [-]	$\hat{u}^2/(g\Delta D_{n50})$	0.44	–	3.59
Ratio wave height water depth [-]	H_s/h	0.25	–	0.42
Ratio wave height depth at crest [-]	H_s/h_c	0.29	–	0.50
Ratio depth at crest depth [-]	h_c/h	0.62	–	0.86
Stability parameter [-]	$H_s/(\Delta D_{n50})$	10	–	55

Table 2.2: Physical scale model test ranges of Lomónaco.

$$S_{1000} = 21.4 \cdot \tan(\alpha)\theta^{2.25}$$
$$\theta = \frac{\hat{u}^2}{g\Delta D_{n50}} \tag{2.19}$$

Klomp and Lomónaco do however give a time dependency. This dependency is shown in Equation 2.20.

$$S_N = S_{1000}\left(\frac{N}{1000}\right)^b = 21.4 \cdot \tan(\alpha)\theta^{2.25}\left(\frac{N}{1000}\right)^b \tag{2.20}$$

In this formula S_N is the damage parameter after N waves. The parameter b can be calculated using Equation 2.21 and 2.22.

$$S'_{1000} = \frac{A_e}{D_{n50}B_c} \tag{2.21}$$

$$\begin{aligned} \text{For } S'_{1000} \leq 100 \qquad & b = 1 - \frac{S'_{1000}}{200} \\ \text{For } S'_{1000} > 100 \qquad & b = 0.5 \end{aligned} \tag{2.22}$$

The defined relations should be used with care because most test were stopped after 2000 waves. Besides this, a lot of scatter is present in the design formula so the verification is still limited. Another conclusion is that the damage developments stops in time and that the dependency to the number of waves agrees well with the relationship derived for breakwaters. Van der Meer [1988] found that the storm duration versus damage could be described best by the parameter $S/\sqrt{N}$ which is the same parameter proposed here when $b = 0.5$.

In Lomónaco and Klomp [1997] more research is done based on the M.Sc. thesis of Lomónaco. In the paper they mention the correlations of the damage with rock transport formulas which are not described in present thesis. Besides this, also reference is made to Equation 2.19 where the θ parameter should be calculated with linear-wave theory at depth h_c. They mention that this formulation predicts the damage within a 90% confidence interval. However, they point out that more research into this formulation has to be done and it can only be used for a conceptual design. In this paper they also mention the time dependency that the structure is observed to be stable after approximately 1000 waves. This observation is done within the limits of their tests and might not be valid for each near-bed structure.

Levit.

Levit [1996] tried to validate in his M.Sc. thesis the formulas found by Klomp and Lomónaco [1995] with additional scale model tests. These scale model tests were done with currents and regular waves. He found that the formulas provided by Klomp where not correlating well with his scale model tests which could be because Levit used regular waves. Besides this, Levit found that structures under currents and waves were more stable than structures under waves alone, which is quite strange. Levit mentions that the initial rate of deformation under waves alone was much more severe than the theory from Klomp predicts. In the later stages of his test deformations were reducing which would indicate that a stable profile was developing. Levit did not make any changes to the formulas provided by Klomp.

The test ranges for Levit's scale model tests using regular waves are shown in Table 2.3. Note that Levit actually measured his maximum bottom velocities so that the velocity parameter could be calculated with these values.

Parameter [unit]	Symbol	Range		
Stone diameter [mm]	D_{n50}		4.3	
Crest width [m]	B_c		0.2	
Front side slope [-]	m_0	2	–	5
Relative buoyant density [-]	Δ		1.67	
Number of waves [-]	N	15	–	3825
Fictitious wave steepness [-]	s_m		0.04	
Velocity parameter (from measured velocity) [-]	$\hat{u}^2/(g\Delta D_{n50})$	4	–	12.3
Velocity parameter (from calculated velocity) [-]	$\hat{u}^2/(g\Delta D_{n50})$		3.00	
Ratio wave height water depth [-]	H_s/h		0.5	
Ratio wave height depth at crest [-]	H_s/h_c		0.625	
Ratio depth at crest depth [-]	h_c/h		0.80	
Stability parameter [-]	$H_s/(\Delta D_{n50})$		34.8	

Table 2.3: Physical scale model test ranges of Levit.

Levit et al. [1997] is a research based on Levit's M.Sc. thesis and investigates the forces acting on a submarine pipeline cover. In this paper they mention that the near bed velocities are increased on the slope and return back to the increased normal velocity on top of the near-bed structure because of the lower depth. They conclude that the flow velocities follow the linear wave theory except on the slope of the structure. In the first 30 seconds of waves, in the waves only model, they already notice rounding off crest corners. In the waves and current model they mention that the structure showed surprisingly little deformation. Even the rounding off from corners was not so significantly as for the waves alone tests. By exposing the structure to more than 1000 waves this resulted in not much additional deformation. Levit et al. conclude that the structure is largely unaffected by the surrounding fluid motion.

Vidal et al.

Vidal et al. [1998] did scale model tests in order to improve the existing theory about the stability of near-bed structures where he paid special attention to the initial stages of damage. He used regular waves to test the stability of near-bed structures. The reflection of the near-bed structure proved to be less than 5% for longer wave periods. Comparisons were made with a Morison parameter, a mobility parameter approach (Shields) and the Hudson number presented as $N_s = H_s/(\Delta D_{n50})$. The Hudson number is presented in this thesis as the stability number. In this formula N_s is the Hudson parameter. In contrast to earlier studies described here Vidal et al. concluded that the mobility parameter can be used to predict damage to the structure. They did not look at comparisons to the velocity parameter which other studies had shown to be the best parameter. They proposed a new mobility parameter based on the shear stress from Jonsson [1966] (Equation B.30). Vidal et al. their design formula can be seen in Equation 2.23 and 2.24.

Their formula to calculate the damage is not time dependent and thus no number of waves are present. The velocity $\hat{u}$ in the design formulas should be calculated using linear wave theory on depth h_c assuming the depth is equal to h everywhere. This is a little different than other studies have shown which recommend to calculate the bottom velocity where the depth should be equal to h_c everywhere. This velocity is called u_c in this thesis.

$$M_p = \frac{\tau_0}{\rho_w g \Delta D_{n50}}$$
$$\tau_0 = \frac{1}{2} c_f \rho_w \hat{u}_c^2$$

$$(2.23)$$

$$\begin{array}{ll} \text{For } M_p < 0.4 & S = 37.03 \cdot M_p - 0.415 \\ \text{For } M_p > 0.4 & S = 0.124 \cdot \exp(53.49 M_p) \end{array}$$

$$(2.24)$$

In Vidal et al. [2002] this approach was compared with a real situation. They concluded that if the 50 largest mobility parameters are used the damage correlates well with this approach. In reality the 50 largest mobility parameters are hard to obtain because this requires the 50 largest wave heights. This would require a statistical approach which is unwanted in a design case. In a real situation most of the time only the parameter H_s is known. Besides this, Vidal et al recommend a near-bed structure should be designed for $M_p = 0.06$, giving $S = 3$. This seems a rather strict requirement because of the large stones used in this real situation.

Vidal et al. [2007] deals with the stability of low crested-structures and submerged breakwaters. This paper is based on re-analysed data of Lomónaco [1994], Vidal et al. [1998] and Vidal et al. [2002]. The submerged structures can be compared to near-bed structures but are a little higher than normal near-bed structures. Apart from the tests an investigation with the COBRAS-UC numerical computer model has been carried out (This computer model is the precursor of the 2VOF model from IH-Cantabria). They compared the results to the velocity parameter, mobility parameter and the stability parameter. In contrast to his earlier observations Vidal et al. advise in this paper that a velocity parameter is the best way to calculate the damage. The maximum velocity should be calculated at the rear edge of the submerged structure with the numerical model. They even improved this function a little by defining a new formula. M_p Should be replaced by $M_{p\,crit}$ which is defined as the difference between the maximum velocity on the rear end of the crest, and the velocity for the threshold of motion for the rubble $U_{max} - U_{crit}$. The formula to calculate the damage with Vidal et al. their new formula can be seen in Equation 2.25 and 2.26.

$$M_{p\,crit} = \frac{\left[\left(\dfrac{U_{max}}{U_{crit}} - 1 \right) \cdot U_{crit} \right]^2}{\Delta g D_{50}} \quad \text{if} \quad U_{max} - U_{crit} > 0$$

$$(2.25)$$

$$S = 3.2 \cdot M_{p\,crit}^{1.45} - 0.30$$

$$(2.26)$$

In Equation 2.25 the parameter U_{max}/U_{crit} should be calculated with the numerical model. U_{crit} Is defined as Equation 2.27 and can be calculated using Equation 2.28. Here Ψ is the Shields coefficient which is explained in Appendix B. Vidal et al. gives a formula for the relation between the critical and maximum velocity which is the best fit for their data and can be seen in Equation 2.29. In this formula H_{50} are the 50 largest waves that has been discussed in the work of Vidal previously. Vidal concludes that this formula slightly overestimates the damage for $S < 1$ while for high damage levels ($S > 7$) it underestimates the damage.

$$U_{crit} = \left(2 \cdot (\rho_s - \rho_w) \cdot g \cdot D_{50} \cdot \frac{\psi_{crit}}{\rho_w \cdot c_f} \right)^{0.5}$$

$$(2.27)$$

$$\psi_{crit} = \frac{0.24}{0.25 \cdot D_{50}} + 0.055 \cdot \left(1 - \exp^{-0.005 \cdot D_{50}}\right) \tag{2.28}$$

$$\frac{U_{max}}{U_{crit}} = 0.73 \cdot \ln\left(\frac{-H_{50}}{h_c}\right) + 2.3 \tag{2.29}$$

Van Gent and Wallast.
Van Gent and Wallast [2001] and Wallast and Van Gent [2002] are a research document and a paper respectively, investigating stability of near-bed structures. Wallast and Van Gent did scale model tests to investigate the stability of near-bed structures under waves and currents. They used a JONSWAP spectrum to describe the irregular waves and used data from Lomónaco [1994] as well. Wallast and Van Gent also tried to correlate their new data with a velocity -, mobility -, Morison parameter and stability number. They found that the velocity based stability parameter, θ, describes the damage in the best way. Besides this, they also found that a current could be neglected when $\theta^2/(g\Delta D_{n50}) < 3.5$. Outside of this range more research would be necessary. The damage development formula from Wallast and Van Gent is shown in Equation 2.30 and 2.31. In this formula S is defined as Equation 2.18.

$$\frac{S}{\sqrt{N}} = 0.2\theta^3 \tag{2.30}$$

$$\theta = \frac{\hat{u}^2}{g\Delta D_{n50}} \tag{2.31}$$

Wallast and Van Gent define $\hat{u}$ with linear wave theory using H_s, T_m and height h_c which is the same way as Lomónaco and Klomp [1997] defined it using Equation 2.16. These formulations from Wallast and Van Gent to calculate the damage to near-bed structures have been included in the Rock Manual [CIRIA, 2007]. The Rock Manual states that because still a lot of scatter is present this formulation should be used with care. An upper safe bound is to include an α factor in the formulations of Wallast and Van Gent. This formulation can be seen in Equation 2.32. This factor should be 3 to create a safe upper bound.

$$\frac{S}{\sqrt{N}} = \alpha \cdot 0.2\theta^3 \tag{2.32}$$

The Rock Manual also states that it is not clear how to design a near-bed structure where perpendicular currents and waves to the crest width are present. It advises to do physical scale model testing for this phenomenon and when designing a near-bed structure outside of the ranges were Wallast and Van Gent have tested with. The test ranges that Wallast and Van Gent have tested are shown in Table 2.4.

Saers.
Saers [2005] did additional scale model tests with irregular waves (JONSWAP spectrum) without an added current. He concluded that Wallast and Van Gent generally overestimated the damage based on his tests. Because of this, Saers found that the number of waves could better be expressed with another function. Saers his design formula is shown in Equation 2.33.

$$\frac{S}{\log N} = 0.8\theta^{2.5}$$
$$\theta = \frac{\hat{u}^2}{g\Delta D_{n50}} \tag{2.33}$$

The velocity $\hat{u}$ is defined in the same way as Lomónaco and Wallast and Van Gent. Lomónaco and Levit mentioned that the slope might influence the erosion of the near-bed structure. Therefore

Parameter [unit]	Symbol	Range		
Stone diameter [mm]	D_{n50}	3.1	–	8.3
Crest width [m]	B_c	0.06	–	0.25
Front side slope [-]	m_0	1	–	8
Relative buoyant density [-]	Δ	1.45	–	1.70
Number of waves [-]	N	1000	–	3000
Fictitious wave steepness [-]	s_m	0.03	–	0.07
Velocity parameter [-]	$\hat{u}^2/(g\Delta D_{n50})$	0	–	10.8
Ratio wave height water depth [-]	H_s/h	0.15	–	0.5
Ratio wave height depth at crest [-]	H_s/h_c	0.2	–	0.9
Ratio depth at crest depth [-]	h_c/h	0.66	–	0.75
Stability parameter [-]	$H_s/(\Delta D_{n50})$	5	–	50

Table 2.4: Physical scale model test ranges of Wallast and Van Gent.

Saers established a factor to correct the damage to the near-bed structure based on this conclusion and his own physical scale model tests. Saers called this 'streamline contraction' because of the acceleration which is present on top of the near-bed structure. He defines this parameter, called the Saers parameter by Van den Bos [2006], as the ratio of the structure height multiplied by the slope over the wave orbital motion. For steep slopes and heigh structures the streamline contraction is larger. The Saers parameter is defined as Equation 2.34. Saers mentions this parameter, but does not conclude that this parameter should be implemented or works out this concept any further.

$$Sa = \frac{z_c m_o}{\hat{a}_0} \tag{2.34}$$

The test ranges from Saers physical scale model tests using irregular waves are shown in Table 2.5.

Parameter [unit]	Symbol	Range		
Stone diameter [mm]	D_{n50}	3.7	–	3.7
Crest width [m]	B_c	0.04	–	0.04
Front side slope [-]	m_0	2.5	–	2.5
Relative buoyant density [-]	Δ	1.47	–	1.47
Number of waves [-]	N	980	–	6546
Fictitious wave steepness [-]	s_m	0.036	–	0.046
Velocity parameter [-]	$\hat{u}^2/(g\Delta D_{n50})$	1.86	–	2.93
Ratio wave height water depth [-]	H_s/h	0.37	–	0.42
Ratio wave height depth at crest [-]	H_s/h_c	0.41	–	0.48
Ratio depth at crest depth [-]	h_c/h	0.85	–	0.91
Stability parameter [-]	$H_s/(\Delta D_{n50})$	27	–	39

Table 2.5: Physical scale model test ranges of Saers.

Van den Bos.
Van den Bos [2006] did his M.Sc. thesis on the design of near-bed structures in currents and waves. He looked at various ways to design and calculate near-bed structures. The damage based method of Van den Bos was based on re-analysed data of Lomónaco [1994], Van Gent and Wallast [2001] and Saers [2005]. He found that the dimensionless erosion area was only depended on the number of waves N, the side slope m_0, the dimensionless crest width B_c/D_{n50} and the velocity parameter θ. Van den Bos developed a new damage development formula which can be seen in Equation 2.35 and 2.36. Note that the dimensionless crest width is not present in this formula.

$$\frac{S^*}{N^{0.3}} = 0.048 \cdot (\theta_{hc\ 1\%})^{1.6} \cdot m_0^{-0.6} \tag{2.35}$$

$$\theta_{hc\ 1\%} = \frac{(\hat{u}_{hc\ 1\%})^2}{g\Delta D_{n50}} \tag{2.36}$$

In this formula $\theta_{hc\ 1\%}$ and S^* are new parameters. $\theta_{hc\ 1\%}$ is calculated with the peak period T_p and the wave height which is exceeded by 1% of the waves, $H_{1\%}$. The formulas to calculate these values are shown in Equation 2.37, 2.38 and 2.39 [WL|Hydraulics, 1985 cf. Van den Bos, 2006]. The peak period T_p can be calculated by $T_m/0.8$.

$$\hat{u}_{hc\ 1\%} = \frac{\pi H_{1\%}}{T_p} \frac{1}{\sinh(k_c h_c)} \tag{2.37}$$

$$\frac{2\pi}{T_p} = \sqrt{gk_c \tanh(k_c h_c)} \qquad \text{Local dispersion relation} \tag{2.38}$$

$$H_{1\%} = H_s \frac{\sqrt{\frac{1}{2}\ln(100)}}{\sqrt[3]{1 + \frac{H_s}{h}}} = H_s \frac{1.52}{\sqrt[3]{1 + \frac{H_s}{h}}} \tag{2.39}$$

S^* is the dimensionless erosion area per unit of crest width. The formula to calculate the erosion area A_e from S^* can be seen in Equation 2.40. Note that Van den Bos implicitly incorporated the dimensionless crest width in S^* here.

$$S^* = \frac{A_e}{B_c D_{n50}} \tag{2.40}$$

Van den Bos states that S^* can be seen as the number of stones removed as a layer from the crest of the structure. S^* can be calculated from S by Equation 2.41.

$$S^* = S \cdot \frac{D_{n50}}{B_c} \tag{2.41}$$

A qualitative damage assessment for pipeline covers was also made by Van den Bos. No damage corresponds to $S^* < 1$ and severe damage to $S^* > 4.2$. The boundary between initial damage and intermediate damage lies at $S^* = 2.5$. In Table 2.6 the qualitative damage assessment is shown.

Dimensionless erosion area per unit width	Damage assessment
$S^* < 1$	No damage or rounding off of corners
$1 < S^* < 2.5$	Initial damage
$2.5 < S^* < 4.5$	Intermediate damage
$S^* > 4.5$	Severe damage

Table 2.6: Qualitative damage assessment for pipeline covers. Taken from Van den Bos [2006].

Tørum et al.
Kuester [2007] did additional scale model tests at the Norwegian Hydrotechnical Laboratory at the SINTEF research campus in Trondheim. Kuester used a JONSWAP spectrum and did tests with and without a current. The point of these tests was to investigate the influence of fairly

deep water and low velocity parameters because in the tests done in the past a large amount of scatter was still present. The analysis of this tests were done by Tørum et al. [2008] who included data of Lomónaco [1994] and Van Gent and Wallast [2001]. Interesting conclusions were that Tørum notices a significant difference in tests done with different slopes. He advises that the analysis method should be revised for this. An interesting observation was that damage occurred only when a current was present, except for one test. The damage that occurred only in one test might be because the very low velocity parameters used in these tests. Although other researchers did observe damage with these velocity parameters. Tørum also finds that just outside the range Wallast and Van Gent described a current could be neglected, a large amount of damage was caused by a current. Tørum does not make any conclusions about this. He recommends a maximum 'acceptable damage' for near-bed structures could be set at $S = 50$ for stone sizes from $D_{n50} < 0.05 - 0.10$ m. For larger stone sizes S should be set lower based on the circumstances. An important conclusion that Tørum draws is that for near-bed structures with (1) slopes steeper then 1:2–1:3, (2) small damage values and (3) a velocity parameter in the range 1.0–1.5, a slightly different formula should be used than the formulation provided by Wallast and Van Gent. This formulation can be seen in Equation 2.42.

$$\frac{S}{\sqrt{N}} = 3\theta \qquad \text{for } \theta < 1.5$$

$$\theta = \frac{\hat{u}^2}{g\Delta D_{n50}}$$

(2.42)

In this formulation $\hat{u}$ is calculated in the same way as Lomónaco and Wallast and Van Gent. The test ranges from the scale model tests Kuester did are shown in Table 2.7.

Parameter [unit]	Symbol	Range		
Stone diameter [mm]	D_{n50}	1.9	–	3.3
Crest width [m]	B_c	0.075	–	0.075
Front side slope [-]	m_0	2	–	3
Relative buoyant density [-]	Δ	1.80	–	1.80
Number of waves [-]	N	476	–	3569
Fictitious wave steepness [-]	s_m	0.031	–	0.053
Velocity parameter [-]	$\hat{u}^2/(g\Delta D_{n50})$	0.06	–	0.8
Ratio wave height water depth [-]	H_s/h	0.14	–	0.21
Ratio wave height depth at crest [-]	H_s/h_c	0.15	–	0.23
Ratio depth at crest depth [-]	h_c/h	0.90	–	0.90
Stability parameter [-]	$H_s/(\Delta D_{n50})$	12	–	31

Table 2.7: Physical scale model test ranges of Kuester.

Tørum et al. [2011] is a paper based on this work. Remarkable is that Tørum mentions his new formula is valid for a velocity parameter smaller than 2 rather than between $1.0 - 1.5$. Other than this, they come to the same conclusions in this paper.

2.3.2 Multiple storms

No design methods are available for near-bed structures to assess the damage during multiple storms. Presently a method is applied comparable to the design of breakwaters [Van der Meer, 1999]. In this method a certain amount of damage is calculated with one of the storms present in the lifetime of the structure. For the next storm the number of waves are calculated for the first storm, with the hydraulic conditions of the new storm, to get the same amount of damage as the previous storm. The calculated number of waves is then added to the waves which are

already present in the second storm. This process is visualised in Figure 2.6. This almost always means the range of $1000 - 3000$ waves for the design range from Wallast and Van Gent which is recommended by the Rock Manual is exceeded. It is therefore of great importance to know what the damage is with multiple storms on a near-bed structure. As stated before, this method has been developed for breakwaters and it is not known if this is also valid for near-bed structures. In a formula form the new number of waves for storm two can be calculated from Equation 2.43 where the damage development equation from Van Gent and Wallast is used.
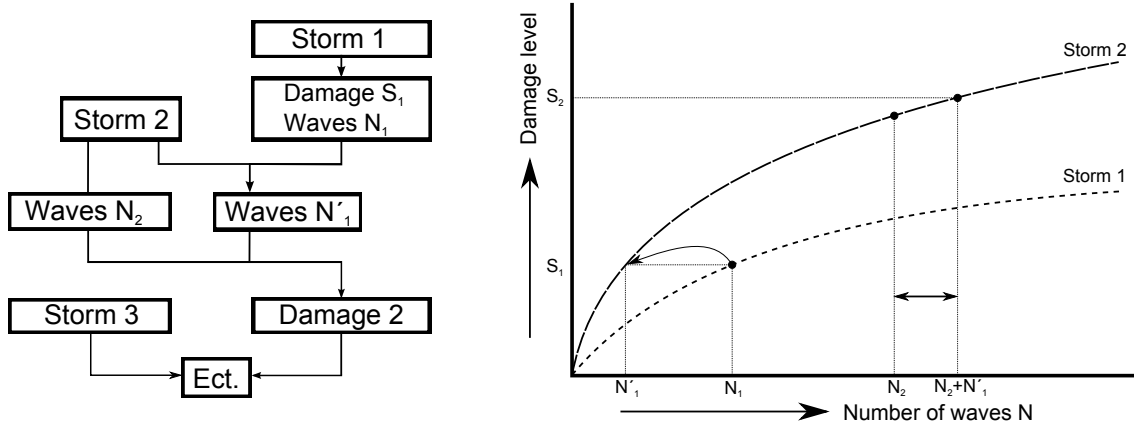
Figure 2.6: Process of incorporating multiple storms

$$N_{tot} = \left(\frac{S_{i-1}}{0.2 \cdot \theta_i^3} \right)^{\frac{1}{0.5}} + N_i \tag{2.43}$$

Another method by Melby and Kobayashi [1998] cf. Suh et al. [2013] is available for designing cumulative damage. However, this method is not applicable to calculate the cumulative damage to near-bed structures because the damage formula for calculating damage with breakwaters is rewritten in this formula which is only applicable for breakwaters.

In this thesis the word multiple storms is used to describe several storms with separate significant wave heights and periods. In reality a storm can be described by several values of the significant wave height because the highest waves present in a storm are only there for a limited amount of time. In other words, there is a distribution of the wave height already present in a storm. From Figure 2.7 the time dependency of the significant wave height is shown. In this thesis this time dependency is not investigated but might also be used together with the method to determine damage during multiple storms.
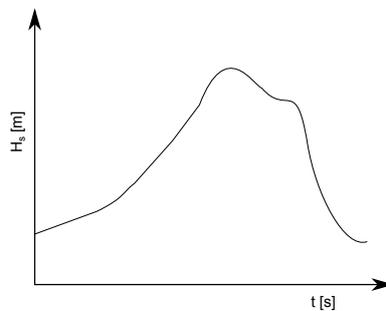
Figure 2.7: Time dependency of H_s in a storm.

2.4   Predicting deformation of near-bed structures

A relatively small amount of research has been done on damage development in near-bed structures compared to bottom protections or breakwaters. In Paragraph 2.3 all the present research has been explained. All these formulas have a damage parameter S [Broderick, 1983] or S^* to calculate the damage. These parameters are defined as Equation 2.18 and 2.40 .

$$S = \frac{A_e}{D_{n50}^2} \tag{2.18}$$

$$S^* = \frac{A_e}{B_c D_{n50}} \tag{2.40}$$

There are several methods available to calculate the new height of the near-bed structure after damage. Van den Bos [2006] investigated which method works the best and concludes that the 'sliced' and 'combination' profile respectively over predicts and under predicts the height reduction of the near-bed structure. His advise is to use an average between these two, which is adopted in this thesis. In Figure 2.8 the sliced and combination profile are shown.
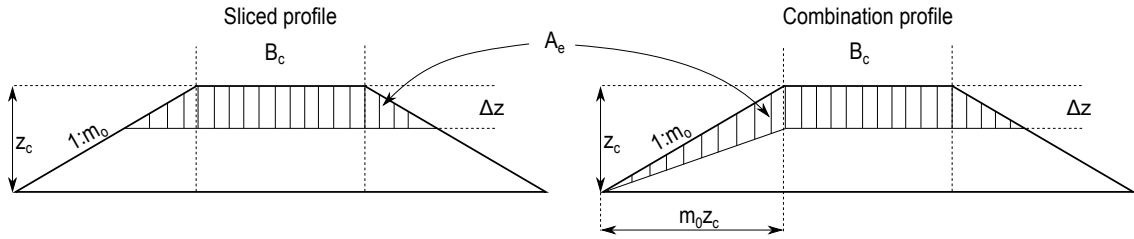
Figure 2.8: Damage profiles

The left schematisation in Figure 2.8 is the sliced profile and is a very simple profile. In this profile it is assumed that there is a constant thickness Δz removed from the crest of the near-bed structure. The erosion area (hatched area) can be calculated as the surface of a trapezoid using Equation 2.44.

$$A_e = \Delta z (B_c + m_o \Delta z) \tag{2.44}$$

The erosion height Δz can be calculated from this using Equation 2.45.

$$\Delta z = \frac{-B_c + \sqrt{B_c^2 + 4m_0 A_e}}{2m_o} \tag{2.45}$$

The right schematisation in Figure 2.8 is the combination profile. Because the sliced profile only takes an erosion from the top of the structure it is easy to imagine that this is not the case in reality. In this profile it is assumed that the transition point between the slope and the crest is exactly below the original transition point. Because not much damage in other tests occurred at the downstream point no damage is taken into account here. The total damage area can be calculated using Equation 2.46.

$$A_e = \Delta z B_c + \frac{1}{2}(\Delta z)^2 m_0 + \frac{1}{2} z_c m_0 \Delta z \tag{2.46}$$

The erosion height Δz can be calculated from this using Equation 2.47.

$$\Delta z = \frac{-(B_c + z_c m_0/2) + \sqrt{(B_c + z_c m_0/2)^2 + 2m_0 A_e}}{m_0} \tag{2.47}$$

As stated before, the height reduction Δz is the average between the sliced and combination profile.

2.5 Scaling laws

Physical scale model testing is the process of doing research at a simplified and smaller scale than reality, which is referred to as the prototype. Normally scale model tests are used because they are cheaper and easier to execute than tests in reality. There needs to be a degree of similarity between the processes in the scale model and the processes that take place in the prototype. Several physical properties must be scaled correctly so that the test results can be applied on real case situations. Often this is done with dimensionless numbers. These dimensionless numbers must be the same in the scale model tests as in the prototype in order to produce valid results. The two most used scaling laws are those of Froude and Reynolds scaling.

The Froude relationships describes the relation between inertial and gravitational forces in a fluid. This relationship can be seen in Equation 2.48 [Van Schijndel et al., 2011]. In this equation the indices m stands for model and p for prototype.

$$Fr_m = Fr_p = \frac{u}{\sqrt{gh}} \tag{2.48}$$

From this the length -, time - , velocity - and force scale can be determined. For Froude scaling the scaling factors are represented respectively in Equation 2.49. In this λ is the scale factor. In these scale factors the density differences have been included.

$$
\begin{aligned}
\frac{L_p}{L_m} &= \lambda \\
\frac{t_p}{t_m} &= \sqrt{\lambda} \\
\frac{U_p}{U_m} &= \sqrt{\lambda} \\
\frac{F_p}{F_m} &= \lambda^3 \cdot \frac{\rho_p}{\rho_m}
\end{aligned} \tag{2.49}
$$

The second scaling law is the ratio of inertial forces and viscous forces which must be correctly scaled. This scaling is called Reynolds scaling and is represented by Equation 2.50.

$$Re = \frac{uL}{\nu} \tag{2.50}$$

It is however not possible to get the same Reynolds number in both the prototype and the scale model. Therefore the transition of turbulent to laminar flow is the starting point for Reynolds related scale effects. Because of this the Reynolds number need to be large enough (say $Re_w >$ 10.000).

In the scale model tests done in this thesis Froude scaling is used. The dimensionless parameters in the formula of Van den Bos are recalculated at the scale which is going to be present in the scale model tests. This is called dimensionless scaling, but is actually the same as Froude scaling.

Froude scaling is considered to be the best scaling method for physical scale model tests which include waves. This is because it represents the relation between the inertial and gravitational forces of a fluid which needs to be scaled correctly when using waves [Van Schijndel et al., 2011]. The damage prediction research described in this chapter have all made use of physical model testing with the Froude scaling method.

2.6   Syntheses

In this section uncertainties are described which are found in the literature study of this chapter. Each important subject is summarized, including the unknown aspects and the differences between several researchers. Besides this, a real case example calculation is done for the damage development formulas in this paragraph.

There are several stability parameters described in this chapter (some are described in Appendix B but for completeness are still included here) which are used to describe the damage development of a near-bed structure. Below a list of the available parameters is shown which have been used in order to get a damage development formula for near-bed structures:

Mobility parameter The mobility parameter in this thesis is also called the shields parameter and is based on the shear stress around a stone.

Stability parameter The stability parameter in this thesis is a Morison-type stability parameter. This stability parameter is a parameter based on the velocities and accelerations around a stone.

Stability number The stability number in this thesis is a Hudson type stability parameter.

Velocity parameter The velocity parameter in this thesis is a stability parameter based on the near-bed velocity.

Research done so far has concluded that the velocity parameter is the best parameter to describe the damage to a near-bed structure. However, there seems to be no consensus on the parameters that should be included in the design formula of a near-bed structure. The way to include the number of waves is different in each formula proposed by researchers. Besides this, some researches impose the side slope as an acting parameter while others do not. Also the way how the velocity parameter should be included in the formulation is different. The next paragraph deals with each difference separately.

Velocity parameter
The velocity parameter is a stability parameter based on the velocity near the bed. The velocity in this parameter is the velocity on the bottom calculated using linear wave theory. The velocity parameter is shown in Equation 2.51.

$$\theta = \frac{\hat{u}_0}{g\Delta D_{n50}} \qquad (2.51)$$

Most of the research done in the past concludes that the velocity parameter is the best to describe damage to a near-bed structure. Actually the velocity parameter could be seen as a Morison stability parameter without the accelerations (Equation B.14 is the original Morison stability parameter). There are several velocities for near-bed structures which can be used in the velocity parameter. Figure 2.9 gives different velocities that can be calculated using linear wave theory. Vidal et al. [1998] used the undisturbed velocity on the crest height of the near-bed structure $\hat{u}_c$. All other researchers use the velocity on top of the structure $\hat{u}_{hc}$ as if the water depth is everywhere equal to h_c. Vidal et al. [2007] uses a numerical model to calculate the governing velocity on top

of the near-bed structure. Because it is unclear which velocity to use and if this is actually the right velocity at all, more research is necessary. Van Gent and Wallast [2001] concluded that in some cases the added currents could be neglected. However it must be stated that these tests were done with wave dominated situations. Tørum et al. [2008] found that only damage occurred with the added currents. However, here can be concluded that Tørum tested with very low velocity parameters which would give very low damages.
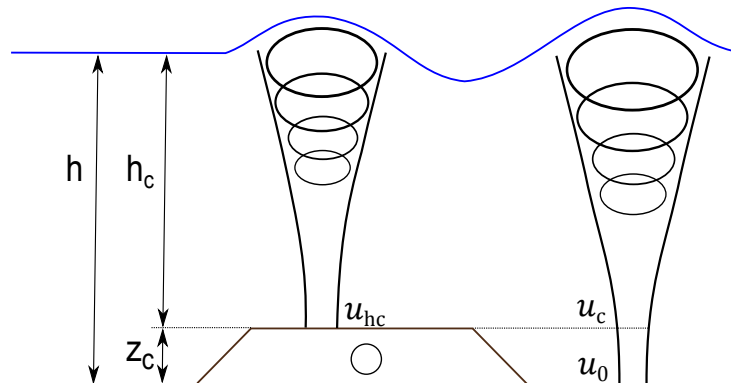

Figure 2.9: Definitions of wave orbital velocities

Time

In many reports it was observed that the damage reduced and even stopped after time. They reported this as armouring against waves and means that after some time the reshaped structure has larger resistance against the wave load. However, this has not been tested to a large extend and is only a prediction. Time is now indirectly incorporated in most formulas by the number of waves N. When some damage is allowed in time, it is not known what approximately the damage in time is under given conditions. Does a structure armour itself in time or does the damage development remain constant over time?

Van der Meer [1988] was the first researcher to couple the number of waves to the damage parameter S for the research he did on breakwaters. Klomp and Lomónaco [1995] were the first researchers who included the number of waves in their damage formulation to calculate damage to near-bed structures. Equation 2.19 and 2.20 give the time dependency for their formulation. It can be seen that if S'_{1000} is large, the parameter b becomes 0.5 which means the root of the number of waves is taken. Wallast and Van Gent [2002] force their dependency on $S/\sqrt{N}$ based on analysis by Van der Meer [1988]. Saers [2005] changes this dependency to a $S/\log(N)$ function. He concluded that this formula could better predict the erosion to near-bed structures than the root function. Van den Bos [2006] again changes the dependency on the number of waves. Van den Bos changes the relationship into $S/N^{0.3}$. This is just between the $\log(N)$ and the $\sqrt{N}$ function. Later research by Tørum et al. [2008] does not change the relationship forced by Wallast and Van Gent. All these formulations dampen out looking at the number of waves. The question remains: how should the number of waves be represented in damage development formulations? Will the damage really dampen out after a large number of waves?

To show the influence of the number of waves the dependency from Wallast and Van Gent, Saers and Van den Bos are plotted in Figure 2.10. Note that this is a very large extrapolation and tests have only been conducted up to the blue line which is why all lines cross exactly this point. The influence for more waves than this number is made clear with this. The relation from Wallast and Van Gent goes much faster than the relation from Saers and Van den Bos. However, Van der Meer concluded that the dependency on $\sqrt{N}$ was only valid up to 10,000 waves for breakwaters. The actual relation is investigated in the remainder of this thesis.
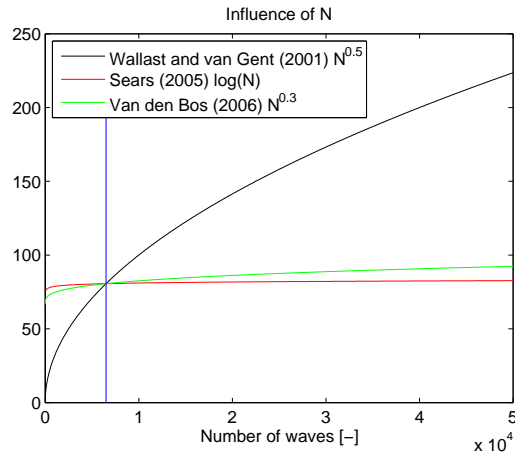
Figure 2.10: Extrapolation of the number of waves in the way they are incorporated in several formulas. The blue line indicates the maximum number of waves tested until now by Saers [2005]. Other researchers have used no more than 3000 waves.

The results from Figure 2.10 give a clear influence how the number of waves N is included in every design formula. However, all the formulas are different and not only differ on the number of waves. To closely investigate this, a comparison must be done on what the predicted damage of these formulas is for a real case situation. For a real situation similar results can be found which indicates the scatter is largely influenced by the number of waves for which the formulations are designed. The result can be seen in Figure 2.11. This Figure includes relations from the most important research done in the past. The top plot is a large extrapolation of the number of waves which is far outside of the ranges for which the formulations are tested and designed for.
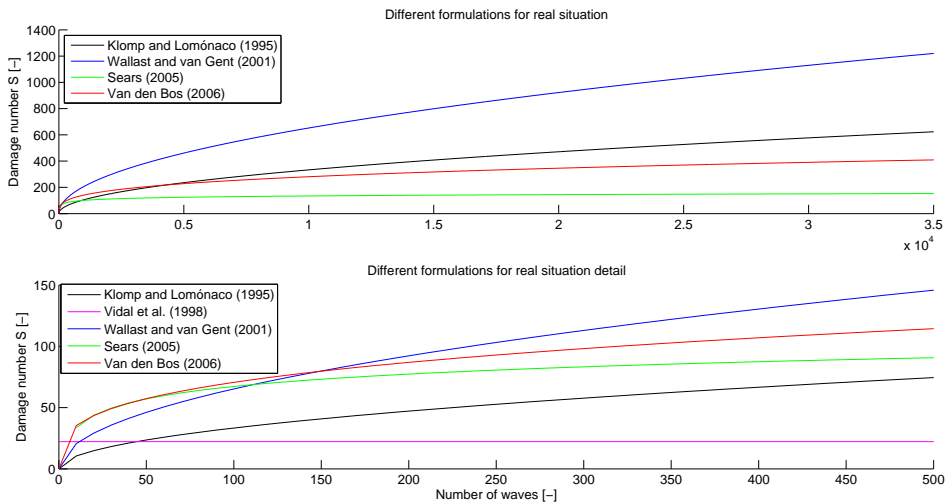
Figure 2.11: Damage number for different formulations in real situation with a $\theta = 3.19$. $H_s = 9$ m, $T_m = 11.3$ s, $h = 20$ m, $z_c = 2$ m and $D_{n50} = 0.15$ m. The top figure is an extrapolation of the number of waves and the bottom figure is zoomed in for the first 500 waves.

Because Tørum et al. [2011] advised that for a low mobility parameters another formula should be used. Figure 2.12 shows a real situation with a low velocity parameter. If only the wave height changes a lower velocity parameter can be obtained. Note the difference between most formulations and Van den Bos and Tørum. Here it must be stated that the formula of Tørum is

only valid for low damage parameters but still the difference with the other formulations is quite large and it is questionable if this is correct.
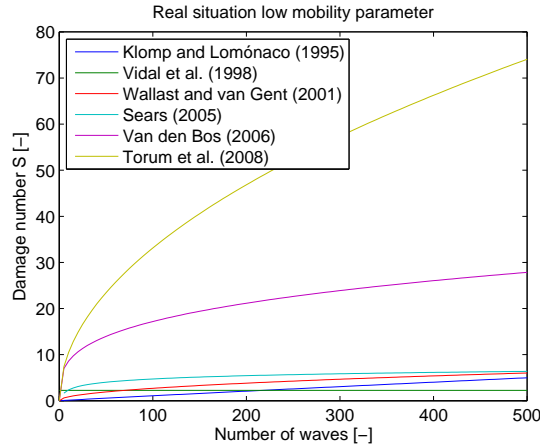
Figure 2.12: Damage number for different formulations in real situation with a low velocity parameter with a $\theta = 1.10$. $H_s = 6$ m, $T_m = 9.2$ s, $h = 20$ m, $z_c = 2$ m and $D_{n50} = 0.15$ m.

Another aspect that has not been investigated for near-bed structures is the way to incorporate several storms. In a prototype situation always several storms pass over a near-bed structure in its lifetime. Currently a method is used from Van der Meer [1999]. This method was developed for breakwaters and might therefore not be applicable for near-bed structures.

Structure parameters
The slope of the structure is not incorporated in most formulas. Van den Bos [2006] is the only researcher that included the slope of the structure. Saers [2005] and Tørum et al. [2008] only mention it is important but do not change their design formulations to coop with the slope of the near-bed structure.

2.6.1 Aspects of research

To investigate all questions that have been drawn out of this synthesis physical scale model testing is necessary. In this physical scale model testing the focus lays on understanding how the damage develops during many waves, and how a near-bed structure behaves in multiple storms. In Chapter 3 the complete scale model is described, which parameters are important and how all variables are measured. In Chapter 4 the test results from the physical scale model tests are described and observations are made.

The most important aspect of this research is the actual relation between damage and number of waves. To correctly test this a near-bed structure is rebuild on scale. In this research the slope, height and width of the near-bed structure are of importance. Because in reality almost only near-bed structures are built with slopes of 1:3, this aspect is not treated in present research but only 1:3 slopes are investigated. The width and height change to find a relation between damage and number of waves which might change with different structure boundary conditions. In the physical scale model tests all these parameters should change in a subsequent test to show their particular influence. The wave height and water depth should change in a particular test as well. From the literature it is known that if these parameters change the velocity calculated by linear wave theory changes as well. By changing these parameters it can be investigated if the damage changes accordingly to this velocity. All these relative changes should be tested in a test with a large number of waves present to find the relation between damage and time.

The second important aspect that is investigated during the physical scale model tests is how a near-bed structure behaves in multiple wave conditions or multiple storms. From the literature study it is known that currently nothing is known about the behaviour of near-bed structures in multiple storm conditions and therefore this aspect is researched in this thesis. This and the part with a large number of waves are the main focus of the physical scale model testing described in Chapter 3. A choice has been made to test within the range tested by other researchers.

There are several important dimensional and non-dimensional parameters which are chosen to be in the same range as the parameters tested in the past. All the parameters from previous research are listed in Table 2.8 and below the dimensionless parameters are explained that were not described in this chapter so far.

- Wave steepness s_m and ratio between wave height and water depth H_s/h.

  The ratio between wave height and water depth defines if waves are breaking. Waves start to break when this factor is larger than 0.5. The wave steepness defined as Equation 2.7 must be in the same order of magnitude of 4.5% for all of the experiments. If the wave steepness is different for each test it is harder to make comparisons.

- Ratio between structure height and water depth z_c/h, stone diameter z_c/D_{n50}.

  The structure height over water depth can determine if there is similar flow around the near-bed structures. When this parameter is significantly high the flow can be considered horizontally orientated. This means the ratio h_c/h must be as large as possible within the dimensions of the wave flume. The structure height over the stone diameter eventually says how many stones are placed on top of each other in the structure profile.

- Ratio between structure width and wavelength B_c/L, stone diameter B_c/D_{n50}.

  The ratio between structure width and wavelength must be significantly low to make sure the structure can be treated as a near-bed structure. If this ratio becomes larger, it can not be seen as a near-bed structure any more but as a weir or a bottom protection. The flow over these kind of structures is not comparable with the flow over near-bed structures and is not treated. The ratio between structure width and stone diameter can be seen as the number of stones covering the crest of the near-bed structure.

	Parameter	Symbol	Range		
Dimensional parameters	Stone diameter [mm]	D_{n50}	1.90	-	8.33
	Stone shape [-]	–	Round	angular	irregular
	Stone density [kg/m]	ρ_s	2463	-	2800
	Relative density [-]	Δ	1.46	-	1.80
	Wave height [m]	H_s	0.07	-	0.29
	Wave period [s]	T_m	0.85	-	2.10
	Water depth [m]	h	0.375	-	0.900
	Structure crest width [m]	B_c	0.04	-	0.25
	Structure slope [-]	$1:m_0$	1	-	8
	Structure height [m]	z_c	0.03	-	0.26
Non-dimensional parameters	Velocity parameter	θ	0.16	-	3.61
	Wave height	H_s/h	0.14	-	0.50
	Wave steepness	s_m	0.028	-	0.071
	Number of waves	N	900	-	6500
	Relative structure height	h_c/h	0.63	-	0.97
	Relative structure height 2	z_c/D_{n50}	8.17	-	40.33
	Relative structure width	B_c/L	0.087	-	0.12
	Relative structure width 2	B_c/D_{n50}	10.81	-	48.75

Table 2.8: Current test ranges of Lomónaco, Wallast and van Gent, Saers and Tørum. Adapted from Van den Bos [2006].

Part II

Physical Scale Model Tests

Chapter 3

Introduction and test scheme

This chapter deals with the set-up of the physical scale model tests that are executed as part of this thesis. The test facilities are introduced, the parameters that are important are explained and which instruments are used for measuring are presented.

3.1 Model tests set-up

The physical scale model tests are performed in the long wave flume of the Fluid Mechanics Laboratory of the TU Delft. The flume is 42 m long, 0.8 m wide and 1 m high. At the beginning of the wave flume an electro mechanically piston type wave generator is installed with a maximum stroke length of 2 m. A schematic overview of the wave flume is presented in Figure 3.1. In this figure the wave paddle, wave gauges, near-bed structure and a rock slope at the end of the wave flume for wave dissipation are shown. The wave flume is divided in two sections separated by a thin board. In this way it is possible to test two near-bed structures at the same time. Because the board is very thin and spans several wavelengths before and after the near-bed structure, the influence on the test results are expected to be negligible. A photo of the wave flume, wave dissipation slope, wave generator and the separation board is shown in Figures 3.2 until 3.5. In the middle of Figure 3.5 the separation board can be seen which cuts the flume in half. The exact coordinates of all wave gauges can be seen in Appendix C.
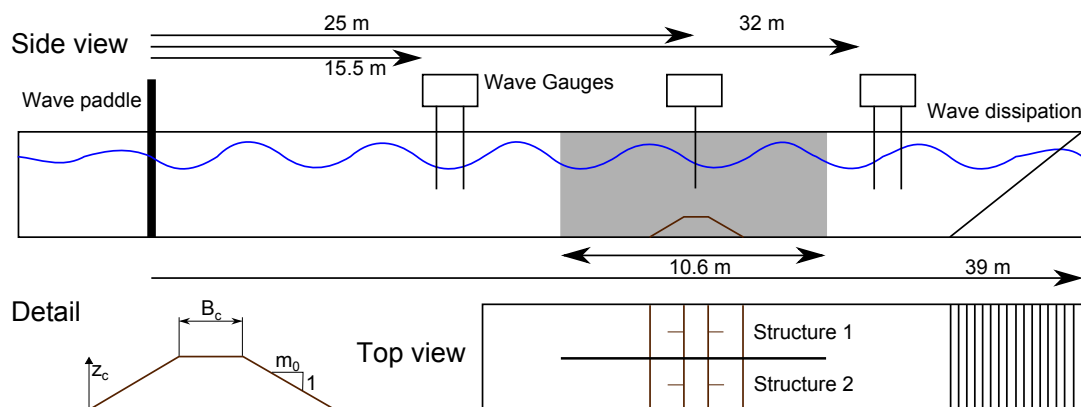
Figure 3.1: Side and top view of the wave flume and an detailed view of the near-bed structure. The grey field represents the screen that cuts the wave flume in half.

Figure 3.2: Photo of rock slope which is used for wave dissipation at the end of the flume.

Figure 3.3: Wave flume located in the water laboratory of the TU Delft. In the middle the separation board can be seen.

Figure 3.4: The piston type wave generator at the start of the flume which generates the waves in these experiments by moving back and forth.

Figure 3.5: Overview of the near-bed structures. At both sides of the flume a different near-bed structure can be seen with the separation board in between.

3.2 Scale model testing

In this paragraph the parameters that change in a test are described and the total test program is explained which is used in this thesis. Subsequently the test procedure is explained which is used during physical scale model testing.

3.2.1 Parameters

Several parameters in the physical scale model test are considered very important to change in a consecutive tests which was concluded in Chapter 2. In Table 3.1 the most important parameters for this modelling are shown and whether they change in a particular test. Only the parameters that were concluded in Chapter 2 to be of importance differ in the physical scale model tests. Because of this, the (1) crest width, (2) crest height, (3) water depth and (4) wave height change in a tests to show their particular influence. The waves are generated by the wave paddle which creates a JONSWAP spectrum with a large number of waves. No wave angles are included because this research is conducted as a two dimensional process.

Parameter	Symbol	Unit	Changes
Structure			
Crest width	B_c	[m]	Yes
Crest height	z_c	[m]	Yes
Slope	$1 : m_0$	[-]	
Environmental properties			
Wave height	H	[m]	Yes
Wave period	T	[s]	Yes
Water depth	h	[m]	Yes
Water density	ρ_w	[kg/m^3]	
Number of waves	N	[-]	Yes
Material properties			
Nominal stone diameter	D_{n50}	[m]	Yes
Gradation	(W_{85}/W_{15})	[-]	Yes
Stone density	ρ_s	[kg/m^3]	Yes

Table 3.1: Parameters involved in the model tests

In the steering file which controls the wave generator a H_{m0} and T_p have to be entered where the wave computer creates a JONSWAP spectrum with. Because the highest waves in the spectrum are breaking just behind the wave paddle, the actual load on the near-bed structure is lower than this H_{m0} entered in the computer. Wave gauges have been installed in the wave flume to determine the exact wave forces on the near-bed structure which can be used to calculate the significant wave height H_s on the near-bed structure. No wave heights higher than H_{m0} of 0.20 m are possible with 0.50 m water depth because of limitations of the wave generator.

3.2.2 Test scheme

This research focusses on two important subjects and correspondingly two parts are present in the physical scale model testing. The two parts of this scale model testing are shown below:

- Large number of waves.

- Multiple consecutive wave conditions to represent multiple storm events.

For the first part the test scheme is shown in Table 3.2. These tests are performed for two stone types (A and B). To check the results from the physical scale model testing two tests have been repeated which is denoted with a 'v2' behind the name of the test. Besides this, in two tests so much stone movement occurred that halfway of a test, one of the structures has been rebuild. This is denoted by a '2' behind the name of the test.

The first test (1A and 1B) is a reference test and in subsequent tests only one parameter changes. The water depth for the first part with a large number of waves is in the order of 0.45 m, the structure height is in the order of 8 to 12.5 cm and the structure width in the order of 15 to 30 cm. For all these tests it has been checked if the dimensionless parameters are in between the parameters tested in the past (Table 2.8). For the following parameters this is not the case:

- The number of waves N. This research focusses on the number of waves and is taken much higher than other researchers have used. 30,000 Waves are used in this thesis which represents approximately 10 storms and is 5 times more than has been done in previous research. For test 2v2 only 17,000 waves are used because of time limitations.

- The crest width B_c. The width is made larger than previously tested to show the particular influence with a large change in width compared to the initial condition.

- Nominal stone diameter D_{n50}. Two types of stones are used in this thesis for test 1-5. One type of stones turned out to be smaller than expected. In Chapter 4 it is determined if this smaller stone type is applicable and can be compared to real near-bed structures.

The parameters from Table 3.2 are determined mostly by the limitations of the wave flume. On forehand calculations have been performed with the damage development equation from Van den Bos [2006] to approximately determine the damage. In this way it was checked if damage would develop and how high the hydrodynamic conditions should be. In this way, and with dimensionless scaling described in Chapter 2, the test program has been put together.

Test number	D_{n50} [m]	h [m]	z_c [m]	B_c [m]	H_{m0} [m]	T_m [s]	m_0 [-]	N_{tot} [-]
1A	0.0015	0.45	0.080	0.15	0.160	1.51	3	10,000
1A2	0.0015	0.45	0.080	0.15	0.160	1.51	3	20,000
1B	0.0034	0.45	0.080	0.15	0.160	1.51	3	30,000
1Av2	0.0015	0.45	0.080	0.15	0.160	1.51	3	30,000
1Bv2	0.0034	0.45	0.080	0.15	0.160	1.51	3	30,000
2A	0.0015	0.40	0.080	0.15	0.160	1.51	3	30,000
2B	0.0034	0.40	0.080	0.15	0.160	1.51	3	30,000
2Av2	0.0015	0.40	0.08	0.15	0.160	1.51	3	17,000
2Bv2	0.0034	0.40	0.08	0.15	0.160	1.51	3	17,000
3A	0.0015	0.45	0.080	0.15	0.190	1.64	3	15,000
3A2	0.0034	0.45	0.080	0.15	0.190	1.64	3	15,000
3B	0.0034	0.45	0.080	0.15	0.190	1.64	3	30,000
4A	0.0015	0.45	0.100	0.15	0.160	1.51	3	30,000
4B	0.0034	0.45	0.125	0.15	0.160	1.51	3	30,000
5A	0.0015	0.45	0.080	0.30	0.160	1.51	3	30,000
5B	0.0034	0.45	0.080	0.30	0.160	1.51	3	30,000

Table 3.2: Test scheme for tests 1-5.

In the second part of the testing, three tests are performed for testing the stability of the near-bed structure in multiple wave events. For these tests only one stone type is used. The test scheme for this part of the tests can be seen in Table 3.3. Because of a breakdown of the wave generator test 7 has been repeated which is denoted by a 'v2'.

In this part of the tests different wave conditions are used where the wave height and number of waves change. The structure parameters remain the same as in test 1. In tests 6 there are 6,000 waves present in each wave series and the wave height increases from 10 to 20 cm with steps of 2 and 1 cm. In this way the influence of higher wave conditions after each other can be made visible and consequently a different storm. In test 7 and 7v2 wave heights are tested of 10, 15, 17.5 and 20 cm with accordingly a number of waves. These waves heights are randomly after each other so it can be seen if for instance a smaller storm still develops damage after a big storm. The number of waves in this test varies per wave height from 3,000 to 6,000. A small wave condition has 6,000 waves where a heavy wave condition has 3,000 waves. The wave period changes accordingly with the wave height to keep a constant steepness of 4.5%.

Test #	D_{n50} [m]	h [m]	z_c [m]	B_c [m]	H_{m0} [m]	m_0 [-]	N_{tot} [-]
6B	0.0034	0.5	0.080	0.15	0,10 - 0,12 -0,14 - 0,16 - 0,18 - 0,19 - 0,20	3	42,000
7B	0.0034	0.5	0.080	0.15	0,10 - 0,15 - 0,175 - 0,20	3	19,000
7Bv2	0.0034	0.5	0.080	0.15	0,10 - 0,15 - 0,175 - 0,20 - 0,15 - 0,175 - 0,15 - 0,20	3	36,000

Table 3.3: Test scheme for tests 6-7.

3.2.3 Granular material

Two types of stones are used for the physical scale model testing where one type of stone is put on each side of the wave flume separated by a thin board. The characteristic values of the stones are very important because these determine for a great part the response of the near-bed structure to the waves inside the physical scale model. The stones used for these tests are very small stones which are scaled approximately 55 and 100 times compared with reality. Normal rubble mound rock in a near-bed structure has a density between 2600 and 2700 kg/m^3 and is kept the same in these tests. The two types of stones that are used are Yellow Sun and Ardenner split. These stones are comparable in shape and have approximately the same density compared with reality which can be seen in Table 3.4. The calculation method of the density and some photos of the stones can be seen in Appendix D. In Table 3.4 and Figure 3.6 the non-exceeded weight percentages of the diameter are shown. These percentages have been calculated by weighing the stones individually. The Yellow Sun has also been sieved because this type was small enough to fit through the sieves. A first observation is that stone type A is not in the range of parameters tested by previous researchers. Because of this the applicability of this stone type is further examined in Chapter 4.

The weighing of the stones was done very accurately by a measuring device which could measure weights accurate until 10^{-5} g.

Non-exceeded percentages	Program	5%	15%	50%	90%	98%	Density [kg/m^3]
Yellow Sun D [mm]	A	0.99	1.16	1.50	2.06	2.50	2679
Yellow Sun D_n [mm]	A	0.99	1.09	1.50	2.13	2.39	2679
Ardenner split D_n [mm]	B	2.09	2.41	3.39	4.54	4.65	2691

Table 3.4: Granular material properties with the non-exceeded weight percentages.

A remarkable observation is that the shape factor is not 0.84 as described in Chapter 2 but approximately 1.0 for the Yellow Sun stone type A which can be seen in Equation 2.2. It has recently been observed that for a small type of stones the shape factor would become larger than 0.84, going towards 1.0 [Jansen, 2013]. However, a shape factor of 1.0 has not been observed in this report.

$$\frac{D_n}{D} = \sqrt[3]{s_f} \longrightarrow \frac{D_{50}}{D_{50}} \approx 1 \tag{2.2}$$

Figure 3.6: Non-exceeded curve for the used test materials.

3.2.4   Test procedure

In each test the structure was built up with approximately 20 cm of water in the flume. If the structure would be built in dry conditions, it would be severely damaged by filling the flume with water. Underwater, with a ruler, the near-bed structure is made as good as possible with the theoretical profile drawn on the glass of the flume as a reference. The stones were not compacted and flattened as little as possible to prevent compacting as well. After each test the stones are mixed to prevent influences from compacting and de-mixing. This can means that for example only the larger stones of the stone gradation are on top of the near-bed structure so less damage will occur.

After building up, the structure is measured and the waves can be generated. After 1000, 3000, 5000 and then every 5000 waves the structure profile is measured and the damage to the structure can be determined accordingly. The significant wave height and reflections are calculated afterwards from the time series of the wave gauges.

3.3   Measurements

In this paragraph it is described how several parameters are measured. The methods and devices which have been used for this are explained and the accuracy is given. For each test the following parameters are measured with instruments:

- Water depth.
- The wave signal in time at eight locations.
- Height profiles before, during and after the tests.

The water depth is put on exactly the height specified for that particular test. The water level was read from two tape-measures on the wave flume with an accuracy of approximately 1 mm. Because of the thick glass the operator had to be in a straight line with the water level to correctly read the height and avoid any deviation by the glass.

3.3.1 Wave conditions

There are eight wave gauges installed in the wave flume for this experiment. Three wave gauges are placed in front of the structure, two on top and three wave gauges after the near-bed structure. The placement of the wave gauges is visualised in Figure 3.1. The three wave gauges in front and after the structure have 0.3 and 0.4 m distance between them to calculate the incoming and reflected wave. The wave gauges above the near-bed structure are used to calculate the significant wave height H_s on each side of the separation board to which the near-bed structure is directly exposed. The difference between these two wave heights was as expected very low ($< 1\%$). Because of this in the analysis only the wave height from one wave gauge on top of the near-bed structure has been used.

A wave gauge consists of two parallel electric wires placed in the water. The resistance of the wires is measured by sending a voltage through these wires. From this voltage a height can be calculated which represents the water level. Before doing this the wave gauges are calibrated to find which voltage represents which height of a wave gauge. The eight wave gauges measure the voltage each 0.01 s and send this to a program called DASYLab[1]. With the use of Matlab [Mathworks, 2013] the exported voltages have been transferred to water level variations. In Appendix C the measured values to convert the voltages from a wave gauge to a water level are shown. With the obtained water level variations a time series of each wave gauge can be drawn where several calculations have been performed on. The accuracy of the water level is in the order of 2 mm.

3.3.2 Structure parameters

The shape of the near-bed structure is measured with the use of an echo-sounder. This echo-sounder measures the vertical height within millimetric ($\pm$ 0.001 m) accuracy. The echo-sounder is placed on a small cart which moves horizontally over the near-bed structure. On this cart there is a small wheel which rotates over the track it follows. Attached to this wheel is a pulse generator which generates an electric pulse each 0.5 mm. This pulse is send to the echo-sounder which measures the vertical height at this pulse. In this way a height measurement is obtained each 0.5 mm. It has been checked several times if this 0.5 mm per pulse was accurate, and a small error in the order of 1 mm was found several times for a horizontal direction of several meters. However, this error might be because of the error that the exact location were the cart stopped was slightly wrong. Because of this the x-length for height measurements is very accurate. The place where this height measurement is taken is less accurate. Because the echo-sounder emits a pulse there is a certain footprint on which this pulse reflects. Because of this footprint there is a certain measurement error on the height profile. It is not known how large this measurement error is on forehand, so this is investigated in Chapter 4.

The echo-sounder works with an ultrasonic-impulse-travel time procedure. This means that the echo-sounder emits an acoustic pulse which is reflected by the bottom or the target it is above. The travel time between sending and receiving the pulse can be translated into a distance. The echo sounder is placed just inside the water because the connection was not waterproof. The results from the height measurement are imported in DASYLab and from here the data is saved and exported to Matlab for analysis.

The height of the near-bed structure is measured in five rows per side when the separation board is in the wave flume, and in nine rows without the board present. Each row is 5 cm apart from each other and row number 3 is exactly in the middle of a side and number 5 exactly in the middle without the separation board present. The measuring lines are visualised in Figure 3.7. In this figure also a reference bar can be seen in front of the near-bed structure (vertical grey line). Because this reference bar does move in wave conditions, the measured height profiles can be placed very accurately over each other and can be compared in this way. In this way it is

---

[1]DASYLab, Data Acquisition System Laboratory. `www.dasylab.com`

known where the height measurement actually starts. After a several thousand waves the wave generator is paused and the height profile is measured.
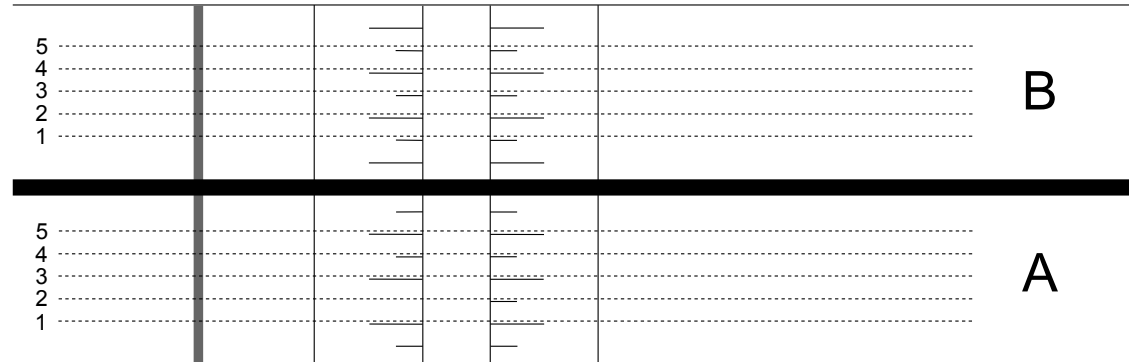
Figure 3.7: Top view of measuring rows for structure A and B. In front of the structure the vertical grey line is the reference bar.

The first few times that measurements were conducted with the echo-sounder unusable profiles were obtained because an extreme amount of scatter was present. It was found that too much vibration of the echo-sounder was one of the problems. By securing the echo-sounder better and removing a part on the moving cart helped to fix the problem. After this, height measurements were quite accurate and only the large footprint of the echo sounder is a limitation.

A big disadvantage of the echo-sounder is that it measures in lines. An optimal procedure would have been to scan the entire structure and get a 3D image of the near-bed structure and the stones that would fall and roll off the near-bed structure. Because lines are used in these tests, a gap or a bump could be missed entirely because it would not fall over a measuring row. By measuring the structure in five or nine rows this error is averaged and is expected to not play a significant role.

3.4 Syntheses

In this chapter the physical scale model testing scheme has been described, how several parameters are measured and how the tests are performed. The test scheme was constructed from parameters that were observed to be important in Chapter 2. In Chapter 4 the test results are shown and observations are described. The measured results are compared against theories found in Chapter 2 and deviations are given. The observations are presented in a clear way so that conclusions can be drawn and these can be linked to the analysis of the main objective in Chapter 5.

Chapter 4

Test results

In this chapter the results and observations of the physical scale model testing are described. First the hydrodynamical conditions are determined which were actually present during the tests. Secondly the structure characteristics such as the height and damage are determined. Finally observations from the physical scale model tests are described, small calculations are performed to visualise the damage to a near-bed structure in time and it is investigated if stone type A is applicable.

4.1   Wave conditions

In this section the wave conditions from the physical scale model tests are described. The wave height, wave period and water depth that were measured during the tests are described and analysed. Secondly the wave reflection that was present in the physical scale model tests is calculated.

With the use of a Matlab script several wave parameters could easily be determined from the physical scale model tests. The time series from DASYLab were imported to Matlab and analysed. From this the wave heights H_s, $H_{1\%}$ and $H_{0.1\%}$ and consequently the wave periods T_m and T_p are calculated. These values were determined by calculating the zero crossing period and the maximum wave height in between these zero crossing periods [Holthuijsen, 2007]. The exceedance graphs for the wave height from every test can be found in Appendix C.

Eight series of waves were performed for test 1-5. First approximately 1000 waves, then 2000, 3000, 5000 and 5000 is repeated until a total number of 30,000 waves is reached. In these wave series the conditions per test were constant, only the duration (number of waves) changed. In Table 4.1 the wave conditions for test 1-5 are shown. These are shown for a complete test (not per wave series) and not per side of the separation board because these are equal. In Table 4.2 the measured hydraulic conditions for test 6 and 7 are shown per wave condition present in these tests. Test 2A and 4A stopped early because to much damage had already occurred and were rebuild halfway which is denoted by the '2'.

An analysis for the differences between the measured and calculated $H_{1\%}$ was performed. The calculated $H_{1\%}$, with the use of Equation 2.39, was on average 3% (with a maximum of 7%) higher than measured. This is a rather good and small deviation. The measured and calculated wave heights can be seen in Appendix C. The measured values of $H_{1\%}$ have not been used for analysis of these experiments because these values are not known for all other researchers. A more recent method is available from Battjes and Groenendijk [2000] to calculate $H_{1\%}$. This method is not

Test	h [m]	H_s [m]	T_p [s]	T_m [s]	s_m	N_{tot} [-]
1	0.45	0.143	1.99	1.59	0.036	30485
1v2	0.45	0.144	2.00	1.60	0.036	30519
2	0.40	0.141	2.03	1.62	0.034	29883
2v2	0.40	0.139	2.01	1.61	0.034	17227
3	0.45	0.166	2.19	1.75	0.035	30707
4	0.45	0.141	1.98	1.58	0.036	31703
5	0.45	0.143	1.99	1.59	0.036	31545

Table 4.1: Measured wave conditions.

Series	1	2	3	4	5	6	7	8
h [m]	0.5	0.5	0.5	0.5	0.5	0.5	0.5	0.5
Test 6								
H_s [m]	0.092	0.094	0.111	0.129	0.147	0.162	0.172	0.180
T_p [s]	1.57	1.56	1.68	1.82	1.97	2.09	2.17	2.27
T_m [s]	1.26	1.25	1.34	1.46	1.58	1.67	1.74	1.81
s_m [-]	0.038	0.038	0.039	0.039	0.038	0.037	0.037	0.035
N [-]	1017	5120	5837	5952	6023	5797	5825	5556
Test 7								
H_s [m]	0.094	0.138	0.161	0.178				
T_p [s]	1.57	1.89	2.08	2.20				
T_m [s]	1.26	1.51	1.66	1.76				
s_m [-]	0.038	0.039	0.037	0.037				
N [-]	6057	7498	2890	2565				
Test 7v2								
H_s [m]	0.094	0.138	0.160	0.180	0.137	0.160	0.137	0.179
T_p [s]	1.56	1.89	2.07	2.27	1.88	2.08	1.89	2.26
T_m [s]	1.25	1.51	1.66	1.82	1.66	1.51	1.81	1.81
N [-]	5730	6162	3044	2973	6020	3051	5978	3001
s_m [-]	0.039	0.039	0.037	0.035	0.039	0.037	0.039	0.035

Table 4.2: Measured hydraulic conditions for test 6 and 7.

used for analysing the results with $H_{1\%}$ in this thesis because larger deviations were found than with Equation 2.39. The calculated wave heights for this method with low probabilities are lower than the measured wave height. The differences can be seen from the red line in Appendix C in Figure C.1 and C.2. This method has been used to calculate $H_{0.1\%}$ which is used in the analysis as well. Here deviations are present with the measured results as well, but no other methods to calculate $H_{0.1\%}$ were available.

$$H_{1\%} = H_s \frac{\sqrt{\frac{1}{2}\ln(100)}}{\sqrt[3]{1 + \frac{H_s}{h}}} = H_s \frac{1.52}{\sqrt[3]{1 + \frac{H_s}{h}}} \tag{2.39}$$

4.1.1   Wave reflection

At the end of the wave flume a rip rap slope is placed to absorb the incoming waves. The rip rap has a size of 85-125 mm and is placed on a 1:5 slope. If the incoming wave is reflected too much, it could influence the test. On forehand the reflection coefficient has been calculated using Equation 4.1. In this equation C_r is the reflection coefficient, ξ is the breaker parameter and a and b are constants from Allsop and Channel [1989] cf. CIRIA [2007]. The breaker parameter is

defined as $\xi = \tan(\alpha)/\sqrt{H_s/L_0}$ where L_0 is the wavelength in deep water. From this equation it was calculated that the reflection would be in the order of 12% with a H_s of 15 cm.

$$C_r = a\xi^b \tag{4.1}$$

Both groups of wave gauges in front and after the structure are able to calculate the wave reflection observed in the scale model tests. A Matlab program called 'Decomp' calculates the incoming and reflected wave signal after a method of Zelt and Skjelbreia [1992] cf. [De Vree, 2013]. It was tried to have the least amount of reflection as possible to not influence the damage occurring to the near-bed structure. The reflection percentages which occurred in the tests can be seen in Table 4.3. In Appendix C the calculated incoming and reflected wave spectra can be seen for each test. From the table with reflection percentages an observation is that the reflection percentages without a near-bed structure present are not equal in front and behind the near-bed structure. This can be explained due to white capping and dissipation of the waves by for example friction. Besides this, it can be seen that there is more difference in reflection with a near-bed structure present in the wave flume. This can be explained by that there is now also reflection because of the near-bed structure itself. This reflection is compensated by the wave generator which has reflection compensation. The reflection behind the structure is the reflection because of the rock slope at the end of the flume. It can be observed that the actual reflection is a little higher (order of 2%) than the on forehand calculated reflection. Because the wave height is measured exactly on the near-bed structure, reflection is also included in this measurement. Therefore the loads on the near-bed structure are known and reflections are expected not to be of influence to the test results and have not been processed in any way in the analysis.

Reflection percentages	Reflection before structure	Reflection behind structure
Without structure Hs = 13 cm	10.6%	8.4%
Without structure Hs = 17 cm	10.4%	15.1%
Test 1	16.9%	12.4%
Test 1v2	16.9%	12.8%
Test 2	20.0%	17.8%
Test 2v2	19.5%	17.7%
Test 3	21.5%	20.5%
Test 4	18.1%	12.8%
Test 5	17.3%	12.7%
Average from tests	18.6%	15.3%

Table 4.3: Reflection percentages of each test.

4.2 Structure characteristics

In this section the structure boundary conditions for the near-bed structure are described. First it is described what the height measurements are and how they have been determined. Secondly it is explained how the damage is calculated and what the results from this calculation are. The last part of this section describes the tests that have been done to measure the accuracy of the echo-sounder.

4.2.1 Height measurements

In Figure 4.1 the five measured rows from test 3B can be seen. The arrow in the near-bed structure indicates the wave direction and the little bump in front of the near bed structure is the reference

bar. The dotted line represents the theoretical profile on the average height of the initial structure and, as can be seen, some damage has already occurred after 5000 waves. In Figure 4.2 the average profiles of the five measured rows are shown after each wave series. Here the blue near-bed structure on the bottom of the figure is a reference near-bed structure where the begin and end of the structure are on the same place as the initial structure. The deviation of the average row compared to each separate measured row is on average 2% with a maximal deviation of 9%. In Appendix E the figures on the left side of the pages give the average measured profiles from each tests.
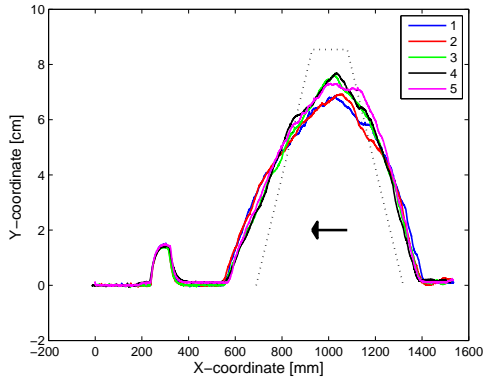
Figure 4.1: Different rows test 3B after 5411 waves.
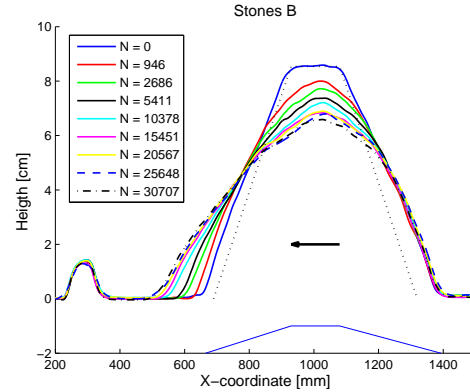
Figure 4.2: Average profiles test 3B.

In Table 4.4 the initial structure height of each test is displayed. This height is the average from the average height of the crest width from each measured structure.

Test number	Initial structure height z_c [cm]
Test 1A	9.19
Test 1A2	9.20
Test 1B	8.22
Test 1Av2	8.38
Test 1Bv2	8.47
Test 2A	8.71
Test 2B	8.82
Test 2Av2	8.73
Test 2Bv2	8.20
Test 3A	8.31
Test 3A2	7.85
Test 3B	8.54
Test 4A	10.55
Test 4B	13.43
Test 5A	8.72
Test 5B	8.90
Test 6B	8.47
Test 7B	8.53

Table 4.4: Initial structure height.

4.2.2 Damage measurements

After each wave series a height measurement was performed on the profile. To calculate the erosion area from this, first it has to be known what the definition of erosion to a structure really is. With this definition the damage can be calculated. Van der Meer [1988] defines the erosion area A_e for breakwaters as the part of the structure that has gone below the initial profile. This definition is used in this thesis as well which is the same way as Saers [2005] and Van Gent and Wallast [2001] define their damage. In Figure 4.3 the definition of damage which is used in this thesis is shown. The hatched part of this near-bed structure is the erosion area A_e. It is checked per row where the profile after a wave series is below the initial profile. This area is then calculated and consequently the damage can be calculated. However, another method which is internationally used for physical scale model testing is to first determine the average row and subsequently calculate the damage. The calculated erosion areas from both methods are shown in Appendix F. Also the differences compared to both methods are shown where a negative value indicates that the method which calculates first the average row is smaller than the other method. A general observation is that if there is a difference present, the method that first calculates the average row is always lower than the other method. Another observation is that in the beginning of a test a large deviation is present which is in the order of 18%. The explanation for both observations are that if the average row is calculated first, the peaks are smoothed out which results in a lower damage. At the end of the tests the differences between subsequent damage profiles are much lower and thus both methods are very comparable and an average difference of 3% is present. In the analysis of this thesis the method that first calculates the average row and subsequently the damage is used for analysis
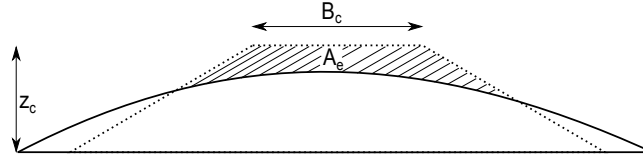
Figure 4.3: Definition of erosion parameter A_e.

In Appendix G, the total data set is included. Here the data is shown for every research done to near-bed structures in the past where for tests done in this thesis the average damage by first calculating the average row are shown. From these measurements the damage parameter S and S^* can be determined with Equation 2.18 and 2.40. In Table 4.5 the ranges from the erosion area and damage parameters are shown for all the tests.

$$S = \frac{A_e}{D_{n50}^2} \tag{2.18}$$

$$S^* = \frac{A_e}{B_c D_{n50}} \tag{2.40}$$

	A_e		S		S^*	
	min	max	min	max	min	max
A	2.57E-03	1.84E-02	1136.8	8125.8	5.7	81.4
B	7.95E-04	1.93E-02	69.1	1682.6	1.2	38.0

Table 4.5: Range of erosion and damage parameters for the scale model tests.

In Appendix F the calculated (based on Equation 2.45 and 2.47 from Chapter 2) and measured structure height have been compared to each other. If the actual near-bed structure is higher than the calculated height, the percentage is negative. It can be seen that the calculated height

with Equation 2.45 and 2.47 overpredicts the height reduction because almost all percentages are negative. Especially for stone size A the calculated height is lower than the actual present height. Note that for the height measurement the average height of the highest point of the rows has been used in present research. This is because the near-bed structure in time tends to converge to a Gaussian shaped profile and no 'average' height can be determined. It can be concluded that the calculated height for the near-bed structure overpredicts the height reduction a little. For stone type A the difference is on average 8% with a maximum of 43%. For this stone type the height reduction is over predicted especially after more then 10,000 waves. For stone type B the height reduction is calculated very reasonable and only a small deviation is present. The calculated height reduction is on average 4% larger than the actual height reduction with a maximum of 20%.

4.2.3   Precision of echo-sounder

The precision of the echo-sounder has been tested where the height turned out to be accurate in the order of 1 mm. However, the x-coordinate where the height is measured is taken is proven not to be so accurate. The highest point of a measurement is usually correct, but the less high points are influenced by the higher points around because of the footprint of the echo-sounder. A footprint is the area on the measuring surface where the echo-sounder measures the height. This footprint should be as small as possible to get accurate results in both x and y directions. The theoretical beam angle of the echo-sounder can be calculated with Equation 4.2 [General Acoustics, 2013 and e-mail communication with them]. In this equation V is the velocity of sound in water, D the diameter of the transducer and F the frequency of the transducer.

$$\sin(\theta) = 1.2 \frac{V}{D \cdot F} \tag{4.2}$$

For the echo-sounder used in this thesis it can be calculated that with $V = 1480$ m/s (20°), $D = 2.2$ cm and $F = 1,000,000$ cycles/second that the angle $\theta = 4.63°$. The beam of the echo-sounder first travels straight for approximately 8 cm and after this point the beam deviates with the angle calculated. From this it can be calculated that the theoretical footprint in 50 cm of water depth is 56 mm.

In every height measurement some scatter is present because of small vibrations of the echo-sounder. To remove this scatter an average is taken over 40 x-points where 20 points are in front and 20 points after the point that is measured. In this way a smooth profile is obtained which is within the footprint of the echo-sounder, because 40 x-points can be converted to an actual distance of 2 cm. In Figure 4.4 an measurement with the echo-sounder can be seen for different distances between two bars in 50 cm of water depth. It can be seen that the theoretical footprint of 56 mm is also the case in these measurements. In the actual height measurement of the near-bed structure height transitions are not this abrupt. General Acoustics mentions that the height measurement then is represented more accurate and a smaller deviation is present. Because of this measurement error an analysis is made what the influence of this measurement error is in the determination of the damage which can be seen in Appendix H. The total error and its influence on the damage is examined in Chapter 5.
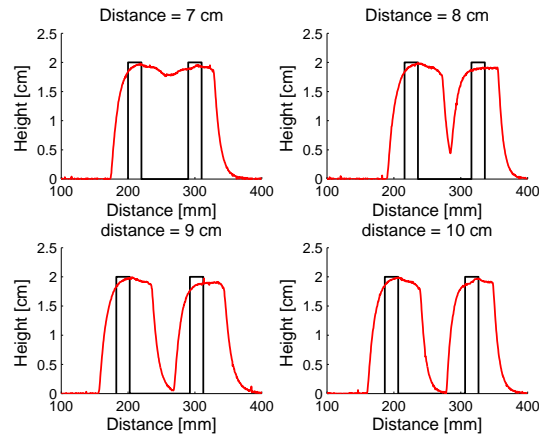
Figure 4.4: Measurements with echo-sounder for a different distance between two bars of 20x20 mm.

4.3 Observations

During the tests observations have been made which could be important for the analysis of the main objective in Chapter 5 and understanding of the results obtained. The observations can be about anything that happened during the testing.

For almost all tests the biggest waves in the JONSWAP spectra broke immediately after generation by the wave generator. This could be caused by a locally too high wave steepness, but depth induced breaking seems a more logical explanation because locally the relation $H_s/h > 0.5$. No wave breaking was seen on or close to the near-bed structure which could influence the movement of the stones in the near-bed structure. However, some white capping did occur in the wave flume. This is because in a wave spectra different waves travel at different speeds. In this way a wave could become locally to big when a wave catches up to another one and dissipate through white capping.

Quick tests with hand made waves very close to the wave dissipation berm showed very little reflection. Higher waves made by the wave generator are also absorbed reasonable but little reflections can be observed. Most waves act on this permeable rocky berm as a spilling breaker. This would also be expected by filling in the breaker parameter: $\xi = 0.26$. Only with the highest waves in the spectra an occasional plunging breaker was observed.

In the beginning of a test always a lot of stone movement occurred. The unfavourable placed stones are moving in the oscillatory movement of the waves. Also some rounding of crest corners can be observed very quickly after the first waves. Eroded stones are mainly deposited on the downstream slope of the structure. The slope of the structure tends to flatten in time and the whole structure tends to flatten towards a sort of Gaussian shaped profile (it has not been checked if this is a real Gaussian shaped profile, but is only used to indicate the approximate form). This could be observed well with the small stone type A. Because a lot of damage occurred, after a while a Gaussian shaped profile was created. This profile was more directed towards the downstream slope as more stones moved towards this side. This can be seen in Figure 4.5 and 4.6. After many waves the movement of stones became less for both stone types, but stones were still moving under the highest waves of the spectrum. Because of this the height of the profile would reduce a little every time a height measurement would take place after a wave series. Stones were observed to move under the highest waves of the spectrum in groups of up to 10 stones. From these observations it can be concluded that in the first thousand waves a lot of reshaping occurs and this damage developments reduces in time. In a few tests little pits were also observed which would fill up again after many waves.

Figure 4.5: Photo of test 2Av2 after 10,000 waves where the Gaussian shaped profile can be seen.
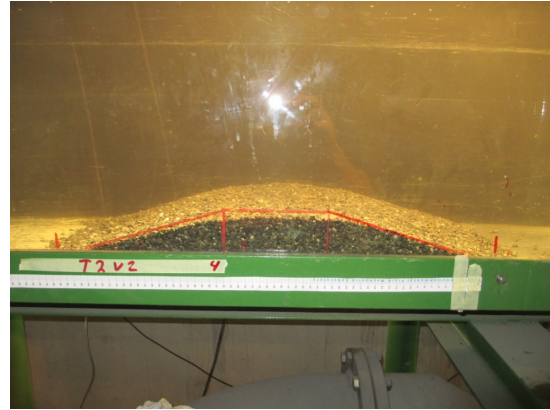
Figure 4.6: Photo of test 2Bv2 after 10,000 waves where beginning of the Gaussian shaped profile can be seen.

When stones were removed from the structure they would not find a stable position on the bottom of the flume and would always be transported away from the near-bed structure towards the downstream side which can be seen in Figure 4.7. On the upstream side of the near-bed structure just before the near-bed structure flow velocities were reduced. This could be seen by the accumulating dust and small stones on the bottom and can be seen in Figure 4.8. They would form little humps and showed almost no movement. This can be explained by the reduction in velocity on the bottom because of the near-bed structure. The height of the near-bed structure influences the orbital velocity on the upstream side of the near-bed structure.

Figure 4.7: Photo of stones removed from the profile of the near-bed structure which travel downstream.

Figure 4.8: Photo of accumulating dust and small stones in front of the near-bed structure.

The structure height and width seemed to have a significant influence in the stability of a near-bed structure. In test 4, which had a higher near-bed structure than the other tests, it could be observed that a lot more stones were removed from the crest which resulted in a lower crest height. This observation can be linked to the higher velocities present on the crest of the near-bed structure because of less available depth. In test 5, which had a wider near-bed structure than the other tests, it could be observed that the structure seemed more stable because the reduction in crest height seemed smaller. Because more stones are present on the crest of the near-bed structure less damage occurs.

The difference in structure geometry over the whole flume because of the glass or the separation board was minimal. Differences in height were observed close to the glass wall where the profile tended to be lower which can be seen in Figure 4.9. Because the structure was measured in the middle, this lower height was not measured and therefore not important for these tests. The total profile of the near-bed structure was a little 'crooked' towards the glass profile on the downstream side of the near-bed structure which can be seen in Figure 4.10. The end of the slope of the near-bed structure started here earlier than in the rest of the flume. This was not observed without the separation board present in the flume. The crooked profile does not influence the measurements of the near-bed structure because these have been made in the middle of the near-bed structure where it is not crooked.

Figure 4.9: Photo of different height near the glass wall.
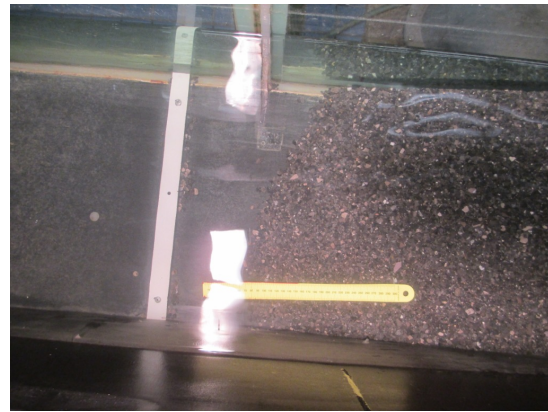
Figure 4.10: Photo of a crooked near-bed structure.

In test 3A2 an interesting observation was made. After rebuilding the structure underwater, because in test 3A already to much damage had occurred, a dune was formed after a several hundred waves which can be seen in Figure 4.11. In this test, with the highest wave condition, stones would fly off the crest of the dune and were almost always deposited on the downstream side of the dune. In this way the dune moved across the crest towards the downstream side of the near-bed structure. After a while the dune completely disappeared and the 'normal' Gaussian shaped profile was seen again. In no other tests a dune was observed and thus it was a whole new phenomenon in this test. Because of this dune and that stone type is smaller than tested in previous research the next section investigates the applicability of this stone type. A first observation why this dune occurred is the steep slope present in the beginning of this test. Because the near-bed structure was made with 45 cm of water still present in the flume, and stones B could not be disturbed, the profile was made under water with a broom. By trying to sweep the stones back together underwater the best possible near-bed structure is made. To make an accurate near-bed structure is with a broom and under water extremely hard. This is why there was a steep slope present and already a little dune could be seen on the photographs of the initial profile. Secondly, the stones were not stirred up again and because of this the packing density could be larger and less water can flow through the near-bed structure. This results in less damping velocity from inside the structure just after the slope. In combination with the steep slope and the small dune present in the initial profile this also contributes to dune forming. In total two times a structure was remade underwater with a broom. In the other test where this was done no dune occurred.

For the tests with multiple wave conditions after each other, test 6, 7 and 7v2, almost no movement of stones was observed in the first few wave conditions as expected. In the biggest wave condition however a lot of movement was seen. In these wave conditions a lot of stone movement was seen in the first hundred waves of the new condition. This movement gradually decreased again. In test 7v2 the movement seemed to stop when a lower wave condition was present when already a higher condition had been imposed to the structure.
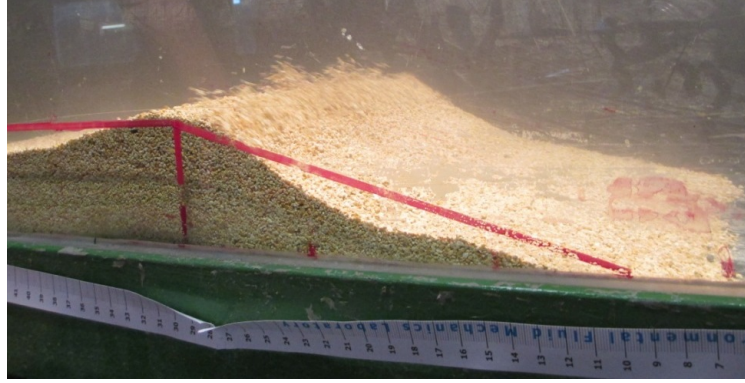
Figure 4.11: The occurred dune in test 3A2 with some flying of the stones over the dune crest.

4.4   Validity of stone types

In Chapter 3 it was described that the diameter of stone type B was in the range of the parameters tested by previous researchers. The diameter of stone type A was not in this range, and because of the dune that formed in test 3A2, it is unclear if this stone type is too small. It might be that other physical effects would start to play a role and these stones are not comparable any more to real near-bed structures. This can be translated in that too much scale effects take place with these smaller stones. Before comparing all the results, it is checked if this stone type is applicable.

A first indication of validity should be the wave-Reynolds number which is defined as Equation 4.3. This parameter can be used together with the the dimensionless bed roughness a_0/k_s to assess the flow regime in the wave boundary layer. In this thesis k_s has been calculated using $2 \cdot D_{n50}$. More about the wave boundary layer can be seen in Appendix B.

$$Re_w = \frac{\hat{u}_0 a_0}{\nu} \tag{4.3}$$

A graph made by Jonsson [1966] helps to determine the flow regime in the boundary layer (Calculated with H_s and T_p). With the corresponding data points of the physical scale model tests, this should point out that every test is in the rough turbulent regime. If the points are in the transition between laminar and rough turbulent, viscous effects may play a role. In Figure 4.12 the flow regime for the physical scale model tests are shown.
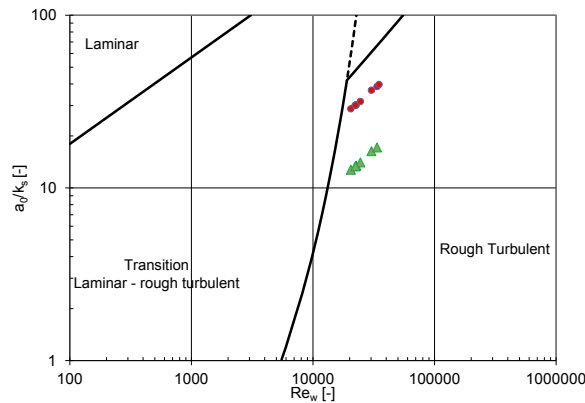
Figure 4.12: Flow regime for physical scale model tests. Red points are data from stone type A and green triangles are data from stone type B.

It can be seen that all tests are in the rough turbulent regime which would also be the case for a real situation. Because of this, it is concluded that all tests are applicable and no viscous effects play a role in these tests. However, because of the dune in test 3A2 and that stone type A is smaller than tested in the past, the validity of stone type A is further examined.

The critical shear stress, which is explained in Appendix B in Figure B.4, is lower for stones in these physical scale model tests than for stones in reality. This means that the tested stones would move earlier than stones in a real near-bed structure. It is expected that this has only minor consequences on the test results and both stone types can be used in relation with the critical shear stress.

Validity of stone type A

Stone type A size turned out to be smaller than expected and is therefore not in the range of parameters tested in the past. Because of this, and the dune from test 3A2, it is investigated if bottom transport is present with this stone type. This can be done using the Rouse number which describes if a stone is suspended or bed load transport under a given flow velocity. The Rouse number is defined by Equation 4.4 [Van Rijn, 1993].

$$P = \frac{w_s}{\kappa u_*} \tag{4.4}$$

In this Equation w_s is the fall velocity of a stone and κ is the von Kármán constant. In this equation u_* can be calculated using the critical shear concept described in Appendix B in Equation B.20 and Figure B.4. When the Rouse number is larger than 2.5, bed load transport is present. For stone type A this is the case ($P = 14.1$ [-]) for all the tests using a fall velocity defined by Van Rijn [1993] as Equation 4.5. Because of this, it can be expected that this smaller type of stone does not impose problems in the physical scale model tests. However, because of the dune this is further examined.

$$w_s = 1.1 \cdot \sqrt{\Delta g D_{50}} \tag{4.5}$$

Suspended transport[1] of stones was observed over the dune in test 3A2 which could be an indication that the transport cannot be considered bed-load transport (Figure 4.11). During testing with an innovative cobble shore for Maasvlakte 2, also flying of stones was observed. For this scale model testing described in Loman et al. [2010], it was concluded that almost no scaling errors occurred by testing the cobble shore on a large scale and small scale. When the environmental conditions are extreme enough, stones always behave like suspended transport with little jumps. Because the highest wave conditions were present when the dune occurred, this might be an indication of the still applicable results. However, it does not explain why the dune occurred.

The dune occurred in test 3A2, which was a repetition of test 3A. This repetition was built halfway of the total wave test, with water still present in the flume because too much damage had occurred to the near-bed structure. The relative change with the reference test 1 was that in test 3 the waves were higher. A interesting observation is that in test 3A no dune occurred and in test 3A2 one did occur. A possible explanation for the occurrence of the dune is the steep slope which was already present in the initial stage of the structure in this test. In test 1A this steep slope was also present, but with lower wave conditions. The steep slope from the initial structure of test 3A2 can be seen in Figure 4.13. In the top right corner of the structure the profile is a centimetre higher than in the rest of the profile. Because of this, and the steep slope occurring, turbulent releasing points occurring on this transition are larger than in other tests. Besides this, the stones were not mixed again for test 3A2 which would mean a larger compaction is present. Because the

---

[1]The observed stone movement is not really suspended transport. The stones are 'flying' over the crest of the dune in a large wave and return to the bed quickly.

stones are compacted more than they would be in a normal built of the structure, less flow travels through the structure because less pore space is available. This flow acts as a sort of damping force to the velocity that acts on the top right corner of the crest of the near-bed structure. Another observation that points out that the results from this test are applicable, is that the damage after a number of waves is approximately the same for test 3A as for test 3A2 after the dune disappeared. This can be seen from Figure 5.1 which is explained in the next chapter.
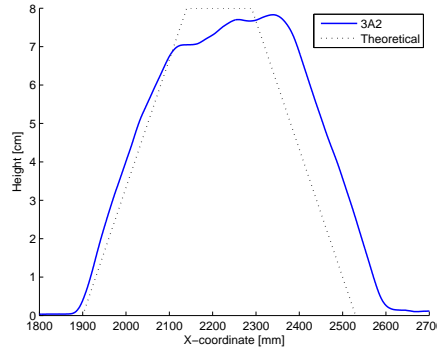
Figure 4.13: Initial profile of test 3A2.

An indicative method to check the scaling errors is to compare the falling velocity w_s of the stones against the velocity on the bottom u_0 in the physical model tests compared to a prototype situation. The velocity obtained with linear wave theory is scaled up to a prototype situation using Froude scaling. With the use of Equation 4.5 for the fall velocity of the small stones and Equation 4.6 [De Reus, 2004] for the fall velocity of up-scaled the prototype stones, the factors w_s/u_0 have been calculated for a prototype and model situation. These two factors have been compared to each other where the difference would be an approximation of the scaling errors present in the physical scale model tests for these stones. It turned out that the scaling error was approximately 7% for stone type A and 5% for stone type B which is considered acceptable for physical scale model testing in this thesis.

$$w_s = \sqrt{2\Delta \frac{g \cdot D_{n50}}{C_d}} \tag{4.6}$$

Based on (1) the Rouse number, (2) the suspended transport of cobbles for Maasvlakte 2, (3) the steep slope present in the initial stage of the structure, (4) less compaction in this initial stage and (5) the indicative way to check scaling errors it is concluded that the results of the tests with stone type A can be used. However, real near-bed structures would be designed with lower velocity parameters than are always present with stone type A. Because of this, a distinction between stone type A and B is given in the rest of this thesis. In this way a better conclusions can be drawn on the part were real near-bed structures are constructed in. A reason to build a near-bed structure with higher velocity parameters could be for 'building with nature' and thus allowing large movement of stones.

4.5   Damage development in time

An important part of this thesis is to examine the relation of the damage development in time for a near-bed structure exposed to wave loads. In this paragraph observations are done on the structure profiles in time and observations are made on which parameters are expected to be important in damage development. This section is split up in two parts where the first part describes the tests with a large number of waves and the second part the tests with multiple storms.

4.5.1 Large number of waves

In Figure 4.14 the profiles during test 4 for stone type B can be seen. Here it can be seen that the stones from the structure are mostly transported in the direction of the waves, which is indicated by the arrow. Besides this, it seems that the damage development is reducing after time. This can be seen because after approximately 1000 waves a lot of damage occurs which reduces in the last condition where not much damage occurs in approximately 4000 waves. From this observation it can be concluded that the damage development reduces in time but does not stop under the limitations of this test. It is however likely that the damage development stops in time when so much damage has occurred that there is almost no transition (or streamline contraction) between the bottom and the near-bed structure or that the height has reduced so far the critical velocity does not move the stones any more. Streamline contraction can be seen as how much the orbital velocity is influenced by the near-bed structure. Because a lower depth is available, the streamlines are compacted more towards each other. This concept is explained more in the analysis done in Chapter 5.

The real damage development can be shown in a more representative way by comparing the structure to the initial profile. In Figure 4.15 the relative changes compared to the initial profile can be seen. Negative values indicate that stones have been removed and positive values that stones have been accumulated. From this figure it can be seen even better that the stones are transported more towards the downstream slope of the near-bed structure. The most erosion occurs on the crest and the transition from the crest towards the slope. Only small changes occur on the upstream slope of the near-bed structure. Here only a small amount of stones accumulate. This can better be observed by investigating stone type A where a lot of damage occurs. All profiles for each test can be seen in Appendix E.
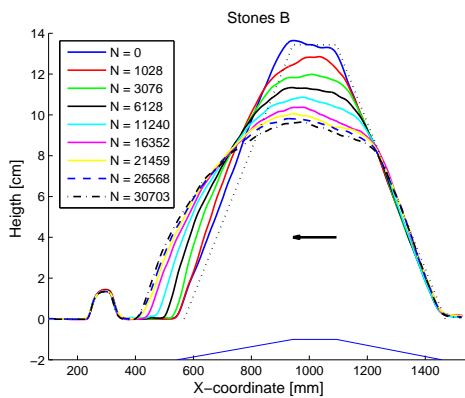
Figure 4.14: Profiles test 4B
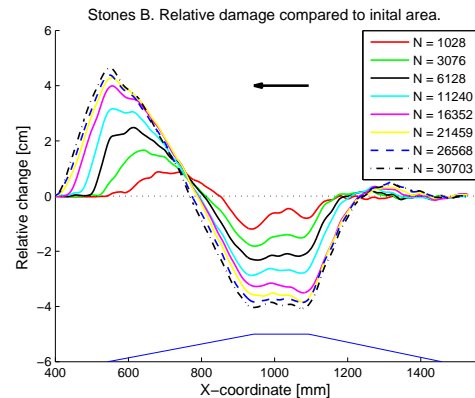
Figure 4.15: Relative changes test 4B

In Figure 4.16 and 4.17 the profile and relative change for test 4 for stone type A can be seen. Because more damage occurs in these tests relative to stone type B, the damage development in time becomes easier to analyse. Again it can be seen that the stones are transported more towards the downstream slope. However, also a smaller amount is transported to the upstream slope. Especially in the relative damage plot this can be observed very well by the hump on the upstream side of the near-bed structure. A sort of Gaussian profile is obtained in time after a large number of waves. The damage development in time for stone type A seems to slow down. However, because more damage occurs here, the damage reduction in time is lower than for stone type B as well.

From these and other relative damage profiles in Appendix E it can be seen that in the first few wave conditions mainly smoothing of the damage profile occurs. If the profile is too high somewhere or a bump is present compared to the rest of the structure, this part is smoothed away

quite fast. Another example is that the structure slope is too gentile so that stones can easily be transported over the slope towards the crest. In other words, the first few wave conditions seem to smooth out irregularities. This is the explanation that some of the relative damage profiles in this appendix seem quite odd and not logical for the first few wave conditions (For example see Figure E.6).
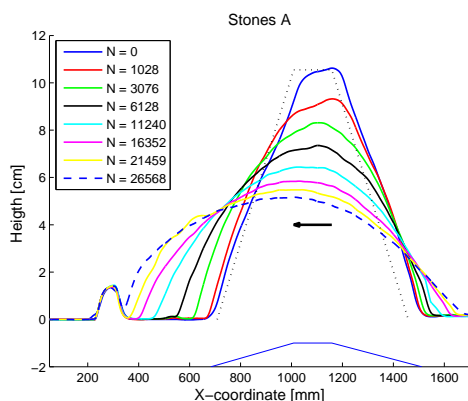
Figure 4.16: Profiles test 4A
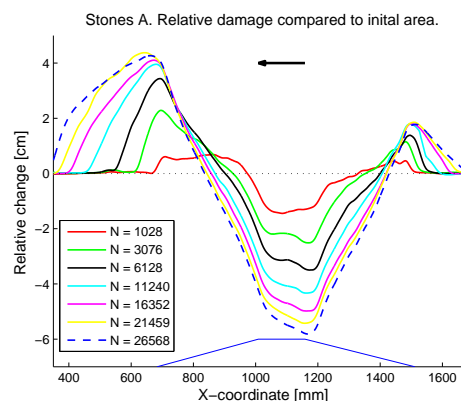
Figure 4.17: Relative changes test 4A

It can be concluded from these figures that:

- The first few waves tend to smooth the profile and remove irregularities

- Stones are transported mainly towards the downstream slope.

- The test all show similar erosion patterns where most of the material is transported towards the downstream side and the crest height reduces.

- Erosion reduces but does not stop in time under these test conditions.

- A smooth Gaussian shaped profile is obtained after a large number of waves with enough damage.

4.5.2 Multiple storm conditions

One of the main parts of this thesis is to investigate the damage during multiple storms. In this paragraph the height profiles are investigated that where observed during the physical scale model testing. Test 7 has been repeated because in this test the wave generator broke down.

The hydraulic conditions from the physical scale model tests with multiple storm conditions can be seen in Table 4.2 or Appendix G. In Figure 4.18 and 4.19 the profiles and relative damage from test 6 can be seen. For test 7 these results can be seen in Appendix E. In test 6 and 7 the wave conditions are from low to high. It can be seen that in the first few wave conditions with a low velocity parameter very low damage occurs as expected. Only during the last four conditions significant damage occurred.

From these figures it can be seen some rounding of crest corners and probably movement of unfavourable placed stones in the first few wave conditions. In the higher wave conditions (from $N > 24,000$) the observed damages are quite large. By an observation it was concluded that when a condition increased from the first wave condition towards a higher second condition, in the first few high waves always reshaping occurred. Additional rounding of the crest and more movement of unfavourable placed stones could be seen. This can be explained by the velocity on the bottom which has increased again and which thus moves more stones. Unfavourable placed stones which
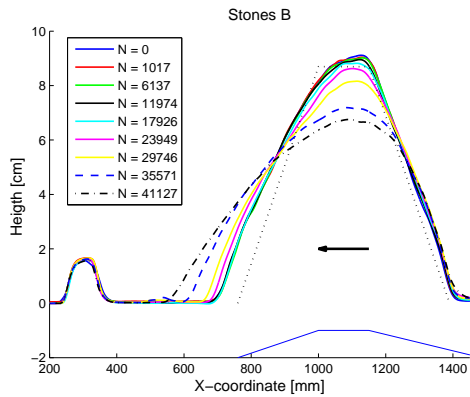
Figure 4.18: Profiles test 6.
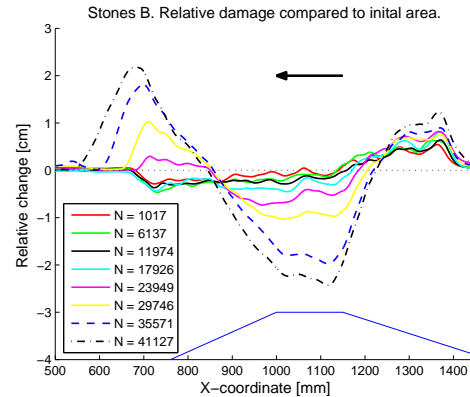
Figure 4.19: Relative changes test 6.

would not move in a lower velocity do move in the velocity from this new condition. Another observation was that movement reduces in time but stone movement has not been observed to stop. This can also be seen in the relative damage in Figure 4.19. In the last condition quite some extra damage occurred. Although test 7 has not been finished, the same observations can be done here. Damage developed mostly at the crest and on the transition to the slope.

In test 7v2, which is the repeated test 7, some interesting observations are made. Test 7v2 was very interesting compared to test 6 because in this test multiple wave conditions were present in a random order and with a different number of waves. The profiles and relative damage for test 7v2 can be seen in Figures 4.20 and 4.21. Form these profiles it can be seen that not a lot of damage occurs in test 7v2. If the profiles are closely examined it seems that in a lower storm condition no or very little damage occurs compared to the previous higher condition. This must be examined in more detail which is done in the next chapter. The damage can better be observed by looking at the relative profiles in Figure 4.21. It can be seen here that relatively low damage occurred on the crest in comparison with other damage tests. Although, the 'normal' general observations can be made that stones are transported towards the downstream side of the near-bed structure. In comparison with test 6, very low damage occurred because the relative changes are much lower for this test. This was to be expected because fewer waves and lower wave conditions were used here. An interesting observation is that the damage seems to stop after wave condition four ($N = 17909$). However, this can not be observed very well in this relative change plot, so this is investigated further in Chapter 5.
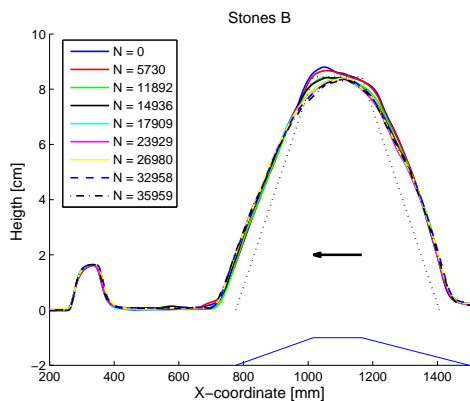
Figure 4.20: Profiles test 7v2.
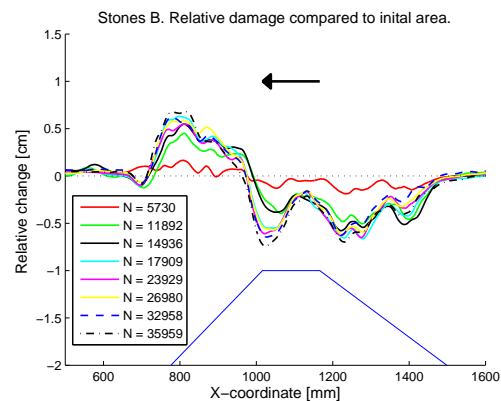
Figure 4.21: Relative changes test 7v2.

4.6 Accuracy and limitations of the damage prediction

In this chapter the initial measurement errors are described and in Paragraph 4.2.3 the precision of the echo-sounder was examined. There are always deviations in the results of physical scale model testing because the measurement devices are not perfect. This section sums up the measurement errors so that these can be worked out in the analysis from Chapter 5.

In Appendix H the measurement error of the echo-sounder was investigated. It was concluded in this appendix that the measurement error because of the footprint of the echo-sounder is never constant. If the relative changes between different heights are large, a large error can be made. When differences are lower the measured height is more accurate. It was concluded that because of the footprint the erosion area could maximally be 23% smaller and 10% larger. The 23% is an absolute maximum percentage because some assumptions have been made which were all on the maximum side and can be seen in Appendix H. Besides the echo-sounder there are more measurements done in the physical scale model tests which can included errors. The measurement error for the number of waves has been estimated and it is expected that this number is determined very accurately by Matlab and thus an error of 1% can be present. The peak period showed more deviation and thus this error is expected to be larger in the order of 5%. Because of the larger number of waves used in this thesis the significant wave height is estimated to be rather accurate and a smaller error is expected here than with the peak period in the order of 2.5%. The height of the near-bed structure was measured by the echo-sounder. Although the maximum height measurement is quite accurate, an average height in the crest has been taken. Because of this an error of 5% is expected to be present in the average height of the near-bed structure. The water depth, which was read by eye, also has a measurement error present estimated in the order of 5%. For the stones approximately 5% deviation is present as well by weighing errors. Because the density tests have been repeated several times the deviation for this is lower than for the stones. In Table 4.6 the quantified measurement errors are showed for every measurement done from the physical scale model tests which are further worked out in Chapter 5.

Parameter	Error	Background
h	± 5%	The water depth was measured using a tape-measure which could be read accurately within 1 mm.
H_s	± 2.5%	The significant wave height is based on a Matlab script.
T_p	± 5%	The peak period is based on a Matlab script but can show some deviations.
N	± 1%	The counting of waves is based on a Matlab script.
A_e	+10% −23%	Based on the considerations of Appendix H due to the measurement errors of the echo-sounder.
z_c	± 2.5%	Based on accurate height measurements of the echo-sounder
D_{n50}	± 5%	Based on the measurement errors because of weighing the stones.
Δ	± 2.5%	Based on density measurements.
g	–	Negligible error

Table 4.6: Quantified measurement errors based on all measurements.

4.7 Syntheses

In this chapter the initial results from the physical scale model tests have been given. With the hydrodynamic conditions linked to the damage several damage development formulas found in Chapter 2 can be investigated. In Chapter 5 these analyses are made and comparisons are done.

For the test 1-5 the relation between damage and the number of waves is analysed. With this actual relation a new damage development formula which predicts the damage to a higher degree of accuracy is developed if the current way to describe the damage is not sufficient. For test 6 and 7 it is analysed what happens in multiple storm conditions and if the damage prediction methods for this are accurate. For each test comparisons are made to the visual observations from previous paragraphs.

Part III

Analysis and Conclusions

Chapter 5

Analysis

In this chapter the results from the physical scale model testing are analysed. The measurements and observations from Chapter 4 are processed in a clear way. In the first part the damage versus number of waves is investigated more closely. In the second part it is tried to find a new design formula which correctly incorporates the damage versus time factor. In the third part the damage occurring in the tests with multiple storms are investigated more closely and finally the current method from chapter 2 to quantify damage in multiple storms is described in relation with how well this method performs.

5.1 Damage versus number of waves

In this section the damage versus the number of waves for test $1 - 5$ is investigated. This paragraph continues on the observations done from these tests in Chapter 4. In this paragraph it is tried to link processes to damage development and the actual relation between damage and time is investigated.

A more accurate analyses can be made from the damage during a large number of waves by comparing the damage against the number of waves. In Figure 5.1 and 5.2 the number of waves are compared with the damage for stone type A and B.
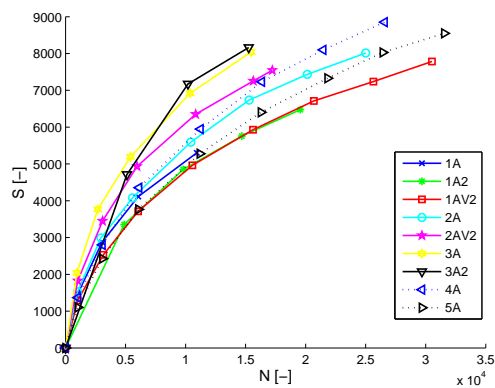
Figure 5.1: Damage versus number of waves for stone type A.
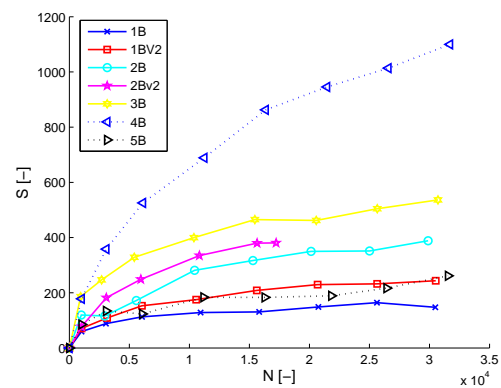
Figure 5.2: Damage versus number of waves for stone type B.

A first observation from Figure 5.1 is that all the occurring damages are relatively close together. Besides this, in each test not a stable equilibrium is reached when the tests were stopped. A closer examination reveals that for the tests that have been repeated, the occurring damage trends are very equal to each other. The damage development for test 1A, 1A2 and 1Av2 are approximately the same. The repeated test 2A and 2Av2 are further apart but still comparable to each other. The differences which are present are mainly because of the first two wave conditions. Even the test where the dune occurred, test 3A2, gives a similar damage development as test 3A where no dune occurred. It can be seen that the damages in this test with very high waves are developing the fastest and the damage is significantly higher than reference test 1. This was to be expected because a larger velocity on the near-bed structure is present because of the higher wave heights. Test 2, with a lower water depth, also gives more damage as the reference test while test 4, with a higher near-bed structure, gives significantly more damage. This is remarkable, because in both tests a larger near-bed velocity would be expected because less water depth is available. Test 5, with a wider near-bed structure gives little more damage than the reference test. It can be concluded that each adjustment influences the damage where the wave height and height of the near-bed structure seems to be the most important parameters. Of course this depends on the actual velocity which is present on the near-bed structure which is shown later in this paragraph.

From stone type B in Figure 5.2 a first observation is that although most damage curves are almost horizontally, damage development never really stops. The repeated tests do not give very similar answers like was seen with stone type A. These answers are close together, but they do differ, which points out that similar conditions can give different results, or errors are made by doing the tests. By rechecking the whole set-up of the physical scale model it has been made certain no errors were made with measuring or setting up the scale model. Because the actual damage development in time is about the same for these tests, the difference in results can be because of randomness still present in damage development in near-bed structures. This randomness is mostly observed in the first few wave conditions of a test. Sometimes a lot of damage occurs and sometimes a lot less damage occurs. This has to do with the placement of stones, packing density and irregularities by placing. Because these can not be measured, the damage in the first few wave conditions have a larger spreading.

An observation is that for test 1B, 3B and 5B the damage seems to become less on some points in the graph. This can actually be the case! Stones are moving back and forth, but also sideways and little holes and bumps are formed in a test. This is especially the case if only little damage occurs in a test. If in one test a hole was present which was not there after the next wave series, the damage could become less. This was also observed sometimes in the physical scale model tests as can be seen in Figure 5.3. Here a hole can be seen which was formed in the course of one wave series of 5000 waves. Actually this change in damage can be explained that too little measurement rows have been taken. If more rows were measured, one row would have more damage and another row would have less damage. A bump can for instance occur if the velocity on the near-bed structure is just below the critical velocity of a stone, which is the largest stone of the grading, so that other stones are moving. Other stones around this stone might not move as well because of interlocking and in this way a bump can be formed. This bump can be wiped away easily if a higher velocity is present under for instance the highest wave of the spectrum H_{max}.

From Figure 5.2 it can also be seen that all tests give more damage than reference test 1. Test 2 gives approximately twice the damage of the reference test. Because of the lower water depth the velocity on the near-bed structure must have increased considerable to create the extra damage. Test 3 gives even higher damages than test 2. This can be explained due to the higher waves and thus an even higher velocity present on the near-bed structure. Test 4 has extreme damage compared to the reference test. This test, with a higher near-bed structure, must be of significant influence to the damage development in time. Because the same waves are used as in test 1, the height of the near-bed structure must be of influence to the damage development and to the velocity present on the near-bed structure. The calculated velocity on the near-bed structure is only a little higher and thus other processes must play a role as well (explained further on). The orbital movement on the bottom could be influenced more because of the higher near-bed

Figure 5.3: A hole which occurred in test 2B.

structure. In test 5, with a wider near-bed structure, not much additional damage has been measured than in reference test 1. It can be concluded from both graphs that several parameters play an important role in the damage development over time. It can be seen that the wave height, water depth and structure height play a role in the damage development. Another important conclusion is that the damage development in near-bed structures still contain some randomness. The first few wave conditions are mostly the cause of this because the damage development trend after this is approximately consistent.

In Figure 5.4 the velocity with the use of linear wave theory on height h_c with $H_{1\%}$ and T_p can be compared to each other. The relative changes in each test are visualised in Figure 5.5. It was concluded in previous paragraphs that the wave height was one of the main differences in resulting damage. From these figures it can be seen that indeed the largest velocity occurs in test 3. The near-bed velocity at the crest of the structure is considered to be the main driving force for damage development. However, because test 4 has so much damage and the velocity is the same as in test 1, here the height of the near-bed structure must play a significant influence. The water depth that was changed in test 2 has a higher velocity present on the near-bed structure. It might be that the added damage compared to reference test 1 is because of this added velocity. The water depth could also more influence the damage development than assumed by the calculated velocity. In test 5 the velocity on the near-bed structure is as expected comparable to test 1.
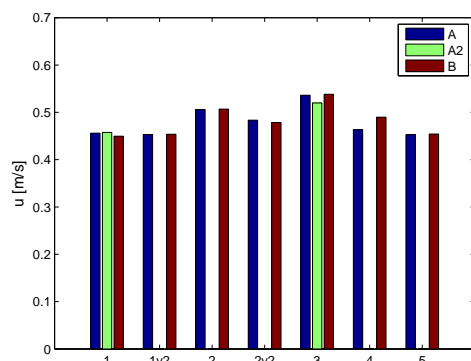
Figure 5.4: Near-bed velocity present in scale model tests.
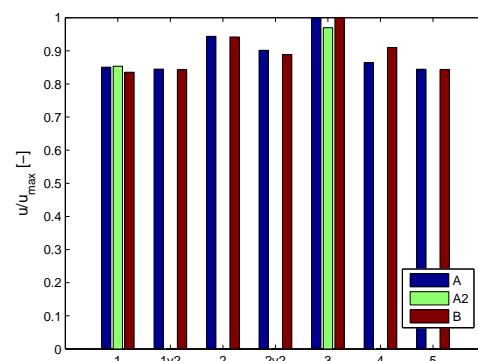
Figure 5.5: Relative velocity present in scale model tests.

A significant difference between stone type A and B is that for stone type B it looks like a lot more damage occurs in test 4. However, for stone type A this near-bed structure is lower and thus differences are smaller compared to the initial test condition. The damage development trend

between stone type A and B is also comparable. It can be seen that test 3, with the highest waves gives significant damage for both stone types. Test 5, with a wider near-bed structure, gives a little more damage than the reference test for both stone types. The overall comparison is that the results from both stone types are very similar.

Based on above observations the following can be concluded:

- In the first few wave conditions randomness in damage development occurs. This is caused by irregularities present in the near-bed profile and different compaction.

- The overall results from both stone types relative to each other are very similar.

- The height of the near-bed structure plays a significant role in damage development.

- The wave height and water depth play an significant role in the damage development.

5.1.1   Accuracy

From Chapter 4 it is known what the measurement errors are and that these influence the results obtained from the physical scale model tests. In the previous section the damage relative to the number of waves was analysed and in this section the measurement errors are taken into account for this part. In this section the measurement errors are investigated to which degree they influence the test results.

In the measurements errors there are three errors present for the relation between damage and number of waves. The first measurement error is in the erosion area A_e which was measured by the echo-sounder. The second and third measurement errors are present in the number of waves N and the median stone diameter D_{n50}. The deviation in the number of waves is small and is expected to be insignificant because of the high number of waves used in this research. Because of this, the error made in estimating the number of waves is ignored in this investigation. In Figure 5.6 and 5.7 the number of waves are plotted against the damage with the error bounds from each measurement. Note that these bounds are the maximum possible deviations. A first observation is that these error bounds get larger after more waves which is of course related to the damage that actually occurs in a test. With more damage the deviation can be larger as well.
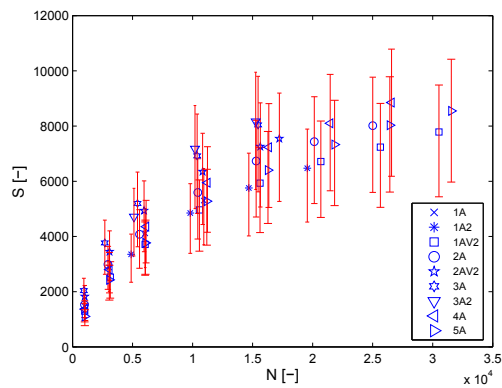
Figure 5.6: Damage versus number of waves for stone type A with error bounds.
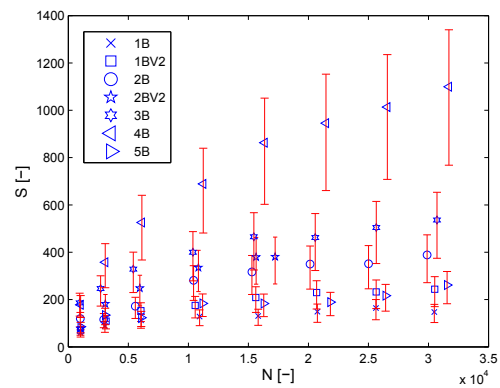
Figure 5.7: Damage versus number of waves for stone type B with error bounds.

A closer investigation into these measurement errors reveals that there is a large error bound for the damage number S. This is because the erosion area measurement has a large deviation in both directions. When more damage occurs, a larger deviation is possible. The maximum deviation can be 26% smaller and 16% larger than actually measured. These deviations have to be taken

into account when the results of the damage predictions are used. In the rest of the analysis these errors are reviewed as well. Because these measurement errors are always present, no standard correction has been introduced to coop with this deviation. The results showed in Appendix G are taken as the best value and are used in analysis.

5.1.2 Exponent of the number of waves

In this section the relation between damage and time is investigated. Because the physical scale model tests were executed with a very large number of waves it is investigated how this relation actually should be, and if relations found by previous researchers are accurate.

Time is in most damage development formulations expressed as the number of waves N. From the literature study it is known that several parameters such as $\sqrt{N}$, $\log{(N)}$ and $N^{0.3}$ have been used by previous researchers to describe the relation between damage and time. By comparing the damage S to the number of waves, an actual relation can be found between damage development and number of waves. Because in previous damage development research by other researchers no more than 6,000 waves have been used, this relation was not found yet.

From the damage observation in time the actual exponent can be found which should be used in damage development formulas. A fit in the form of $S = N$ has been tried for many forms such as linear, exponential, logarithmic and polynomial but it was concluded the power relation worked best for the relation between damage and number of waves. With this power relation a 'best fit' line in the form of $S = a \cdot N^b$ was fitted through the data of each test result. From this the parameters a and b can be determined with the use of the Curve Fitting Toolbox from Matlab using the method of least squares. In Table 5.1 the exponential coefficient, 5% and 95% confidence bounds, mean value and standard deviation are given. The way to calculate the mean and standard deviation is explained in Appendix I. In this table no coefficients are given for other researchers because to few data points per test were present to correctly fit a line through the data and not enough waves were used. It was found that a minimal of four data points was necessary to correctly represent the power function and its confidence bounds.

Test	b	5%	95%	Test	b	5%	95%
1A	0.509	0.366	0.653	1B	0.258	0.186	0.331
1A2	0.463	0.363	0.534	1Bv2	0.345	0.292	0.398
1Av2	0.482	0.435	0.529				
2A	0.473	0.421	0.525	2B	0.421	0.303	0.539
2Av2	0.462	0.394	0.529	2Bv2	0.480	0.360	0.600
3A	0.457	0.385	0.529	3B	0.298	0.259	0.338
3A2	0.489	-0.631	1.609				
4A	0.523	0.465	0.582	4B	0.478	0.425	0.530
5A	0.529	0.473	0.584	5B	0.304	0.187	0.421
Average	0.488	0.407	0.553		0.369	0.287	0.451
Std dev.	0.027	0.043	0.045		0.090	0.087	0.106
Overall	0.436	0.354	0.508				

Table 5.1: Exponential coefficients for N^b with 5% and 95% confidence interval, mean and standard deviation given for stone type A and B.

From Table 5.1 a first observation is that the results from test 3A2 are very different than from the rest of the tests. This is because not enough data points are present to correctly fit a line through. Note that because of this, these results have not been included in the averaging and calculation of the standard deviation. Besides this, it can be concluded that there is not 'one' correct exponential coefficient. In fact, stone type A tends to go towards the conclusion from

Wallast and Van Gent [2002] ($b = 0.5$) while stone type B leans more towards the conclusion of Van den Bos [2006] ($b = 0.3$). For stone type A the standard deviation is low and is only 5.5% of the mean. For stone type B however, the standard deviation is larger, and is 24% of the mean.

For stone type A, where a lot of damage occurs, the standard deviation is low. This might be linked with the damage that occurred in a test which was approximately constant in each test. For stone type B more differences are present. In reference test 1 the differences between test 1B and the repetition 1Bv2 are already 30%. This could also be linked to the damage that develops in a test because for test 1Bv2 the initial damage in the first 2000 waves is larger. For test 2 and 4 the exponent is much larger and tents towards the observation of stone type A. In both tests the velocity on the bottom was increased by other means than the wave height and in both tests quite some damage occurred. In the test with the most damage, test 3, it is then interesting to see that the exponent again tends towards 0.3. It can be concluded that more factors play a role in the actual exponential coefficient of the number of waves than assumed so far in research. This can be concluded because of the still large deviations present per test. The tests that were repeated have both different exponential factors which means that this parameter is influenced by several other factors and might also be influenced by the damage in the first few wave conditions as seen by test 1B and 1Bv2. The exponential factor from test 2B and 4B differs so much from test 1B, 3B and 5B that the parameters which changed in this test must play some sort of role in this exponential factor. Parameters that might influence this exponential coefficient are then the structure height and water depth. Because of the differences in coefficients between stone type A and B the mean diameter must play a role as well. Apart from this, the exponential coefficient might depend on the actual damage that occurs. For instance with a small damage this coefficient should be small as well. To calculate the damage that would occur with this formula, an iteration would be necessary in this way.

For describing parameter b several relations have been examined but no good relation which could predict parameter b was found. A relation could be present for example in the form of Equation 5.1 which is similar to the relation which Klomp and Lomónaco [1995] found. This relation describes that the parameter b is constant after 2000 waves. However, still some scatter was present with this method. Other ways to describe parameter b have been examined in the form of predictive equations. However, a good and high correlation between the actual coefficient and the calculated coefficient were not found. Because a lack of data with for instance multiple stone sizes or more differences in wave height, no further attempts have been made to describe parameter b in an equation. In the remaining of this thesis parameter b is 0.436 for all data and 0.369 for data with stone size B which is the average value for the tests.

$$\frac{S}{S_{2000}} \cong (N - 2000)^b \tag{5.1}$$

If measurement errors from the previous section are introduced to this analyses different exponents than listed in Table 5.1 can be found from each test. When the maximum or the lower bounds are used the same exponent b is found. Differences do occur if for example in the first measurement the actual damage number is the lowest from the lower bound and in the last measurement the damage is the highest of the upper bound. In this way a different exponent would be found for the relation between the number of waves and damage. Because the exponents found in this thesis are approximately the 'best fit' coefficients for this relation, these values are not investigated further and the standard deviation between different tests found in this thesis is assumed correct.

Because of the analysis in this section it can be concluded that parameter b is not 'one' coefficient and this exponential parameter depends on several other factors. In this thesis it is concluded that this parameter is dependent, among others, on the damage that occurs after approximately 2000 waves in a test, the wave height, the stone size, water depth and structure height.

5.2 Deformation analysis

As concluded in the previous section several factors seem to play a role which are not included in current damage development formulas. In this section it is investigated if other damage development formulas calculate the damage to a high degree of accuracy. If this is not the case, a new damage development formula is investigated together with the parameters that were concluded to be important in the previous section.

Van Gent and Wallast

In Figure 5.8 and 5.9 the measured versus the calculated damage for Equation 2.30 and 2.31 from Van Gent and Wallast [2001] is shown for stone type A and B. The dashed line is the calculated damage and the solid line is the measured damage. A first observation is that the calculated damage for test 2A and 2B goes up and down in the graph. It was investigated that this is because of a small change in wave period which results in a different velocity because of linear wave theory.

$$\frac{S}{\sqrt{N}} = 0.2\theta_{hc}^3 \tag{2.30}$$

$$\theta_{hc} = \frac{\hat{u_{hc}}^2}{g\Delta D_{n50}} \tag{2.31}$$
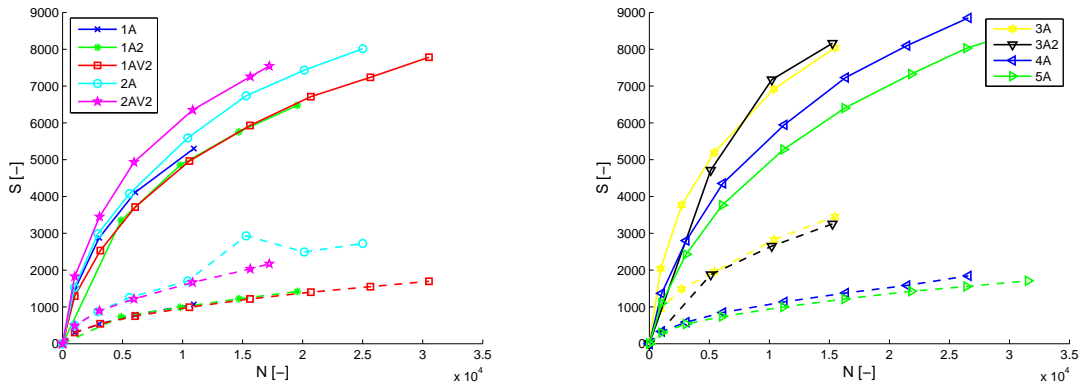
Figure 5.8: Stone type A measured (solid) and calculated (dashed) damage with Equation 2.30 [Van Gent and Wallast, 2001].

From these figures it can be seen that the damage calculated by the formula from Wallast and Van Gent underestimates the damage in each test. This is a whole other observation than made by Saers [2005] who concluded that the formula from Wallast and Van Gent over predicted the damage (see further on in this paragraph for analysis of this). Only test 1B and 5B are calculated closely, but still a large deviation is present. The deviation in test 1B was as large as 160% at the start of the test and reduces to 10% in the end of the test. For test 5B the average deviation was approximately 70%. Especially the damage calculated for stone type A is very under predicted. From this it can be concluded that the formula from Wallast and Van Gent under predicts the damage for high velocity parameters. Besides this, the changes in these tests such as the wave height, waver depth, structure height and structure width all have a different damage. The calculated damage however is approximately the same for test 1A, 4A and 5A. From this it can be concluded that the structure height and structure width must play some role in the damage development formula.
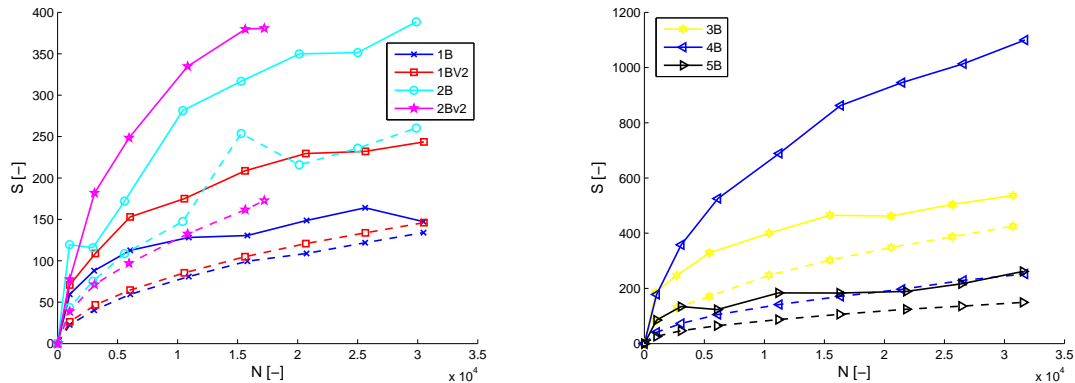
Figure 5.9: Stone type B measured (solid) and calculated (dashed) damage with Equation 2.30 [Van Gent and Wallast, 2001].

For stone type B in Figure 5.9 it can be seen that for test 1B, 3B and 5B, where the damage is calculated the closest, in the beginning the calculated damage is much smaller than the measured damage. With a large N the calculated damage and measured damage seem to converge to each other. This could be because the number of waves is to the power 0.5, which was found in this thesis to be too high compared to other researchers. A main conclusion from these graphs is that the damage until 3000 waves, where this formula was designed upon, does not predict the damage sufficiently. It can be concluded from stone type B that the wave height, water depth and structure height are not represented well in the formula from Wallast and Van Gent because the calculated damages are lower than the occurred damage.

Because Saers [2005] concluded that the damage development formula from Wallast and Van Gent [2002] over predicted the damage development, and tests in this thesis have shown that they under predict the measured damage, an investigation is performed. In Figure 5.10 a comparison between tests done by Saers and stone type B is performed together with the damage development formula from Wallast and Van Gent. It can be seen that indeed the damage development formula generally over predicts damage for Saers his scale model tests and under predicts damage for stone type B. A first observation is that the data of Saers is generally in the higher regions of the velocity parameter compared to tests with stone type B. Saers used just a little larger stone ($D_{n50} = 3.70$ mm compared to $D_{n50} = 3.39$ mm) which would result in lower velocity parameters. Because of this, the wave height in Saers his tests must be significantly larger than used in tests with stone type B. This is odd because test 3 used the largest waves possible in the wave flume and Saers used this same wave flume. In Saers his thesis it is not explained how these larger waves where made, so it remains unknown if this is correct. Another possible reason could be that a lot less damage occurred in Saers his tests. Again this seems odd, because with a larger wave height more damage would be expected. Because it is not known what exactly the reason is for the other observations, data of Saers is used in this thesis. A solution would be to recheck the wave height and damage actually measured by Saers. If it turns out that everything is correct, it is concluded that a large deviation is present in damage development for different near-bed structures. Because of this analysis it is assumed the wave height used in Saers his test is somehow a little too large.

Another reason that the results are so different from the results from Saers his tests could be that measurement errors from scale model test in this thesis have a big impact in the results. In Figure 5.11 the error bounds are shown together with the formula of Wallast and Van Gent [2002]. In this analysis all errors have been included that were introduced in Chapter 4. Because of this there are errors possible in both directions. Note that the bounds in this figure are maximum deviations possible. From this figure it can be concluded that even with the error bounds introduced, the formula of Van Gent and Wallast still underestimates the damage and that measurement errors do not change this conclusion.
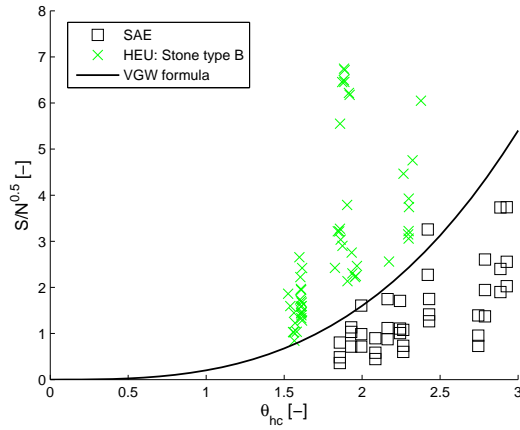
Figure 5.10: Comparison between measurements from Saers [2005] and tests done in this thesis for stone type B.
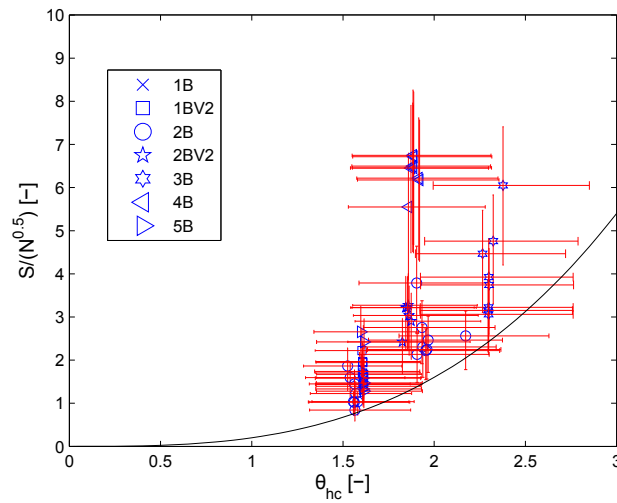
Figure 5.11: Error bounds for test results with method of Wallast and Van Gent [2002].

Van den Bos

In Figure 5.12 the measured and calculated damage with the use of Equation 2.35 and 2.36 from Van den Bos [2006] are shown for stone type A. The dashed line is the calculated damage and the solid line is the measured damage. A first observation is that the damage is still under predicted for stone type A. In Figure 5.13 these profiles are shown for stone type B where the damage seems to be predicted to a higher level of accuracy.

$$\frac{S^*}{N^{0.3}} = 0.048 \cdot (\theta_{hc\ 1\%})^{1.6} \cdot m_0^{-0.6} \tag{2.35}$$

$$\theta_{hc\ 1\%} = \frac{(\hat{u}_{hc\ 1\%})^2}{g\Delta D_{n50}} \tag{2.36}$$

From Figure 5.12 it can be seen that for stone type A the formula of Van den Bos under predicts the damage as well. An interesting difference with the calculation from the formula from Wallast
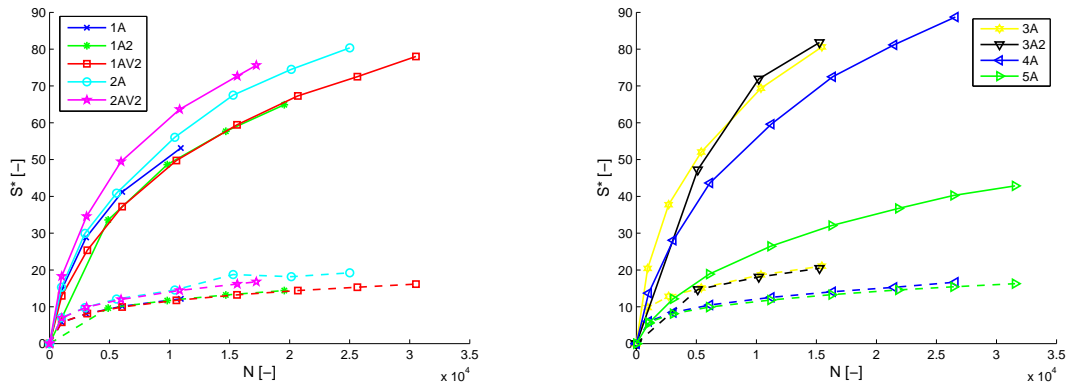
Figure 5.12: Stone type A measured (solid) and calculated (dashed) damage with Equation 2.35 [Van den Bos, 2006].
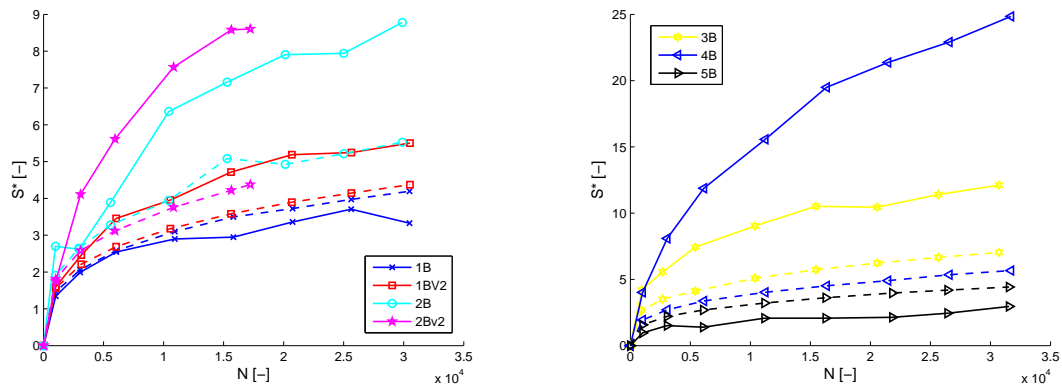
Figure 5.13: Stone type B measured (solid) and calculated (dashed) damage with Equation 2.35 [Van den Bos, 2006].

and Van Gent is that test 5, with the wider near-bed structure, is calculated to a higher degree of accuracy. This might be because of the width which is present in S^*. Concluded can be here that all relative changes compared to the reference test have an influence in calculating the correct damage for stone type A.

A closer investigation of Figure 5.13 reveals that the damage from test 1B is calculated to a very high degree of accuracy with an average deviation of only 10%. Test 1Bv2 seems to have more initial damage in the first two or three wave series so that the overall damage is larger. The damage development trend after the third wave series is approximately the same. In test 2B, with a lower water depth, the calculated damage is further away from the measured damage (average deviation of 28%). In the beginning the calculated damage seems to be really close, but after 5000 waves more deviations start to occur. From this it can be concluded that the water depth influences the damage development more than assumed. The same can be observed in test 2Bv2. In test 3B, with higher waves, the damage is also under predicted. Higher waves seem to have more influence in the initial damage development because the occurring damage trend after 5000 waves seems to be very similar to the calculated damage. In test 4B, with a lower near-bed structure, the actual damage and calculated damage are very different (average deviation of 75%). Even the damage development rate is different. From this it can be concluded that the damage is not calculated accurately for higher near-bed structures and that this influences the damage development more than assumed so far. In test 5, with the wider near bed structure, the calculated damage is a little higher but very similar to the measured damage. In this test the average deviation was still 60%

because of the small damage measured. From stone type B it can be concluded that the water depth, wave height and structure height are not properly represented by the formula of Van den Bos because large deviations are present between the calculated damage and measured damage. Also the width of the structure might have an larger influence that can be seen from Figure 5.13. Because the average deviation was still 60% this must be investigated as well.

From Figures 5.12 and 5.13 it can be concluded that the damage is calculated to a higher degree of accuracy with the formula of Van den Bos than with the formula of Wallast and Van Gent. The overall damage is closer to the measured damage, and not in every test a lower damage is calculated than actually measured. However, the current design formula from Van den Bos still does not calculates the damage sufficiently because on the deviation for all test is still 40%. The damage from test 1B and 1Bv2 have been calculated reasonable (respectively on average 10% and 18% deviation). However, the damage from test 2B, 3B and 4B are not calculated even close (respectively on average 28%, 41% and 71% deviation). Test 5B, with a wider near-bed structure, seemed to be calculated close, but because of the small damage occurring the deviation was on average still 60%. For stone type A the occurring damage was, as was seen as well with Wallast and Van Gent, always much higher than the calculated damage (an average deviation for all tests of approximately 70%). The parameters that are observed to influence the damage are the water depth, wave height, structure height, structure width and stone size.

Because it seems like more parameters than currently in damage development formulas influence the damage development of a near-bed structure, a deformation analysis is made in this chapter in order to find a new design formula which can calculate the damage within a higher degree of accuracy. For this deformation analysis only the velocity parameter, based on the velocity on the bottom, is used as stability parameter. This is because Wallast and Van Gent [2002] and Van den Bos [2006] already concluded that this parameter was the best stability parameter to describe damage to near-bed structures. This seems not logical choice because in previous paragraphs it was seen that still a lot of difference was present by using the velocity parameter. However, because other stability parameters are likely to have even more differences with the calculated damage these are not investigated. First it is checked which dimensionless parameters might influence the damage development with near-bed structures. After this it is investigated which damage classification should be used and how the velocity parameter should be defined. This analysis is done on all data available including data from other researchers for waves only. This dataset can be seen in Appendix G.

5.2.1 Important parameters

The erosion to a near-bed structure can be described by several parameters. From previous research it is known that it currently includes the number of waves, wave height, wave period, water depth, median stone diameter, relative stone density, and the slope of the structure. However, the wave height, wave period and water depth are implicitly incorporated in the damage development formula. Besides these parameters, still many other parameters might influence the erosion as seen in the previous section. These parameters are the crest height and width of the near-bed structure and water depth and wave height for the hydrodynamic conditions. It was seen that some of these parameters were already incorporated implicitly but these effects were not represented accurately.

To improve the current design formula a large number of parameters is tested. A starting point for this are the dimensionless parameters described in Chapter 2. The parameters that are investigated in this thesis are described below:

Relative structure height It was seen from Figure 5.2 that the structure height was of significant influence in damage development. Saers [2005] linked the influence of the structure height to the flow contraction in the Saers parameter $z_c m_0/a_0$. However, there are many more ways to include the structure height. For instance, the structure height can be added

to the design formula with the water depth above the near-bed structure h_c, or with the actual structure height z_c. This factor can be made dimensionless in a lot of ways. Some examples that are tried are the stone diameter D_{n50}, structure width B_c and wave orbital motion a_0 which again can be defined in a number of ways which was seen with the velocity parameter explained in the next section or Figure 2.9.

Relative structure width While for stone type B the damage in test 5, with the wider near-bed structure, was calculated reasonable if compared by eye, the deviation percentage was still high. Although the width of the near-bed structure has already been imposed by using S^*, it was seen with this deviation percentage that the width still influences the damage development more than expected. Because of this it is investigated if the relative width parameter can give a positive influence in describing the damage development formula. The relative width of the near-bed structure can be described by the crest width B_c or the full width B. The relative structure width can be explained as how the wave feels the width of the structure or how many stones are present in this width. Both of these parameters can be related to the stone diameter D_{n50}, wave length L, orbital wave motion a_0 or water depth h. Maybe not the relative crest width is important, but the total length including the slopes which can be defined as $B_c + 2 \cdot \sqrt{z_c^2 + (m_0 z_c)^2}$. Besides this, the total surface could be of importance. This can be defined as the total cross sectional area divided by for example the stone diameter squared or crest height squared. All of these options are investigated in order to find new parameters which defines the relative width and describes the damage to a near-bed structure in a more realistic way.

Structure slope The slope of the structure was included in the design formula of Van den Bos [2006]. It can be seen as a measure for the fluid motion around the near-bed structure. Because the slope parameter m_0 is already dimensionless, it can be added to a number of parameters. It can for instance be included in the relative height or relative width of the near-bed structure. The structure slope was not changed here in tests because in reality almost always near-bed structures with a 1:3 slope are built. However, because the slope was found as an important parameter by Van den Bos this parameter is investigated as well.

5.2.2 Damage and velocity parameter

The velocity parameter can be described in many ways which was seen in the literature study in Chapter 2. By Van den Bos [2006] it was concluded that the velocity parameter $\theta_{hc1\%}$, which is defined on top of the near-bed structure as if the water depth is everywhere equal to h_c, was the best velocity parameter to describe the velocity on the near-bed structure. However, there are many ways to describe the velocity parameter. The first difference can be where the velocity parameter is described (Figure 2.9). Besides this, there are also several other ways to calculate the velocity parameter which make use of different wave heights and periods. With the use of Battjes and Groenendijk [2000] the wave height $H_{0.1\%}$ and with the use of the method from Holthuijsen [2007] the wave height H_{max} was found. H_{max} can be defined as $H_{max} = 2 \cdot H_s$. Together with the period T_m and T_p a few new forms of the velocity parameters can be calculated. It turned out that the velocity parameter proposed by Van den Bos [2006] is on average 4% better than the velocity parameter proposed by Wallast and Van Gent [2002] by comparing both velocity parameters inside the formula of Van den Bos. The Equation to calculate the velocity for the velocity parameter which Van den Bos proposed is shown in Equation 2.37. For the velocity parameter which make use of H_{max} and $H_{0.1\%}$ together with T_p, differences compared to the velocity parameter from Van den Bos were negligible. H_{max} and $H_{0.1\%}$ together with the mean period T_m actually performed worse than the velocity parameter imposed by Van den Bos. Because of this, from now on the velocity parameter that is described with $H_{1\%}$ (Equation 2.39) and T_p is used in this thesis. It was observed in this analysis that the T_p had a major influence in describing a velocity on the bottom.

$$\hat{u}_{hc\ 1\%} = \frac{\pi H_{1\%}}{T_p} \frac{1}{\sinh(k_c h_c)} \tag{2.37}$$

In literature two definitions are found for describing the damage to near-bed structures, which are shown in Equation 2.18 and 2.40. These are damage numbers where S is more commonly used in research with for example breakwaters. Van den Bos [2006] concluded that S^* works better in describing the damage to near-bed structures than S. This statement is checked in this thesis by comparing both damage numbers with each other including the new data. By using the Curve Fitting Toolbox of Matlab together with the formula of Van den Bos it is found that a better way to describe the damage to a near-bed structure is with the use of S^* rather than S. S^* works 10% better for all the data, and even 23% for all data excluding stones A. This is based on comparing the RMSE and R^2 defined in Appendix I. The differences with the damage development equation from Van den Bos are showed in Figure 5.14 and 5.15 for all data excluding stone type A. Here the difference in fit can be seen very well. Because of this, from this point parameter S^* is used in this thesis to describe the damage to near-bed structures.

$$S = \frac{A_e}{D_{n50}^2} \tag{2.18}$$

$$S^* = \frac{A_e}{B_c D_{n50}} \tag{2.40}$$
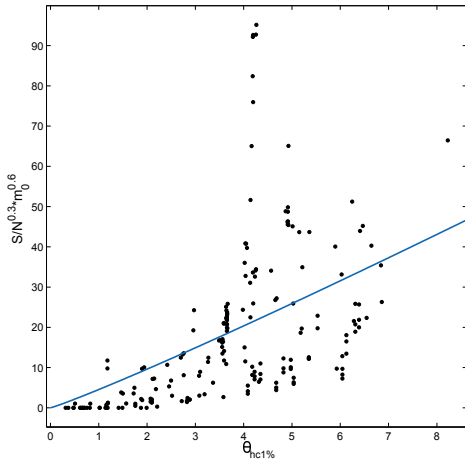
Figure 5.14: S versus $\theta_{hc1\%}$ for the formula from Van den Bos with a best fit of $R^2 = 0.27$.
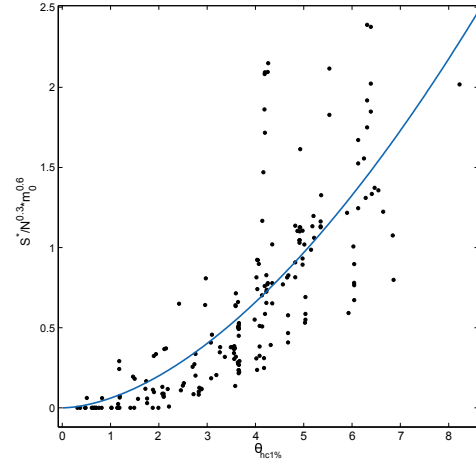
Figure 5.15: S^* versus $\theta_{hc1\%}$ for the formula from Van den Bos with a best fit of $R^2 = 0.63$.

5.2.3 Damage prediction

In the previous paragraph several parameters were described which are important to the damage development of a near-bed structure. In this paragraph it is tried to find a new damage development formula. A general form of this damage development formula is shown in Equation 5.2. In this equation parameters A, a, c, d and e are all random parameters. Parameter b is fixed with the average values found from Table 5.1.

$$S^* = A \cdot (\text{velocity parameter})^a \cdot (\text{N})^b \cdot (\text{relative structure height})^c$$
$$\cdot (\text{relative structure width})^d \cdot (\text{structure slope})^e \tag{5.2}$$

To find a value for these parameters a multivariate linear regression analysis has been performed. Because of this, the general equation first has to be made linear. This can be done by using the natural logarithm. The transformation using the natural logarithm from Equation 5.2 can be seen in Equation 5.3.

$$\ln(S^*) = \ln(A) + a \cdot \ln(\text{velocity parameter}) + b \cdot \ln(\text{N}) + c \cdot \ln(\text{relative structure height})$$
$$+ d \cdot \ln(\text{relative structure width}) + e \cdot \ln(\text{structure slope}) \tag{5.3}$$

From this point a stepwise linear regression analysis on our dataset and the data of other researchers who have tested with waves only is performed. This is done with Matlab which uses the method of least squares. To determine the fit of the model, and if the imposed parameter is a good addition to the model, the coefficient of determination $\bar{R}^2$, RMSE, p-value and Lack-of-fit are used. These values are explained in detail in Appendix I. In general the $\bar{R}^2$ must be as close as possible to 1 and the RMSE must be as small as possible compared to for example the mean value. A p-value determines the probability that the 0-hypothesis is right. The definition of the 0-hypothesis is that no model is better than the imposed model. A p-value can be given for each parameter, and for the total model. So if the p-value is too large (>0.05), the imposed model or parameter is rejected. The lack of fit gives the total lack of fit by the model which should be compared to the total model. A lack of fit is present because there are multiple answers for the same input value which is statistically impossible. This is further explained in the rest of this paragraph.

During the linear regression several points are very important to monitor which are described below. It might be possible that a model with no physical background is obtained. This is possible because several parameters depend on for instance the water depth or wave height. When these parameters are in the formula several times, a good fit can occur but with no physical background behind it.

Including a parameter and lack of fit Including a parameter is based upon the p-test from the regression analysis. A p-value denotes the probability that the model has improved by random data. If this p-value is larger than 5% the introduced parameter is rejected. If this parameter is sufficient, the adjusted $\bar{R}^2$ and RMSE are used to assess if the fit has improved. This was actually always the case compared to the initial formula if the p-value was sufficient. Subsequently, the research continued if there was an even better parameter to describe the damage. In our model there are different velocity parameters for which the measured damage was the same. Because of this, Matlab introduces a lack of fit and a pure error. It is statistically impossible to have two different input values that give the same output. The lack of fit is a good parameter to describe the still present uncernities which are always present in physical scale model testing. Besides this parameter, Matlab also provides a pure error which can be seen as a sort of measurement error. This error should be sufficiently low compared to the total model ($<5\%$).

Physical reality Physical reality is very important in compiling a new formula. As for instance the exponent of the velocity parameter becomes negative, it would mean that there would be less damage with a higher velocity parameter. This is of course not possible. Because of this, every parameter is checked of its physical reality when it is added to the model.

Collinearity The goodness of fit is determined from a linear regression in Matlab with several predicting variables. However, if several of these predicting variables are related or depended on each other, this could unrealistically improve the goodness of fit. If parameters are related to each other it can be determined by collinearity which is obtained by a calculation in Matlab as explained in Appendix I. The condition index which is obtained from this calculation must be lower than 10 which indicates a weak or no collinearity present [Friendly and Kwan, 2009].

From more than 75 combinations of all possible options of the parameters described, the p-values, RMSE, adjusted $\bar{R}^2$ and collinearity have been checked. From this analysis it was found that several parameters could be included in the damage development formula to describe the damage to near-bed structure in a more accurate way. Besides the number of waves and the velocity parameter, it was found that the slope parameter m_0, relative structure width B_c/D_{n50} and relative height parameter a_0/z_c had a significant positive influence on the damage prediction. This formula, with the best fit parameters by a linear regression obtained from Matlab for all data with waves only, is shown in Equation 5.4. In this equation a_0 is represented in the undisturbed situation on depth h with the significant wave height H_s and mean period T_m.

$$\frac{S^*}{N^{0.44}} = 0.0195 \cdot \theta_{hc1\%}^{2.96} \cdot m_0^{-1.05} \cdot \left(\frac{B_c}{D_{n50}}\right)^{-0.39} \cdot \left(\frac{a_0}{z_c}\right)^{-1.05} \tag{5.4}$$

From this equation several observations can be made. The exponent of the slope parameter is negative, which indicates that the damage reduces when the slope flattens out. This is very logical as the contraction of the streamlines becomes less which can be seen in Figure 5.16. The exponent of the relative width is negative as well. This means that if the width increases, the damage reduces. It also means that if the D_{n50} increases, the damage increases. This is not the case because the D_{n50} is also present in the velocity parameter which is more important than the relative width parameter. The next parameter is a parameter that describes how much the undisturbed movement is influenced by the near-bed structure, which is called the relative height parameter. Because in the undisturbed bottom movement a near-bed structure is placed with a specific height, this movement is influenced by the near-bed structure which then influences the damage accordingly. This process is visualised in Figure 5.16. The exponent of the relative height parameter is also negative, which indicates that if the height of the near-bed structure increases, the movement is disturbed more so more damage occurs. The undisturbed movement also depends on the velocity parameter although calculated with a different period and wave height. This is why the exponent of this parameter suggests that if the movement increases, the damage reduces. This is again not the case because the velocity parameter changes as well.
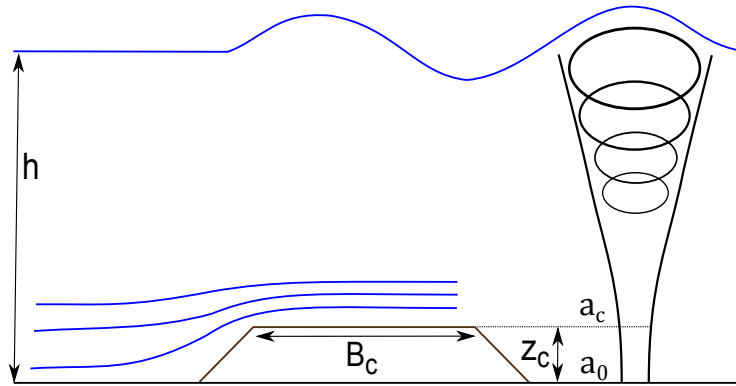
Figure 5.16: Influence of slope and relative height.

In literature a bottom protection or a statically stable near-bed structure is calculated using Shields or Isbash (see Appendix B). When a slope is included in the design an extra parameter

has to be added which represents the increase in velocity present on the slope. This parameter can be described by a extra destabilizing component of the weight along the slope and the weight perpendicular to the slope. This parameter is defined as a strength reduction factor and is represented by $\sqrt{1 - \sin^2(\alpha)/\sin^2(\phi)}$ [CIRIA, 2007]. In this α is the slope of the near-bed structure and ϕ is the angle of repose. This is the angle of friction and can be defined as the maximum angle when stones are still stable on a slope. This parameter is different from the parameter m_0 that this is just the slope of the structure, which induces contraction of flow. It was tried to fit this well known increase in velocity into the formula instead of the slope parameter m_0. Unfortunately this parameter seemed to work less than the slope parameter m_0. Because of this, this reduction parameter is not inserted into the equation instead of m_0.

From a literature study on the relative height parameter, it turned out that this parameter is already used in hydraulic engineering. This parameter is used to determine the forces and scour around vertical piles in water. This factor is called the Keulegan-Carpenter number and is represented in Equation 5.5 [Sumer et al., 1992]. In this equation u_0 is the velocity calculated with linear wave theory on the bottom and with H_s, T_m and D which is the diameter of the pile. The parameter found by this analysis and the Keulegan-Carpenter number differs a constant factor of 2π with each other. Because of this, the Keulegan-Carpenter number divided by 2π from now on is used to represent the relative height parameter. Instead of flow around the diameter of the pile, it is now the flow across the height of the near-bed structure. Because of this, not the diameter from the pile the height is used but the height of the near-bed structure z_c which is shown in Equation 5.6.

$$Kc = \frac{u_0 T_m}{D} = \frac{a_0 \cdot 2\pi}{D} \tag{5.5}$$

$$\frac{Kc}{2\pi} = \frac{a_0}{z_c} \tag{5.6}$$

From Equation 5.4 it can be seen that the exponent from the slope and the relative height parameter are the same. This means they can be joined together into one parameter. The parameter that can be obtained from this is $m_0 \cdot \frac{Kc}{2\pi}$. An interesting observation from this is that this parameter is very close to the Saers parameter found in the literature study. This comparison can be seen in Equation 5.7. The difference is that the slope m_0 has changed position in the relative height parameter found in this thesis. Saers [2005] explains his parameter as in how much width the streamline contraction occurs. The parameter found in this thesis describes how much the undisturbed bottom velocity which is increased by the width of the structure, is influenced by the height of the structure. If the slope increases, the undisturbed bottom movement becomes larger in this parameter and is therefore less influenced by the height of the near-bed structure. Because the exponent of this relative height parameter is negative, it means that less damage occurs. Because the streamline contraction is influenced more by the height of the structure than by the width of the slope, it is concluded that the relative height parameter which is imposed in this thesis represents the actual processes more realistic than imposed by Saers. A total comparison cannot be made with Saers his parameter because he does not give an exponent or an 'best fit'. By comparing the results of the statistical parameters it was concluded again that the relative height parameter in this thesis improves the fit more than the Saers parameter.

$$Sa = \frac{z_c m_o}{a_0} \neq \frac{z_c}{m_0 a_0} \tag{5.7}$$

The total best-fit formula which includes all parameters described in previous paragraphs can be described as Equation 5.8 for all the data and as Equation 5.9 for all the data without stone type A. The 2π which was showed together with the Keulegan-Carpenter number has been processed in the constant which was called parameter A in Equation 5.2. All the statistical data which includes

p-values per parameter, p-values of the total model, RMSE and R^2 values of these formulas can be found in Appendix I. Some of these parameters are described in the remainder of this paragraph for comparisons.

$$\frac{S^*}{N^{0.44}} = 0.134 \cdot \theta_{hc1\%}^{2.96} \cdot \left(\frac{B_c}{D_{n50}}\right)^{-0.39} \cdot (m_0 \cdot Kc)^{-1.05} \tag{5.8}$$

$$\frac{S^*}{N^{0.37}} = 0.238 \cdot \theta_{hc1\%}^{2.69} \cdot \left(\frac{B_c}{D_{n50}}\right)^{-0.40} \cdot (m_0 \cdot Kc)^{-0.90} \tag{5.9}$$

These equations can be calculated with Equations 2.36, 2.37, 2.39 and 2.38. For the Keulegan-Carpenter number the dispersion relation and orbital velocity should be calculated on depth h with H_s and T_m in the undisturbed situation. The total range for Equation 5.8 and 5.9 is shown in Table 5.2 for these tests and includes the ranges from other researchers.

$$\theta_{hc\ 1\%} = \frac{(\hat{u}_{hc\ 1\%})^2}{g\Delta D_{n50}} \tag{2.36}$$

$$u_{hc\ 1\%} = \frac{\pi H_{1\%}}{T_p}\frac{1}{\sinh(k_c h_c)} \tag{2.37}$$

$$H_{1\%} = H_s \frac{\sqrt{\frac{1}{2}\ln(100)}}{\sqrt[3]{1+\dfrac{H_s}{h}}} = H_s \frac{1.52}{\sqrt[3]{1+\dfrac{H_s}{h}}} \tag{2.39}$$

$$\frac{2\pi}{T_p} = \sqrt{gk_c\tanh(k_ch_c)} \qquad \text{Local dispersion relation} \tag{2.38}$$

	Parameter	Symbol	Minimal Range			Maximum range		
			Eq. 5.8	Eq. 5.9	Old	Old	Eq. 5.8	Eq. 5.9
Model	Stone diameter [mm]	D_{n50}	1.50	3.35	1.90	–	8.33	1.50	3.35
parameters	Stone shape [-]	–	irregular	irregular	Round	angular	irregular	irregular	irregular
	Stone density [kg/m]	ρ_s	2679	2691	2463	–	2800	2679	2691
	Relative density [-]	Δ	1.68	1.69	1.46	–	1.80	1.68	1.69
	Wave height [m]	H_s	0.142	0.142	0.07	–	0.29	0.172	0.172
	Wave period [s]	T_m	1.58	1.58	0.85	–	2.10	1.78	1.78
	Water depth [m]	h	0.40	0.40	0.375	–	0.900	0.45	0.45
	Structure crest width [m]	B_c	0.15	0.15	0.04	–	0.25	0.3	0.3
	Structure slope [-]	$1:m_0$	3	3	1	–	8	3	3
	Structure height [m]	z_c	0.10	0.08	0.03	–	0.26	0.10	0.13
Dimensionless	Velocity parameter	θ_{hc}	3.60	1.52	0.16	–	3.61	5.35	2.37
parameters	Wave height	H_s/h	0.355	0.355	0.14	–	0.50	0.38	0.38
	Wave steepness	s_m	0.034	0.034	0.028	–	0.071	0.036	0.036
	Wave length	L/h	6.35	6.35	2.76	–	13.95	6.91	6.91
	Number of waves	N	10935	17227	900	–	6500	31703	31703
	Relative structure height	h_c/h	0.79	0.79	0.63	–	0.97	0.78	0.71
	Relative structure height 2	z_c/D_{n50}	55.87	24.54	8.17	–	40.32	66.67	38.81
	Relative structure width	B_c/L	0.059	0.059	0.0087	–	0.12	0.10	0.10
	Relative structure width 2	B_c/D_{n50}	10	4.48	10.81	–	48.74	20.00	8.96

Table 5.2: Current test ranges of all research done on near-bed structures.

In Figure 5.17 and 5.18 the Equations are shown together with their data. This is the best fit for all the data on which the formula is based. In the rest of this thesis the name 'Other + A + B' indicates that all data is used together with all the data of other researchers (Lomónaco, Wallast and Van Gent, Saers and Tørum). 'Other + B' indicates that all data is used from each researcher

together with data from stone type B. The difference between both equations is that Equation 5.8 predicts a little higher damage than Equation 5.9. Especially in the higher regions of the velocity parameter more damage is calculated. This is because of more observations are present in the higher region of the velocity parameter where the formula is also fitted upon.

The relative width parameter (B_c/D_{n50}) is present twice in Equation 5.8 and 5.9 because it is also implicitly incorporated in S^*. The damage number S^* can be rewritten into S with the use of Equation 2.41 which can be seen in Equation 5.10 and 5.11. The exponent of the relative width parameter changes from negative to positive in this transformation which means that if the width increases, the damage S increases as well. Besides this, if the median diameter increases the damage would decrease because of this parameter as well. This is contrary to what was observed with the damage number S^*. If the width increases here, less damage is observed. This is because of the different definition of both damage numbers because in both cases the same erosion area A_e can be calculated. This also reveals the problem of S^*. If the width is extremely large, less damage is calculated than would be expected. Because of this, a real near-bed structure needs to be in the dimensionless parameters described in Table 5.2. Because S^* can also be used to determine which state of damage development is present (Table 2.6), this damage number is used in the remainder of this thesis.

$$S^* = S \cdot \frac{D_{n50}}{B_c} \tag{2.41}$$

$$\frac{S}{N^{0.44}} = 0.134 \cdot \theta_{hc1\%}^{2.96} \cdot \left(\frac{B_c}{D_{n50}} \right)^{0.61} \cdot (m_0 \cdot Kc)^{-1.05} \tag{5.10}$$

$$\frac{S}{N^{0.37}} = 0.238 \cdot \theta_{hc1\%}^{2.69} \cdot \left(\frac{B_c}{D_{n50}} \right)^{0.60} \cdot (m_0 \cdot Kc)^{-0.90} \tag{5.11}$$

In reality mostly structures are designed with low velocity parameters ($\theta_{hc1\%} < 3$) and consequently low damages. Because of this, Figure 5.18 is zoomed in for low velocity parameters in Figure 5.19. In these scale model tests no tests have been performed which resulted in low velocity parameters. It can be seen that the general fit is rather good but most observations are below the formula. To compare this fit on the lower velocity parameters in Figure 5.20 the formula of Van den Bos is showed for these same velocity parameters. A visual observation reveals that the equation of Van den Bos generally calculates a lower damage on low velocity parameters. However, much more observations are above the fit for Van den Bos his formula. This means that the uncertainty is larger and more damage can easily be present in real situations. Further on in this chapter the statistical results on the low velocity parameters are described.
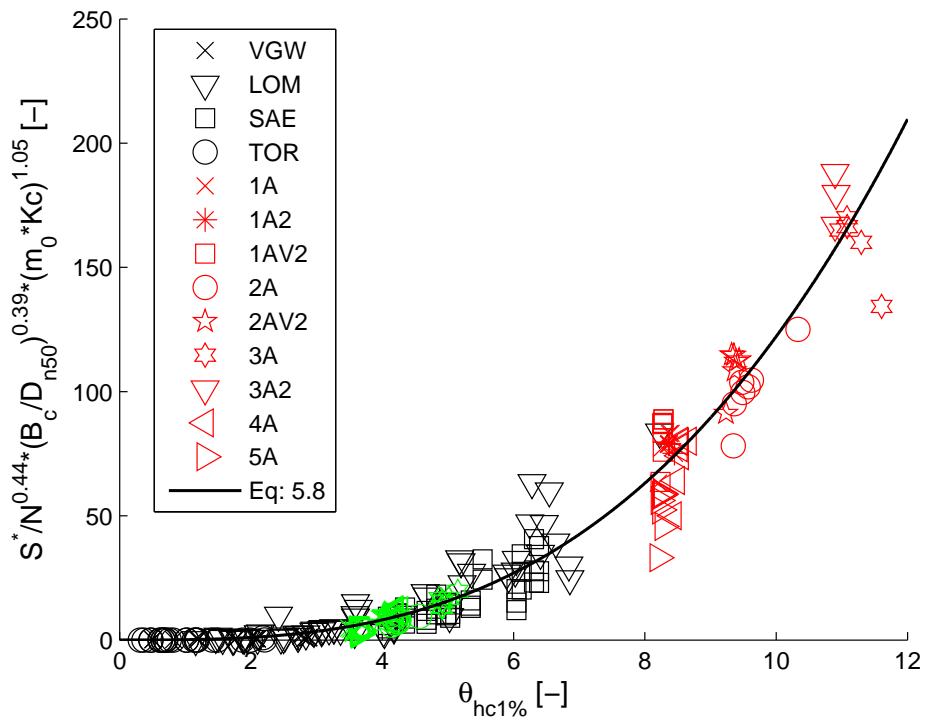
Figure 5.17: Equation 5.8 with all data.
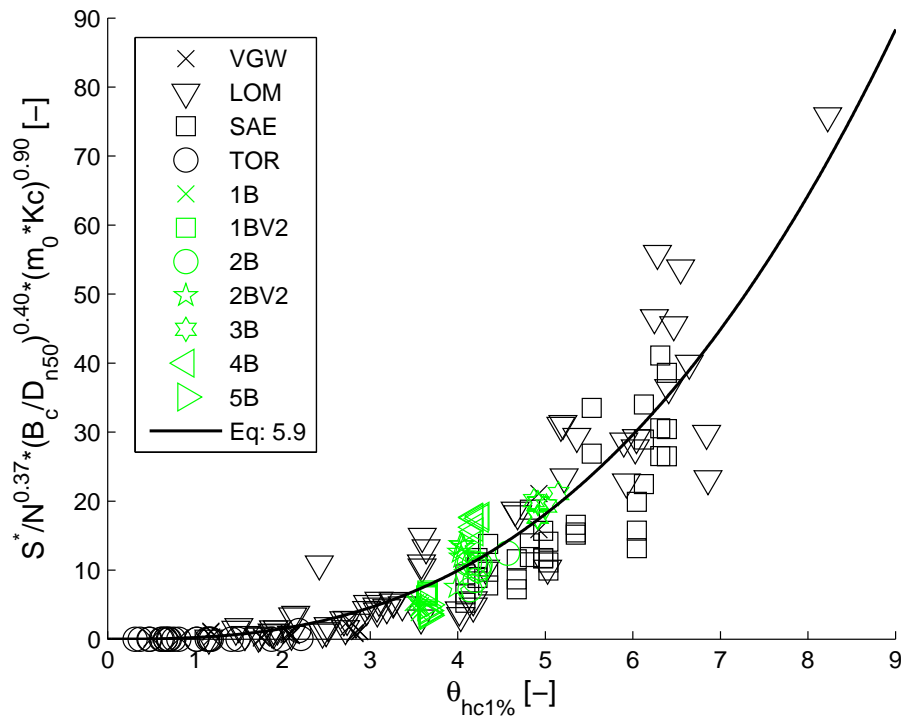
Figure 5.18: Equation 5.9 with all data except stone type A.
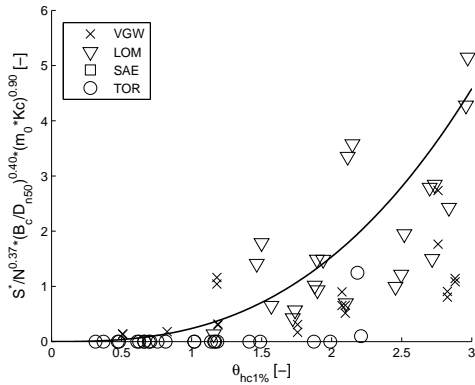
Figure 5.19: Equation 5.9 for low velocity parameters.
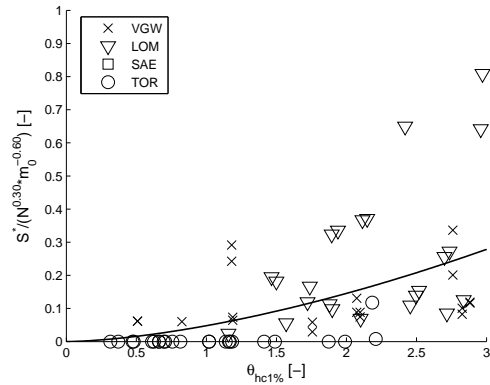
Figure 5.20: Equation 2.35 from Van den Bos [2006] for low velocity parameters.

Statistics of new equations

In Table 5.3 the RMSE of the actual damage calculation, R^2 of the actual damage calculation and the R^2 of the logarithmic calculation are shown. The logarithmic calculation is used here as well because this is also used by Van den Bos to compare his results. From this table and from Tables I.4 and I.5 in Appendix I it can be concluded that the fit for both formulas found in this thesis are rather good. The RMSE is for Equation 5.8 higher than for Equation 5.9 because more data in the higher region of the velocity parameter are present and the scatter is higher in this case. Because of this the RMSE is showed relative to the mean error as well to get a indication of its magnitude and to compare the RMSE to other formulas. The R^2 is higher for equation 5.8 because stone type A strengthens the fit in the higher regions of the velocity parameter. From Table I.2 it is known that a high fit is present if $R^2 > 0.7$ which is the case for both equations.

	Dataset	RMSE	Perc. relative to mean	R^2 (REAL)	R^2 (LOG)
Eq: 5.8	Other + A + B	3.33	25%	0.97	0.88
Eq: 5.9	Other + B	1.91	48%	0.80	0.73

Table 5.3: Determination of fit from Equation 5.8 and 5.9.

To really determine if this formula is better than other equations for damage development present in literature, comparisons need to be done with these formulas to the datasets which other researchers have used. In this way the new obtained formulas can be compared to formulas obtained by other researchers.

In Table 5.4 the comparison from Equation 5.8 and 5.9 with the formulas from Wallast and Van Gent [2002] and Van den Bos [2006] can be seen. From this table it can be concluded that the formula from Van den Bos has a lower RMSE and can calculate the damage to a higher degree of accuracy than the formula by Wallast and Van Gent. Besides this, a conclusion can be made that the formulas obtained in this thesis have a lower RMSE than both Wallast and Van Gent and Van den Bos. The obtained formulas also work better for the dataset Van den Bos used in his thesis. This can be seen from the percentage of the RMSE which is lower in both cases for the equations found in this thesis. Besides the RMSE, the R^2 is higher too for the real situation and for the logarithmic situation.

A closer investigation of Table 5.4 shows that the that the real R^2 changes more than the logarithmic R^2. Compared with the logarithmic R^2 Equation 5.8 and 5.9 improved slightly by looking at the dataset of Lomónaco, Van Gent and Wallast and Saers. However, this might be because the

Formula	Dataset	RMSE	Perc. relative to mean	R^2 (REAL)	R^2 (LOG)
VDB	Other + A + B	18,48	140%	0,22	0,70
VGW	Other + A + B	1911,00	161%	0,31	0,57
VDB	Other + B	3,37	84%	0,38	0,67
VGW	Other + B	144,10	117%	0,29	0,42
VDB	LOM, VGW, SAE	2,23	62%	0,53	0,70
VGW	LOM, VGW, SAE	72,38	113%	0,33	0,38
Eq: 5.8	LOM, VGW, SAE	1,77	49%	0,71	0,72
Eq: 5.9	LOM, VGW, SAE	1,74	48%	0,73	0,72

Table 5.4: Comparison between formulas for different datasets.

formulas found in this thesis were not fit on this data. The real R^2 shows considerable improvement which was also seen by the RMSE in previous paragraph. It can be seen that the logarithmic R^2 for Van den Bos is 0.67 for the dataset Other+B while for the complete dataset this is higher which is probably because more data is present.

In Table 5.5 the statistical results for lower velocity parameters are shown. In real situations mostly near-bed structures are constructed with lower damage and consequently lower velocity parameters. Because of this the statistical results for velocity parameters $\theta_{hc1\%} < 3$. As was seen in Figure 5.19 and 5.20 the fit for Equation 5.9 is a little lower than the formula of Van den Bos. However, there is more spreading in the formula of Van den Bos and a lot of the observed damages are larger than calculated (see Figure 5.20). A general conclusion is that the fit for both formulas has a very low fit for velocity parameters smaller than 3. This can be linked to the observation that in the initial conditions randomness in damage development is present. Because of the low velocity parameter and consequently low damage, not much extra damage can be expected after the damage that occurred due to randomness. Concluded can be that if a near-bed structure is designed for low velocity parameters a safe confidence bound needs to be taken because damage cannot be calculated to a high degree because of randomness. The formula of Van Gent and Wallast again has a much larger deviation than the other formulas.

Formula	Dataset	RMSE	Perc. relative to mean	R^2 (REAL)	$\bar{R}^2$ (LOG)
JVDB	$\theta_{hc1\%} < 3$	0.73	114%	0.35	0.04
VGW	$\theta_{hc1\%} < 3$	25.36	151%	0.00	0.00
Eq: 5.9	$\theta_{hc1\%} < 3$	0.76	118%	0.31	0.02

Table 5.5: Determination of fit for low velocity parameters.

From these tables and the work done by Van den Bos [2006] in his thesis, it can be concluded that the damage prediction formula from Van den Bos works better than the damage prediction formula from Wallast and Van Gent [2002]. Because of this no comparisons are made to their formula any more but only to the formula of Van den Bos.

Another way to compare the data from both formulas is to calculate with the measured damage the exact parameter A from Equation 5.2. In this way the variance within the formulations can be visualised by using a box plot. In Figure 5.21 a box plot can be seen from Equations 5.8 and 5.9 compared to the damage development formula by Van den Bos and divided by the 'best fit' parameter A to compare the formulations. Here LGS represents the dataset from Lomónaco, Van Gent and Wallast and Saers which Van den Bos used in his thesis. In this box plot the box represents 50% of the data while the whiskers represent a 25% and 75% confidence bound which then extends to the nearest value. The red plus signs represent outlying data while the red line represents the median value. For Equations 5.8 and 5.9 the median is exactly the parameter A, which is why the red line is placed on exactly 1. For the equation of Van den Bos with his dataset, this is not the case which could be because of rounding errors. It can be seen that the variances

in both Equation 5.8 and 5.9 are lower than in the Equation from Van den Bos. This means that the spreading is lower and thus the damage can be calculated to a higher degree of accuracy. Especially the dataset where Van den Bos designed his formula on (indicated by LGS in the box plot) can be used to compare both equations. It can be seen here that both Equation 5.8 and 5.9 have a lower variance present because of the size of the box plot. The variances in the equations obtained in this thesis are in the same order of magnitude.
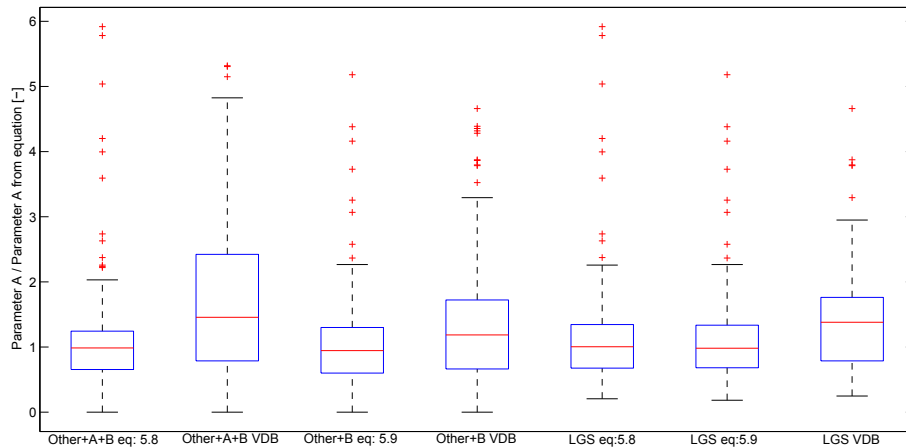
Figure 5.21: Box plot of the variability of parameter A (Equation 5.2) relative to Van den Bos. LGS indicates the dataset from Lomónaco, Van Gent and Wallast and Saers.

Performance formulas on physical scale model tests

In Figure 5.22 and 5.23 the measured versus the calculated damage for both obtained formulas is shown. In Figure 5.22 it can be seen that for high regions of measured damage Equation 5.8 under predicts the damage. For the lower regions the damage is a little over predicted. In total this equation calculates the damage to a higher degree of accuracy than then damage development formula from Van den Bos. From this figure it can be concluded that the more damage is observed, the higher the deviations in damage occur relative to damage development equation. Because in reality a near-bed structure is never made which allows this much damage, the first concern are the lower regions of damage. In Figure 5.23 the average trend of the calculated damage by Equation 5.9 is relatively good. For test 4B, the test with the extra high near-bed structure, the calculated damage is significantly lower than the measured damage. This should be an indication that a high near-bed structure behaves in a different way and might not be applicable as a near-bed structure. When designing a high near-bed structure this should be kept in mind.

For the tests done in this thesis the measured damage and calculated damage versus the number of waves are shown in Figure 5.24 and 5.25. A first observation is that the calculated damages for stone type A and B are calculated to a higher degree of accuracy than the formula of Wallast and Gent and Van den Bos did. A more detailed investigation reveals that the damage for stone type A is calculated very accurately with on average only 13% deviation between the measured and calculated damage. Test 2A was calculated the most accurate with an average deviation of only 6%. Test 5A, with the wide near-bed structure has the largest deviation with on average 30% difference between the measured and calculated damage.

For stone type B in Figure 5.25 the average deviation from all the tests between the measured and calculated damage is 30%. From a visual observation it can be seen that apart from test
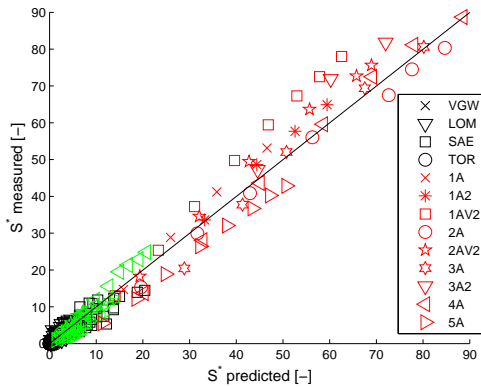
Figure 5.22: S^* measured versus calculated for all data with Equation 5.8.
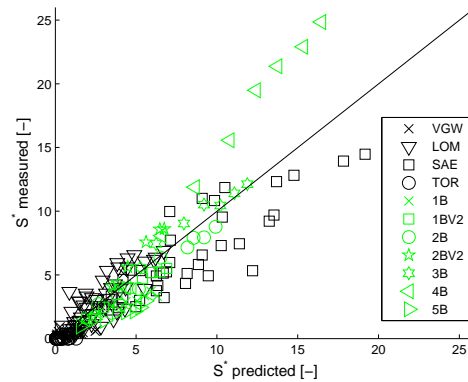
Figure 5.23: S^* measured versus calculated for all data with Equation 5.9.
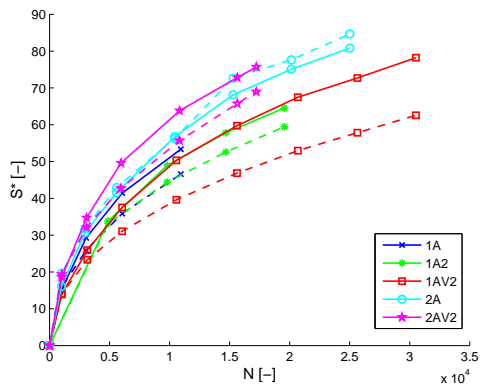
Figure 5.24: Stone type A measured (solid) and calculated (dashed) damage with Equation 5.8.
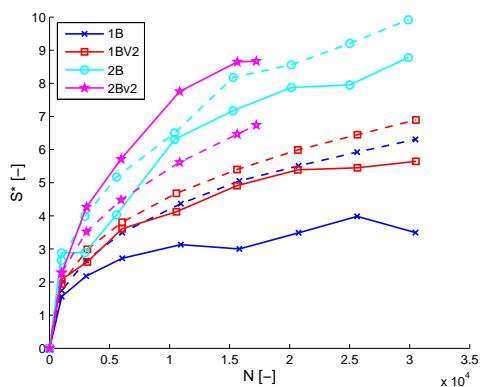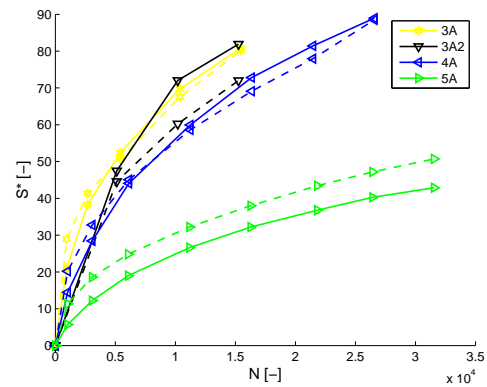
Figure 5.25: Stone type B measured (solid) and calculated (dashed) damage with Equation 5.9.
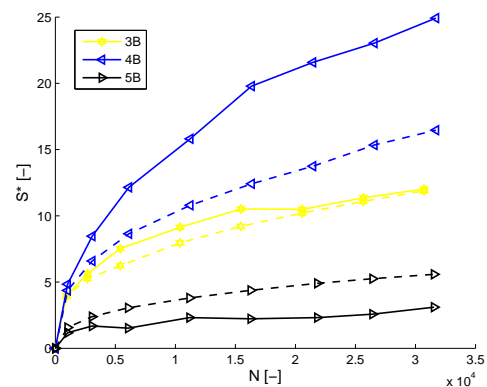
1B and 4B the damage is calculated to a high degree of accuracy. The differences between the measured and calculated damage where for these tests respectively 45% and 30%. However the largest deviation was for test 5B because low damage occurred here. The deviation was here on average 75%. The lowest deviation was found for test 3B with only 7%.

Confidence interval

In this section the confidence bounds of Equation 5.8 and 5.9 are determined. Confidence bounds are bounds for which only a certain percentage of observations is above. for example a 95% confidence bound means that only 5% of the data is above this bound and thus can be seen as a 'safe' parameter to design a near-bed structure.

The confidence bounds of 5% and 95% from both equations are obtained by the regression analysis in Matlab as well. All the unknown parameters for Equation 5.12 are shown in Table 5.6. From a comparison between the two formulas it can be concluded that Equation 5.8 calculates a higher damage for the higher regions of the velocity parameter. In the lower regions of the velocity parameter both formulas calculate approximately the same damage.

$$\frac{S^*}{N^b} = A \cdot \theta^a \cdot \left(\frac{B_c}{D_{n50}}\right)^c \cdot \left(m_0 \cdot \frac{Kc}{2\pi}\right)^d \tag{5.12}$$

Confidence bounds	Parameter	5%	50%	95%
Equation 5.8	A	0.130	0.134	0.138
	a	2.75	2.96	3.17
	b	0.44	0.44	0.44
	c	-0.51	-0.39	-0.27
	d	-1.24	-1.05	-0.86
Equation 5.9	A	0.215	0.238	0.2623
	a	2.38	2.69	3.00
	b	0.34	0.34	0.34
	c	-0.55	-0.40	-0.25
	d	-1.14	-0.90	-0.66

Table 5.6: Confidence bounds for coefficients calculated by Matlab.

Because in this method all parameters change, this is a rather difficult method. It would be easier to only change parameter A and by changing this parameter giving the 5% and 95% confidence bounds. By analysing the obtained data for calculating each parameter A, it was found that a normal distribution was the closest to the available data. For this conclusions all available distributions have been determined and how well parameter A would fit this distribution was checked by eye. In Figure 5.26 it can be seen that for both equations parameter A is almost normally distributed. The plus signs are the data while the dotted line is the theoretical normal distribution. From this distribution the 5% and 95% confidence bounds can be calculated as well by $1.96 \cdot \sigma \pm B$. Here is B the coefficient calculated by the linear regression or the median from A. However, in this thesis the results are obtained from the graph shown in Figure 5.26 with an assumption of a totally normal distributed sample. The results from this can be seen in Table 5.7. Here 95% of the data lies above and 95% of the data lies underneath the lower and upper bound and thus represents the 90% confidence interval. Because only parameter A changed in this analysis it is much easier to calculate these confidence bounds.

Confidence bounds	5%	50%	95%	σ_A
Equation 5.8	0.0524	0.1340	0.1962	0.0919
Equation 5.9	0.0908	0.2376	0.3582	0.1397

Table 5.7: Simplified confidence bounds for parameter A.
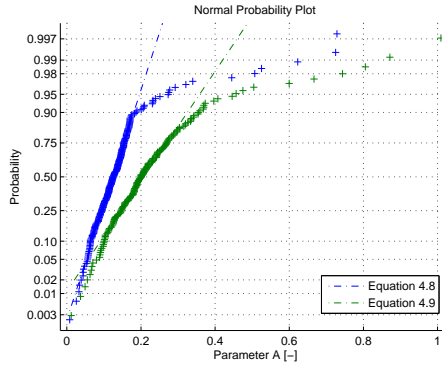
Figure 5.26: Probability plot for parameter A.

From Table 5.7 the 90% confidence interval with the data for both formulations can be seen in Figure 5.27 and 5.28. It can be observed from these figures that the lower bound is further of the 'best fit' than the upper bound.
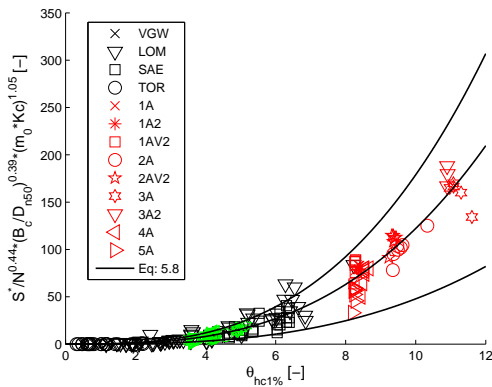
Figure 5.27: Confidence interval for Equation 5.8. The top line is the 95% and the bottom line the 5% confidence bound.
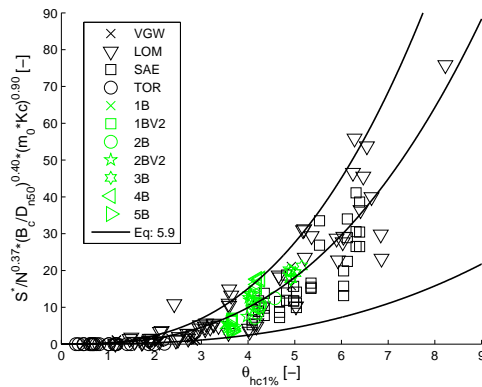
Figure 5.28: Confidence interval for Equation 5.9. The top line is the 95% and the bottom line the 5% confidence bound.

The final step is to link the low velocity parameters where most near-bed structures are designed upon to the confidence bounds. In Figure 5.29 the confidence bound for low velocity parameters for Equation 5.9 is shown. It can be seen that the lower bound is further below the 'best fit' than the upper bound is above this 'best fit'. This confidence bound can be compared to the confidence bound of Van den Bos [2006] which can be seen in Figure 5.30 ($A = 0.02$ for the 5% bound and $A = 0.12$ for the 95% bound). A first observation for this is that the lower confidence bound of the formula of Van den Bos is further below the 'best fit' than the upper bound is above this fit. Besides this, it can be observed that the confidence bound of Van den Bos has more data inside but it also seems that this confidence bound is larger than for Equation 5.9. If this is actually the case is investigated by the tests with multiple storms further on in this chapter. This concludes the investigation into a better damage prediction method that presently available in literature.
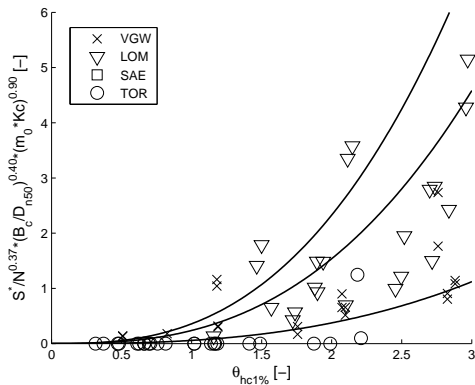
Figure 5.29: Confidence interval for Equation 5.9 with low velocity parameters. The top line is the 95% and the bottom line the 5% confidence bound.
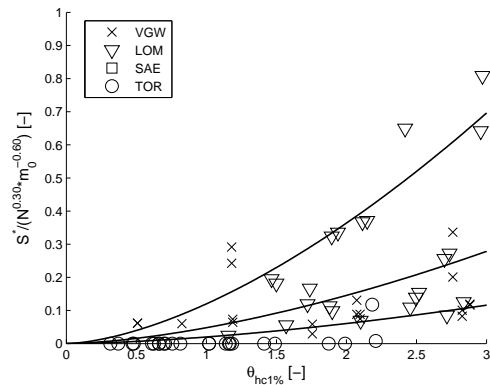
Figure 5.30: Confidence interval for Equation 2.35 from Van den Bos [2006] with low velocity parameters. The top line is the 95% and the bottom line the 5% confidence bound.

Accuracy

With the newly obtained formulas and confidence bounds, the measurement errors are investigated which have been described in Chapter 4. In the best case the measurement errors would be inside the confidence bounds of the obtained formulas. If this is the case, the confidence bounds can be used to take the measurement errors into consideration.

For the determination of the measurement errors which are present all measurement errors described in Table 4.6 are used. In Figure 5.31 and 5.32 the velocity parameter and damage divided by the formula are shown for Equation 5.8 and 5.9. The error in the velocity parameter is mostly depended on the variation in the wave height and wave period while the error on the Y-axis is mostly because of differences in the erosion area. In Figure 5.31 the measurements in the higher region of the velocity parameter are all for stone type A. It can be seen that most of the errors are inside the confidence bounds of the obtained formula and only small ranges outside the confidence bounds are possible. Note that the error bounds are the maximum possible deviation and the actual error might be much smaller than this maximum. The maximum value for the velocity parameter is 15% smaller and 18% larger than the obtained parameter. For the Y-axis with Equation 5.8 the maximum value is 23% smaller and 11% larger. From this it can be concluded that this error is almost entirely due to measurement errors from the erosion area.

For Figure 5.32, which is only for stone type B, it can be seen that for tests 4B the 'best fit' measurement is already on the confidence bound. Together with the measurement error the actual position of this test in the graph can be different. For the other tests the measurement errors are observed to be mostly inside the confidence bounds and would thus not effect the outcome of the result. The maximum value for the velocity parameter is 15% smaller and 18% larger than the obtained parameter. For the Y-axis with Equation 5.9 the maximum value is 23% smaller and 11% larger.

From these figures it can be concluded that measurement errors from the physical scale model test influence the results. For the obtained formulas the actual results are used without including these measurement errors. For this thesis it is considered that the confidence bounds obtained for Equation 5.8 and 5.9 are a good approximation to include measurement errors. Further on in this thesis are because of this only the confidence bounds used to classify the uncertainty and errors in measurements. If single test results are used these uncernities have to be taken into consideration.
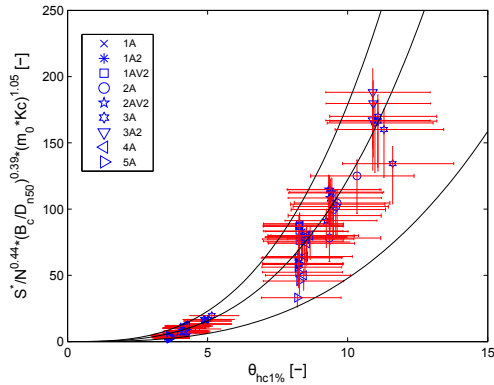
Figure 5.31: Confidence interval for Equation 5.8 with error bounds. The top line is the 95% and the bottom line the 5% confidence bound.
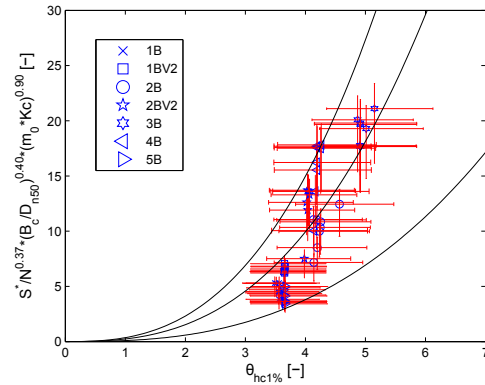
Figure 5.32: Confidence interval for Equation 5.9 with error bounds. The top line is the 95% and the bottom line the 5% confidence bound.

Conclusions

The relation between the number of waves and the damage that occurs is clear. The time dependency shows two different stages. In the first 1000 waves the erosion is very strong and subsequently the damage development seems to reduce. Rounding of crest corners and lowering of the crest is the most observed damage. The time dependency of damage on the number of waves N is not one parameter as assumed in previous research. This parameter turned out to be far but constant for each test that has been executed. It is observed in this thesis that this parameter is depended on (1) the damage that occurs after 2000 waves, (2) the wave height, (3) the mean stone size and (4) the water depth. A good relation between these parameters was never found and thus the average of the parameter b is implemented in this thesis.

It was found that the deformation in time was influenced by several factors which were not present in current design formulas. The parameters that were found to influence the deformation of a near-bed structure are the water depth, wave height, structure height, structure width and stone size. By trying to include these parameters into the design formula two extra parameters came to light which are not present in current damage development formulas. The first parameter, B_c/D_{n50} seemed to strengthen the fit. This parameter can be seen as the amount of stones present on the crest of a near-bed structure. If the width increases, the damage reduces. The next parameter which was found is the Keulegan-Carpenter number multiplied by the slope of the near-bed structure and divided by 2π. This parameter can be seen as the amount of which the undisturbed oscillatory movement on the bottom is influenced by the height and slope of the near-bed structure. The diameter in the Keulegan-Carpenter number should be changed to the structure height z_c of the near-bed structure. From this analysis Equation 5.8 and 5.9 were found. For both equations the RMSE and variations were lower than for previous damage development formulas.

To compare all formulas with each other a fictional 'real case' scenario is described in Appendix J. In this scenario a fixed amount of damage is allowed and accordingly a median stone diameter has to be determined for which no more damage than a certain limit occurs. To make sure this limit is not exceeded, the confidence interval of all equations is used as well. Because of the smaller confidence bounds of Equation 5.8 and 5.9 the calculated stone diameter was significantly lower compared to the formula of Wallast and Van Gent [2002] and Van den Bos [2006]. For a real case scenario this reduction in stone diameter can reduce the costs of rocks considerable. The total calculations and analysis on this can be seen in Appendix J.

5.3　Multiple storms

A main part of this thesis is to investigate the damage during multiple storms. Nowadays, nothing is known about the stability of stones in near-bed structures during several storms. From the physical scale model tests it is analysed what happens to near-bed structures when the wave conditions vary. Does the near-bed structure armour itself against damage so that in a lower storm condition no movement of stones occurs, or does the movement of stones just reduce? In the physical scale model tests this has been tested by test 6, 7 and 7v2 which have only been executed for stone type B. Test 7 has been repeated because in this test the wave generator broke down. In this paragraph the influence of multiple storms on the stability of near-bed structures are explained through the model tests that have been executed for this purpose. This section continues from the observation during these tests from Chapter 4.

To make a more accurate comparison of the observations from test 6, 7 and 7v2, the damage is showed against the number of waves which can be seen in Figure 5.33. The bar above represents the conditions for test 7v2 and the bar below the test represents test 6. The wave conditions during these tests can be seen in the table next to this figure. A first observation is that the damage for test 7 and 7v2 are not exactly the same but very similar. This indicates that no large errors have been made during the testing and similar damage development occurs. After the first wave condition the damage from test 6, 7 and 7v2 is very similar which is expected because the same wave condition are present in these tests. In tests 6 the damage in each wave condition developed as was already seen from the relative profile. In test 7v2 the damage development stops after wave condition four, with the highest waves, and continues again in wave condition eight.

Condition	T6 H_s [cm]	T7v2 H_s [cm]
1	9.28	9.39
2	11.11	13.79
3	12.90	15.99
4	14.65	18.02
5	16.24	13.72
6	17.22	15.97
7	18.01	13.73
8		17.93
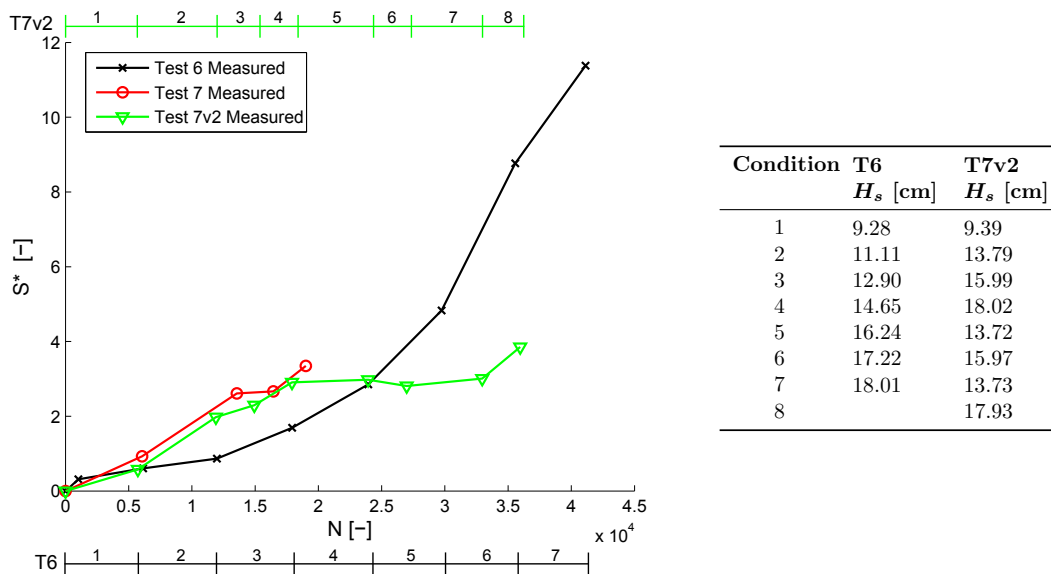
Figure 5.33: Damage for test 6, 7 and 7v2 against the number of waves with above and below a bar where the storm conditions are shown. In the table the H_s is shown for each condition in test 6 and 7v2.

A closer examination of Figure 5.33 reveals that in the first three wave conditions of test 6 the damage development is approximately constant if the first 1000 waves are not included. This can especially be observed well in Figure 5.34. After the third wave condition the damage development starts to increase where in condition seven the damage development slightly reduces again. Because the velocity parameter was increased with 11% relative to the previous condition, it can be concluded that some armouring is present because the damage development reduces with a higher velocity parameter. An observation is that this happens from an S^* of approximately 8. A

comparison with the previous section, where many waves were investigated, is that approximately the same damage was observed for test 3 with the highest wave conditions.

For test 7v2 it can be seen that the damage development reduces slightly after the second wave condition, which can also be seen in Figure 5.35. This is not to be expected because the wave height increases in this condition. However, in test 7 roughly the same was seen where only very minor damage occurred. This makes us wonder what really changed in comparison with the second condition in test 7v2. The third condition had only 3000 waves where the second condition had 6000 waves present. The H_s changed with about 2 cm which could be too small. A visual observation from this test confirms that stones were moving. Because stones were moving, it can be concluded that only minor reshaping of the structure was done and because of the limited number of waves not a lot of stones were transported downstream. In the fourth wave condition, which is the heaviest in this test, damage developed again as expected in both tests. In the fifth, sixth and seventh condition for test 7v2, which are all lower wave conditions than condition four, the damage did not develop any further and only very minor stone movement was observed. In the sixth condition it can be seen that the damage reduces in relation to earlier conditions. As said before in this thesis, this damage reduction is actually possible. Stones in the near-bed structure can make small holes or move directly under a measurement line which would result in a lower damage. In the seventh condition these stones were moved again and approximately the same damage was observed in relation to the fifth condition. In the last wave condition damage starts to develop again which is the same hydrodynamic condition as in condition four. From test 7v2 it can be concluded that if a lower wave condition passes the near-bed structure after a higher condition, none or very minor damage occurs. When the same or a higher condition moves over the near-bed structure damage starts to develop again.
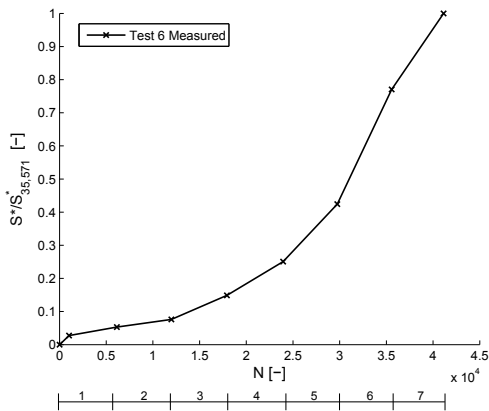
Figure 5.34: Relative damage test 6.
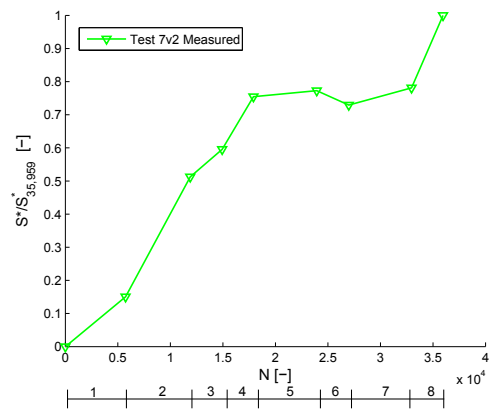
Figure 5.35: Relative damage test 7v2.

Accuracy

In Figure 5.36 the measurement errors for the results of test 6 and 7v2 for multiple storms are shown. From this calculation it can be seen clearly that for test 6, because of the higher damage, a larger deviation is present than for test 7v2. From the last section it is known that the damage can be 26% smaller and 16% larger than actually measured. In these errors the height of the near-bed structure, water depth and erosion area are included and the maximum possible deviation is shown in this figure. These deviations are not taken into account in the rest of the research into damage development for multiple storms. For the prediction of damage during multiple storms it is considered that the confidence bounds of the predicting formulas include measurement errors.
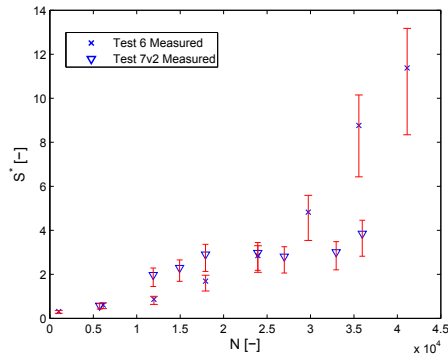
Figure 5.36: Measurement error in damage measurements for multiple storms.

5.3.1   Comparison

In this paragraph the damage development in many waves is compared to multiple storm conditions. This is to see if another damage development is present or that this can be compared.

In Figure 5.37 the comparison between damage for the first 10,000 waves from test 3B and the highest conditions from test 6 and 7v2 can be seen. Note that in test 3 the water depth was lower but also the wave height was slightly lower. However, this resulted in approximately the same velocity on the bottom (3B = 0.52 m/s and 6, 7v2 = 0.53 m/s). Comparing test 3B with the last condition from test 6, it can be seen that a lower damage occurs when already some damage is present which can be related to armouring. The same can be seen for the highest conditions from test 7v2 compared to test 3B. From this it can be concluded that a lower damage occurs when already some damage is present in the near-bed structure. Another interesting observation is that the first high condition from test 7v2 more damage occurs than in the last high condition. It might be that because several weaker storm conditions have passed the near-bed structure before condition 8 was imposed, the stones are more interlocked by each other and have found more stable places in weaker conditions with lower stone movement.
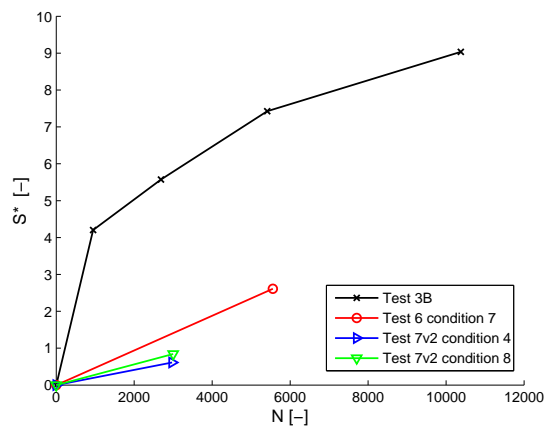
Figure 5.37: Comparsion between test 3B, 6 and 7v2.

5.3.2   Damage prediction

In the literature study one method was found that could describe the damage during multiple
storm conditions. However, this method was not developed and validated to calculate the damage
for near-bed structures. In this paragraph this method is compared with the physical scale model
tests for the damage development formula from Van den Bos and Equation 5.8 and 5.9 found in
this thesis. In the last section it was concluded that test 7 and 7v2 were very similar. Because of
this, not every result from test 7 is shown.

Added damage

A method of calculating the damage in multiple storms might be that the damage is calculated
in each separate wave condition and with these damages added to each other the total damage
can be determined. In Figure 5.38 the added damage for each storm can be seen against the
measured damage. A general conclusion from this method is that the calculated damage is much
more than the measured damage. An explanation for this is that the structure armours itself so
that less damage occurs in a subsequent storm which was observed in the last section. Besides
this, in the literature study it was observed that in the begin always a lot of damage occurred
which reduced after a large number of waves which is not present in this method. To include the
effect of multiple subsequent wave conditions there is one method available which is performed in
the next paragraph.
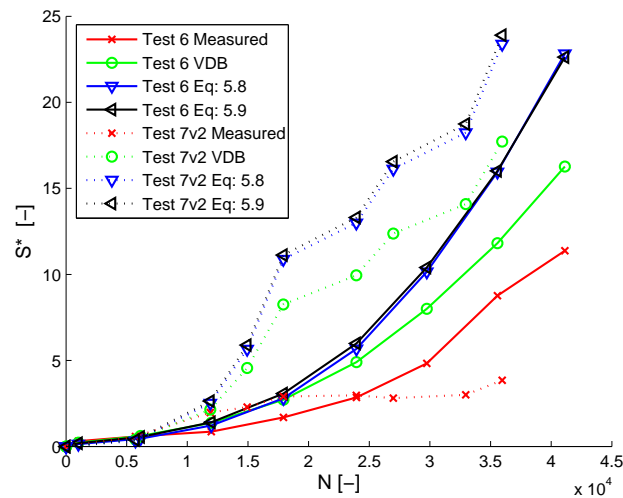
Figure 5.38: Damage predicted for test 6 and 7 for multiple storms by adding the damages.

Van der Meer Method

The method developed by Van der Meer [1999], as explained in Figure 2.6, is used in combination
with the damage development equation from Van den Bos and the equations found in this thesis. In
short, the method from Van der Meer calculates the number of waves with the hydraulic conditions
of the second storm for the damage of the first storm. Then this number of waves is added to
the number already present in storm two, which gives the cumulative damage. Figure 5.39 gives
the results of the calculation performed with the method from Van der Meer. In this figure the
measured damage and the calculated damage with the formula of Van den Bos (VDB), Equation 5.8
and 5.9 are shown.
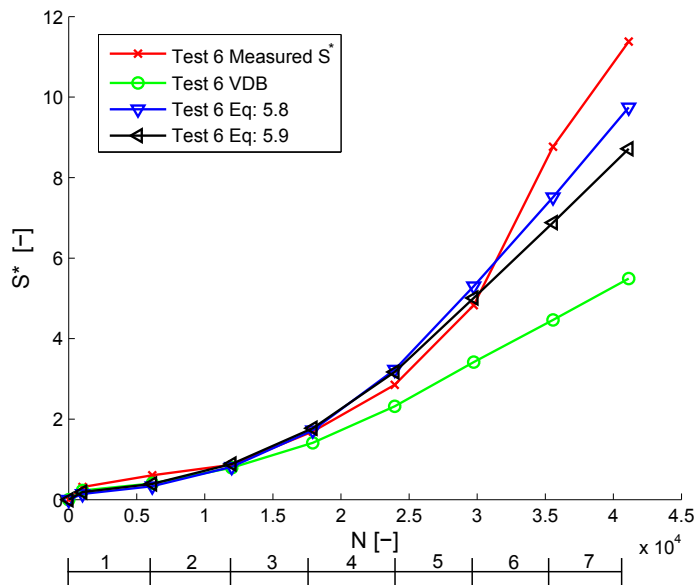
Figure 5.39: Damage predicted for test 6 for multiple storms with the method from Van der Meer. Below the figure is a bar with the storm conditions.

It can be seen that for test 6 that the damage development for the first four wave conditions is similar with all damage prediction methods (The exact conditions were shown in Table 4.2). Equation 5.8 and 5.9 have on average approximately 18% difference between the calculated and measured damage while the formula of Van den Bos has approximately 30% difference. However, the calculated damage seems to be to small for each method in the first few conditions compared to the measured damage. After the fourth wave condition the calculated damage starts to vary where Equation 5.8 calculates the measured damage the closest. Interesting to see is that it is not Equation 5.9, but Equation 5.8 that calculates the damage the closest of these two formulations. A possible explanation could be that because stone type A is present in this data, more data points are present in the high range of the velocity parameter. It could be that because of the shift in the higher regions of the velocity parameter, the overall fit is better. Besides this, it could also be that the predicted damage is still inside the 95% confidence interval. This is checked later in this paragraph. It can be concluded from test 6 that the overall trend of the calculated damage is the same as the measured damage.

For the 7 and 7v2 the results are shown in Figure 5.40. The calculated results are shown only for test 7v2, which do not deviate a lot from test 7. A first observation from this figure is that the calculated damage by Equation 5.8 and 5.9 both over predict the damage and the damage development formula from Van den Bos calculates the damage to a higher degree of accuracy. The difference between the measured and calculated damage from Equation 5.8 and 5.9 is on average 85% while the formula from Van den Bos has on average approximately 35% difference.

From a closer examination of Figure 5.40 it can be seen for test 7v2 that all three formulas calculate the same damage development trend as the measured damage. The initial measured damage is higher in this test than the calculated damage, which was also seen in test 6. After the third wave condition all three formulas calculate the damage to a very high degree of accuracy. In the fourth wave condition, with the highest waves, Equation 5.8 and 5.9 both over predict the damage while the formula from Van den Bos still calculates the damage to a high degree of accuracy. Subsequently, the general trend in all three formulas is approximately the same but because of the deviation from condition 4, the deviations with Equation 5.8 and 5.9 remain high. It can be concluded from this that in test 7v2 the formula from Van den Bos calculates the damage
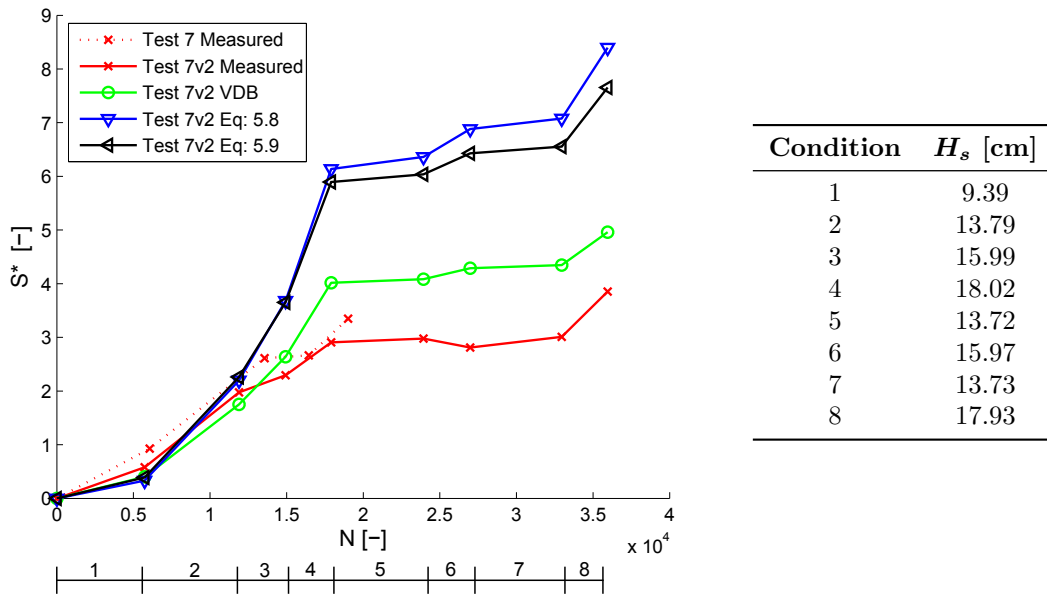
Figure 5.40: Damage predicted for test 7v2 for multiple storms with the method of Van der Meer and measured damage for test 7. Below the figure is a bar with the storm conditions.

to the highest degree of accuracy. Another conclusion is again that for all three formulas the damage development trend compared to the measured damage is relatively good with the formula of Van der Meer. However, because the damage calculated with Equation 5.8 and 5.9 differs from the measured results, it is not known if the measured results are still in the confidence interval available for these formulas.

It can be concluded from Figure 5.39 and 5.40 that the method from Van der Meer calculates the cumulative damage in multiple storms well. In the first few wave conditions the calculated damage is always lower than the actual occurred damage. After three wave conditions the calculated damage is for all three formulas very close to the measured damage. From the fourth wave conditions most deviations start to occur. The general damage development trend is still very comparable to the actual damage development in multiple wave conditions. When even more conditions were included, the measured and calculated damages started to differ more. In other words, the uncertainty in the calculated damage becomes larger. In each test a different formula calculated the damage the closest. In test 6 Equation 5.8 calculates the damage the closest, in test 7 Equation 5.9 and in test 7v2 the formula from Van den Bos.

In previous section a 90% confidence interval for the damage development formulas was described. If it turns out that the measured damage is not within the confidence interval, the damage development equation is not applicable for calculating damage during multiple storms. Because of the large deviation with the calculated and measured damage in test 7v2 for Equation 5.8 and 5.9, it is investigated if the measured damage is still inside the confidence interval. For this confidence interval the method of Van der Meer has been used as well. Because the formula of Van den Bos [2006] and Equation 5.8 and 5.9 are fitted on a different datasets and thus different confidence bounds are present, a new confidence bound for the formula of Van den Bos is investigated. Again it turned out that the normal distribution was the closest distribution available. The distribution of parameter A for Van den Bos his formula can be seen in Figure 5.41. It can be seen that the distribution is further away from the normal distribution that was present in the formulas found in this thesis. Assuming a normal distribution and using the dataset Other+B the lower and upper bound can be determined for the 5% and 95% confidence bounds. The upper bound was found to be the same which Van den Bos used in his thesis, 0.12. The lower bound was found by Van den

Bos as 0.02 and this research showed that it is 0.0071. These new confidence bounds are used for the formula of Van den Bos.
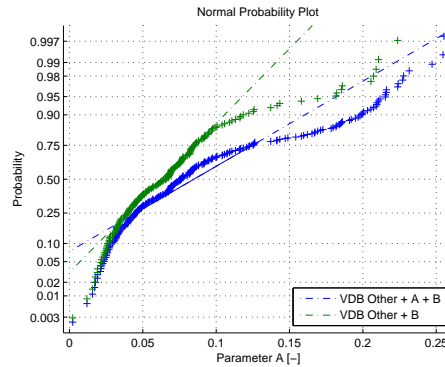
Figure 5.41: The normal distribution of parameter A for the formula of Van den Bos.

The results from calculation with the method of Van der Meer with confidence bounds can be seen in Figure 5.42 and 5.43. From these figures it can be concluded that the measured damage for test 6 and 7v2 are within the confidence intervals for each researcher. In these two tests the confidence interval for the damage development formula from Van den Bos is the largest and covers almost the entire interval. The upper bound is approximately the same for each formula. However, because the calculated damage for Equation 5.8 and 5.9 are higher than for the formula of Van den Bos, the actual present confidence interval is much lower than for the formula of Van den Bos.

For test 7v2 it can be seen in Figure 5.43 that the measured damage is just within the confidence interval of Equation 5.8 and 5.9. It might be that very low damage occurred in this test because relatively few damage occurred in the first few wave conditions. The packing density could be larger than in other tests or the the larger stones of the grading are on top of the structure so that little damage is measured. Because the measured damage is still within the confidence interval of the test no errors are expected to be present inside this test.
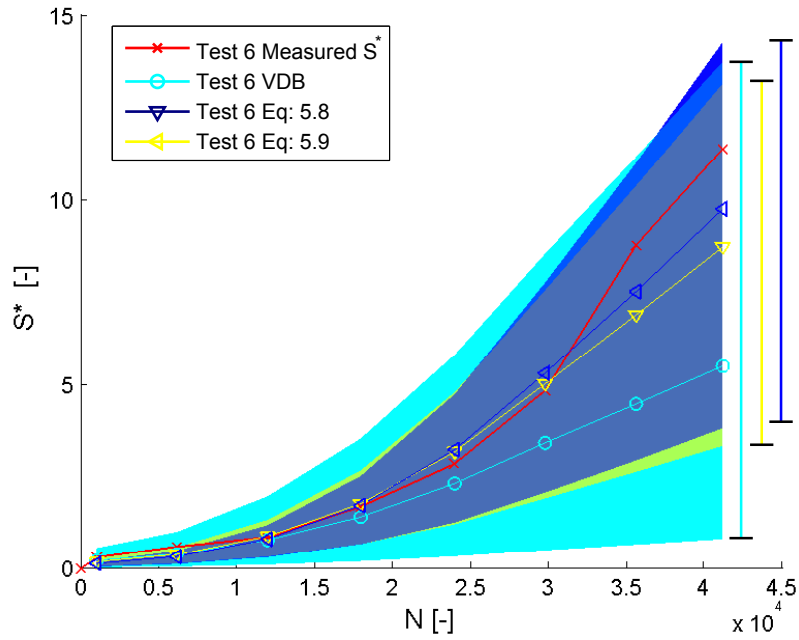
Figure 5.42: Confidence interval for test 6.
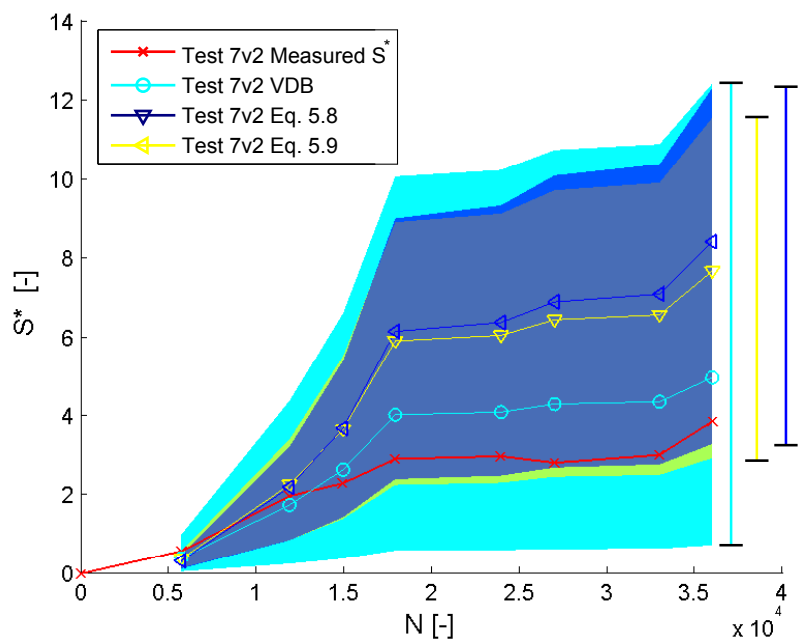
Figure 5.43: Confidence interval for test 7v2.

Chapter 6

Conclusions and recommendations

In this chapter conclusions and recommendations are reviewed and discussed. In the first part the most important observations of the physical scale model test are explained. In the second part general conclusions are formed and in the third part recommendations for further research are given. In this chapter an answer to the main objective of this thesis is given. In Chapter 1 this objective was described and is repeated below:

> *To investigate the effect of multiple storms and a large number of waves on the stability of near-bed structures and to develop a design method to include this effect.*

6.1 Observations

In this section the most important observations of the physical scale model test are described. These observations form an important part of the conclusions, because they describe how a near-bed structure behaves in a wave condition.

- In this thesis irregular waves were used represented by a JONSWAP spectrum. The largest waves present in the spectrum almost always broke immediately after generation by the wave generator. This was caused by depth induced breaking because locally the relation $H_s/h > 0.5$ was exceeded. In the rest of the wave flume no wave breaking was observed and occasional some white capping was present. At the end of the wave flume the wave dissipation slope absorbed the incoming waves as good as possible and little reflections were present. Reflections caused by the near-bed structure were absorbed with the reflection compensation from the wave generator.

- In the first few waves of each test, a lot of stone movement occurred. Unfavourable placed stones are moving in the oscillatory movement of the waves and irregularities are smoothed. These conditions were observed in the first 1000 to 2000 waves.

- The movement of the stones in the physical scale model tests can be described by rolling and sliding. Some stones travelled from the crest to the upstream slope. More stones travelled from the crest towards the downstream slope, where sometimes they would completely be removed from the structure and sometimes they would find a stable position on the slope. After many waves a sort of Gaussian shaped profile was created, which leans towards the downstream side. Occasionally irregularities to the profile were created in the course of a few thousand waves in the middle of a test. After many waves these holes or bumps were

smoothed out again. This was observed more for stone type B, where less damage occurred. Because so much damage occurred for stone type A this was not observed. These holes or bumps are created by the near-bed velocity. Sometimes the velocity is just not high enough to transport a larger stone of the gradation but does transport the smaller stones. In this way a bump is formed or a hole if too much small stones are together which all move under an average wave.

- Stone movement was never observed to stop in these scale model tests, but did reduce in time. Stone movement still occurred after a lot of waves ($N > 25,000$) in the highest waves of the spectra where, because of this, still erosion occurred. After the first few conditions stones were observed to move in groups of up to 10 stones at a time in the highest waves of the spectra. Sometimes they would fall of the crest and others remained on the crest and moved back and forth in the oscillatory movement of the waves.

- In test 3A2, a repetition of test 3A, a dune occurred where on this dune suspended transport (flying of a few seconds) of stones was observed. This dune started on the upstream side of the near-bed structure and was observed moving towards the downstream side. After approximately 7,000 waves the dune disappeared completely and the normal damage profile was observed again.

- In the test with multiple wave conditions in sequence with increasing wave height (test 6), always a lot of reshaping of the near-bed structure occurred at the start the new wave condition. In the lowest wave condition little stone movement occurred. Here stones remained mostly on the crest and did not fall onto the slope of the near-bed structure.

- In the test with multiple random wave conditions in sequence (test 7 and 7v2), almost no stone movement was observed in a lower condition when a high condition had already been imposed to the near-bed structure. When the same high condition was imposed to the near-bed structure, stone movement was again observed.

6.2   Conclusions

This section deals with the conclusions that are drawn from the observations during the physical scale model tests in Chapter 4 and the analysis from Chapter 5. This section is split up in two parts:

- Large number of waves
- Multiple storm conditions

6.2.1   Large number of waves

In this first part conclusions are drawn from the physical scale model tests which deals with a large number of waves. Here the conclusions about the actual relation between damage and the number of waves are presented. Besides this, conclusions about the new damage development formula are described.

The following conclusions are drawn:

- In the first few wave conditions (N up to 2000) randomness in damage development occurs. These wave conditions tend to remove irregularities and smooth the profile. Concluded can be that this is because little bumps are eroded away, small holes are filled with stones, unfavourable placed stones are moved, compacting of the structure and rounding of the crest corners take place. How much damage during the first few conditions occurs is largely determined by these factors. The damage development seems to decrease in time when these factors are not present any more.

- The rate of damage development to near-bed structures seems to reduce in time, but has never been observed to stop under the tested conditions which was seen in Figure 5.1 and 5.2. Lomónaco [1994] and Lomónaco and Klomp [1997] had concluded that near-bed structures would be stable after approximately 2000 waves. This conclusion is not valid for these tests under the tested hydraulic conditions. For stone type B the damage starts to decrease after approximately 5000 waves but has still been observed after more than 25,000 waves in the highest waves of the spectrum. The stones are mainly transported to the downstream slope of the near-bed structure. After a large amount of damage a sort of Gaussian shaped profile can be observed and the profile is completely smoothed. When low damage occurs in a test, gaps can be formed which are later smoothed out again. Hypothesis about damage development in time is that the damage development never stops until so much damage has occurred that the stones form a very smooth structure with a small height difference compared to the bottom. In this thesis stone movement under the highest waves of the JONSWAP spectra was always present.

- Stone type A (D_{n50} = 1.50 mm) is applicable and can be compared with real near-bed structures. A first indication for the applicability of this stone type is the Rouse number, which indicates bed load transport for stone type A. Besides this, by testing the innovative cobble shore for Maasvlakte 2 also suspended transport of stones was observed, a steep slope was present and an indicative method pointed that only an scaling error of 7% was present. This is rather low and indicates it can be compared to reality. Because in reality near-bed structures are built with lower velocity parameters (and consequently lower damage), a distinction between both stone types is given in this thesis. In this way a better fit on the lower regions of the velocity parameter is obtained.

- The erosion patterns in time of the tests with stone type A are similar to the tests with stone type B. In both tests the wave height, structure height, structure width and water depth played a role in damage development. It is concluded that not only the velocity parameter is a main driving force for the damage to near-beds structures, but also these parameters that effect the velocity on the near-bed structure play a major role. Some of these forces are already present in the velocity parameter used to describe damage to near-bed structures. However, their particular influence is larger and different than the velocity parameter describes.

- In previous research the relation between damage and the number of waves is presented in several ways. By comparing the damage S to the number of waves N it has been found that the exponent from the number of waves is not 'one' or constant parameter, but depends on several other factors. This implies that the relation cannot be described by S/N^b, but it was concluded that this is not the case. This exponential relation was found in this thesis to be the best suitable relation to describe the relation between damage and time. In this thesis there is reason to believe the exponent b is dependent on the wave height, water depth, stone size, structure height and the actual damage that occurs in a test after 2000 waves. This is concluded because this parameter changed in each test where one of these factors was investigated. To include the damage after 2000 waves removes the uncertain first stages of damage development due to randomness. The rate of damage development depends on these parameters and thus the relation between damage and time does as well. In this thesis the mean has been taken as the exponent of the number of waves. This parameter is 0.44 for all data (velocity parameter $\theta_{hc1\% max} > 7$) and 0.37 for all data without stone size A ($\theta_{hc1\% max} < 7$). For stone type A (large mobility) this parameter tends to go to the observation from Van der Meer [1988] ($b = 0.5$), while the data for stone type B (smaller mobility) tends towards the conclusion of Van den Bos [2006] ($b = 0.3$).

- The velocity parameter which makes use of $H_{1\%}$ and T_p on depth h_c is the best velocity parameter to describe the damage to near-bed structures. This parameter introduced by Van den Bos works 4% better than the velocity parameter described by Wallast and Van Gent

to describe the damage to near-bed structures. The velocity parameter from Van den Bos has been used in this thesis as well and can be calculated by using Equations 2.36, 2.37, 2.38 and 2.39.

$$\theta_{hc\,1\%} = \frac{(\hat{u}_{hc\,1\%})^2}{g\Delta D_{n50}} \tag{2.36}$$

$$u_{hc\,1\%} = \frac{\pi H_{1\%}}{T_p} \frac{1}{\sinh(k_c h_c)} \tag{2.37}$$

$$\frac{2\pi}{T_p} = \sqrt{gk_c \tanh(k_c h_c)} \qquad \text{Local dispersion relation} \tag{2.38}$$

$$H_{1\%} = H_s \frac{\sqrt{\frac{1}{2}\ln(100)}}{\sqrt[3]{1 + \frac{H_s}{h}}} = H_s \frac{1.52}{\sqrt[3]{1 + \frac{H_s}{h}}} \tag{2.39}$$

- The damage parameter S^* is better to describe damage to near-bed structures than the damage parameter S which was seen in Figure 5.14 and 5.15. This damage parameter, which was introduced by Van den Bos [2006], worked approximately 10% better for all data and even 23% for all data excluding stone type A. The damage parameter S^* can be calculated by using Equation 2.40.

$$S^* = \frac{A_e}{B_c D_{n50}} \tag{2.40}$$

- The damage development formula from Wallast and Van Gent [2002] has more spreading and a higher RMSE relative to the mean than the damage development method from Van den Bos [2006] which was seen in Table 5.4. Both damage development methods were compared against the measured damages of the physical scale model tests. The prediction method from Van den Bos calculated the damage for three tests with stone type B very close. For stone type A however the occurred damage was always much higher than the predicted damage. The prediction method from Wallast and Van Gent underestimated the damage in each test. This conclusion is very different than Saers [2005] made, who concluded Van Gent and Wallast over predict the damage. An investigation into this problem showed in Figure 5.10 turned out that it is likely that the wave height is calculated too high for Saers his tests. The main parameters that were different in the tests that are not calculated to a high degree of accuracy by Wallast and Van Gent and Van den Bos were concluded to be the water depth, wave height, structure height and structure width. With this information a new damage development method was investigated.

- This thesis has led by an investigation into the relevant parameters and processes to a new damage development formula which differs from the formula of Van den Bos [2006] in two ways. A relative width parameter has been added, which describes how many stones are present on the crest of the near-bed structure. This parameter is implicitly also present in S^* but was found to further improve the fit. If the width increases, the near-bed structure becomes more stable and thus damage reduces. The second parameter is called the relative height parameter and consists of the Keulegan-Carpenter number and the structure slope. This parameter can be seen as the amount of which the undisturbed oscillatory movement on the bottom is influenced by the height and slope of the near-bed structure. As the height of the near-bed structure increases the undisturbed movement is influenced more and thus more damage occurs. This parameter is very close but different from the Saers parameter. It is concluded that this is because Saers linked the undisturbed bottom movement to the width

of the slope, while it should actually be linked to the height of the structure. If the height increases, the undisturbed movement is influenced more. The new damage development formula which uses this can be seen in Equation 5.8 and 5.9. These equations can be calculated using the velocity parameter described above and makes use of the Keulegan-Carpenter number which is shown in Equation 5.6. Parameter α in this Equation can be seen with its confidence bounds and standard deviation in Table 6.1. Both equations are the best fit from a dataset from Lomónaco, Wallast and Van Gent, Saers, Tørum and the scale model tests performed in this thesis. Equation 5.8 is for all data where Equation 5.9 is for all data excluding stone type A. Both equations are visualised in Figure 6.1 and 6.2. These formulas are valid in the dimensionless ranges specified in Table 5.2. Equation 5.8 can be used when $\theta_{hc1\% \, max} > 7$ and Equation 5.9 when $\theta_{hc1\% \, max} < 7$. Both Equations have a better fit and lower variance than all damage development equations found in literature. Besides this, with datasets other researchers have used, these formulas have lower variances and a better fit of on this data. Another point of improvement is that the relation between the damage and number of waves is actually investigated for a very large number of waves. Note that these formulas have been derived from a dataset with waves only.

$$\frac{S^*}{N^{0.44}} = \alpha \cdot \theta_{hc1\%}^{2.96} \cdot \left(\frac{B_c}{D_{n50}} \right)^{-0.39} \cdot (m_0 \cdot Kc)^{-1.05} \tag{5.8}$$

$$\frac{S^*}{N^{0.37}} = \alpha \cdot \theta_{hc1\%}^{2.69} \cdot \left(\frac{B_c}{D_{n50}} \right)^{-0.40} \cdot (m_0 \cdot Kc)^{-0.90} \tag{5.9}$$

$$Kc = \frac{u_0 T_m}{z_c} \tag{5.6}$$

Confidence bounds	5%	50%	95%	σ_α
Equation 5.8	0.0524	0.1340	0.1962	0.0919
Equation 5.9	0.0908	0.2376	0.3582	0.1397

Table 6.1: Confidence bounds and standard deviation for parameter α.
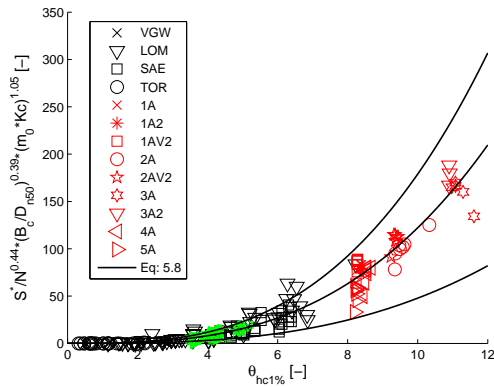
Figure 6.1: Confidence interval for Equation 5.8. The top line is the 95% and the bottom line the 5% confidence bound.
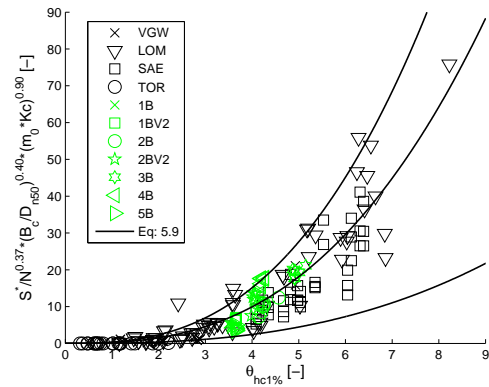
Figure 6.2: Confidence interval for Equation 5.8. The top line is the 95% and the bottom line the 5% confidence bound.

- With low velocity parameters ($\theta_{hc1\%} < 3$) Equation 5.9 performs relatively good although the statistical fit parameters are very bad because of a lot of scatter. From Figure 5.19 and 5.20 it was observed that for Equation 5.9 almost all observations are underneath the best fit line and with the formula of Van den Bos more observations are above (the formula of Van den Bos also has very bad statistical fit parameters for low velocity parameters). It is concluded that because with low velocity parameters randomness plays an important role in the total damage development, it is more safe to use an upper bound. The confidence bounds for low velocity parameters can be seen for Equation 5.9 in Figure 6.3 and for the formula of Van den Bos in Figure 6.4. From this it can be concluded that for low velocity parameters Equation 5.9 should be preferred for the 50% confidence bound because more safety is present and the confidence bound is somewhat smaller (see next conclusion).
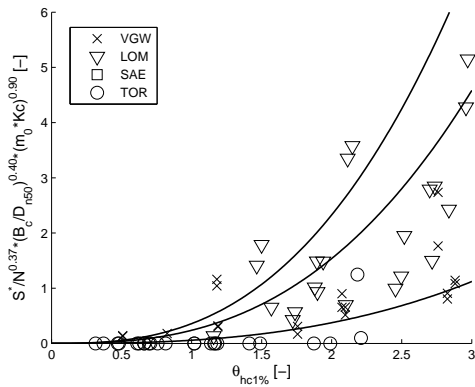
Figure 6.3: Confidence interval for Equation 5.9 with low velocity parameters. The top line is the 95% and the bottom line the 5% confidence bound.
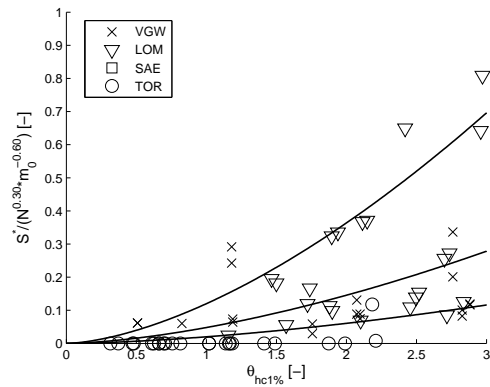
Figure 6.4: Confidence interval for Equation 2.35 from Van den Bos [2006] with low velocity parameters. The top line is the 95% and the bottom line the 5% confidence bound.

- With a real case scenario with a fixed damage level the stone size calculated with Equation 5.9 on the 95% confidence bound was smaller than calculated with the formula of Van den Bos. The calculation for this scenario can be seen in Appendix J. By using the 95% confidence bound a safe limit is used so that it is made certain no more damage occurs than this fixed level.

6.2.2 Multiple wave conditions

In this second part conclusions are drawn from the part of this thesis which deals with multiple wave conditions. In this part the behaviour of a near-bed structure is examined in multiple wave conditions. Besides this, conclusions are drawn from the current way to calculate the cumulative damage for several storms.

The following conclusions are drawn:

- When a low wave condition passes the near-bed structure after a higher wave condition already passed the structure, none or very few damage occurs to the near-bed structure which was seen in Figure 5.33. This can be related to armouring or that the near-bed structure has a higher resistance such that the stones in the structure do not move under a lower velocity. Because no damage was observed in a lower wave condition, it can be concluded that a near-bed structure has a better 'armour' against a low storm when an extreme storm event has already passed. This can also be concluded by comparing the part

with a lot of waves to the part with multiple storms. It can be concluded that if some damage already has occurred, lower damage develops to the near-bed structure in the same hydrodynamic conditions which was seen in Figure 5.37.

- With increasing wave conditions the damage develops in every new condition continuously which was observed in Figure 5.33. After a number of wave conditions the damage development starts to reduce again when a lot of damage has already occurred, in test 6 observed from $S^* > 8$.

- The damage prediction method for cumulative damage from Van der Meer [1999] is usable for calculating the damage in multiple wave conditions with the formula of Van den Bos [2006] and Equation 5.8 and 5.9 from this thesis. For test 6 there was on average 16% difference between the calculated and measured value. For test 7v2 there was on average 85% difference between the measured and calculated damage which seems high. The occurring damage development trend is very similar with the method of Van der Meer and because low damages occurred in this test the relative percentages are high. It has been observed that te method of Van der Meer underestimates the damage in the first few storm conditions for each formula. After several storm conditions this method calculates the damage to a high degree of accuracy (deviations within 10% for both tests) and after more storm conditions the deviations with the measured damage start to develop. For all tests the measured damages were in the 90% confidence interval of the formulas which can be seen in Figure 6.5 and 6.6. For test 6 Equation 5.8 calculates the damage the closest, for test 7 Equation 5.9 and for test 7v2 the equation from Van den Bos.
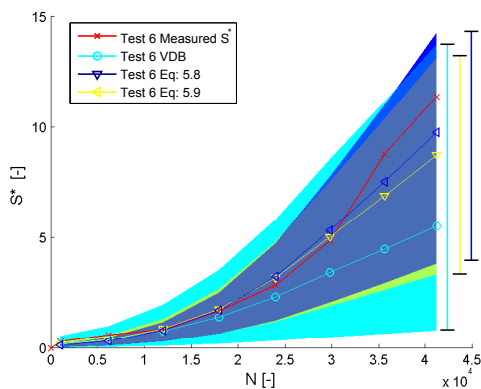
Figure 6.5: Confidence interval for test 6.
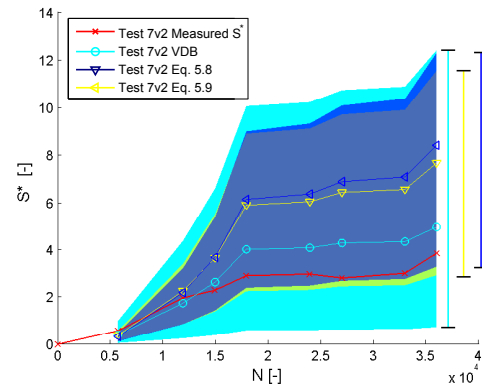
Figure 6.6: Confidence interval for test 7v2.

- With the confidence interval printed in Figure 6.5 and 6.6 it can be concluded that while there is less variation in Equation 5.8 and 5.9 compared to the equation from Van den Bos, calculating damage to near-bed structures still has a large variability.

6.3   Recommendations

In this paragraph recommendations are given for further research.

- In this thesis it was observed that the relation between the number of waves and damage was not a constant exponent but depended on several factors. More tests should be done to determine this parameter or an equation to calculate this parameter. In this investigation multiple stone sizes, wave heights and crest heights should be used which were found to be

of importance in this parameter. In each test another parameter should change and with the use of around 10,000 waves and by measuring the structure at least four times a relation can be determined.

- Additional scale model tests should be performed to check the validity of stone type A. This can be verified by rebuilding on scale a tests of stone type B with stone type A. With the use of Froude scaling this near-bed structure can be scaled down and the same damage should occur to stone type A if this stone type is not too small. In this thesis it is expected that this stone type is still applicable and thus no differences are expected to occur.

- Velocity

  - Tests to check the influence of the bottom velocity in damage development for near-bed structures are recommended. Different waves which have the same peak velocity with a smaller or larger wave steepness can be used to determine the actual influence of the velocity. The peak velocity would in this case be the same, but would last longer or shorter in one direction. This could for instance develop more or less damage.

  - In this thesis linear wave theory has been used to calculate the velocity on the crest of near-bed structures. Actually second or third order theories should be used to calculate this velocity. An investigation into these velocities might give better results with the velocity parameter than the velocity used with linear-wave theory. Besides this, the velocity can be actually measured in the physical scale model tests. By comparing this velocity to the calculated velocity it can be made clear which theory should be used.

  - In this thesis it is assumed after a conclusion from Van Gent and Wallast [2001] that an added current does not influence the damage development to a large degree in wave dominated situations. Additional scale model tests should be performed to check when a current has more influence to the damage development than waves. This can be tested by setting one standard type of waves and increasing the current. If the current becomes too high it can be observed that the damage development occurs mostly because of the added current than from the waves.

  - In the tests which were done with the numerical model (IH-2VOF), described in Appendix A, it was observed that a peak velocity was present just above the near-bed structure on the top corner of the downstream direction. This peak velocity might be the actual velocity which should be used in the velocity parameter. Besides this, there are newer models available which can calculate movement of stones which can be used to determine the damage to near-bed structures (for instance PFEM[1]).

- Damage

  - More research could be done on the first stages of damage development in near-bed structures and very low velocity parameters. Because of randomness present in the early stages of damage development a maximum allowable damage can be set on low velocity parameters. Because in reality mostly near-bed structures are built with low velocity parameters, a maximum allowable damage is then determined and can be used to design dynamically stable near-bed structures.

  - A more accurate method to measure the total damage to the structure can be helpful in future experiments. In this thesis the profile was measured with an echo-sounder in multiple rows. A better method could for instance be stereo photography where the total structure can be measured and the 3D images can be translated to an erosion area. Because some stones might be transported sideways, and are not measured in a row by the echo sounder, these can be visualised with 3D images from stereo photography. In this way the measuring accuracy would improve considerable compared to tests in this thesis.

---

[1]Particle Finite Element (PFEM), `http://www.cimne.com/pfem/`

– When a near-bed structure is constructed with fall-pipe vessels in reality, there might be more damage because of a lower compaction and more irregularities to the structure profile. It can be tested by for example with a bucket and a hose, to represent the fall-pipe vessel, the real construction of a near-bed structure. It might be that this structure would have much more damage than tested in this thesis. Another conclusion can be where irregularities should be avoided.

- In this thesis no research was done on wave direction. When the wave direction is for instance perpendicular to the crest width, a completely different damage development could be present.

- Tests on a larger scale, such as the Delta Flume in the Netherlands, can be used to check the validity of the damage development equation found in this thesis. In this way it would be clear if scale effects occur and if the damage development remains to be the same relative to these tests. Also testing here with multiple wave conditions could be important to determine if the Van der Meer relation for cumulative damage also holds for larger scales.

- In Figure 2.7 a distribution was given for the significant wave height in a storm. In this research only one significant wave height has been used per storm to determine the damage. Because in a storm there is a distribution present in wave height, the method to include multiple storms might also work to include several significant wave heights in one storm. In this way the damage during this one storm might be calculated more closely. A method to validate this is to include the method of Van der Meer in tests with large number of waves which are performed in this thesis.

Bibliography

J.A. Battjes and H.W. Groenendijk. Wave height distributions on shallow foreshores. In *Coastal engineering*, volume 40, number 3, pages 161–182. Elsevier, 2000.

J.S. Bendat and A.G. Piersol. *Random data: analysis and measurement procedures*, volume 729. John Wiley & Sons, 2011.

J.P. van den Bos. Design of granular near-bed structures in waves and currents. Master's thesis, TU Delft, Delft, The Netherlands, 2006.

L. Broderick. Riprap stability, a progress report. In *Proceedings special conference design, construct, maintenance and performance coastal structures*, pages 320–330. ASCE, New York, USA, 1983.

CETMEF CIRIA, CUR. *The Rock Manual. The use of rock in hydraulic engineering.* C683, CIRIA, London, 2007.

F.M. Dekking, C. Kraaikamp, H.P. Lopuhaä, and L.E. Meester. *A Modern Introduction to Probability and Statistics: Understanding why and how.* Springer, 2005.

M. Dessens. The influence of flow acceleration on stone stability. Master's thesis, TU Delft, Delft, The Netherlands, 2004.

M. Friendly and E. Kwan. Where's waldo? visualizing collinearity diagnostics. In *The American Statistician*, volume 63, number 1, 2009.

N. Garcia, J.L. Lara, and I.J. Losada. 2-d numerical analysis of near-field flow at low-crested permeable breakwaters. In *Coastal Engineering*, volume 51, number 10, pages 991 – 1020, 2004.

General Acoustics. Ultralab uws, 2013. URL http://www.generalacoustics.com/. Accessed june 17.

M.R.A. van Gent and I. Wallast. Stability of near-bed structures and bed protections; analysis of physical model tests with waves and currents. In *WL|Delft Hydraulics, Delft, The Netherlands*. Delft cluster report HC030204H3804, 2001.

R. Guanche, I.J. Losada, and J.L. Lara. Numerical analysis of wave loads for coastal structure stability. In *Coastal Engineering*, volume 56, number 5, pages 543–558. Elsevier, 2009.

P.H.A. Hendrickx. Personal communication. Papendrecht, Boskalis, 2013.

B. Hofland. *Rock and roll: Turbulence-induced damage to granular bed protections.* PhD thesis, 2005.

L.H. Holthuijsen. *Waves in oceanic and coastal waters.* Cambridge University Press, 2007.

IH-Cantabria. *IH-2VOF Course manual.* 2012.

L.J.M. Jansen. Breuksteen. De bepaling van de relatie tussen D_x en D_{nx} en de invloed van enkele factoren daarop. B.Sc. thesis in Dutch, not yet published, 2013.

I.G. Jonsson. Wave boundary layers and friction factors. In *Proceedings of the International Conference on Coastal Engineering*, volume 1, number 10, pages 127–148. ASCE, New York, USA, 1966.

W.H.G. Klomp and P. Lomónaco. Pipeline cover stability. In *The proceedings of the 5th International Offshore and Polar Engineering Conference*, volume 2, pages 15–22. ISOPE, Golden, Colorado, USA, 1995.

C. Kuester. Waves and currents on near-bed structures. data summary report. In *Norwegian University of Science and Technology, Department of Civil and Transport Engineering/Valle Scandinavian Scholarship and Exchange Program.*, 2007.

J.L. Lara, N. Garcia, and I.J. Losada. Rans modelling applied to random wave interaction with submerged permeable structures. In *Coastal Engineering*, volume 53, number 5, pages 395–417. Elsevier, 2006a.

J.L. Lara, I.J. Losada, and P.L.F. Liu. Breaking waves over a mild gravel slope: experimental and numerical analysis. In *Journal of Geophysical Research: Oceans (1978–2012)*, volume 111, number C11. Wiley Online Library, 2006b.

B. Lau. Matlab code for diagnosing collinearity in a regression design matrix, 2013. URL `http://www.subcortex.net/home`. Accessed august 6.

M. Levit. Stability of pipeline cover material. Master's thesis, TU Delft, Delft, The Netherlands, 1996.

M. Levit, M.R.A van Gent, and W.W. Massie. Stability of pipeline covers under waves and currents'. In *Proceedings of the 8th International Conference on the behaviour of offshore structures*, volume 1, pages 195–210, 1997.

G.J.A. Loman, M.R.A. van Gent, and J.W. Markvoort. Physical model testing of an innovative cobble shore, part i: Verification of cross-shore profile deformation. In *Preparation for the Proc. International Coastlab Conference*, 2010.

P. Lomónaco. Design of rock cover for underwater pipelines. Master's thesis, International Institute for Infrastructural Hydraulic and Environmental Engineering (IHE), Delft, The Netherlands, 1994.

P. Lomónaco and W.G.H. Klomp. Pipeline rock cover damage assessment. In *Proceedings of the 8th International Conference on the behaviour of offshore structures*, volume 1, pages 179–193, 1997.

P. Lomonaco, C. Vidal, I.J. Losada, N. Garcia, and J.L. Lara. Flow measurements and numerical simulation on low-crested structures for coastal protection. In *Environmentally Friendly Coastal Protection*, pages 191–210. Springer, The Netherlands, 2005.

Mathworks. Matlab documentation center, 2013. URL `http://www.mathworks.nl`. Accessed throughout the whole thesis.

J.W. van der Meer. *Rock slopes and gravel beaches under wave attack*. PhD thesis, Technische Universiteit Delft, 1988.

J.W. van der Meer. Design of concrete armour layers. In *Proceedings of the International Conference Coastal Structures*, volume 1, pages 213–221, 1999.

J.R. Morison, J.W. Johnson, and S.A. Schaaf. The force exerted by surface waves on piles. In *Journal of Petroleum Technology*, volume 2, number 5, pages 149–154. Society of Petroleum Engineers, 1950.

J.S. de Reus. Het valgedrag van stortsteen onder invloed van stroming. Master's thesis, Delft University of Technology, In Dutch, 2004.

L.C. van Rijn. *Principles of sediment transport in rivers, estuaries and coastal seas*, volume 1006. Aqua publications Amsterdam, 1993.

W. Saers. Erosion of rubble mound near-bed structures under irregular waves. Master's thesis, TU Delft, Delft, The Netherlands, 2005.

G.J. Schiereck. *Introduction to bed, bank and shore protection*. Delft University Press, Delft, The Netherlands, 2001.

S. van Schijndel, L.E. Frostick, S.J. McLelland, and T.G. Mercer. *Users Guide to Physical Modelling and Experimentation: Experience of the HYDRALAB Network*. CRC Press, 2011.

A. Shields. Anwendung der ahnlichkeitsmechanik und der turbulenz forschung auf die geschiebe bewegung. In *Mitteilungen der Preuszichen Versuchsanhalt für Wasserbau und Schiffbau, Berlin, Germany*, volume 26, pages 524–526, 1936.

K.D. Suh, M. Kim, and S.W. Kim. Comparison of calculation methods of cumulative damage of breakwater armor layer. In *Journal of Waterway, Port, Coastal, and Ocean Engineering*. ASCE, New York, USA, 2013.

B.M. Sumer, J. Fredsøe, and N. Christiansen. Scour around vertical pile in waves. In *Journal of waterway, port, coastal, and ocean engineering*, volume 118, number 3, pages 15–31. ASCE, New York, USA, 1992.

E. Terrile. The threshold of motion of coarse sediment particles by regular non-breaking waves. Master's thesis, TU Delft, Delft, The Netherlands, 2004.

D.M. Thompson and R.M. Shuttler. Riprap design for wind wave attack. a laboratory study in random waves. *HRS, Wallingford, Report EX*, 707, 1975.

A. Tørum, C. Kuester, and Ø.A. Arntsen. Stability against waves and currents of rubble mounds over pipelines. In *Norwegian University of Science and Technology, Department of Civil and Transport Engineering*. Report number BAT/MB-R1/2008, 2008.

A. Tørum, Ø.A. Arntsen, and C. Kuester. Stability against waves and currents of gravel ruble mounds over pipelines and flat gravel beds. In *Proceedings of the International Conference on Coastal Engineering*, volume 1, pages 48–59, 2011.

M. Tromp. The influence that fluid accelerations have on threshold of motion. Master's thesis, TU Delft, Delft, The Netherlands, 2004.

M. van de Velde. Rockdumping, 2013. URL `http://www.theartofdredging.com/rockdumping`. Accessed march 15, 2013.

C.P. Vidal, I.J. Losada, and F.L. Martin. Stability of near-bed rubble-mound structures. In *Proceedings of the International Conference on Coastal Engineering*, volume 2, pages 1730–1743. ASCE, New York, USA, 1998.

C.P. Vidal, P. Lomónaco, and F.L. Martín. Prototype analysis of stability of rubble mound protections for submarine outfalls. In *Proceedings of the 28th International Conference on Coastal Engineering*, volume 2, pages 1936–1948. ASCE, New York, USA, 2002.

C.P. Vidal, I.R. Losada, and F.M. López. Stability analysis of low crested and submerged rubble mound breakwaters: Relationship between flow characteristics and measured damage and stability formulae for low crested and submerged breakwaters. In *Proceedings of the 5th Coastal Structures International Conference*, volume 1, pages 939–950, 2007.

S. de Vree. Laboratory of Fluid Mechanics, Delft University of Technology. Internal unpublished communication, 2013.

I. Wallast and M.R.A. van Gent. Stability of near-bed structures under waves and currents. In *Proceedings of the 28th International Conference on Coastal Engineering*, volume 2, pages 1744–1756. ASCE, New York, USA, 2002.

Appendix A

IH-2VOF computer model

Because of breakdown of the wave generator tests have not been performed to validate the numerical model. For future research everything about the numerical model which was already performed in this thesis can be found in this appendix.

IH-2VOF is a relatively new numerical wave-structure interaction model. This model is developed at the Environmental Hydraulic Institute of IH-Cantabria. VOF stands for Volume Of Fluid which is a numerical technique for tracking and locating the free surface. One of the important features from this model is that it is able to calculate numerical tests on model and prototype scale. The IH-2VOF model solves the Reynolds Averaged Navier-Stokes (RANS) equations [IH-Cantabria, 2012]. In this chapter the background formulas behind the IH-2VOF model are described shortly, the model set-up, what tests should be done and the results from these tests for the numerical model are described. The overall performance of the model is reviewed as well.

The IH-2VOF numerical model has several interfaces to build a model. To build a structure and a mesh where the calculations are performed, the program CORAL is needed. In this program the structure and a calculating mesh can be made. After building the structure waves such as regular, irregular (JONSWAP spectrum) and solitary waves can be simulated with the IH-2VOF numerical model [IH-Cantabria, 2012].

A.1 Background and research

In this paragraph the mathematical background and validation of the numerical model is described. A lot of research has been done in the past which aims to validate this numerical model. This research is described shortly and some general checks are made about the model.

A.1.1 Mathematical background

The IH-2VOF model solves the RANS equations where Reynolds decomposition refers to separating the flow and pressure into a mean (time averaged, denoted by the overbar) and fluctuating component (denoted by the accent). This decomposition is given by Formula A.1.

$$u_i = \overline{u_i} + u_i' \quad \text{and} \quad p = \overline{p} + p' \tag{A.1}$$

In these formulas i stands for direction which can be in x or y direction. Here the x direction is in the length of the flume and the y direction is the height of the flume. The RANS equations can

be derived from the Navier-Stokes equations with this formula and assuming the fluid is incompressible. The RANS equations are given in Equation A.2. Because of the Reynolds properties the fluctuating component in the average velocity over an x-direction must be zero.

$$\frac{\partial \overline{u_i}}{\partial x_i} = 0$$
$$\frac{\partial \overline{u_i}}{\partial t} + \overline{u_j}\frac{\partial \overline{u_i}}{\partial x_j} = -\frac{1}{\rho}\frac{\partial \overline{p}}{\partial x_i} + g_i + \frac{1}{\rho}\frac{\partial \overline{\tau_{ij}}}{\partial x_j} - \frac{\partial(\overline{u_i'u_j'})}{\partial x_j} \tag{A.2}$$

In this formula τ_{ij} is a viscous stress tensor which can be calculated by the boussinesq assumption in Equation A.3. The first term on the left hand side of Equation A.2 is the change of velocity in time. The second term is the change in mean momentum of a fluid element. These terms are balanced by the right-hand side of the equation which are stresses, external forces such as gravity, viscous stresses and Reynolds stresses. The Reynold stresses can be calculated using the non-linear $k - \epsilon$ model [Shih et al., 1996, Lin and Liu, 1998 cf IH-Cantabria, 2012]. In this model k is the turbulent kinetic energy and ϵ the dissipation rate of the turbulent kinetic energy.

$$\tau_{ij} = \nu \left(\frac{\partial u_i}{\partial x_j} + \frac{\partial u_j}{\partial x_i} \right) \tag{A.3}$$

A.1.2 Research

The IH-2VOF model has a small amount of semi-empirical parameters. Thus, the results obtained from this model has to be correct and the processes need to be presented well by the model. For instance, waves, wave induced currents, reflections, transmissions, over-topping and wave breaking have to be included in the model correctly. To validate the model several researchers have compared the model to physical scale model tests. However, no validation has been done so far concerning flow characteristics around a near-bed structures. The first researchers that looked at the model investigated the predecessor of the IH-2VOF model called COBRAS which was developed by Lin and Lui [1998] cf. Garcia et al. [2004].

In Garcia et al. [2004] conclusions were made that the COBRAS model simulates the propagation of regular waves over a low-crested breakwater to a satisfactory degree. These conclusions were made by comparing the computer tests to a physical scale model. The reflection, transmissions, pressures inside the structure, shoaling and velocities are very comparable with the scale model tests. Flow velocities on the bottom and slope of the structure are also quite good represented by the model which is important for flow around near-bed structures. As a conclusion Garcia et al. mentions that the COBRAS model reproduces the water movement around a low-crested breakwater to a very high degree of accuracy.

In Lara et al. [2006a] further research is done with the COBRAS computer model using irregular waves which are again compared to a low-crested breakwater. First it is tested if irregular waves are represented in a correct way by the computer model which seems to be the case. However, the model seems to underestimate the the height of the highest waves which could be a problem in our case. Still a conclusion in this paper is that the model reproduces the wave spectrum generally in a correct way. In a later paper by Lara et al. [2006b] wave breaking, pressure and undertow have been examined. These can be simulated reasonable with the COBRAS model. However, the velocity field under broken waves are represented very well which could be important in our case if wave breaking on the near-bed structure occurs. In a later paper by Guanche et al. [2009] this was concluded as well. They also concluded that flow in a porous medium such as in a near-bed structure is calculated to a high degree of satisfactory.

A.2   Set-up of the IH-2VOF model

In this chapter it is explained which mesh size is used, which boundary conditions are imposed and how the model is validated. Some small tests have been used in order to validate the numerical model.

A.2.1   Mesh size

The first step in setting up a model is to create a structured mesh with CORAL. This mesh can be defined very accurate near the interest area and can get coarser moving away from the interest area. The manual states however that the use of a uniform (constant cell size) mesh is recommended. This is because the scheme used to calculate this is in this way only first order accurate and the resulting errors can be considerable [IH-Cantabria, 2012].

To create a structure CORAL is needed as well. For building a structure there two possibilities. The first is an obstacle which represents an incompressible and non-porous medium that can be made in any possible shape. The second option is to create a porous medium which is used in this thesis to represent a near-bed structure. For this the porosity, linear friction coefficient, non-linear friction coefficient, added mass coefficient and D_{n50} need to be entered in CORAL. Added mass is inertia added to a system because an accelerating or decelerating body of fluid must move some volume of surrounding fluid with it as it moves through or alongside an object. The last step in CORAL is imposing the water level h which can be made on any height required.

A.2.2   Boundary conditions

After building the structure in CORAL, waves can be simulated. There are three wave types possible in the IH-2VOF numerical model which are regular waves, irregular waves and a solitary wave. For every wave type the height, cycle period and sampling frequency need to be specified. The sampling frequency is standard set on 30 Hz. For the regular and irregular wave field a wave period needs to be entered into the model. Besides this, in the irregular wave field a γ for representing a JONSWAP spectrum needs to be specified. This γ value is set to 3.3 which is considered the best value for representing a JONSWAP spectrum in the North Sea [Hasselman et al. cf Holthuijsen, 2007].

There are solid and open boundary conditions possible in the numerical model to absorb or reflect the incoming wave. The absorption or reflection of both boundaries can be turned on or off. At one side in the model waves are generated which is done by a Dirichlet boundary condition. For this boundary condition horizontal and vertical velocity components are generated. These velocities are generated in advance of running the computer model. The second option to generate waves is with a moving boundary (flap) which generates the waves just like this is done in the wave flume. Both produce the same waves so the easy stationary boundary is used in this thesis. The last step in creating the model is to define the fluid density of water, turn the boundary absorptions on and insert 'wave gauges'. These gauges tell the numerical model at which point in the grid the data needs to be saved. It saves the water level, horizontal and vertical velocities and pressures if this is required.

A.2.3   Validation

Before actual tests are done with the IH-2VOF model, the model is validated with respect to boundary reflections and velocity fields on the bottom. In the numerical model two options are present with respect to boundary conditions: Left boundary absorption and right boundary absorption. Normally these options should be on, but to see if these boundary absorptions are

working properly some small tests have been performed with this. In Table A.1 the results are given. These tests are performed in an 15 m long and 1 m high grid with a mesh size of 2x1 cm and regular waves with $H = 15$ cm. The left boundary is the boundary where the waves are generated and the right boundary is where they are absorbed or reflected. It can be seen that reflection percentages are not 100% when both boundary absorptions are turned off. When a wave is reflected by the boundary, a standing (fully reflected) wave is generated. Because of the limited water depth, the wave 'feels' the bottom and will start to break. In this way not the fully reflected wave will be measured by the wave gauge and less reflection will be present. The little reflection that is present when both boundary conditions are turned on can be explained by wave dissipation which is present in the model. It can be concluded that the right boundary condition is very important and must be turned on at all times to minimize the effect of reflected waves.

Absorption on or off		Reflection percentage [%]
Left Boundary **ON**	Right Boundary **ON**	7.1%
Left Boundary **OFF**	Right Boundary **ON**	7.4%
Left Boundary **ON**	Right Boundary **OFF**	69.2%
Left Boundary **OFF**	Right Boundary **OFF**	70.9%

Table A.1: Reflections when boundary absorptions are turned on or off.

With this calculating grid the velocity profile for a linear wave has been checked as well. This velocity is compared to the velocity which can be calculated using linear wave theory (Equation 2.6). The result from this test can be seen in Figure A.1. It can be seen that these velocities are almost the same and the same curve is present in both lines. The average error is only 4% and the maximum error is 9%.
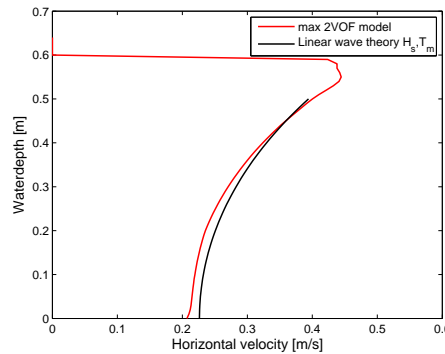
Figure A.1: A velocity profile from the 2VOF model and linear wave theory. $H = 0.15$ m and $T_m = 1.46$ s.

A.2.4 Optimization of the numerical model

The turn around times for the IH-2VOF model are very high. A typical calculating time for 1000 waves is a few days. To minimize the calculating time the mesh size is optimized. Besides this, it was determined how many waves are needed to correctly represent a JONSWAP spectrum.

The first step is to look what the largest possible mesh size is, where the maximum calculated velocity is still near the calculated maximum velocity from the smallest mesh size. The model is set-up which x the horizontal and y the vertical direction. A general rule of thumb for this model is that $\Delta x < 2.5\Delta y$ which means that the step size in the x direction can be almost 2.5 times larger than the step size in y direction. IH-Cantabria [2012] advises furthermore to put a minimum of 4

y-points in one wave height. For example with 15 cm waves this would mean $\Delta y < 3.75$ cm which gives $\Delta x < 9.4$ cm. Because it is not known if this represents the actual velocities in a right way, verification tests are performed. The maximum velocities on the bottom under a regular wave are compared to each other in order to choose which mesh size is used in the later stages of this research. Only uniform (one mesh size in the entire calculating grid) mesh sizes are used in this thesis as recommended to prevent calculating errors [IH-Cantabria, 2012]. Square and rectangle mesh sizes have been used in a 15 m long flume to reduce turn around times. In Figure A.2 the overall velocity before and on top of the near-bed structure are shown (mesh = XXXYYY where X and Y are sizes in mm). In Figure A.3 the zoomed, and thus more detailed, results of the computer model with the mesh tests are shown. In these figures a lot of maximum horizontal velocities under regular waves for different mesh sizes are shown where mesh sizes larger than these values did not provide an answer. In Figure A.3a the velocity before the near-bed structure is shown and in Figure A.3b the velocity on the near-bed structure is shown which is considered more important in this thesis. In Figure A.3a it can be seen that the results are practically the same for all mesh sizes. In Figure A.3b the velocities on the near-bed structure differ a lot. It is important to model the 'peak' velocity in a right way because this is the highest velocity present on the structure and results in deformation in a real case. Assuming the best results are obtained from the smallest mesh size, the 'peak' velocity is only modelled correctly for mesh sizes smaller than $\Delta x = 2$ cm and $\Delta y = 1$. This can better be observed from Table A.2. This table includes the turn around times, the maximal velocities on the near-bed structure and the percentage of the maximum. From the comparison of the maximum velocity and keeping in mind the turn around times, a uniform mesh size of $\Delta x = 2$ cm and $\Delta y = 1$ cm is chosen. It is concluded that the maximum flow velocity for the $\Delta x = 2$ cm and $\Delta y = 1$ cm is 0.058 m/s smaller than the smallest mesh size which is considered appropriate. This mesh size means that there are 15 y calculating points in one wave of 15 cm. A more understandable term in numerical modelling is the number of x calculating points in a wavelength which should be far above 50. In a mean wavelength with this mesh size and in this test there are 142 x calculating points which is considered very high and thus accurate. Although there is a little difference with the smallest mesh size, the computational times are so extensive that this is not considered feasible. With the 2x1 mesh size the simulations are done. Lara et al. [2006a] did also use this mesh size to validate the IH-2VOF numerical model. The total velocity profiles from these tests can be seen in Figure A.2.

(a) Velocity profile before the near-bed structure   **(b)** Velocity profile on top of the near-bed structure
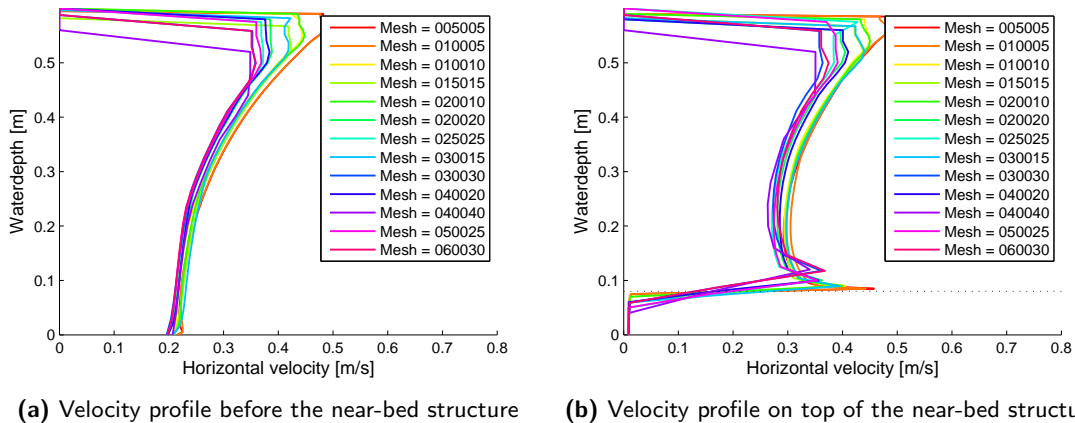
Figure A.2: Total horizontal velocity profile for the mesh test. The initial set-up of this test is $H = 0.15$ m and $T_m = 1.46$ s.

Apart from the mesh size the number of waves is also an important factor in the computational time. The JONSWAP spectrum needs to be represented in a statistical right way and for this a certain number of waves need to be simulated. A test has been done to determine how many waves are at least necessary to represent a JONSWAP spectrum. It has been checked when the significant

(a) Velocity profile before the near-bed structure   **(b)** Velocity profile on top of the near-bed structure
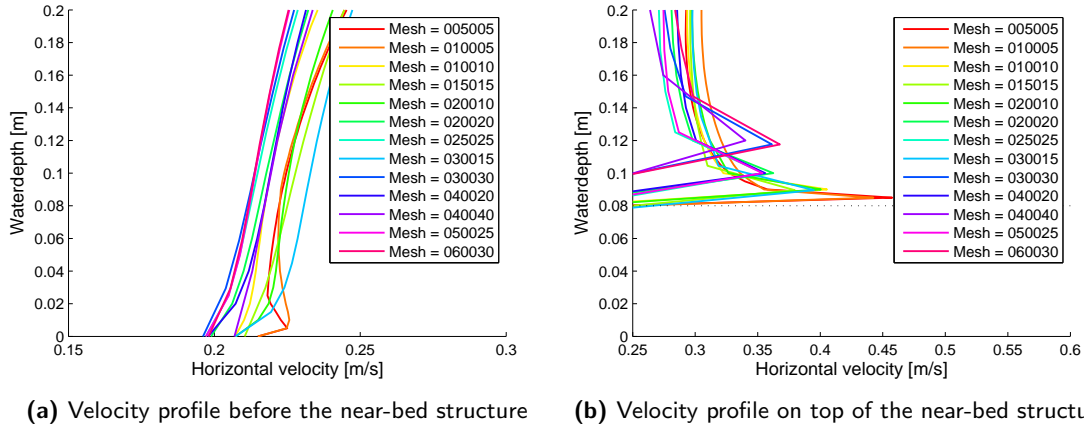
Figure A.3: Detail of horizontal velocities for the mesh test. The initial set-up of this test is $H = 0.15$ m and $T_m = 1.46$ s.

Mesh = XXXYYY [mm]	Near-bed structure maximal velocity [m/s]	percentage of maximum [%]	Indication turn around times for 1000 waves
Mesh = 005005	0.458	100%	7 days
Mesh = 010005	0.443	97%	4 days
Mesh = 010010	0.405	89%	3 days
Mesh = 015015	0.380	83%	2 days
Mesh = 020010	0.400	88%	1 day
Mesh = 020020	0.362	79%	18 hours
Mesh = 025025	0.370	81%	15 hours
Mesh = 030015	0.395	86%	15 hours
Mesh = 030030	0.364	80%	11 hours
Mesh = 040020	0.356	78%	9 hours
Mesh = 040040	0.351	77%	6 hours
Mesh = 050025	0.377	82%	5 hours
Mesh = 060030	0.375	82%	2 hours

Table A.2: Maximal velocity with a certain mesh.

wave height for a scale model did not change any more. This test can be seen in Figure A.4. It can be seen that the significant wave height is stable after 1000 waves. This number of waves should minimal be used to correctly represent a JONSWAP spectrum.

In Figure A.3 it was seen a 'peak' velocity on top of the near-bed structure is seen. At this point it is uncertain if this velocity is correct or that this is a physical error in the model. However, during the literature study this peak velocity was also found in other literature so it is assumed there is no numerical error in this case.
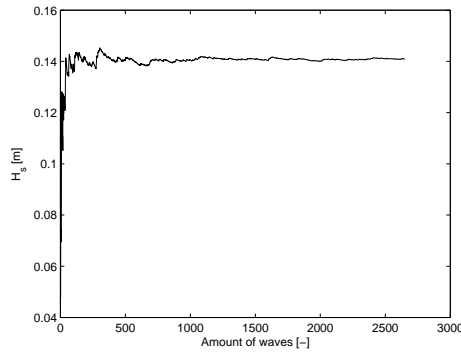
Figure A.4: JONSWAP tests for significant wave height.

A.3   Physical model tests

Besides the damage tests which are used in this thesis, verification tests for the numerical model can be done as well. With the IH-2VOF model a part of the physical scale model tests can be rebuild and simulated. It should be checked if the velocity which is present on the near-bed structure is comparable to the velocities measured in the physical scale model. For this a velocity meter should be placed in front and on top of the near-bed structure. Table A.3 shows which tests should be done to compare the flow velocities with the physical scale model and the expected horizontal velocities. For these tests Ardenner split is glued together so that no damage can occur. No damage is allowed because in the numerical model no damage can occur as well. Irregular and regular waves are used to test the flow velocities. Regular waves are used because the flow velocities are better to compare if the same wave passes by each time. In a random wave field very different velocities can be expected because of the different wave heights. Figure A.5 shows the places where the velocity should be measured. In the numerical model the velocity is measured on exactly this place as well.

Test	Wavetype	h [m]	z_c [m]	B_c [m]	H_s [m]	T_m [s]	m_0 [-]	N [-]	u_{hc}	$u_{hc1\%}$	Remarks
8B	Regular	0.5	0.08	0.15	0.15	1.46	3	100	0.27	0.27	Repeated 7 times with velocity meter on different places
9B	Regular	0.5	0.08	0.15	0.2	1.69	3	100	0.39	0.39	Repeated 7 times with velocity meter on different places
10B	Irregular	0.5	0.08	0.15	0.15	1.46	3	1000	0.27	0.42	Repeated 7 times with velocity meter on different places
11B	Irregular	0.5	0.08	0.15	0.2	1.69	3	1000	0.39	0.57	Repeated 7 times with velocity meter on different places

Table A.3: Tests for the near-bed velocity.
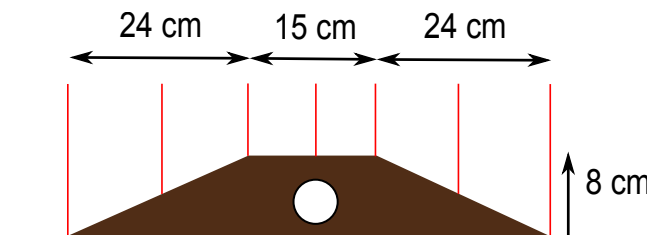
Figure A.5: Places where the velocity meter should be placed for the physical scale model tests.

A.4 Numerical Model

In this paragraph it is explained what the results for the numerical model for different tests are. The overview of the test can be seen in Table A.3 in the previous section of this appendix. The tests to compare the results from the numerical model to the physical scale model tests have not been performed. In this section only the numerical results are described.

A.4.1 Results

In this paragraph numerical results from the test program in Table A.3 are explained. In Figure A.6 the maximum horizontal velocity profile from test 8B is shown for different places on the near-bed structure where the velocity is measured. The velocity is on a 1:10 scale. It can be seen that the 'peak' in the velocity is not present in the beginning but it starts to grow over the near-bed structure. This peak is maximal in the top right corner and becomes weaker towards the end. In Figure A.7 the maximum horizontal velocity profiles from test 10B are shown. This test is done with irregular waves and thus higher velocities are expected. The same trend in the peak velocity can be seen as before.
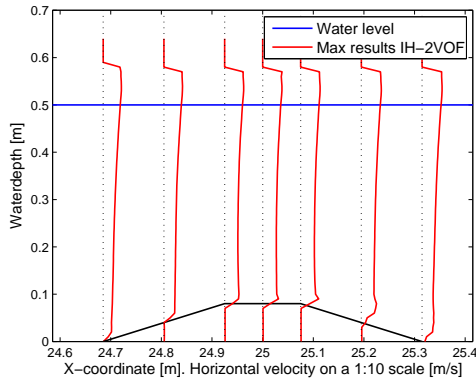
Figure A.6: Numerical model results from test 8B. Input: $z_c = 8$ cm, $B_c = 15$ cm, $H = 15$ cm and $T_m = 1.46$ s. The velocities are on a 1:10 scale.
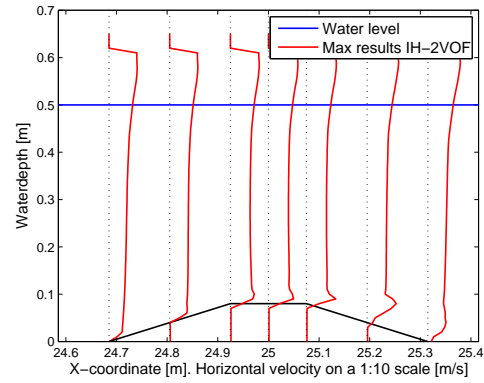
Figure A.7: Numerical model results from test 10B. Input: $z_c = 8$ cm, $B_c = 15$ cm, $H_s = 15$ cm and $T_p = 1.82$ s. The velocities are on a 1:10 scale.

In Figure A.6 and A.7 it is not very clear what the flow velocities are. In Table A.4 the numeric values of the velocities are given on a certain height. In the max column the maximum velocity in the 'peak' are given.

Because Figures A.6 and A.7 only show the maximum horizontal flow velocity results, this is not representable for an entire irregular wave field. There are of course many more waves in an irregular wave field with different velocities. In Figure A.8 the non-exceeded horizontal velocity is shown for the irregular wave field from test 10B and 11B. In this figure also the velocities from linear wave theory, which are used in the damage formulations, are plotted. Both velocities are calculated on height h_c and show velocity u_{hc} with H_s, T_m and $H_{1\%}, T_p$.

| Test | h | X1 [m/s] | X2 [m/s] | X3 [m/s] | X4 [m/s] | X5 [m/s] | X6 [m/s] | X7 [m/s] |
	Height near-bed structure	0	0.04	0.08	0.08	0.08	0.04	0
8B	0.01	0.10	0.01	0.01	0.01	0.01	0.01	0.09
	0.05	0.17	0.12	0.01	0.01	0.01	0.11	0.23
	0.10	0.19	0.22	0.28	0.28	0.30	0.25	0.22
	0.15	0.20	0.23	0.27	0.27	0.28	0.25	0.23
	0.20	0.21	0.23	0.26	0.27	0.27	0.26	0.24
	0.25	0.22	0.24	0.26	0.27	0.28	0.27	0.26
	max	0.17	0.21	0.27	0.31	0.36	0.30	0.23
10B	0.01	0.16	0.01	0.01	0.01	0.01	0.01	0.12
	0.05	0.28	0.20	0.01	0.01	0.01	0.16	0.34
	0.10	0.31	0.35	0.47	0.48	0.45	0.36	0.32
	0.15	0.33	0.36	0.41	0.41	0.41	0.38	0.34
	0.20	0.34	0.36	0.40	0.40	0.40	0.38	0.35
	0.25	0.35	0.37	0.39	0.40	0.40	0.38	0.36
	max	0.27	0.35	0.47	0.50	0.58	0.58	0.36

Table A.4: Horizontal velocities per test on a certain height. In this X is the place where the velocity is taken where X1 is point on the left of the near-bed structure and X7 is the point the most to the right.
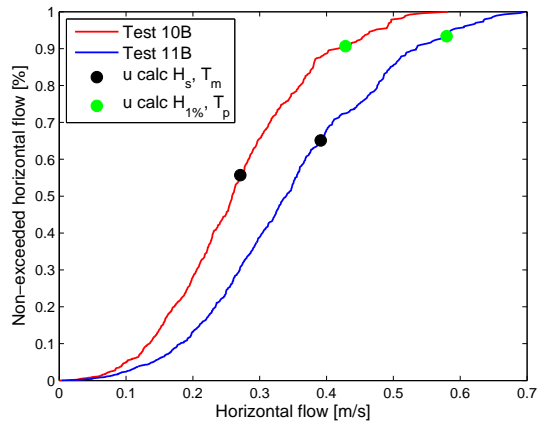
Figure A.8: Non-exceeded velocity for test 10B and 11B. In test 10B $H_s = 15$ cm and test 11B $H_s = 20$ cm. U calc is the calculated horizontal velocity using linear wave theory on depth h_c.

Appendix B

Literature

In this Appendix several investigations that have been performed in this thesis are explained. These investigations are important, but not of significance for the analysis of the damage development investigated in this thesis. These matters that are not of extreme importance are explained in this appendix. This appendix is about the following subjects:

- Boundary layer under waves

- Forces on a single stone

- Imitation of motion

- Design practice using Shields

- Shields for waves

B.1 Boundary layer under waves

The boundary conditions to solve the balance equation for linear wave theory is that the velocity in the x direction on the bottom should be zero. However, near the bottom is a boundary layer where the flow is highly rotational and the assumptions on which linear wave formulations are based are no longer valid. The boundary layer is very small so it is still allowed to use linear wave theory in the remaining depth. The boundary layer or viscous sub layer can be expected in a relatively thin region near the bottom. The boundary layer is responsible for high shear stresses under short waves. Because of the relatively small wave period the boundary layer is never fully developed. There is insufficient time in a wave period to develop a velocity profile over the whole height which for instance is possible with flow in rivers.

Jonsson [1966] measured the logarithmic velocity profiles and he proposed a maximum boundary layer thickness for waves as Equation B.1. In this formula ν is the kinematic viscosity. In Figure B.1 a horizontal velocity profile under a wave with rotational flow in a full profile and in a boundary layer is shown. The zoomed version of the boundary layer shows a certain increase in velocity just above the boundary layer which was measured by Jonsson [1966]. This was not observed by Tromp [2004] and Terrile [2004] because they used measurement devices which had to be put away to far from the bottom. They do however mention this extra velocity is present. Hofland [2005] also measured an increase in velocity just above the boundary layer. He measured this for currents without waves present.

$$\delta = \frac{1}{2}\sqrt{\nu \pi T} \qquad\qquad (B.1)$$
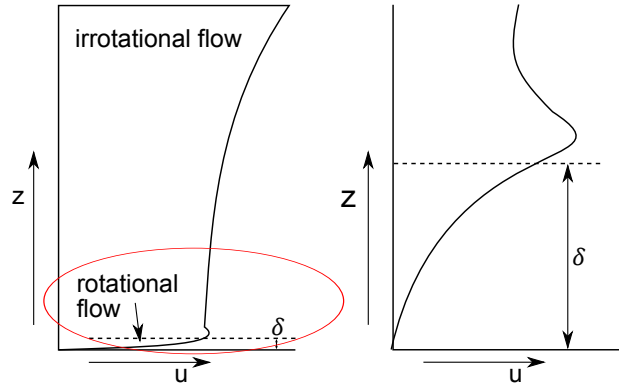
Figure B.1: Horizontal velocity profile under a wave with rotational flow in the boundary layer. To the left is a full velocity profile and to the right is a zoomed graph of the boundary layer from measurements after Jonsson [1966].

The accelerations in waves vary in time but not in place. The growth or height of the boundary layer can be approximated by Equation B.2 [Booij, 1992 cf. Schiereck, 2001]. In this formula κ is the von Kàrmàn constant.

$$\frac{d\delta}{dt} \approx \kappa u_* \approx 0.4 u_* \qquad\qquad (B.2)$$

The shear velocity u_* [-] can be approximated by the driving velocity on the bottom, $u_* = 0.1 \cdot u_0$. In a wave the boundary layer can only grow during half the wave period and has to start all over again when the flow reverses. The growth of this boundary layer with Equation B.2 applies for a flat bed without irregularities such as a near-bed structure. The boundary layer created in front of the near-bed structure influences the horizontal velocity and therefore the near-bed structure.

B.2   Design approaches

In this paragraph first the forces on a single stone are explained. Secondly the stable design approach using the bed shear stress is explained. This is the stable method to design a near-bed structure.

B.2.1   Forces on a single stone

From the previous section and from Chapter 2 it is know that there is a orbital flow velocity on the bottom of the sea because of the waves. These flow forces can cause instability of near-bed material. In this paragraph a stability parameter that is directly based on analysis of the stabilizing and destabilizing forces is treated. This approach does take the flow acceleration into account and is generally called the Morison approach after their research of wave forces on piles [Morison et al., 1950]. Besides this research several MSc students have looked at this problem [Dessens, 2004, Tromp, 2004 and Terrile, 2004]. Van den Bos [2006] summarises all the approaches of these students. This paragraph is based on all of these researches.

In Figure B.2 the forces that act on a bed material particle that is subject to passing flow are shown. There are six different forces that can be distinguished.
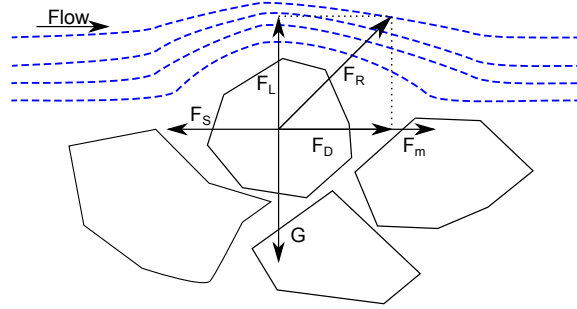
Figure B.2: Forces on bed particle.

Gravity: G**.** The underwater weight of the stone can be related to its volume V. In Equation B.3 this relation can be seen.

$$G = (\rho_s - \rho_w)gV \tag{B.3}$$

Drag Force: F_D**.** When a flow goes past an object the object experiences a drag force from this flow. The drag force is thus in the direction of the flow. Via Equation B.4 the drag force can be calculated.

$$F_D = \frac{1}{2}\rho_w C_D u^2 A_D \tag{B.4}$$

In this Equation C_D is an empirical drag coefficient that depends on the shape of the object and A_D is the cross sectional area of the object in the direction of the flow. The drag coefficient is hard to determine because of the irregularities to every stone. Besides this, the local velocity is different at every depth. Also the area is hard to determine because of the irregularities and the stone might be embedded in the structure.

Lift force: F_L**.** As the flow passes the stones streamlines are contracting which can be seen in Figure B.2. This results in higher velocities and a reduction in pressure. Because of the higher velocities around the stone and a reduction in pressure the stone is pulled out of the bed by a lift force. The lift force is perpendicular to the flow direction and can be calculated with Equation B.5. In this Equation C_L is the empirical lift coefficient and A_L is the cross sectional area of the stone perpendicular to the stone.

$$F_L = \frac{1}{2}C_L\rho_w u^2 A_L \tag{B.5}$$

Because the lift force and the drag force are both difficult to calculate these are most of the time combined into a resultant force F_R. This force can be calculated using Equation B.6. In this Equation C_B is the bulk coefficient that combines the effect of the lift and drag forces. The area A in this Equation has been assumed to be the same for the lift and drag force, $A_D = A_L$.

$$F_R = \frac{1}{2}\rho_w C_B u^2 A \tag{B.6}$$

From Figure B.2 it can be seen that the resultant force is $F_R = \sqrt{F_L^2 + F_D^2}$ and it follows the bulk coefficient has to be calculated in the same way, $C_B = \sqrt{C_L^2 + C_D^2}$. The angle on which this force acts depends on the magnitude of the drag and lift force.

Inertia force: F_M**.** If accelerations are present in the flow, there is a pressure gradient over the stone. This causes an extra force in the flow direction. This force can be calculated using

the theoretical Equation B.7. It is assumed the dp/dx over a stone length is constant. In this Equation p is the pressure.

$$F_M = \iiint \frac{dp}{dx} dxdydz = V\frac{dp}{dx} \tag{B.7}$$

Because this formula is a theoretical formula the stones do not move accordingly to this. The stones are partially bedded which means that not the full volume V is active. Besides this, not only the stones are accelerated but also the water volume around the stone. This introduces extra mass which is called the added mass. This can be compensated by introducing again an empirical coefficient C_M. Equation B.7 can be calculated with the use of the simplified equations of motions from the 1-dimensional Euler Equation. This formula can be seen in Equation B.8.

$$\frac{dp}{dx} = \rho_w \frac{Du}{Dt} = -\rho_w \left(\frac{\delta u}{\delta t} + u\frac{\delta u}{\delta x} \right) \tag{B.8}$$

Using the empirical added mass coefficient C_M and substituting Equation B.8 in B.7 gives Equation B.9. Here Du/Dt is the material derivative which are the accelerations that cause the inertia force due to a temporal acceleration.

$$F_M = C_M \rho_w V \frac{Du}{Dt} \tag{B.9}$$

Shear force: F_S. Schiereck [2001] also mentions the shear force. The shear force is caused by the moving velocity along the stone. The shear force can be calculated using Equation B.10. C_S is the empirical shear coefficient and A_S the exposed surface area.

$$F_S = \frac{1}{2}\rho_w C_S u^2 A_S \tag{B.10}$$

Van den Bos [2006] mentions that the shear force is implicitly included in the drag force F_D because this is also proportional to u^2 and works in the flow direction. He bases this conclusion on work by Dessens [2004], Tromp [2004] and Terrile [2004].

Friction force: F_F. Another force that is present on a stone is the friction force. This force is caused by interlocking with other stones. Together with the weight of the stone this force is the resistant factor towards movement against currents. The friction force can also be called the stability of the stone. A visualisation can be seen in Figure B.3 where F_R is used instead of the drag and lift force.
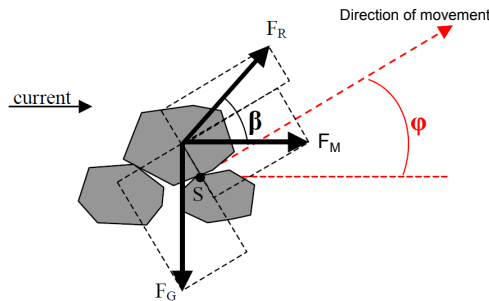
Figure B.3: Stability of a bed particle. Taken from Dessens [2004].

In Figure B.3 the current tries to move the stone in the direction of the flow around point S. The resultant force and the inertia force act under an angle β. This angle depends on the contribution

of the lift, drag and turbulent forces. It is assumed the stone starts to move at a certain angle which is called the escape angle ϕ. This angle depends on the position of point S. The smaller the this angle, the more exposed the stone is [Tromp, 2004].

What force is necessary to move the stone can be found through a force balance in the direction of the current [Dessens, 2004 and Tromp, 2004]. The force balance is shown in Equation B.11.

$$F_G \sin(\phi) = F_R \cos(\phi - \beta) + F_M \cos(\phi) \tag{B.11}$$

Stones start to move if $F_G < F_{R,M}$. This describes a threshold of motion and a stability parameter Θ can be derived from this which is done in Equation B.12.

$$\Theta = \frac{F}{G} = \frac{F_r \dfrac{\cos(\beta - \phi)}{\sin(\phi)} + F_M \dfrac{\cos(\phi)}{\sin(\phi)}}{G} \tag{B.12}$$

With Equation B.3, B.6 and B.9 substituted into each other, $A = D_{n50}^2$ and $V = D_{n50}^3$ this gives Equation B.13.

$$\Theta = \frac{\dfrac{1}{2} C_B \dfrac{\cos(\beta - \phi)}{\sin(\phi)} u^2 + C_M \dfrac{\cos(\phi)}{\sin(\phi)} \dfrac{Du}{Dt} D_{n50}}{\Delta g D_{n50}} \tag{B.13}$$

The effects of ϕ and β are assumed to be implicity included in the coefficients C_B and C_M. Dessens [2004] and Tromp [2004] give the stability parameter as Equation B.14.

$$\Theta = \frac{\dfrac{1}{2} C_B u^2 + C_M \dfrac{Du}{Dt} D_{n50}}{\Delta g D_{n50}} \tag{B.14}$$

The values of the coefficients are hard to determine and there is not much literature available on the this subject. The only coefficients that have been investigated a lot are the drag and lift coefficients. Below is stated what the ranges of each coefficient is and on what research it is based.

- Drag coefficient C_D. The drag coefficient has been investigated intensively and the following range can be given: $C_D = 0.15 - 0.35$ [Hofland et al, 2004 cf. Tromp, 2004].

- Lift coefficient C_L. The lift coefficient has also been investigated intensively and the following range can be given: $C_L = 0.15 - 0.22$ [Hofland et al, 2004 cf. Tromp, 2004].

- Bulk coefficient C_B. As stated before, the bulk coefficient can be calculated using the drag and lift coefficient: $C_B = \sqrt{C_L^2 + C_D^2}$.

- Inertia coefficient C_M. The research of the inertia coefficient is done after Dalrymple, 1991 cf. Tromp, 2004. Here a formula is given in the form of: $C_M = 1 + k_m$ where k_m is called the added mass which depends on the object. Tromp advises to take a value of 2 - 3 for the inertia coefficient.

B.2.2 Initiation of motion

In the past a lot of research has been done on the initiation of motion. The most important research has been done by Izbash [1930] cf. Schiereck [2001] and Shields [1936]. They developed a relationship whether or not a particle is stable under given flow conditions. An important concept

in this is the so-called threshold of motion. This can be defined as the load when stones start to move. It is often described as the exceeding of critical values of shear stress.

Izbash defined the threshold of motion by a critical velocity. When the flow velocity is higher then the critical velocity stones start to move. Izbash his formula is shown in Equation B.15. Here D is the diameter of the stones and Δ is the relative stone weight defined as $(\rho_s - \rho_w)/\rho_w$.

$$u_c = 1.2\sqrt{2\Delta g D} \tag{B.15}$$

The place of the flow velocity u_c is however not defined and neither it is very clear how the diameter of stones is incorporated. This formula is a good tool to use with first approximations of the size of stone that is needed.

More research on this topic was done by Shields [1936] which is still being used today. He reasoned that the destabilising forces could be represented by Equation B.16.

$$F = a\zeta D^2 \left(\frac{1}{2}\rho u_k^2\right) \tag{B.16}$$

Here ζ is a coefficient that includes drag, shear and lift. This coefficient represents actually the forces that are present on the bed particle. $\frac{1}{2}\rho u_k^2$ Represents a dynamic pressure related to the local velocity near the stone. In this equation a is a constant which mainly depends on the grain shape but also depends slightly on other variables. The velocity u_k is assumed to be at level $z = c \cdot D$ where c is a constant in the order of one. Shields showed that this velocity depends on the particle Reynolds number where he assumes a logarithmic velocity profile near the bed. The particle Reynolds number is a measure in fluid mechanics to consider the nature of the flow around an object. Shields his formula can be seen in Equation B.17.

$$u_k = u_* f_1 \left(Re_*\right) = u_* f_1 \left(\frac{u_* D}{\nu}\right) \tag{B.17}$$

In this equation Re_* is the particle Reynolds number, u_* is the shear velocity which can be defined as $u_* = \nu(\tau_0/\rho)$, ν is the kinematic viscosity of the fluid, τ_0 is the bed shear stress which can be calculated with $\tau_0 = \rho u_*^2$ and the function f_1 depends on grain shape. Shields hereby links the shear stress to the destabilising forces instead of to the velocity u_k. These destabilising forces, ζ in Equation B.16, are also a function of the particle Reynolds number around a stone. This function can be seen in Equation B.18.

$$\zeta = f_2 \left(\frac{u_k D}{\nu}\right) = f_2 \left(\frac{u_* f_1 Re_* D}{\nu}\right) = f_3(Re_*) \tag{B.18}$$

It can be seen that from Equation B.17 and B.18 all unknown variables in Equation B.16 are functions of the grain shape and Re_*. Because of this it is possible to rewrite Equation B.16 into B.19.

$$F = D^2(\rho u_*^2) f_4(Re_*) \tag{B.19}$$

The motion of a stone starts when the forces are equal or higher than the resulting forces caused by the weight of the stone ($F \geq G$), which is also referred to as the initiation of motion. As showed before the gravity force of an underwater stone can be calculated with Equation B.3. In the most critical situation the destabilising forces are equal to the resistance forces. Combining this with Equations B.3 and B.19 this can be rewritten in the form of Equation B.20.

$$\frac{\tau_{0cr}}{(\rho_s - \rho_w)gD} = \frac{u_{*cr}^2}{\Delta gD} = f(Re_*) \tag{B.20}$$

This formula is the original Shields formula which is shown in many textbooks. In this thesis this is referred to as the mobility parameter. Here the subscript cr is used to denote the critical situation. The left side of this Equation is called the Shields parameter Ψ_{cr} and is a stability parameter which is defined using a critical value of the (shear) velocity. Figure B.4a is the classical shields curve. For high numbers of Re_*, the Shields parameter Ψ_{cr} becomes constant. Iteration is necessary because u_{*cr} appears on both axes of the graph.
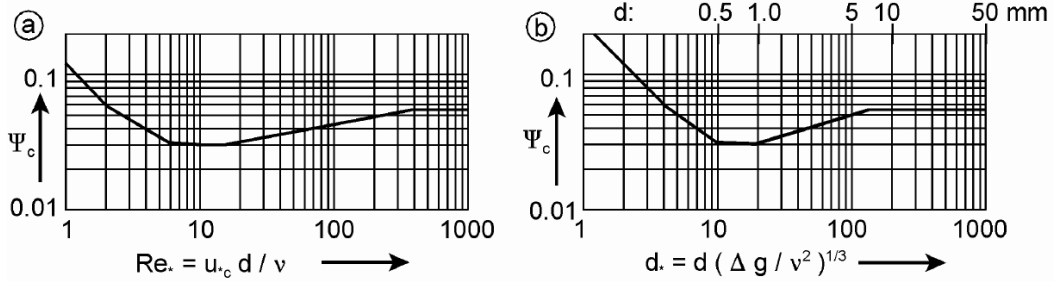
Figure B.4: Critical shear stress according to Shields [1936] and Van Rijn [1984]. Taken from Schiereck [2001].

Figure B.4b gives the same relation, but Re_* is replaced by a dimensionless particle diameter D_*, which was introduced by van Rijn [1984] cf. Schiereck [2001]. The dimensionless particle diameter is given by Equation B.21.

$$D_* = D \left(\frac{\Delta g}{\nu^2} \right) \tag{B.21}$$

The advantage of this formula is that iteration of u_{*cr} is no longer necessary. For particles bigger then $D = 6\text{-}7$ mm the Shields value becomes constant wit a value of approximately $\Psi_{cr} = 0.055$.

Design practice with Shields

Near-bed structures are currently designed often with the use of the Shields formula (Equation B.20). For a given acting bed shear stress τ the stone and mobility parameter Ψ can be calculated. As said before, when Ψ is lower than the critical value Ψ_{cr} stones start to move. When no stones should be moving, a design formula for the size of the stones can be determined. Rewriting of Equation B.20 gives Equation B.22.

$$D = \frac{\tau_0}{(\rho_s - \rho_w)\Psi_{cr}} \tag{B.22}$$

From a momentum balance the bottom shear stress can be determined for uniform gravity driven flow. The bottom shear stress τ_0 can be calculated using Equation B.23. In this formula R is the hydraulic radius which is defined as A/P, P is the perimeter and i_b is the slope of the bottom.

$$\tau_0 = \rho_w g R i_b \tag{B.23}$$

The Chézy relationship holds when a logarithmic velocity profile is assumed over the water depth. The classical Chézy formula is shown in Equation B.24. In this formula C is the Chézy parameter and $\bar{\bar{u}}$ is the depth averaged velocity.

$$\overline{\overline{u}} = C\sqrt{Ri_b} \tag{B.24}$$

By a combination of Equation B.24, B.23 and knowing $\tau_0 = \rho_w u_*^2$, two Equations can be derived. These formulas can be seen in Equation B.25 and B.26.

$$u_* = \frac{\sqrt{g}}{C}\overline{\overline{u}} \tag{B.25}$$

$$\tau_0 = \rho_w u_*^2 = \rho_w \frac{g}{C^2}\overline{\overline{u}}^2 \tag{B.26}$$

To combine these Equations with the design formula from Shield in Equation B.22 a design formula with more appropriate parameters can be derived. This design formula is shown in Equation B.27.

$$D = \frac{\overline{\overline{u}}^2}{\Psi_{cr}\Delta C^2} \tag{B.27}$$

This is the main design formula to design a stable near-bed structure or bottom protection. The Chézy coefficient in this formula can be calculated using Equation B.28. In this formula the horizontal roughness parameter k_s can be calculated using $k_s = 2 \cdot D_{n50}$ which is recommended by Schiereck [2001].

$$C = 18\log\left(\frac{12h}{k_s}\right) \tag{B.28}$$

Another important factor is the value which is taken for the Shields number Ψ_{cr}. As said before, the Shields value becomes constant for large Reynolds numbers which gives a value of $\Psi_{cr} = 0.055$. For smaller values of this number it was said that the stones would begin to move. However, in reality there is no such thing as the threshold of motion. Stones always tend to move even below the Shields parameter for threshold of motion. Schiereck [2001] distinguishes seven types of stone movement from 'No movement at all' to 'general transport of all grains'. It was investigated that the Shields criterion fits stage six the best which is defined as 'continuous movement of at all locations'. For save design purposes a choice of $\Psi_{cr} = 0.03$ is recommended and means very small or no transport at all of stones should be present.

The size of the stones in the Shields formula is another point of debate. It is assumed the D value in Equation B.27 is the D_{n50}. However, this means that 50% of the stones are lighter and thus move. Because also 50% of the stones are heavier than the D value it is assumed the stones are interlocked, and that the D_{n50} is an appropriate value.

Shields for waves

So far the stability calculated by Shields was for uniform flow only. This excludes non developed flow, non-uniform flow, stability during waves, sloping beds and on places where increased turbulence is expected like along weirs and structures. Several reduction parameters have been developed to coop with these problems. However, the most important topic of this thesis, the stability of stones under waves, has not been included in these factors.

Several researchers have investigated the shear-stress under waves. The friction factor τ_0 has to be redefined for the use with waves which includes oscillatory flow situations. The bed shear stress under waves can be linked to the horizontal orbital velocity close to the bed. The horizontal velocity varies over a wave and consequently so does the shear stress. An overall value for the shear stress could be the maximum shear which is defined by a hat ($\hat{\tau}$) or the averaged shear value ($\overline{\tau}$). Jonsson [1966] mentions that the friction factor for waves is defined as Equation B.29.

Here the subscript w is used for waves, $\hat{u}_0$ is the maximum velocity on the bottom which can be calculated using linear wave theory and c_f is the friction factor.

$$\hat{\tau}_w = \frac{1}{2}\rho_w c_f \hat{u}_0 \tag{B.29}$$

Jonsson also found a way to describe the friction factor. This factor has been rewritten by Swart [1974] cf. Saers [2005]. The friction factor can be seen in Equation B.30.

$$c_f = \exp\left[-6.0 + 5.2\left(\frac{a_0}{k_s}\right)^{-0.19}\right] \qquad \text{with} \qquad c_{fmax} = 0.3 \tag{B.30}$$

Within this friction factor a_0 is the amplitude of the horizontal wave motion near the bed. This can be defined according to linear wave theory as $\hat{u}_0 T/2\pi$, which is also shown in Equation 2.6. Many other factors for the friction factor exist. These factors are not described in this thesis.

With this shear stress the stability relation by Shields can be used again. The result from this approach differs a little bit from the original Shields graph (Figure B.4). These results are probably different because other boundary developments are present in an oscillating situation. Sleath [1978] summarized a lot of measurements in non breaking waves from different authors. The graph made by Sleath can be seen in Figure B.5.
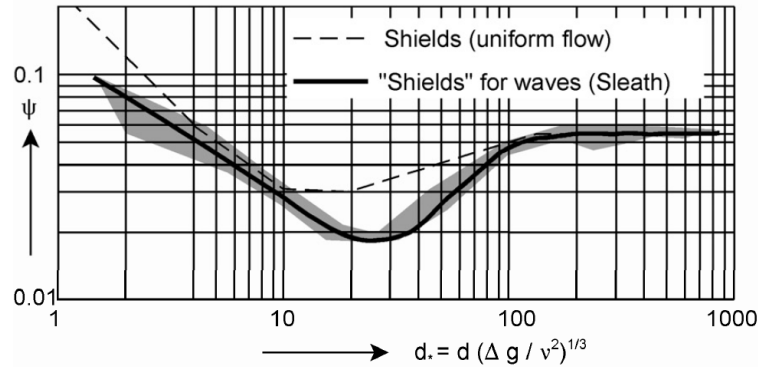
Figure B.5: Modified Shields diagram for non-breaking waves. Taken from Schiereck [2001].

Sleath also uses the dimensionless shear stress Ψ and the dimensionless grain diameter used by Van Rijn. For large values of d_* Sleath found the $\Psi = 0.055$ which is the same value as Shields used first. The Shields number for waves can be obtained to insert Equation B.29 in B.20. The answer to this is shown in Equation B.31.

$$\Psi_{wcr} = \frac{\hat{\tau}_{0,w}}{(\rho_s - \rho_w)gD} \tag{B.31}$$

Appendix C

Measured hydraulic conditions

In Figure C.1 the wave height distribution is drawn for test 1. This is done with an adapted Matlab script from H.J. Verhagen and P.B. Smit to determine the wave properties. The blue dots are the observed values, the red line is the Battjes and Groenendijk [2000] relation and the blue line is the Rayleigh distribution. The red dot in this formula is the calculated wave height with the use of Equation 2.39. For the other tests this wave height distribution is very similar, because the same waves have been imposed at the wave generator. For test 3 higher waves were used, this wave height distribution can be seen in Figure C.2. Both Figures are made with approximately 5000 waves which is more than enough to represent a JONSWAP spectrum. Because the saved files from Dasylab are recorded in volts Table C.1 gives the scaling factors to meters. Besides this, also the exact coordinates of the wave gauges are given here in meters from the starting position of the wave board.

$$H_{1\%} = H_s \frac{\sqrt{\frac{1}{2}\ln(100)}}{\sqrt[3]{1 + \frac{H_s}{h}}} = H_s \frac{1.52}{\sqrt[3]{1 + \frac{H_s}{h}}} \tag{2.39}$$

G18	G19	G20	G21	G22	G23	G25	G27	Unit
0,025478	0,02398	0,026874	0,024055	0,026144	0,024883	0,024359	0,022644	[m/volt]
15.50	15.80	16.20	25.00	25.00	32.00	32.30	32.70	[m]

Table C.1: Scaling factors for Dasylab data files and exact distance from wave board.

In Figure C.3 and C.4 the incident and reflected wave spectra are shown for test 1 before and after the near-bed structure. The spectra's for other test are very similar when the same wave height was used. It can be seen that the spectrum is a little distorted after passing the near-bed structure and in both cases very few reflection is present. In Figure C.5 and C.6 the incident and reflected wave spectra are shown for test 3 before and after the near-bed structure. Here more reflection is present because higher waves are used. Both wave spectra's for test 1 and 3 are made with approximately 5000 waves.

H_mean (m) 0.096
H_rms (m) 0.1
H_1/3 (m) 0.14
T_mean (s) 1.6
T_1/3 (s) 2.1
H_tr(m)(acc BG) 0.011
Bed slope 1:1000000
         obs   Rayleigh   BG(red)
H_2%(m) 0.185   0.2   0.162
H_1%(m) 0.196   0.214   0.17
H_0.1%(m) 0.229   0.265   0.19
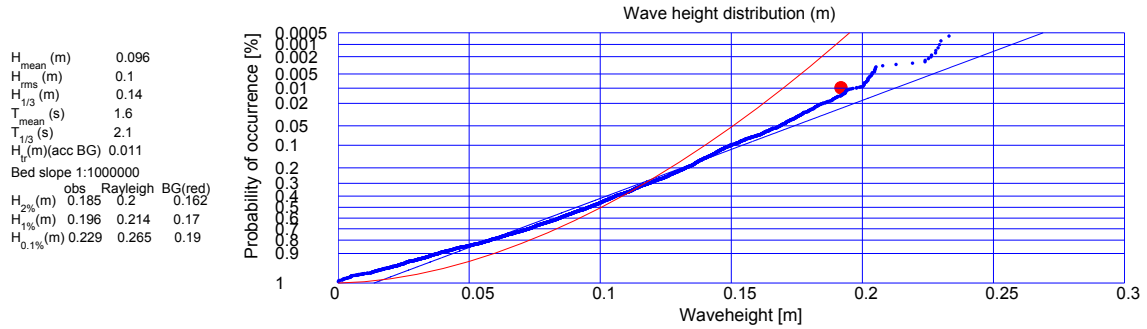
Figure C.1: Wave height distribution test 1.

H_mean (m) 0.11
H_rms (m) 0.12
H_1/3 (m) 0.16
T_mean (s) 1.8
T_1/3 (s) 2.4
H_tr(m)(acc BG) 0.018
Bed slope 1:1000000
         obs   Rayleigh   BG(red)
H_2%(m) 0.208   0.23   0.186
H_1%(m) 0.217   0.246   0.194
H_0.1%(m) 0.245   0.304   0.217
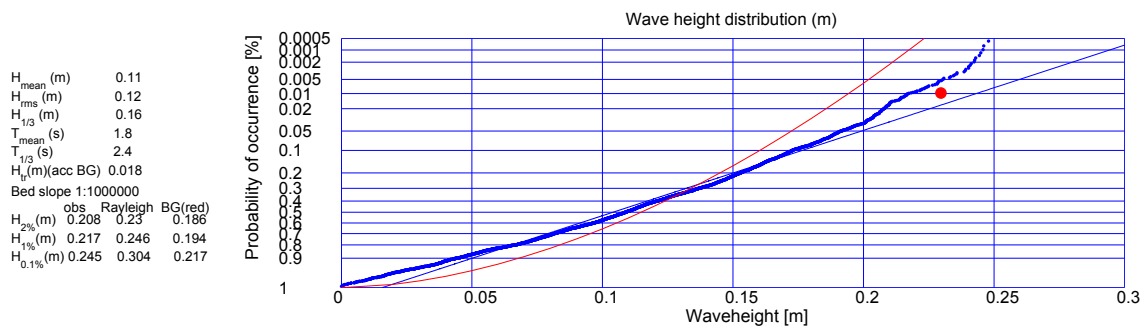
Figure C.2: Wave height distribution test 3.

In Table C.2 the hydraulic conditions for each test are shown. The calculated wave height $H_{1\%calc}$ is calculated with Equation 2.39. The wave heights H_s, $H_{1\%meas}$, $H_{0.1\%meas}$, period T_m and number of waves N is calculated from analysing the zero crossing period and the maximum wave height in between this period [Holthuijsen, 2007]. The number of waves is taken cumulative for each tests. To get the number of waves in each separate wave condition the previous condition should be subtracted from this. The peak period T_p is calculated using $T_p = \frac{T_m}{0.8}$.

Test #	H_s	$H_{1\%calc}$	$H_{1\%meas}$	$H_{0.1\%meas}$	T_m	T_p	N_{cum}
[-]	[m]	[m]	[m]	[m]	[s]	[s]	[-]
1A 1	0.142	0.197	0.192	0.231	1.58	1.98	1018
1A 2	0.142	0.197	0.193	0.233	1.59	1.98	3048
1A 3	0.143	0.198	0.194	0.234	1.59	1.99	6054
1A 4	0.143	0.198	0.195	0.234	1.60	2.00	10935
1A2 1	0.143	0.199	0.196	0.235	1.60	2.00	4881
1A2 2	0.143	0.198	0.196	0.229	1.59	1.98	9806
1A2 3	0.143	0.198	0.195	0.234	1.60	2.00	14684
1A2 4	0.143	0.198	0.195	0.234	1.60	2.00	19550
1B 1	0.142	0.197	0.192	0.231	1.58	1.98	1018
1B 2	0.142	0.197	0.193	0.233	1.59	1.98	3048
1B 3	0.143	0.198	0.194	0.234	1.59	1.99	6054
1B 4	0.143	0.198	0.195	0.234	1.60	2.00	10935
1B 5	0.143	0.199	0.196	0.235	1.60	2.00	15816
1B 6	0.143	0.198	0.196	0.229	1.59	1.98	20741
1B 7	0.143	0.198	0.195	0.234	1.60	2.00	25619
1B 8	0.143	0.198	0.195	0.234	1.60	2.00	30485
1Av2 1	0.144	0.199	0.198	0.230	1.60	2.00	1014
1Av2 2	0.144	0.200	0.197	0.236	1.60	2.00	3144
1Av2 3	0.144	0.200	0.198	0.235	1.59	1.99	6050
1Av2 4	0.144	0.200	0.197	0.236	1.59	1.99	10568
1Av2 5	0.144	0.200	0.197	0.233	1.60	2.00	15619
1Av2 6	0.144	0.200	0.198	0.235	1.60	2.00	20682
1Av2 7	0.144	0.199	0.197	0.239	1.60	2.00	25644
1Av2 8	0.144	0.200	0.196	0.236	1.60	2.00	30519

Test #	H_s	$H_{1\%calc}$	$H_{1\%meas}$	$H_{0.1\%meas}$	T_m	T_p	N_{cum}
[-]	[m]	[m]	[m]	[m]	[s]	[s]	[-]
1Bv2 1	0.144	0.199	0.198	0.230	1.60	2.00	1014
1Bv2 2	0.144	0.200	0.197	0.236	1.60	2.00	3144
1Bv2 3	0.144	0.200	0.198	0.235	1.59	1.99	6050
1Bv2 4	0.144	0.200	0.197	0.236	1.59	1.99	10568
1Bv2 5	0.144	0.200	0.197	0.233	1.60	2.00	15619
1Bv2 6	0.144	0.200	0.198	0.235	1.60	2.00	20682
1Bv2 7	0.144	0.199	0.197	0.239	1.60	2.00	25644
1Bv2 8	0.144	0.200	0.196	0.236	1.60	2.00	30519
2A 1	0.140	0.192	0.183	0.202	1.61	2.01	995
2A 2	0.140	0.192	0.183	0.201	1.60	2.00	2946
2A 3	0.141	0.193	0.184	0.206	1.61	2.01	5579
2A 4	0.141	0.193	0.183	0.207	1.61	2.01	10432
2A 5	0.144	0.198	0.185	0.206	1.76	2.20	15293
2A 6	0.142	0.195	0.185	0.204	1.61	2.01	20139
2A 7	0.141	0.194	0.186	0.206	1.61	2.01	25005
2B 1	0.140	0.192	0.183	0.202	1.61	2.01	995
2B 2	0.140	0.192	0.183	0.201	1.60	2.00	2946
2B 3	0.141	0.193	0.184	0.206	1.61	2.01	5579
2B 4	0.141	0.193	0.183	0.207	1.61	2.01	10432
2B 5	0.144	0.198	0.185	0.206	1.76	2.20	15293
2B 6	0.142	0.195	0.185	0.204	1.61	2.01	20139
2B 7	0.141	0.194	0.186	0.206	1.61	2.01	25005
2B 8	0.142	0.195	0.187	0.207	1.60	2.00	29883
2Av2 1	0.139	0.191	0.182	0.204	1.60	2.01	1020
2Av2 2	0.139	0.192	0.182	0.210	1.62	2.02	3088
2Av2 3	0.139	0.192	0.184	0.208	1.60	2.00	5961
2Av2 4	0.140	0.192	0.185	0.210	1.61	2.01	10840
2Av2 5	0.140	0.192	0.186	0.208	1.61	2.02	15646
2Av2 6	0.140	0.193	0.186	0.207	1.62	2.02	17227
2Bv2 1	0.139	0.191	0.182	0.204	1.60	2.01	1020
2Bv2 2	0.139	0.192	0.182	0.210	1.62	2.02	3088
2Bv2 3	0.139	0.192	0.184	0.208	1.60	2.00	5961
2Bv2 4	0.140	0.192	0.185	0.210	1.61	2.01	10840
2Bv2 5	0.140	0.192	0.186	0.208	1.61	2.02	15646
2Bv2 6	0.140	0.193	0.186	0.207	1.62	2.02	17227
3A 1	0.172	0.234	0.223	0.237	1.67	2.09	946
3A 2	0.168	0.230	0.221	0.246	1.71	2.14	2686
3A 3	0.164	0.225	0.218	0.239	1.75	2.19	5411
3A 4	0.164	0.225	0.219	0.241	1.78	2.22	10378
3A 5	0.164	0.225	0.219	0.243	1.78	2.23	15451
3A2 1	0.164	0.225	0.220	0.247	1.78	2.22	5116
3A2 2	0.164	0.225	0.217	0.245	1.78	2.22	10197
3A2 3	0.164	0.225	0.218	0.249	1.78	2.22	15256
3B 1	0.172	0.234	0.223	0.237	1.67	2.09	946
3B 2	0.168	0.230	0.221	0.246	1.71	2.14	2686
3B 3	0.164	0.225	0.218	0.239	1.75	2.19	5411
3B 4	0.164	0.225	0.219	0.241	1.78	2.22	10378
3B 5	0.164	0.225	0.219	0.243	1.78	2.23	15451
3B 6	0.164	0.225	0.220	0.247	1.78	2.23	20567
3B 7	0.164	0.225	0.217	0.245	1.78	2.22	25648
3B 8	0.164	0.225	0.218	0.249	1.78	2.22	30707
4A 1	0.140	0.194	0.190	0.226	1.58	1.98	1028
4A 2	0.140	0.195	0.192	0.220	1.59	1.99	3076
4A 3	0.141	0.195	0.189	0.221	1.59	1.99	6128
4A 4	0.141	0.195	0.189	0.223	1.59	1.98	11240
4A 5	0.141	0.195	0.190	0.222	1.59	1.98	16352
4A 6	0.141	0.196	0.190	0.221	1.59	1.98	21459
4A 7	0.142	0.197	0.192	0.228	1.59	1.98	26568
4B 1	0.140	0.194	0.190	0.226	1.58	1.98	1028
4B 2	0.140	0.195	0.192	0.220	1.59	1.99	3076
4B 3	0.141	0.195	0.189	0.221	1.59	1.99	6128
4B 4	0.141	0.195	0.189	0.223	1.59	1.98	11240
4B 5	0.141	0.195	0.190	0.222	1.59	1.98	16352
4B 6	0.141	0.196	0.190	0.221	1.59	1.98	21459
4B 7	0.142	0.197	0.192	0.228	1.59	1.98	26568

Test #	H_s	$H_{1\%calc}$	$H_{1\%meas}$	$H_{0.1\%meas}$	T_m	T_p	N_{cum}
[-]	[m]	[m]	[m]	[m]	[s]	[s]	[-]
4B 8	0.142	0.197	0.192	0.229	1.59	1.98	31703
5A 1	0.143	0.198	0.196	0.233	1.59	1.98	1025
5A 2	0.143	0.199	0.198	0.235	1.59	1.99	3065
5A 3	0.143	0.199	0.195	0.234	1.59	1.99	6073
5A 4	0.143	0.198	0.194	0.233	1.59	1.98	11183
5A 5	0.143	0.198	0.194	0.233	1.59	1.99	16278
5A 6	0.143	0.199	0.196	0.235	1.59	1.99	21828
5A 7	0.143	0.199	0.195	0.237	1.59	1.99	26432
5A 8	0.143	0.198	0.193	0.233	1.60	2.00	31545
5B 1	0.143	0.198	0.196	0.233	1.59	1.98	1025
5B 2	0.143	0.199	0.198	0.235	1.59	1.99	3065
5B 3	0.143	0.199	0.195	0.234	1.59	1.99	6073
5B 4	0.143	0.198	0.194	0.233	1.59	1.98	11183
5B 5	0.143	0.198	0.194	0.233	1.59	1.99	16278
5B 6	0.143	0.199	0.196	0.235	1.59	1.99	21828
5B 7	0.143	0.199	0.195	0.237	1.59	1.99	26432
5B 8	0.143	0.198	0.193	0.233	1.60	2.00	31545
6B 1	0.092	0.132	0.137	0.170	1.25	1.57	1017
6B 2	0.094	0.134	0.138	0.174	1.25	1.56	6137
6B 3	0.111	0.158	0.161	0.182	1.34	1.68	11974
6B 4	0.129	0.182	0.189	0.221	1.45	1.82	17926
6B 5	0.147	0.204	0.203	0.227	1.57	1.97	23949
6B 6	0.162	0.225	0.221	0.244	1.67	2.09	29746
6B 7	0.172	0.237	0.231	0.262	1.73	2.17	35571
6B 8	0.180	0.247	0.231	0.252	1.82	2.27	41127
7B 1	0.094	0.135	0.139	0.174	1.25	1.57	6057
7B 2	0.138	0.194	0.200	0.215	1.51	1.89	13555
7B 3	0.161	0.222	0.223	0.241	1.66	2.08	16445
7B 4	0.178	0.244	0.231	0.250	1.76	2.20	19010
7Bv2 1	0.094	0.135	0.139	0.179	1.25	1.56	5730
7Bv2 2	0.138	0.193	0.201	0.214	1.51	1.89	11892
7Bv2 3	0.160	0.222	0.223	0.238	1.66	2.07	14936
7Bv2 4	0.180	0.247	0.231	0.255	1.82	2.27	17909
7Bv2 5	0.137	0.192	0.200	0.214	1.50	1.88	23929
7Bv2 6	0.160	0.221	0.222	0.241	1.67	2.08	26980
7Bv2 7	0.137	0.193	0.200	0.215	1.51	1.89	32958
7Bv2 8	0.179	0.246	0.228	0.253	1.81	2.26	35959

Table C.2: Measured hydraulic conditions
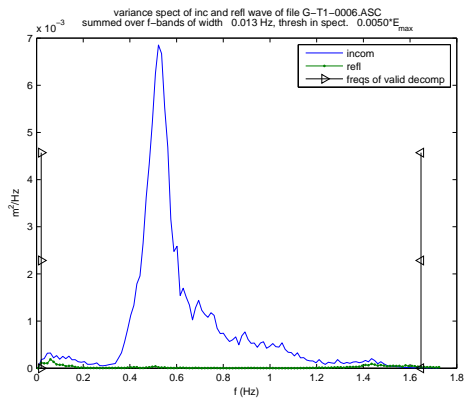
Figure C.3: Incident and reflected wave spectra test 1 calculated before the near-bed structure.
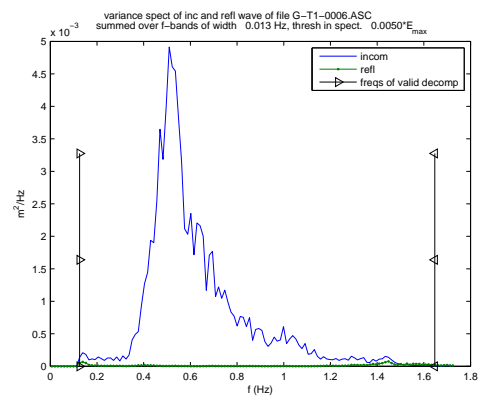
Figure C.4: Incident and reflected wave spectra test 1 calculated after the near-bed structure.
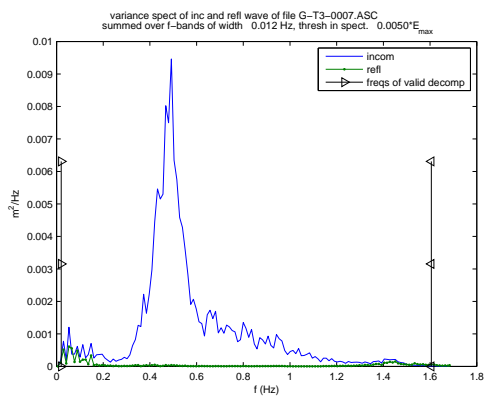
Figure C.5: Incident and reflected wave spectra test 3 calculated before the near-bed structure.
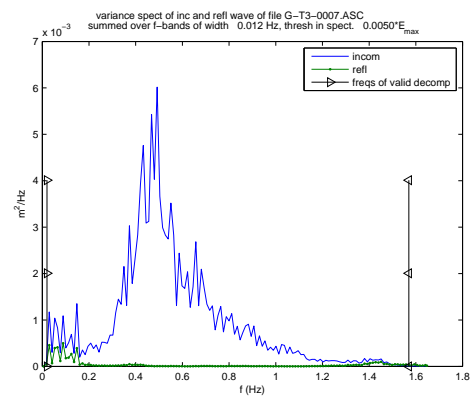
Figure C.6: Incident and reflected wave spectra test 3 calculated after the near-bed structure.

Appendix D

Granular material

In Table D.1 the sieve percentages and the characteristic diameter values for the 1-3 mm Yellow Sun stones are shown. These tests have been done by sieving a sample through seven sieves and weighing the amount of stones that has not gone through the sieve. To obtain the 50% non exceeded weight Gaussian interpolation is used.

Sieve [mm]	% of total weight on the sieve	Diameter [mm]	
3.35	0.0%		
2.8	0.4%	D_{05}	0.99
2	15.2%	D_{15}	1.16
1.7	13.9%	D_{50}	1.50
1.4	28.5%	D_{90}	2.06
1	40.0%	D_{98}	2.50
0.71	1.7%		
rest	0.4%		

Table D.1: Sieve percentages of the 1-3 mm Yellow Sun.

In Table D.2 the test to calculate the density for the 1-3 mm Yellow Sun stones are shown. These tests have been done by weighing the stones i a dry and wet condition. The difference between this is the stone volume. When the dry stone weight is divided by the volume the density is obtained. The same test is repeated for the 2-5 mm Ardenner split and is shown in Table D.3.

Nr.	Dry stone weight [g]	Submerged stone weight [g]	Stone volume [cm^3]	Stone density [kg/m^3]
1	12.914	8.096	4.818	2680
2	13.285	8.338	4.947	2685
3	15.985	10.017	5.968	2679
4	12.128	7.596	4.532	2676
5	11.526	7.217	4.309	2675
average				2679

Table D.2: Stone density test for the 1-3 mm Yellow Sun.

The grading specifications from Table 2.1 in Chapter 2 are for both stone types in the 'wide' gradation which is the same as in a real near-bed structure. Besides this, both stone types have an irregular shape. Photos from the two type of stones can be seen in Figure D.1 until D.4.

Nr.	Dry stone weight [g]	Submerged stone weight [g]	Stone volume [cm^3]	Stone density [kg/m^3]
1	17.533	11.016	6.517	2690
2	10.852	6.834	4.018	2701
3	15.213	9.546	5.667	2684
4	14.137	8.870	5.267	2684
5	15.769	9.924	5.845	2698
average				2691

Table D.3: Stone density test for the 2-5 mm Ardenner split.
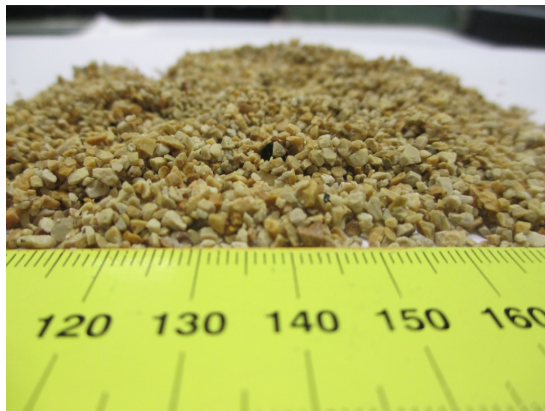
Figure D.1: Photo of stone type A.

Figure D.2: Photo of stone type A.

Figure D.3: Photo of stone type B.

Figure D.4: Photo of stone type B.

Measured damage profiles
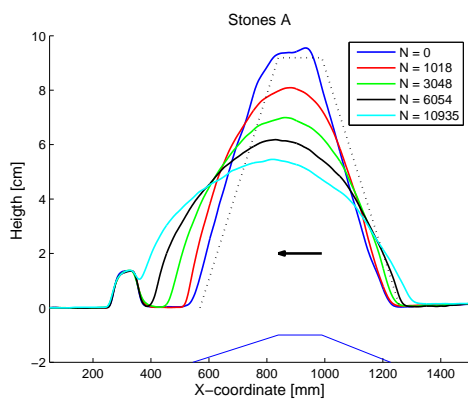
Figure E.1: Profiles test 1A
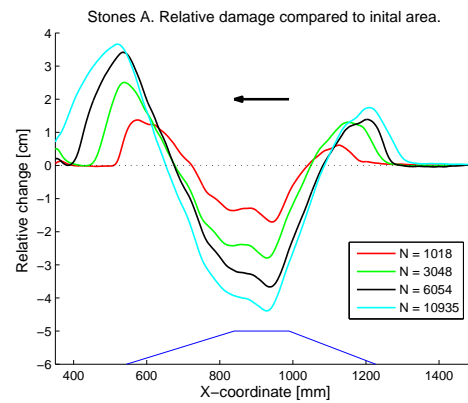
Figure E.2: Relative changes test 1A
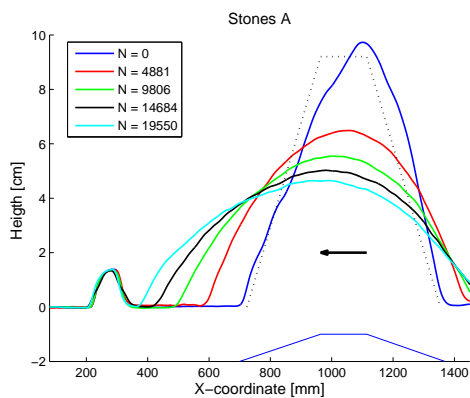
Figure E.3: Profiles test 1A2
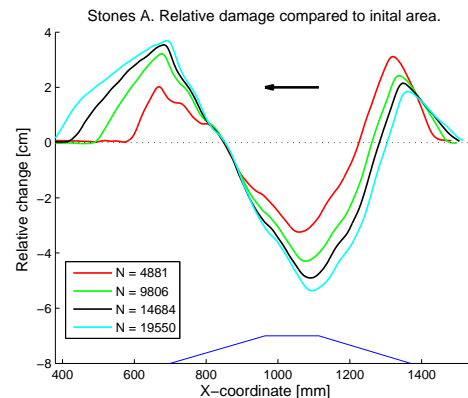
Figure E.4: Relative changes test 1A2
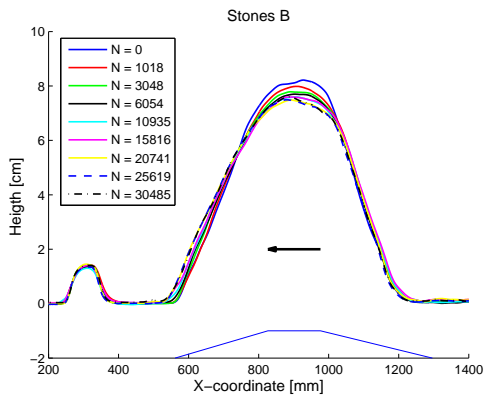
Figure E.5: Profiles test 1B
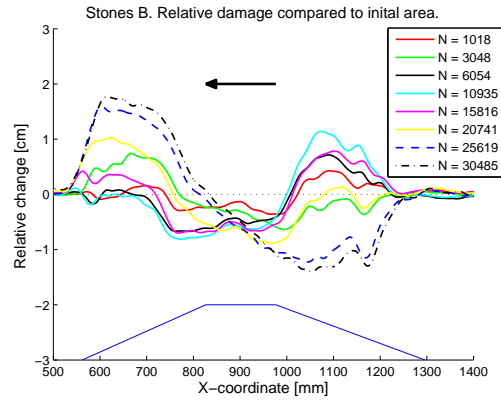
Figure E.6: Relative changes test 1B
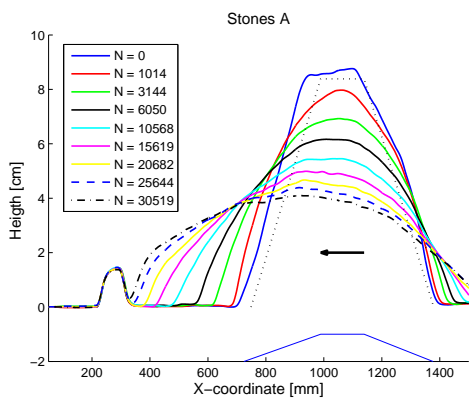
Figure E.7: Profiles test 1Av2
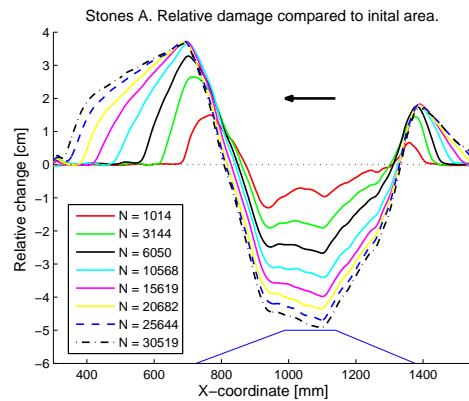
Figure E.8: Relative changes test 1Av2
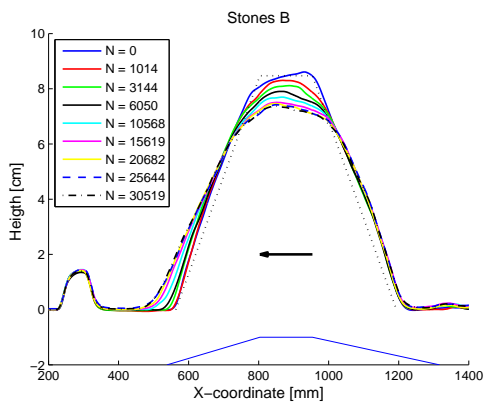
Figure E.9: Profiles test 1Bv2
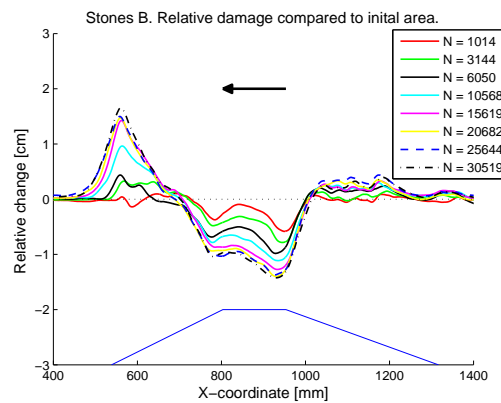
Figure E.10: Relative changes test 1Bv2
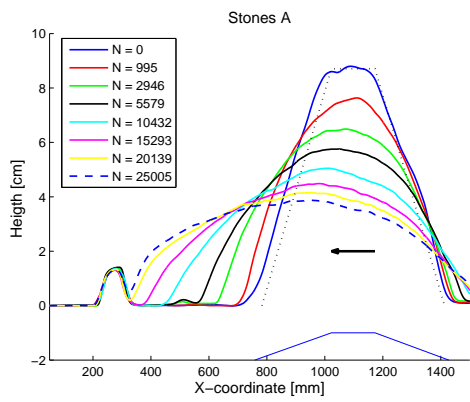
Figure E.11: Profiles test 2A
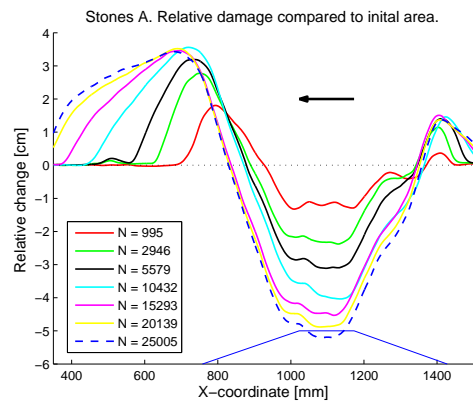
Figure E.12: Relative changes test 2A
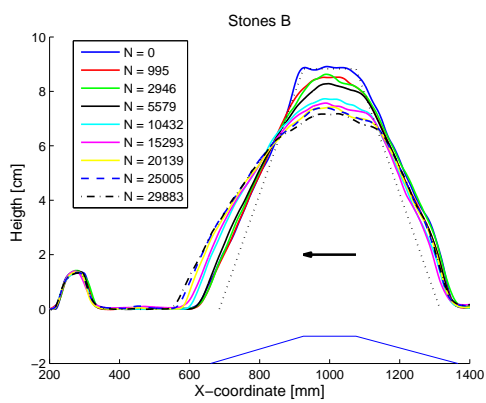
Figure E.13: Profiles test 2B
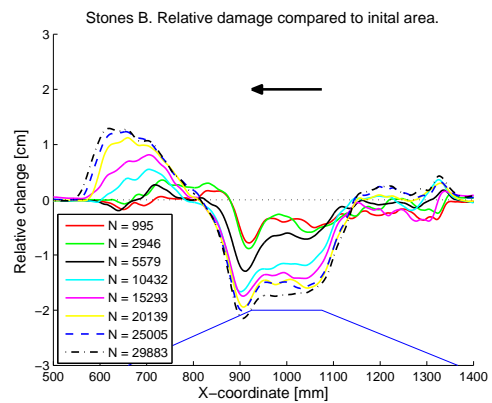
Figure E.14: Relative changes test 2B
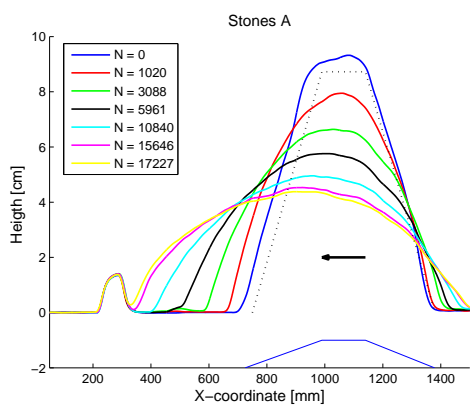
Figure E.15: Profiles test 2Av2
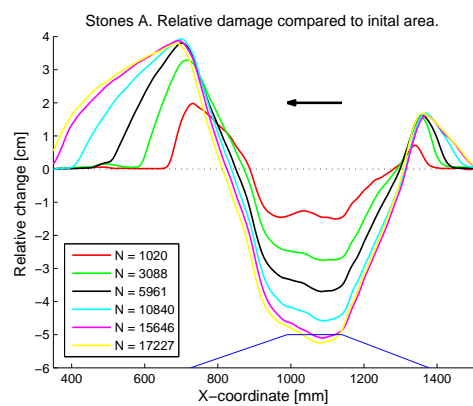
Figure E.16: Relative changes test 2Av2
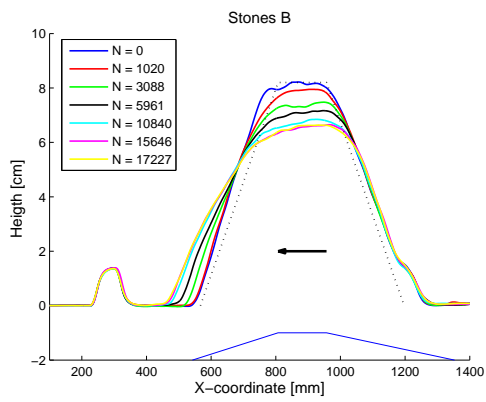
Figure E.17: Profiles test 2Bv2
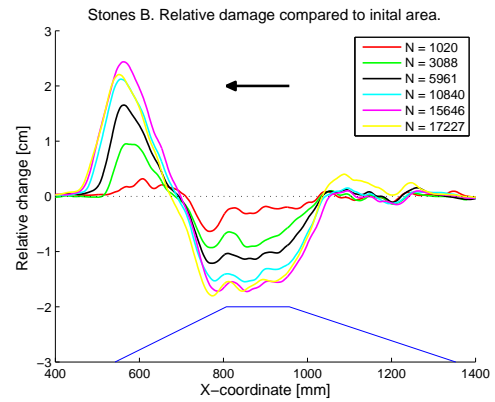
Figure E.18: Relative changes test 2Bv2
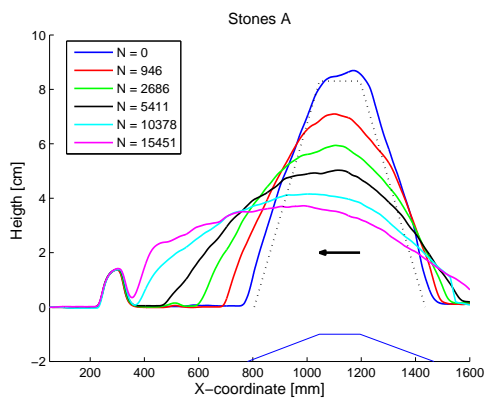
Figure E.19: Profiles test 3A
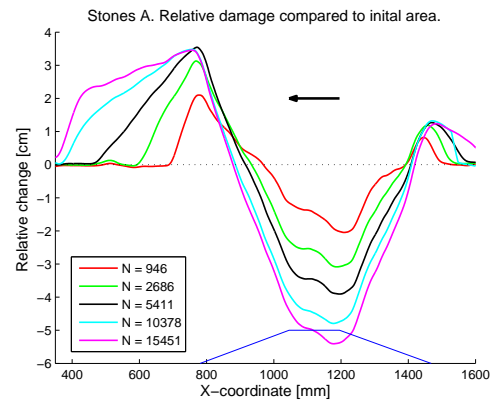
Figure E.20: Relative changes test 3A
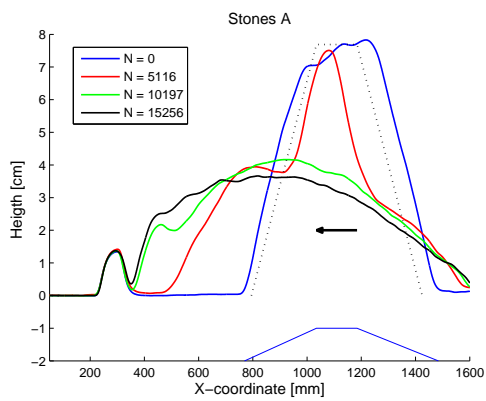
Figure E.21: Profiles test 3A2
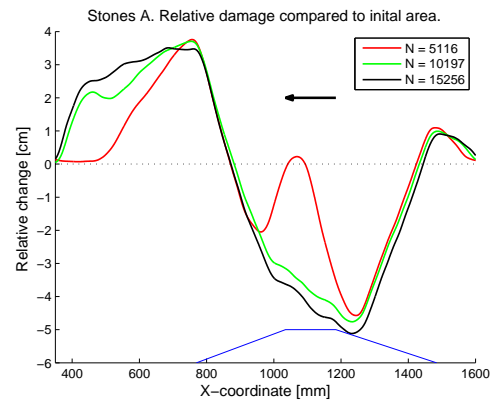
Figure E.22: Relative changes test 3A2
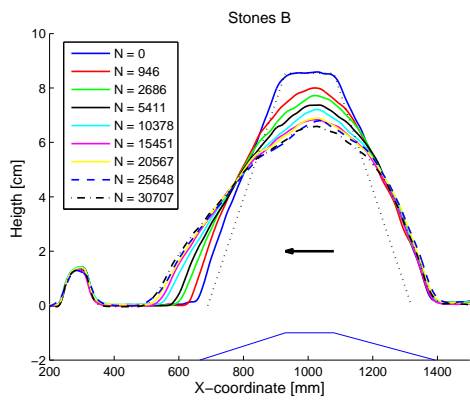
Figure E.23: Profiles test 3B
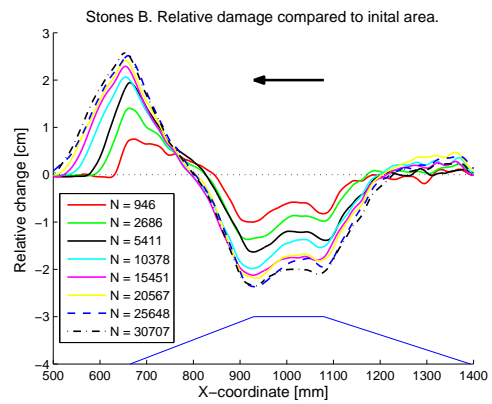
Figure E.24: Relative changes test 3B
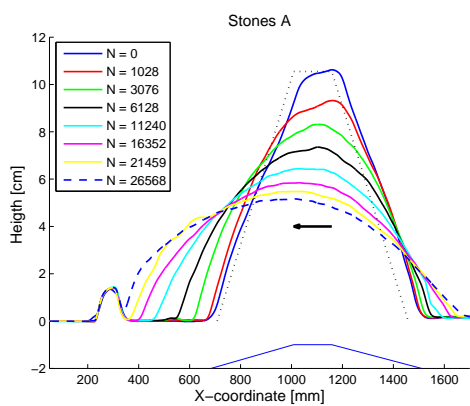
Figure E.25: Profiles test 4A
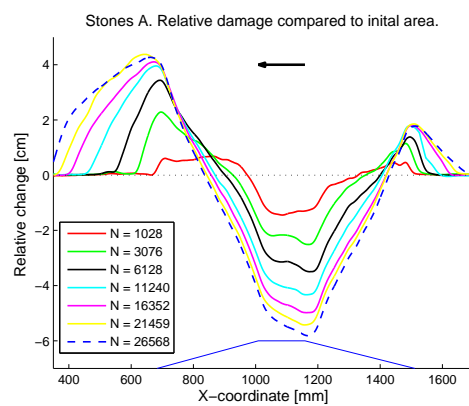
Figure E.26: Relative changes test 4A
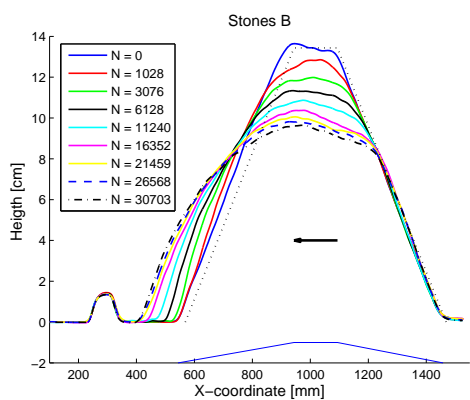
Figure E.27: Profiles test 4B
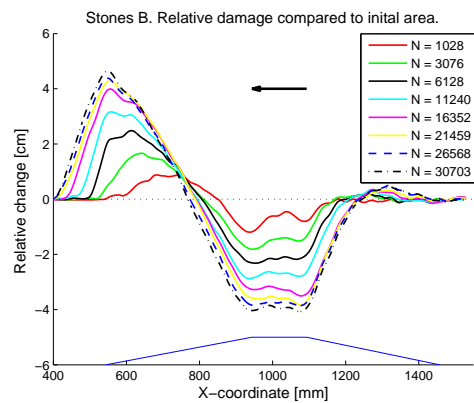
Figure E.28: Relative changes test 4B
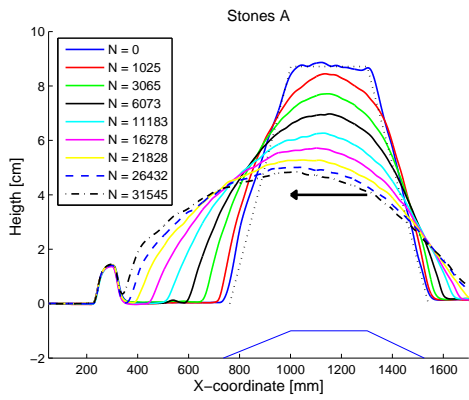
Figure E.29: Profiles test 5A
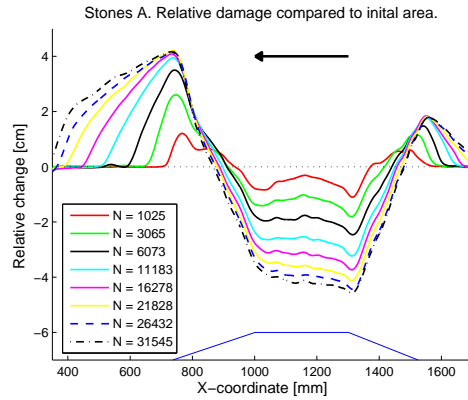
Figure E.30: Relative changes test 5A
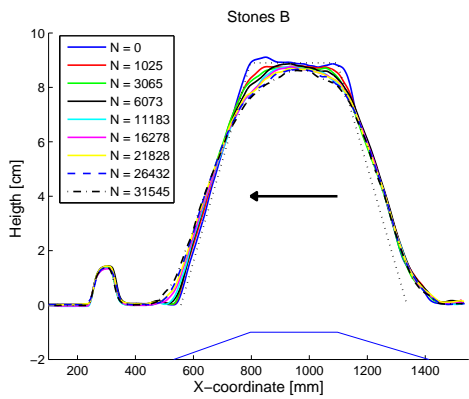
Figure E.31: Profiles test 5B
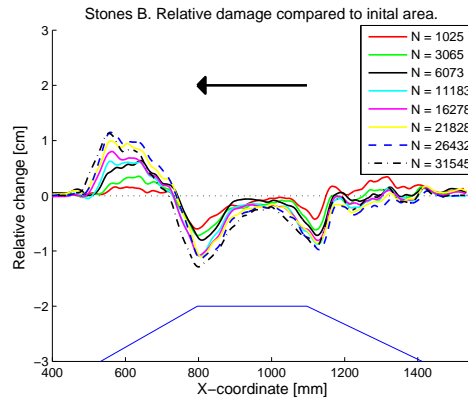
Figure E.32: Relative changes test 5B
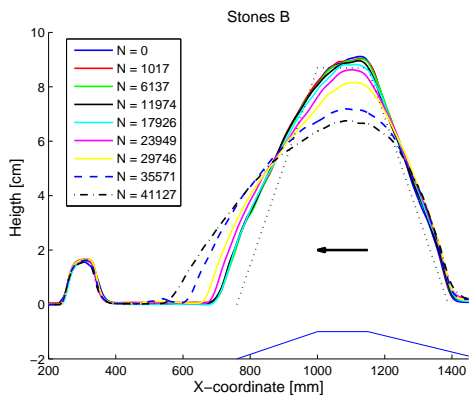
Figure E.33: Profiles test 6B
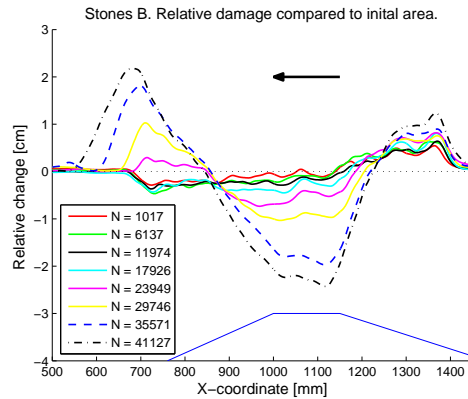
Figure E.34: Relative changes test 6B
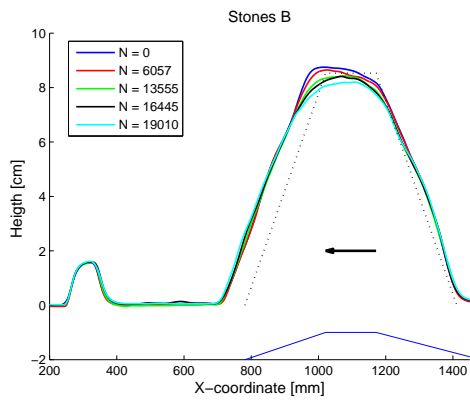
Figure E.35: Profiles test 7B
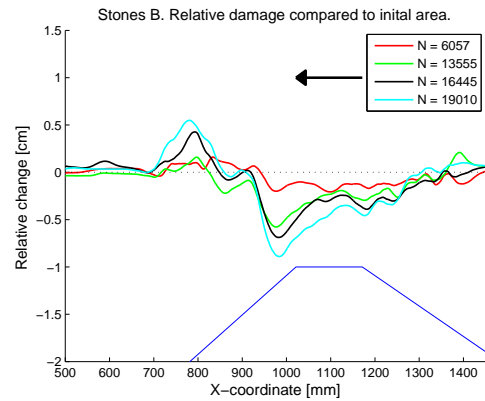
Figure E.36: Relative changes test 7B
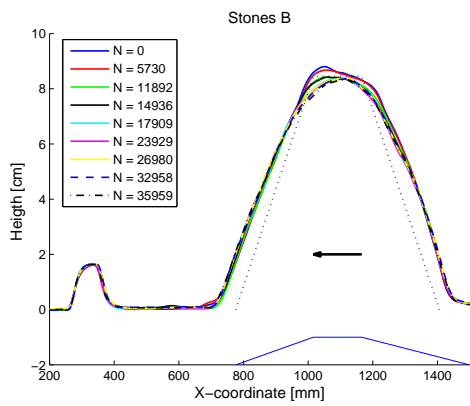
Figure E.37: Profiles test 7Bv2
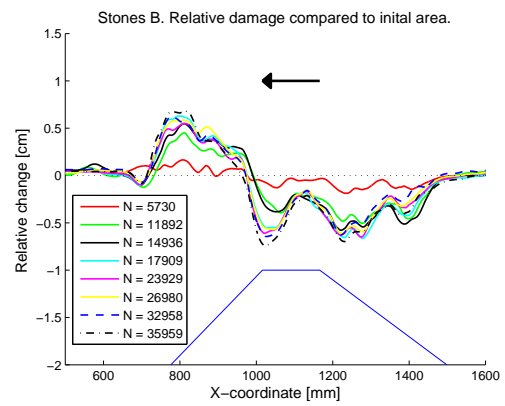
Figure E.38: Relative changes test 7Bv2

Appendix F

Erosion areas

In Table F.1 and F.5 the calculated erosion areas, structure height, calculated structure height from averaging between Equation 2.45 and 2.47 and the percentage that the maximum height and calculated height differ can be seen after each wave series for each test. When the actual height of the near-bed structure is larger than the height calculated, the percentage is minus. The mean A_e is the mean erosion area calculated per row. The erosion area A_{e2} is has been calculated with the average row. The percentage behind this is the difference with the mean erosion area per row.

$$\Delta z = \frac{-B_c + \sqrt{B_c^2 + 4m_0 A_e}}{2m_o} \qquad (2.45)$$

$$\Delta z = \frac{-(B_c + z_c m_0/2) + \sqrt{(B_c + z_c m_0/2)^2 + 2m_0 A_e}}{m_0} \qquad (2.47)$$

| | | Erosion Areas | | | | | | | | Calculations | | Erosion Area 2 | |
Test #	N [-]	1 [m²]	2 [m²]	3 [m²]	4 [m²]	5 [m²]	Mean A_e [m²]	z_d [m]	Δz [m]	$z_c - \Delta z$ [m]	Perc.	A_{e2} [m²]	Perc.
1A 1	1018	3.98E-03	3.53E-03	3.89E-03	3.45E-03	2.35E-03	3.44E-03	0.0775	0.0142	0.0777	0%	3.32E-03	-4%
1A 2	3048	7.78E-03	7.17E-03	6.74E-03	5.99E-03	5.33E-03	6.60E-03	0.0671	0.0244	0.0675	1%	6.51E-03	-1%
1A 3	6054	1.03E-02	9.90E-03	9.77E-03	8.96E-03	7.78E-03	9.34E-03	0.0598	0.0322	0.0597	0%	9.29E-03	0%
1A 4	10935	1.26E-02	1.23E-02	1.25E-02	1.24E-02	1.04E-02	1.20E-02	0.0525	0.0392	0.0527	0%	1.20E-02	0%
1A2 1	4881	8.59E-03	7.35E-03	7.15E-03	6.79E-03	8.27E-03	7.63E-03	0.0623	0.0274	0.0646	4%	7.58E-03	-1%
1A2 2	9806	1.21E-02	1.06E-02	1.06E-02	1.02E-02	1.16E-02	1.10E-02	0.0532	0.0367	0.0554	4%	1.10E-02	-1%
1A2 3	14684	1.46E-02	1.27E-02	1.22E-02	1.21E-02	1.35E-02	1.30E-02	0.0486	0.0417	0.0504	4%	1.30E-02	0%
1A2 4	19550	1.59E-02	1.41E-02	1.38E-02	1.37E-02	1.53E-02	1.46E-02	0.0447	0.0453	0.0468	5%	1.46E-02	1%
1B 1	1018	7.09E-04	5.42E-04	1.26E-03	7.20E-04	7.45E-04	7.95E-04	0.0889	0.0038	0.0784	-12%	6.83E-04	-14%
1B 2	3048	1.53E-03	1.22E-03	1.19E-03	9.17E-04	6.82E-04	1.11E-03	0.0865	0.0052	0.0770	-11%	1.01E-03	-9%
1B 3	6054	1.56E-03	1.34E-03	1.67E-03	1.05E-03	1.29E-03	1.38E-03	0.0952	0.0064	0.0758	-20%	1.29E-03	-6%
1B 4	10935	2.09E-03	1.82E-03	1.49E-03	9.25E-04	1.64E-03	1.59E-03	0.0844	0.0073	0.0749	-11%	1.47E-03	-7%
1B 5	15816	2.57E-03	1.26E-03	1.78E-03	1.17E-03	8.50E-04	1.53E-03	0.0854	0.0070	0.0752	-12%	1.50E-03	-2%
1B 6	20741	2.80E-03	1.76E-03	2.10E-03	1.05E-03	1.15E-03	1.77E-03	0.0834	0.0081	0.0741	-11%	1.71E-03	-4%
1B 7	25619	2.94E-03	2.68E-03	1.94E-03	1.51E-03	1.05E-03	2.03E-03	0.0838	0.0091	0.0731	-13%	1.88E-03	-7%
1B 8	30485	3.25E-03	1.42E-03	1.89E-03	1.14E-03	1.18E-03	1.78E-03	0.0847	0.0081	0.0741	-12%	1.69E-03	-5%
1Av2 1	1014	2.13E-03	3.41E-03	3.48E-03	3.09E-03	3.53E-03	3.13E-03	0.0761	0.0133	0.0706	-7%	2.93E-03	-6%
1Av2 2	3144	4.59E-03	5.34E-03	5.99E-03	6.44E-03	6.86E-03	5.84E-03	0.0662	0.0225	0.0614	-7%	5.72E-03	-2%
1Av2 3	6050	7.10E-03	8.43E-03	8.01E-03	9.30E-03	9.50E-03	8.47E-03	0.0589	0.0303	0.0536	-9%	8.39E-03	-1%
1Av2 4	10568	9.41E-03	1.11E-02	1.16E-02	1.20E-02	1.26E-02	1.13E-02	0.0524	0.0380	0.0458	-13%	1.12E-02	-1%
1Av2 5	15619	1.13E-02	1.33E-02	1.35E-02	1.45E-02	1.47E-02	1.35E-02	0.0479	0.0433	0.0405	-15%	1.34E-02	0%
1Av2 6	20682	1.29E-02	1.50E-02	1.51E-02	1.65E-02	1.66E-02	1.52E-02	0.0448	0.0475	0.0364	-19%	1.52E-02	0%
1Av2 7	25644	1.40E-02	1.57E-02	1.69E-02	1.75E-02	1.78E-02	1.64E-02	0.0420	0.0502	0.0337	-20%	1.64E-02	0%
1Av2 8	30519	1.48E-02	1.72E-02	1.75E-02	1.93E-02	1.94E-02	1.76E-02	0.0394	0.0529	0.0309	-22%	1.76E-02	0%
1Bv2 1	1014	9.69E-04	1.62E-03	8.18E-04	1.05E-03	8.29E-04	1.06E-03	0.0817	0.0050	0.0797	-2%	8.13E-04	-23%
1Bv2 2	3144	1.66E-03	1.97E-03	8.85E-04	1.21E-03	9.01E-04	1.33E-03	0.0805	0.0062	0.0786	-2%	1.25E-03	-6%
1Bv2 3	6050	2.44E-03	2.23E-03	1.17E-03	1.83E-03	1.51E-03	1.84E-03	0.0782	0.0083	0.0764	-2%	1.76E-03	-4%
1Bv2 4	10568	2.80E-03	3.10E-03	1.70E-03	1.43E-03	1.44E-03	2.10E-03	0.0763	0.0093	0.0754	-1%	2.01E-03	-4%
1Bv2 5	15619	3.04E-03	3.73E-03	2.59E-03	1.94E-03	1.19E-03	2.50E-03	0.0746	0.0109	0.0738	-1%	2.40E-03	-4%
1Bv2 6	20682	3.31E-03	4.07E-03	2.78E-03	2.11E-03	1.43E-03	2.74E-03	0.0737	0.0118	0.0729	-1%	2.64E-03	-4%
1Bv2 7	25644	3.67E-03	4.16E-03	2.82E-03	2.16E-03	1.05E-03	2.77E-03	0.0734	0.0119	0.0728	-1%	2.67E-03	-4%
1Bv2 8	30519	3.76E-03	3.97E-03	3.28E-03	2.14E-03	1.21E-03	2.87E-03	0.0732	0.0123	0.0724	-1%	2.80E-03	-2%

Table F.1: Measured damages for the physical model scale tests.

Test		Erosion Areas							Calculations				Erosion Area 2	
Test #	N [-]	1 [m^2]	2 [m^2]	3 [m^2]	4 [m^2]	5 [m^2]	Mean A_e [m^2]	z_d [m]	Δz [m]	$z_c - \Delta z$ [m]	Perc.	A_{e2} [m^2]	Perc.
2A 1	995	3.69E-03	4.33E-03	3.28E-03	3.37E-03	3.45E-03	3.62E-03	0.0750	0.0150	0.0721	-4%	3.45E-03	-5%
2A 2	2946	7.16E-03	6.97E-03	6.42E-03	7.21E-03	6.85E-03	6.92E-03	0.0641	0.0256	0.0615	-4%	6.75E-03	-2%
2A 3	5579	9.90E-03	9.15E-03	9.17E-03	9.07E-03	9.59E-03	9.38E-03	0.0569	0.0326	0.0545	-4%	9.21E-03	-2%
2A 4	10432	1.27E-02	1.33E-02	1.27E-02	1.24E-02	1.29E-02	1.28E-02	0.0498	0.0414	0.0456	-8%	1.26E-02	-1%
2A 5	15293	1.60E-02	1.58E-02	1.50E-02	1.51E-02	1.49E-02	1.54E-02	0.0448	0.0475	0.0395	-12%	1.52E-02	-1%
2A 6	20139	1.69E-02	1.70E-02	1.69E-02	1.66E-02	1.72E-02	1.69E-02	0.0416	0.0511	0.0360	-13%	1.68E-02	-1%
2A 7	25005	1.82E-02	1.85E-02	1.78E-02	1.84E-02	1.82E-02	1.82E-02	0.0384	0.0539	0.0331	-14%	1.81E-02	-1%
2B 1	995	8.06E-04	1.36E-03	1.37E-03	1.30E-03	2.48E-03	1.46E-03	0.0842	0.0067	0.0815	-3%	1.37E-03	-6%
2B 2	2946	8.92E-04	1.67E-03	1.94E-03	1.19E-03	1.65E-03	1.47E-03	0.0848	0.0067	0.0815	-4%	1.33E-03	-9%
2B 3	5579	1.38E-03	2.33E-03	1.84E-03	1.76E-03	2.94E-03	2.05E-03	0.0820	0.0091	0.0791	-4%	1.98E-03	-4%
2B 4	10432	3.86E-03	3.48E-03	2.44E-03	2.56E-03	3.71E-03	3.21E-03	0.0760	0.0135	0.0747	-2%	3.23E-03	1%
2B 5	15293	2.46E-03	3.60E-03	3.70E-03	3.80E-03	4.68E-03	3.65E-03	0.0754	0.0150	0.0732	-3%	3.64E-03	0%
2B 6	20139	3.78E-03	4.67E-03	4.28E-03	3.17E-03	4.11E-03	4.00E-03	0.0738	0.0163	0.0719	-2%	4.02E-03	0%
2B 7	25005	4.00E-03	4.94E-03	4.19E-03	3.17E-03	3.91E-03	4.04E-03	0.0735	0.0164	0.0718	-2%	4.04E-03	0%
2B 8	29883	4.02E-03	5.61E-03	4.50E-03	3.95E-03	4.23E-03	4.46E-03	0.0718	0.0178	0.0704	-2%	4.46E-03	0%
2Av2 1	1020	4.12E-03	4.08E-03	4.22E-03	4.68E-03	3.89E-03	4.20E-03	0.0743	0.0169	0.0703	-5%	4.13E-03	-2%
2Av2 2	3088	7.32E-03	7.44E-03	8.17E-03	8.56E-03	7.66E-03	7.83E-03	0.0620	0.0283	0.0590	-5%	7.80E-03	0%
2Av2 3	5961	1.01E-02	1.11E-02	1.17E-02	1.18E-02	1.12E-02	1.12E-02	0.0540	0.0374	0.0499	-8%	1.12E-02	0%
2Av2 4	10840	1.35E-02	1.45E-02	1.45E-02	1.54E-02	1.41E-02	1.44E-02	0.0465	0.0453	0.0420	-10%	1.43E-02	0%
2Av2 5	15646	1.53E-02	1.60E-02	1.70E-02	1.73E-02	1.64E-02	1.64E-02	0.0425	0.0499	0.0373	-12%	1.64E-02	0%
2Av2 6	17227	1.59E-02	1.70E-02	1.76E-02	1.83E-02	1.65E-02	1.71E-02	0.0411	0.0514	0.0359	-13%	1.71E-02	0%
2Bv2 1	1020	7.53E-04	9.06E-04	1.42E-03	1.55E-03	1.16E-03	1.16E-03	0.0792	0.0055	0.0765	-3%	8.89E-04	-23%
2Bv2 2	3088	1.77E-03	1.37E-03	2.45E-03	2.55E-03	2.72E-03	2.17E-03	0.0751	0.0097	0.0723	-4%	2.09E-03	-4%
2Bv2 3	5961	2.25E-03	2.34E-03	3.61E-03	3.24E-03	3.08E-03	2.91E-03	0.0714	0.0125	0.0695	-3%	2.86E-03	-2%
2Bv2 4	10840	3.25E-03	4.27E-03	4.35E-03	4.16E-03	3.68E-03	3.94E-03	0.0687	0.0162	0.0658	-4%	3.85E-03	-2%
2Bv2 5	15646	3.72E-03	4.72E-03	5.08E-03	4.40E-03	4.06E-03	4.40E-03	0.0666	0.0178	0.0642	-4%	4.36E-03	-1%
2Bv2 6	17227	3.93E-03	4.79E-03	5.13E-03	3.87E-03	4.31E-03	4.41E-03	0.0671	0.0178	0.0642	-4%	4.38E-03	-1%
3A 1	946	3.97E-03	4.52E-03	4.74E-03	5.61E-03	4.86E-03	4.74E-03	0.0680	0.0189	0.0641	-6%	4.61E-03	-3%
3A 2	2686	7.84E-03	8.60E-03	8.61E-03	9.87E-03	8.25E-03	8.63E-03	0.0569	0.0308	0.0523	-8%	8.51E-03	-1%
3A 3	5411	1.10E-02	1.13E-02	1.16E-02	1.29E-02	1.23E-02	1.18E-02	0.0485	0.0393	0.0438	-10%	1.17E-02	-1%
3A 4	10378	1.48E-02	1.53E-02	1.60E-02	1.66E-02	1.59E-02	1.57E-02	0.0399	0.0487	0.0343	-14%	1.56E-02	-1%
3A 5	15451	1.68E-02	1.75E-02	1.81E-02	1.97E-02	1.90E-02	1.82E-02	0.0356	0.0543	0.0288	-19%	1.82E-02	0%
3A2 1	5116	1.14E-02	1.04E-02	1.05E-02	1.04E-02	1.08E-02	1.07E-02	0.0744	0.0367	0.0418	-44%	1.07E-02	0%
3A2 2	10197	1.75E-02	1.54E-02	1.62E-02	1.61E-02	1.61E-02	1.62E-02	0.0415	0.0503	0.0282	-32%	1.62E-02	0%
3A2 3	15256	1.94E-02	1.84E-02	1.77E-02	1.87E-02	1.82E-02	1.85E-02	0.0366	0.0553	0.0232	-37%	1.84E-02	0%

Table F.2: Measured damages for the physical model scale tests (continued).

| Test | | | | Erosion Areas | | | | | Calculations | | | Erosion Area 2 | |
Test #	N [-]	1 [m²]	2 [m²]	3 [m²]	4 [m²]	5 [m²]	Mean A_e [m²]	z_d [m]	Δz [m]	$z_c - \Delta z$ [m]	Perc.	A_{e2} [m²]	Perc.
3B 1	946	2.32E-03	2.65E-03	1.65E-03	1.66E-03	1.85E-03	2.03E-03	0.0787	0.0090	0.0764	-3%	2.14E-03	5%
3B 2	2686	3.02E-03	3.62E-03	2.61E-03	2.55E-03	2.52E-03	2.86E-03	0.0762	0.0123	0.0731	-4%	2.83E-03	-1%
3B 3	5411	4.29E-03	4.90E-03	2.99E-03	3.64E-03	3.32E-03	3.83E-03	0.0730	0.0157	0.0697	-4%	3.78E-03	-1%
3B 4	10378	5.27E-03	5.89E-03	4.03E-03	4.02E-03	4.00E-03	4.64E-03	0.0715	0.0185	0.0669	-6%	4.59E-03	-1%
3B 5	15451	6.02E-03	7.13E-03	4.38E-03	4.45E-03	4.76E-03	5.35E-03	0.0681	0.0208	0.0646	-5%	5.35E-03	0%
3B 6	20567	6.43E-03	6.62E-03	4.81E-03	4.29E-03	4.51E-03	5.33E-03	0.0684	0.0208	0.0646	-6%	5.31E-03	0%
3B 7	25648	6.72E-03	7.55E-03	5.38E-03	4.59E-03	4.65E-03	5.78E-03	0.0677	0.0222	0.0632	-7%	5.80E-03	0%
3B 8	30707	7.11E-03	7.71E-03	5.62E-03	5.64E-03	4.47E-03	6.11E-03	0.0655	0.0232	0.0622	-5%	6.16E-03	1%
4A 1	1028	2.94E-03	3.46E-03	3.92E-03	2.97E-03	3.03E-03	3.27E-03	0.0927	0.0132	0.0923	0%	3.09E-03	-5%
4A 2	3076	6.48E-03	6.29E-03	7.12E-03	5.93E-03	6.27E-03	6.42E-03	0.0822	0.0233	0.0822	0%	6.33E-03	-1%
4A 3	6128	1.00E-02	1.02E-02	1.04E-02	9.42E-03	9.64E-03	9.94E-03	0.0727	0.0331	0.0724	0%	9.84E-03	-1%
4A 4	11240	1.32E-02	1.38E-02	1.40E-02	1.31E-02	1.34E-02	1.35E-02	0.0641	0.0419	0.0636	-1%	1.34E-02	-1%
4A 5	16352	1.63E-02	1.66E-02	1.67E-02	1.61E-02	1.65E-02	1.64E-02	0.0580	0.0485	0.0570	-2%	1.63E-02	0%
4A 6	21459	1.87E-02	1.83E-02	1.87E-02	1.80E-02	1.81E-02	1.84E-02	0.0544	0.0527	0.0528	-3%	1.83E-02	0%
4A 7	26568	2.04E-02	2.02E-02	2.06E-02	1.94E-02	1.96E-02	2.01E-02	0.0512	0.0562	0.0493	-4%	2.00E-02	0%
4B 1	1028	3.06E-03	2.99E-03	2.75E-03	2.00E-03	1.49E-03	2.46E-03	0.1269	0.0099	0.1244	-2%	2.05E-03	-17%
4B 2	3076	5.34E-03	5.48E-03	4.73E-03	3.51E-03	2.45E-03	4.30E-03	0.1180	0.0160	0.1183	0%	4.11E-03	-4%
4B 3	6128	7.24E-03	7.10E-03	6.65E-03	5.88E-03	4.03E-03	6.18E-03	0.1121	0.0216	0.1127	1%	6.04E-03	-2%
4B 4	11240	9.50E-03	9.07E-03	9.55E-03	7.11E-03	4.97E-03	8.04E-03	0.1075	0.0267	0.1076	0%	7.92E-03	-2%
4B 5	16352	1.10E-02	1.16E-02	1.11E-02	1.04E-02	6.22E-03	1.01E-02	0.1029	0.0319	0.1024	0%	9.91E-03	-1%
4B 6	21459	1.22E-02	1.25E-02	1.19E-02	1.06E-02	7.72E-03	1.10E-02	0.1002	0.0342	0.1001	0%	1.09E-02	-1%
4B 7	26568	1.33E-02	1.33E-02	1.21E-02	1.20E-02	7.86E-03	1.17E-02	0.0982	0.0359	0.0984	0%	1.16E-02	-1%
4B 8	31703	1.34E-02	1.36E-02	1.38E-02	1.28E-02	9.77E-03	1.27E-02	0.0961	0.0382	0.0961	0%	1.26E-02	0%
5A 1	1025	2.58E-03	2.71E-03	2.37E-03	2.49E-03	2.69E-03	2.57E-03	0.0833	0.0069	0.0803	-4%	2.49E-03	-3%
5A 2	3065	6.32E-03	6.17E-03	5.40E-03	4.91E-03	4.78E-03	5.52E-03	0.0758	0.0141	0.0731	-4%	5.48E-03	-1%
5A 3	6073	9.44E-03	9.13E-03	8.33E-03	8.06E-03	7.87E-03	8.57E-03	0.0688	0.0209	0.0662	-4%	8.51E-03	-1%
5A 4	11183	1.27E-02	1.29E-02	1.17E-02	1.17E-02	1.09E-02	1.20E-02	0.0616	0.0281	0.0591	-4%	1.19E-02	-1%
5A 5	16278	1.55E-02	1.55E-02	1.41E-02	1.40E-02	1.35E-02	1.45E-02	0.0563	0.0331	0.0541	-4%	1.45E-02	0%
5A 6	21828	1.75E-02	1.69E-02	1.67E-02	1.63E-02	1.57E-02	1.66E-02	0.0525	0.0370	0.0502	-4%	1.66E-02	0%
5A 7	26432	1.90E-02	1.90E-02	1.79E-02	1.77E-02	1.73E-02	1.82E-02	0.0495	0.0399	0.0472	-5%	1.81E-02	0%
5A 8	31545	1.98E-02	2.00E-02	1.90E-02	1.89E-02	1.89E-02	1.93E-02	0.0478	0.0420	0.0451	-6%	1.93E-02	0%

Table F.3: Measured damages for the physical model scale tests (continued).

Test #	N [-]	1 [m²]	2 [m²]	3 [m²]	Erosion Areas 4 [m²]	5 [m²]	Mean A_e [m²]	z_d [m]	Δz [m]	Calculations $z_c - \Delta z$ [m]	Perc.	Erosion Area 2 A_{e2} [m²]	Perc.
5B 1	1025	1.14E-03	1.78E-03	7.47E-04	1.30E-03	1.01E-03	1.19E-03	0.0866	0.0033	0.0857	-1%	9.77E-04	-18%
5B 2	3065	2.05E-03	1.95E-03	1.64E-03	1.85E-03	1.06E-03	1.71E-03	0.0855	0.0046	0.0843	-1%	1.54E-03	-10%
5B 3	6073	2.40E-03	1.68E-03	1.05E-03	1.15E-03	1.46E-03	1.55E-03	0.0864	0.0042	0.0848	-2%	1.42E-03	-9%
5B 4	11183	3.20E-03	2.85E-03	1.55E-03	1.70E-03	2.48E-03	2.36E-03	0.0854	0.0063	0.0826	-3%	2.11E-03	-10%
5B 5	16278	3.06E-03	2.66E-03	1.49E-03	2.03E-03	2.10E-03	2.27E-03	0.0854	0.0061	0.0829	-3%	2.11E-03	-7%
5B 6	21828	3.29E-03	3.37E-03	9.67E-04	2.53E-03	1.62E-03	2.35E-03	0.0854	0.0063	0.0827	-3%	2.17E-03	-8%
5B 7	26432	4.04E-03	3.26E-03	1.71E-03	2.16E-03	1.92E-03	2.62E-03	0.0849	0.0070	0.0820	-3%	2.49E-03	-5%
5B 8	31545	4.56E-03	4.60E-03	1.87E-03	2.46E-03	2.27E-03	3.15E-03	0.0845	0.0083	0.0806	-5%	3.00E-03	-5%

Table F.4: Measured damages for the physical model scale tests (continued).

Test #	N [-]	1 [m²]	2 [m²]	3 [m²]	4 [m²]	Erosion Area 5 [m²]	6 [m²]	7 [m²]	8 [m²]	9 [m²]	Mean A_e [m²]	z_d [m]	Δz [m]	Calculations $z_c - \Delta z$ [m]	Perc.	Erosion Area 2 A_{e2} [m²]	Perc.
6B 1	1017	3.18E-04	3.14E-05	1.90E-04	4.82E-04	1.25E-03	2.81E-04	1.45E-04	5.81E-04	2.75E-04	3.95E-04	0.0844	0.0020	0.0828	-2%	1.59E-04	-60%
6B 2	6137	5.68E-04	5.29E-04	3.26E-04	6.97E-04	1.09E-03	4.10E-04	3.84E-04	6.65E-04	7.90E-04	6.07E-04	0.0837	0.0030	0.0818	-2%	3.08E-04	-49%
6B 3	11974	8.74E-04	5.20E-04	6.78E-04	4.13E-04	1.42E-03	9.52E-04	5.93E-04	6.92E-04	1.01E-03	7.94E-04	0.0833	0.0038	0.0809	-3%	4.40E-04	-45%
6B 4	17926	9.80E-04	7.99E-04	9.91E-04	1.11E-03	1.12E-03	1.27E-03	9.71E-04	1.28E-03	5.98E-04	1.01E-03	0.0822	0.0048	0.0799	-3%	8.60E-04	-15%
6B 5	23949	2.04E-03	1.30E-03	1.22E-03	1.22E-03	1.96E-03	1.21E-03	1.62E-03	1.37E-03	1.49E-03	1.49E-03	0.0810	0.0069	0.0779	-4%	1.45E-03	-3%
6B 6	29746	3.30E-03	2.32E-03	2.28E-03	2.16E-03	2.65E-03	2.58E-03	2.20E-03	2.41E-03	1.94E-03	2.43E-03	0.0782	0.0106	0.0741	-5%	2.46E-03	1%
6B 7	35571	5.33E-03	4.41E-03	5.02E-03	3.99E-03	4.25E-03	4.32E-03	5.36E-03	4.19E-03	3.17E-03	4.45E-03	0.0692	0.0179	0.0668	-3%	4.46E-03	0%
6B 8	41127	5.39E-03	6.05E-03	6.81E-03	5.36E-03	5.71E-03	5.66E-03	6.12E-03	6.18E-03	3.42E-03	5.63E-03	0.0649	0.0218	0.0630	-3%	5.79E-03	3%
7B 1	6057	1.37E-03	8.42E-04	6.57E-04	8.15E-04	1.17E-03	8.17E-04	6.07E-04	5.06E-04	9.41E-04	8.58E-04	0.0846	0.0041	0.0812	-4%	4.72E-04	-45%
7B 2	13555	1.22E-03	1.13E-03	1.60E-03	1.97E-03	2.20E-03	1.88E-03	1.67E-03	1.62E-03	1.56E-03	1.65E-03	0.0819	0.0075	0.0778	-5%	1.33E-03	-19%
7B 3	16445	1.39E-03	1.47E-03	1.73E-03	1.83E-03	1.87E-03	1.87E-03	2.26E-03	1.86E-03	1.52E-03	1.76E-03	0.0817	0.0080	0.0773	-5%	1.35E-03	-23%
7B 4	19010	1.62E-03	1.73E-03	1.67E-03	1.68E-03	2.61E-03	3.00E-03	3.15E-03	2.51E-03	1.85E-03	2.20E-03	0.0794	0.0097	0.0755	-5%	1.70E-03	-23%
7Bv2 1	5730	3.87E-04	7.51E-04	4.51E-04	4.35E-04	5.52E-04	1.06E-03	2.99E-04	1.24E-03	5.61E-04	6.37E-04	0.0836	0.0031	0.0814	-3%	2.95E-04	-54%
7Bv2 2	11892	1.82E-03	1.56E-03	1.08E-03	1.01E-03	1.39E-03	1.23E-03	5.43E-04	1.46E-03	1.68E-03	1.31E-03	0.0819	0.0061	0.0784	-4%	1.00E-03	-23%
7Bv2 3	14936	1.33E-03	1.84E-03	1.30E-03	1.39E-03	1.13E-03	1.54E-03	7.85E-04	9.35E-04	1.34E-03	1.29E-03	0.0816	0.0060	0.0785	-4%	1.17E-03	-9%
7Bv2 4	17909	1.09E-03	2.44E-03	1.14E-03	1.77E-03	1.68E-03	2.18E-03	2.44E-03	2.12E-03	2.61E-03	1.94E-03	0.0801	0.0087	0.0758	-5%	1.48E-03	-24%
7Bv2 5	23929	1.90E-03	1.92E-03	1.74E-03	2.43E-03	1.63E-03	1.71E-03	2.17E-03	1.77E-03	2.08E-03	1.93E-03	0.0801	0.0087	0.0759	-5%	1.51E-03	-21%
7Bv2 6	26980	1.62E-03	1.81E-03	1.53E-03	1.72E-03	2.04E-03	1.86E-03	2.13E-03	1.70E-03	1.83E-03	1.80E-03	0.0801	0.0082	0.0764	-5%	1.43E-03	-21%
7Bv2 7	32958	1.69E-03	2.17E-03	1.53E-03	1.50E-03	1.62E-03	2.52E-03	2.34E-03	2.13E-03	2.38E-03	1.99E-03	0.0798	0.0089	0.0756	-5%	1.53E-03	-23%
7Bv2 8	35959	1.89E-03	2.64E-03	1.64E-03	2.20E-03	2.48E-03	2.26E-03	2.46E-03	2.50E-03	1.93E-03	2.22E-03	0.0797	0.0098	0.0747	-6%	1.96E-03	-12%

Table F.5: Measured damage for test 6 and 7.

Appendix G

Dataset

In this Appendix the data is placed from Lomónaco, Van Gent and Wallast, Saers and Tørum which is used for the comparison with the data from this thesis and can be seen in Table G.1 until G.7. These tables are updated from Van den Bos [2006] and is for the data with 'waves only'. The first row indicates the test number which Van den Bos used supplemented with Tørum and tests done in this thesis. The original test number is the test number which the different researchers used in their research. In the dataset column LOM stands for Lomónaco, VGW for Van Gent and Wallast, SAE for Saers, TOR for Tørum and HEU for Heuvel. The rest of the columns explain itself. The peak period T_p is calculated here with Equation G.1, the specific density Δ with Equation G.2 and the total width B with Equation G.3. The parameter z_d is the height of the near-bed structure after the test which is only given if this is mentioned in the report of the researcher. The parameter A_e is calculated here with the damage from the average row which has also been used for the analysis.

$$T_p = \frac{T_m}{0.8} \tag{G.1}$$

$$\Delta = \frac{\rho_s - \rho_w}{\rho_w} \tag{G.2}$$

$$B = B_c + 2 * z_c * m_0 \tag{G.3}$$

	Test		Hydraulic conditions							Stones			Structure					Damage				
Number	Orig nr	Dataset	H_s	$H_{1\%}$	T_m	T_p	N	h	h_c	ρ_s	D_{n50}	shape	Δ	m_0	z_c	B_c	B	S	S^*	z_d	Duration	A_e
-	-	-	[m]	[m]	[s]	[s]	[-]	[m]	[m]	[kg/m³]	[m]	[-]	[-]	[-]	[m]	[m]	[m]	[-]	[-]	[m]	[s]	[m²]
W1	A310	VGW	0.090	0.129	1.11	1.39	1000	0.50	0.375	2650	7.20E-03	0	1.65	3	0.1250	0.13	0.875	4.4	0.25	0.0000	1110	2.28E-04
W2	A310	VGW	0.090	0.129	1.11	1.39	3000	0.50	0.375	2650	7.20E-03	0	1.65	3	0.1250	0.13	0.875	6.1	0.35	0.0000	3330	3.16E-04
W3	A311	VGW	0.127	0.179	1.32	1.65	1000	0.50	0.375	2650	7.20E-03	0	1.65	3	0.1250	0.13	0.875	4.6	0.26	0.0000	1320	2.38E-04
W4	A311	VGW	0.127	0.179	1.32	1.65	3000	0.50	0.375	2650	7.20E-03	0	1.65	3	0.1250	0.13	0.875	7.3	0.42	0.0000	3960	3.78E-04
W5	A312	VGW	0.163	0.226	1.51	1.89	1000	0.50	0.375	2650	7.20E-03	0	1.65	3	0.1250	0.13	0.875	6.3	0.36	0.0000	1510	3.27E-04
W6	A312	VGW	0.163	0.226	1.51	1.89	3000	0.50	0.375	2650	7.20E-03	0	1.65	3	0.1250	0.13	0.875	7.4	0.43	0.0000	4530	3.84E-04
W7	H312	VGW	0.162	0.224	1.51	1.89	1000	0.50	0.375	2650	7.20E-03	0	1.65	3	0.1250	0.13	0.875	6.3	0.36	0.0000	1510	3.27E-04
W8	H312	VGW	0.162	0.224	1.51	1.89	3000	0.50	0.375	2650	7.20E-03	0	1.65	3	0.1250	0.13	0.875	13.0	0.75	0.0000	4530	6.74E-04
W9	A313	VGW	0.188	0.257	1.66	2.08	1000	0.50	0.375	2650	7.20E-03	0	1.65	3	0.1250	0.13	0.875	8.3	0.48	0.0000	1660	4.30E-04
W10	A313	VGW	0.188	0.257	1.66	2.08	3000	0.50	0.375	2650	7.20E-03	0	1.65	3	0.1250	0.13	0.875	11.8	0.68	0.0000	4980	6.12E-04
W11	H313	VGW	0.186	0.254	1.66	2.08	1000	0.50	0.375	2650	7.20E-03	0	1.65	3	0.1250	0.13	0.875	5.9	0.34	0.0000	1660	3.06E-04
W12	H313	VGW	0.186	0.254	1.66	2.08	3000	0.50	0.375	2650	7.20E-03	0	1.65	3	0.1250	0.13	0.875	10.0	0.58	0.0000	4980	5.18E-04
W13	A320	VGW	0.085	0.121	1.10	1.38	1000	0.38	0.250	2650	7.20E-03	0	1.65	3	0.1250	0.13	0.875	4.3	0.25	0.0000	1100	2.23E-04
W14	A321	VGW	0.119	0.165	1.32	1.65	1000	0.38	0.250	2650	7.20E-03	0	1.65	3	0.1250	0.13	0.875	2.1	0.12	0.0000	1320	1.09E-04
W15	A321	VGW	0.119	0.165	1.32	1.65	3000	0.38	0.250	2650	7.20E-03	0	1.65	3	0.1250	0.13	0.875	5.8	0.33	0.0000	3960	3.01E-04
W16	A410	VGW	0.090	0.129	1.11	1.39	1000	0.50	0.375	2650	3.10E-03	0	1.65	8	0.1250	0.13	2.125	22.3	0.55	0.0000	1110	2.14E-04
W17	A410	VGW	0.090	0.129	1.11	1.39	3000	0.50	0.375	2650	3.10E-03	0	1.65	8	0.1250	0.13	2.125	37.3	0.93	0.0000	3330	3.58E-04
W18	A411	VGW	0.127	0.179	1.32	1.65	1000	0.50	0.375	2650	3.10E-03	0	1.65	8	0.1250	0.13	2.125	18.5	0.46	0.0000	1320	1.78E-04
W19	A411	VGW	0.127	0.179	1.32	1.65	3000	0.50	0.375	2650	3.10E-03	0	1.65	8	0.1250	0.13	2.125	43.0	1.07	0.0000	3960	4.13E-04
W20	A412	VGW	0.164	0.227	1.51	1.89	1000	0.50	0.375	2650	3.10E-03	0	1.65	8	0.1250	0.13	2.125	103.6	2.57	0.0000	1510	9.96E-04
W21	A412	VGW	0.164	0.227	1.51	1.89	3000	0.50	0.375	2650	3.10E-03	0	1.65	8	0.1250	0.13	2.125	206.4	5.12	0.0000	4530	1.98E-03
W22	T1 D2	LOM	0.149	0.207	1.28	1.61	2897	0.50	0.470	2463	3.65E-03	Round	1.46	3	0.0298	0.06	0.239	60.4	3.67	0.0254	3722	8.03E-04
W23	T1 D3	LOM	0.153	0.212	1.26	1.58	2870	0.50	0.444	2512	6.12E-03	Round	1.51	5	0.0562	0.12	0.682	4.5	0.23	0.0562	3616	1.70E-04
W24	T1 D4	LOM	0.149	0.208	1.26	1.58	2845	0.50	0.444	2512	6.12E-03	Round	1.51	3	0.0559	0.12	0.455	20.0	1.02	0.0554	3585	7.50E-04
W25	T1 D5	LOM	0.148	0.206	1.26	1.58	2840	0.50	0.446	2512	6.12E-03	Round	1.51	1	0.0540	0.12	0.228	41.5	2.12	0.0481	3578	1.55E-03
W26	T1 D6	LOM	0.140	0.196	1.28	1.61	2806	0.50	0.375	2712	8.33E-03	Sharp	1.71	3	0.1253	0.25	1.002	4.0	0.13	0.1248	3605	2.81E-04
W27	T2 D2	LOM	0.186	0.254	1.49	1.86	1864	0.50	0.468	2463	3.65E-03	Round	1.46	3	0.0320	0.06	0.252	32.0	1.94	0.0274	2777	4.25E-04
W28	T2 D3	LOM	0.191	0.260	1.49	1.86	1850	0.50	0.441	2512	6.12E-03	Round	1.51	5	0.0589	0.12	0.709	8.9	0.46	0.0579	2756	3.35E-04
W29	T2 D4	LOM	0.183	0.251	1.56	1.95	1853	0.50	0.442	2512	6.12E-03	Round	1.51	3	0.0576	0.12	0.466	8.3	0.42	0.0562	2891	3.10E-04
W30	T2 D5	LOM	0.181	0.248	1.49	1.86	1846	0.50	0.448	2512	6.12E-03	Round	1.51	1	0.0523	0.12	0.225	28.8	1.47	0.0459	2750	1.08E-03
W31	T2 D6	LOM	0.178	0.244	1.56	1.95	1799	0.50	0.374	2712	8.33E-03	Sharp	1.71	3	0.1265	0.25	1.009	10.2	0.34	0.1265	2806	7.06E-04
W32	T3 D2	LOM	0.213	0.288	1.64	2.05	928	0.50	0.470	2463	3.65E-03	Round	1.46	3	0.0298	0.06	0.239	39.1	2.38	0.0252	1520	5.20E-04
W33	T3 D4	LOM	0.209	0.283	1.64	2.05	898	0.50	0.442	2512	6.12E-03	Round	1.51	3	0.0579	0.12	0.467	10.6	0.54	0.0571	1471	3.99E-04
W34	T3 D5	LOM	0.202	0.274	1.64	2.05	919	0.50	0.442	2512	6.12E-03	Round	1.51	1	0.0579	0.12	0.236	48.3	2.46	0.0466	1506	1.81E-03
W35	T5A D2	LOM	0.208	0.290	1.46	1.82	953	0.70	0.670	2463	3.65E-03	Round	1.46	3	0.0300	0.06	0.240	12.3	0.75	0.0286	1388	1.63E-04
W36	T5A D3	LOM	0.233	0.322	1.46	1.82	970	0.70	0.636	2463	3.65E-03	Round	1.46	5	0.0637	0.12	0.757	24.5	0.74	0.0635	1412	3.26E-04
W37	T5A D4	LOM	0.201	0.281	1.49	1.86	950	0.70	0.638	2463	3.65E-03	Round	1.46	3	0.0625	0.12	0.495	46.2	1.40	0.0598	1415	6.13E-04
W38	T5A D5	LOM	0.203	0.283	1.49	1.86	938	0.70	0.640	2512	6.12E-03	Round	1.51	1	0.0598	0.12	0.240	15.0	0.77	0.0586	1397	5.62E-04
W39	T5A D6	LOM	0.202	0.282	1.46	1.82	920	0.70	0.572	2613	5.13E-03	Sharp	1.61	3	0.1280	0.25	1.018	21.3	0.44	0.1272	1340	5.62E-04
W40	T5A D7	LOM	0.180	0.254	1.46	1.82	956	0.70	0.440	2712	8.33E-03	Sharp	1.71	3	0.2601	0.25	1.811	14.5	0.48	0.2584	1392	1.01E-03
W41	T5B D2	LOM	0.208	0.290	1.49	1.86	1897	0.70	0.670	2463	3.65E-03	Round	1.46	3	0.0300	0.06	0.240	16.8	1.02	0.0283	2826	2.23E-04
W42	T5B D3	LOM	0.233	0.322	1.46	1.82	1935	0.70	0.636	2463	3.65E-03	Round	1.46	5	0.0637	0.12	0.757	37.6	1.14	0.0632	2817	5.00E-04

Table G.1: Dataset for pipeline covers. Tests with waves only.

	Test			Hydraulic conditions							Stones		Structure							Damage		
Number	Orig nr	Dataset	H_s	$H_{1\%}$	T_m	T_p	N	h	h_c	ρ_s	D_{n50}	shape	Δ	m_0	z_c	B_c	B	S	S^*	z_d	Duration	A_e
-	-	-	[m]	[m]	[s]	[s]	[-]	[m]	[m]	[kg/m^3]	[m]	[-]	[-]	[-]	[m]	[m]	[m]	[-]	[-]	[m]	[s]	[m^2]
W43	T5B D4	LOM	0.201	0.281	1.49	1.86	1898	0.70	0.638	2463	3.65E-03	Round	1.46	3	0.0625	0.12	0.495	62.1	1.89	0.0591	2827	8.25E-04
W44	T5B D5	LOM	0.202	0.282	1.49	1.86	1876	0.70	0.640	2512	6.12E-03	Round	1.51	1	0.0598	0.12	0.240	21.2	1.08	0.0571	2794	7.96E-04
W45	T5B D6	LOM	0.204	0.284	1.46	1.82	1842	0.70	0.572	2613	5.13E-03	Sharp	1.61	3	0.1280	0.25	1.018	33.5	0.69	0.1272	2682	8.80E-04
W46	T5B D7	LOM	0.181	0.255	1.46	1.82	1908	0.70	0.440	2712	8.33E-03	Sharp	1.71	3	0.2601	0.25	1.811	24.9	0.83	0.2579	2778	1.73E-03
W47	T6A D2	LOM	0.251	0.344	1.64	2.05	932	0.70	0.662	2463	3.65E-03	Round	1.46	3	0.0376	0.06	0.286	75.0	4.56	0.0286	1527	9.97E-04
W48	T6A D3	LOM	0.283	0.384	1.64	2.05	921	0.70	0.636	2463	3.65E-03	Round	1.46	5	0.0640	0.12	0.760	77.6	2.36	0.0608	1509	1.03E-03
W49	T6A D4	LOM	0.244	0.335	1.64	2.05	929	0.70	0.637	2463	3.65E-03	Round	1.46	3	0.0630	0.12	0.498	140.4	4.26	0.0542	1522	1.87E-03
W50	T6A D5	LOM	0.243	0.334	1.68	2.10	920	0.70	0.630	2512	6.12E-03	Round	1.51	1	0.0696	0.12	0.259	69.3	3.54	0.0491	1546	2.60E-03
W51	T6A D6	LOM	0.244	0.335	1.68	2.10	907	0.70	0.572	2613	5.13E-03	Sharp	1.61	3	0.1277	0.25	1.016	46.0	0.94	0.1258	1524	1.21E-03
W52	T6A D7	LOM	0.223	0.309	1.82	2.28	911	0.70	0.442	2712	8.33E-03	Sharp	1.71	3	0.2576	0.25	1.796	77.0	2.56	0.2518	1659	5.34E-03
W53	T6B D2	LOM	0.252	0.345	1.64	2.05	1871	0.70	0.662	2463	3.65E-03	Round	1.46	3	0.0376	0.06	0.286	97.7	5.94	0.0274	3065	1.30E-03
W54	T6B D3	LOM	0.283	0.384	1.64	2.05	1845	0.70	0.636	2463	3.65E-03	Round	1.46	5	0.0640	0.12	0.760	128.7	3.91	0.0576	3023	1.71E-03
W55	T6B D4	LOM	0.244	0.336	1.68	2.10	1852	0.70	0.637	2463	3.65E-03	Round	1.46	3	0.0630	0.12	0.498	215.9	6.56	0.0501	3113	2.87E-03
W56	T6B D5	LOM	0.242	0.333	1.68	2.10	1842	0.70	0.630	2512	6.12E-03	Round	1.51	1	0.0696	0.12	0.259	76.1	3.89	0.0476	3096	2.86E-03
W57	T6B D6	LOM	0.243	0.335	1.68	2.10	1811	0.70	0.572	2613	5.13E-03	Sharp	1.61	3	0.1277	0.25	1.016	73.7	1.51	0.1253	3044	1.94E-03
W58	T6B D7	LOM	0.223	0.310	1.82	2.28	1822	0.70	0.442	2712	8.33E-03	Sharp	1.71	3	0.2576	0.25	1.796	119.3	3.98	0.2449	3317	8.28E-03
W59	T7A D2	LOM	0.255	0.357	1.64	2.05	975	0.90	0.861	2463	3.65E-03	Round	1.46	3	0.0386	0.06	0.292	48.0	2.91	0.0332	1597	6.37E-04
W60	T7A D3	LOM	0.285	0.396	1.64	2.05	960	0.90	0.837	2463	3.65E-03	Round	1.46	5	0.0628	0.12	0.748	80.0	2.43	0.0601	1573	1.06E-03
W61	T7A D4	LOM	0.248	0.347	1.64	2.05	974	0.90	0.837	2463	3.65E-03	Round	1.46	3	0.0632	0.12	0.499	85.9	2.61	0.0584	1596	1.14E-03
W62	T7A D5	LOM	0.252	0.353	1.64	2.05	957	0.90	0.833	2512	6.12E-03	Round	1.51	1	0.0674	0.12	0.255	57.0	2.91	0.0545	1568	2.14E-03
W63	T7A D6	LOM	0.250	0.351	1.64	2.05	960	0.90	0.773	2613	5.13E-03	Sharp	1.61	3	0.1270	0.25	1.012	50.6	1.04	0.1270	1573	1.33E-03
W64	T7A D7	LOM	0.238	0.334	1.64	2.05	936	0.90	0.646	2712	8.33E-03	Sharp	1.71	3	0.2542	0.25	1.775	39.1	1.30	0.2527	1534	2.72E-03
W65	T7B D2	LOM	0.257	0.359	1.64	2.05	1941	0.90	0.861	2463	3.65E-03	Round	1.46	3	0.0386	0.06	0.292	54.5	3.31	0.0332	3180	7.24E-04
W66	T7B D3	LOM	0.286	0.397	1.64	2.05	1921	0.90	0.837	2463	3.65E-03	Round	1.46	5	0.0628	0.12	0.748	100.1	3.04	0.0598	3147	1.33E-03
W67	T7B D4	LOM	0.248	0.347	1.64	2.05	1949	0.90	0.837	2463	3.65E-03	Round	1.46	3	0.0632	0.12	0.499	105.0	3.19	0.0581	3193	1.39E-03
W68	T7B D5	LOM	0.250	0.350	1.64	2.05	1914	0.90	0.833	2512	6.12E-03	Round	1.51	1	0.0674	0.12	0.255	69.4	3.54	0.0508	3136	2.60E-03
W69	T7B D6	LOM	0.252	0.353	1.64	2.05	1910	0.90	0.773	2613	5.13E-03	Sharp	1.61	3	0.1270	0.25	1.012	66.2	1.36	0.1263	3129	1.74E-03
W70	T7B D7	LOM	0.241	0.338	1.64	2.05	1871	0.90	0.646	2712	8.33E-03	Sharp	1.71	3	0.2542	0.25	1.775	49.9	1.66	0.2527	3065	3.46E-03
W71	T9 D2	LOM	0.207	0.280	2.05	2.56	1011	0.50	0.461	2463	3.65E-03	Round	1.46	3	0.0391	0.06	0.295	92.1	5.60	0.0274	2071	1.22E-03
W72	T9 D4	LOM	0.199	0.270	2.05	2.56	976	0.50	0.438	2463	3.65E-03	Round	1.46	3	0.0625	0.12	0.495	184.4	5.60	0.0488	1999	2.45E-03
W73	T9 D5	LOM	0.201	0.273	2.11	2.64	973	0.50	0.441	2463	3.65E-03	Round	1.46	2	0.0589	0.12	0.356	209.4	6.36	0.0440	2057	2.78E-03
W74	T11 D2	LOM	0.263	0.359	1.87	2.34	968	0.70	0.669	2463	3.65E-03	Round	1.46	3	0.0308	0.06	0.245	87.8	5.33	0.0210	1813	1.17E-03
W75	T11 D3	LOM	0.293	0.396	1.87	2.34	973	0.70	0.636	2463	3.65E-03	Round	1.46	5	0.0640	0.12	0.760	199.3	6.05	0.0537	1822	2.65E-03
W76	T11 D4	LOM	0.253	0.347	1.87	2.34	955	0.70	0.640	2463	3.65E-03	Round	1.46	3	0.0601	0.12	0.481	207.6	6.31	0.0459	1789	2.76E-03
W77	T11 D5	LOM	0.257	0.352	1.87	2.34	955	0.70	0.641	2463	3.65E-03	Round	1.46	2	0.0591	0.12	0.356	227.2	6.90	0.0393	1789	3.02E-03
W78	T11 D6	LOM	0.259	0.354	1.96	2.45	919	0.70	0.571	2613	5.13E-03	Sharp	1.61	3	0.1289	0.25	1.023	103.8	2.13	0.1233	1801	2.73E-03
W79	T12 D2	LOM	0.215	0.290	1.64	2.05	931	0.50	0.469	2463	3.65E-03	Round	1.46	3	0.0310	0.06	0.246	51.6	3.14	0.0252	1525	6.86E-04
W80	T12 D4	LOM	0.206	0.278	1.64	2.05	905	0.50	0.443	2463	3.65E-03	Round	1.46	3	0.0571	0.12	0.463	132.2	4.01	0.0481	1483	1.76E-03
W81	T12 D5	LOM	0.203	0.275	1.64	2.05	908	0.50	0.442	2463	3.65E-03	Round	1.46	2	0.0584	0.12	0.354	203.9	6.19	0.0425	1488	2.71E-03
W82	0a6	SAE	0.208	0.284	1.71	2.14	1096	0.55	0.490	2470	3.70E-03	Irregular	1.47	2.5	0.0598	0.04	0.339	107.8	9.97	0.0514	1876	1.48E-03
W83	0a6	SAE	0.208	0.284	1.71	2.14	3177	0.55	0.490	2470	3.70E-03	Irregular	1.47	2.5	0.0598	0.04	0.339	128.2	11.85	0.0508	5439	1.75E-03
W84	1a4	SAE	0.209	0.283	1.71	2.14	1052	0.50	0.455	2470	3.70E-03	Irregular	1.47	2.5	0.0448	0.04	0.264	45.1	4.17	0.0351	1801	6.18E-04

Table G.2: Dataset for pipeline covers (continued).

Number	Test Orig nr	Dataset	H_s	$H_{1\%}$	T_m	T_p	N	h	h_c	ρ_s	D_{n50}	shape	Δ	m_0	z_c	B_c	B	S	S^*	z_d	Duration	A_e
-	-	-	[m]	[m]	[s]	[s]	[-]	[m]	[m]	[kg/m³]	[m]	[-]	[-]	[-]	[m]	[m]	[m]	[-]	[-]	[m]	[s]	[m²]
W85	1a4	SAE	0.209	0.283	1.71	2.14	3114	0.50	0.455	2470	3.70E-03	Irregular	1.47	2.5	0.0448	0.04	0.264	53.3	4.93	0.0340	5331	7.30E-04
W86	1a4	SAE	0.209	0.283	1.71	2.14	6196	0.50	0.455	2470	3.70E-03	Irregular	1.47	2.5	0.0448	0.04	0.264	57.6	5.33	0.0335	10608	7.89E-04
W87	1a5	SAE	0.209	0.283	1.71	2.14	1028	0.50	0.451	2470	3.70E-03	Irregular	1.47	2.5	0.0494	0.04	0.287	83.5	7.72	0.0346	1760	1.14E-03
W88	1a5	SAE	0.209	0.283	1.71	2.14	2820	0.50	0.451	2470	3.70E-03	Irregular	1.47	2.5	0.0494	0.04	0.287	103.1	9.54	0.0325	4828	1.41E-03
W89	1a5	SAE	0.209	0.283	1.71	2.14	5855	0.50	0.451	2470	3.70E-03	Irregular	1.47	2.5	0.0494	0.04	0.287	104.9	9.70	0.0322	10024	1.44E-03
W90	1a6	SAE	0.209	0.283	1.71	2.14	982	0.50	0.436	2470	3.70E-03	Irregular	1.47	2.5	0.0637	0.04	0.359	117.2	10.84	0.0451	1681	1.60E-03
W91	1a6	SAE	0.209	0.283	1.71	2.14	2941	0.50	0.436	2470	3.70E-03	Irregular	1.47	2.5	0.0637	0.04	0.359	138.6	12.82	0.0431	5035	1.90E-03
W92	1a6	SAE	0.209	0.283	1.71	2.14	5961	0.50	0.436	2470	3.70E-03	Irregular	1.47	2.5	0.0637	0.04	0.359	156.5	14.48	0.0419	10205	2.14E-03
W93	1a6 her	SAE	0.209	0.283	1.71	2.14	1015	0.50	0.440	2470	3.70E-03	Irregular	1.47	2.5	0.0596	0.04	0.338	119.0	11.00	0.0407	1738	1.63E-03
W94	1a6 her	SAE	0.209	0.283	1.71	2.14	3079	0.50	0.440	2470	3.70E-03	Irregular	1.47	2.5	0.0596	0.04	0.338	133.2	12.32	0.0395	5271	1.82E-03
W95	1a6 her	SAE	0.209	0.283	1.71	2.14	6296	0.50	0.440	2470	3.70E-03	Irregular	1.47	2.5	0.0596	0.04	0.338	150.6	13.93	0.0375	10779	2.06E-03
W96	1b4	SAE	0.180	0.245	1.62	2.02	1023	0.45	0.408	2470	3.70E-03	Irregular	1.47	2.5	0.0420	0.04	0.250	34.5	3.19	0.0342	1653	4.72E-04
W97	1b4	SAE	0.180	0.245	1.62	2.02	3063	0.45	0.408	2470	3.70E-03	Irregular	1.47	2.5	0.0420	0.04	0.250	40.6	3.76	0.0330	4950	5.56E-04
W98	1b4	SAE	0.180	0.245	1.62	2.02	6083	0.45	0.408	2470	3.70E-03	Irregular	1.47	2.5	0.0420	0.04	0.250	46.9	4.34	0.0321	9830	6.42E-04
W99	1b6	SAE	0.180	0.245	1.62	2.02	1052	0.45	0.390	2470	3.70E-03	Irregular	1.47	2.5	0.0604	0.04	0.342	56.7	5.24	0.0489	1700	7.76E-04
W100	1b6	SAE	0.180	0.245	1.62	2.02	3114	0.45	0.390	2470	3.70E-03	Irregular	1.47	2.5	0.0604	0.04	0.342	78.9	7.30	0.0459	5032	1.08E-03
W101	1b6	SAE	0.180	0.245	1.62	2.02	6196	0.45	0.390	2470	3.70E-03	Irregular	1.47	2.5	0.0604	0.04	0.342	99.6	9.21	0.0435	10013	1.36E-03
W102	2b4	SAE	0.173	0.236	1.62	2.02	1046	0.45	0.409	2470	3.70E-03	Irregular	1.47	2.5	0.0412	0.04	0.246	29.0	2.68	0.0343	1690	3.97E-04
W103	2b4	SAE	0.173	0.236	1.62	2.02	3073	0.45	0.409	2470	3.70E-03	Irregular	1.47	2.5	0.0412	0.04	0.246	32.4	2.99	0.0336	4966	4.43E-04
W104	2b4	SAE	0.173	0.236	1.62	2.02	6128	0.45	0.409	2470	3.70E-03	Irregular	1.47	2.5	0.0412	0.04	0.246	34.8	3.22	0.0332	9903	4.77E-04
W105	2b5	SAE	0.173	0.236	1.62	2.02	1104	0.45	0.399	2470	3.70E-03	Irregular	1.47	2.5	0.0509	0.04	0.295	58.0	5.37	0.0394	1784	7.94E-04
W106	2b5	SAE	0.173	0.236	1.62	2.02	3330	0.45	0.399	2470	3.70E-03	Irregular	1.47	2.5	0.0509	0.04	0.295	64.5	5.97	0.0385	5381	8.83E-04
W107	2b5	SAE	0.173	0.236	1.62	2.02	6546	0.45	0.399	2470	3.70E-03	Irregular	1.47	2.5	0.0509	0.04	0.295	70.9	6.56	0.0377	10578	9.71E-04
W108	2b6	SAE	0.173	0.236	1.62	2.02	1079	0.45	0.390	2470	3.70E-03	Irregular	1.47	2.5	0.0603	0.04	0.342	56.0	5.18	0.0491	1744	7.67E-04
W109	2b6	SAE	0.173	0.236	1.62	2.02	3221	0.45	0.390	2470	3.70E-03	Irregular	1.47	2.5	0.0603	0.04	0.342	62.9	5.82	0.0481	5205	8.61E-04
W110	2b6	SAE	0.173	0.236	1.62	2.02	6369	0.45	0.390	2470	3.70E-03	Irregular	1.47	2.5	0.0603	0.04	0.342	80.5	7.44	0.0459	10292	1.10E-03
W111	3c4	SAE	0.148	0.203	1.61	2.01	990	0.40	0.358	2470	3.70E-03	Irregular	1.47	2.5	0.0425	0.04	0.253	25.3	2.34	0.0364	1592	3.46E-04
W112	3c4	SAE	0.148	0.203	1.61	2.01	2956	0.40	0.358	2470	3.70E-03	Irregular	1.47	2.5	0.0425	0.04	0.253	26.3	2.43	0.0364	4753	3.59E-04
W113	3c4	SAE	0.148	0.203	1.61	2.01	5621	0.40	0.358	2470	3.70E-03	Irregular	1.47	2.5	0.0425	0.04	0.253	27.0	2.50	0.0362	9039	3.70E-04
W114	3c5	SAE	0.148	0.203	1.61	2.01	1014	0.40	0.348	2470	3.70E-03	Irregular	1.47	2.5	0.0518	0.04	0.299	36.1	3.34	0.0439	1631	4.94E-04
W115	3c5	SAE	0.148	0.203	1.61	2.01	3112	0.40	0.348	2470	3.70E-03	Irregular	1.47	2.5	0.0518	0.04	0.299	57.7	5.34	0.0403	5004	7.90E-04
W116	3c5	SAE	0.148	0.203	1.61	2.01	6028	0.40	0.348	2470	3.70E-03	Irregular	1.47	2.5	0.0518	0.04	0.299	55.6	5.14	0.0406	9693	7.61E-04
W117	3c6	SAE	0.148	0.203	1.61	2.01	980	0.40	0.340	2470	3.70E-03	Irregular	1.47	2.5	0.0596	0.04	0.338	50.2	4.65	0.0492	1576	6.88E-04
W118	3c6	SAE	0.148	0.203	1.61	2.01	2910	0.40	0.340	2470	3.70E-03	Irregular	1.47	2.5	0.0596	0.04	0.338	53.1	4.92	0.0488	4679	7.27E-04
W119	3c6	SAE	0.148	0.203	1.61	2.01	5967	0.40	0.340	2470	3.70E-03	Irregular	1.47	2.5	0.0596	0.04	0.338	55.2	5.11	0.0486	9595	7.56E-04
W120	1	TOR	0.071	0.103	0.94	1.18	2806	0.50	0.450	2800	3.30E-03	Irregular	1.80	2	0.0500	0.08	0.275	0.0	0.00	0.0000	2638	0.00E+00
W121	2	TOR	0.091	0.131	1.07	1.34	2908	0.50	0.450	2800	3.30E-03	Irregular	1.80	2	0.0500	0.08	0.275	0.0	0.00	0.0000	3112	0.00E+00
W122	3	TOR	0.099	0.142	1.22	1.53	476	0.50	0.450	2800	3.30E-03	Irregular	1.80	2	0.0500	0.08	0.275	0.0	0.00	0.0000	581	0.00E+00
W123	4	TOR	0.073	0.106	1.10	1.38	3122	0.50	0.450	2800	3.30E-03	Irregular	1.80	2	0.0500	0.08	0.275	0.0	0.00	0.0000	3434	0.00E+00
W124	5	TOR	0.078	0.113	1.24	1.55	3238	0.50	0.450	2800	3.30E-03	Irregular	1.80	2	0.0500	0.08	0.275	0.0	0.00	0.0000	4015	0.00E+00
W125	6	TOR	0.102	0.146	1.29	1.61	3569	0.50	0.450	2800	3.30E-03	Irregular	1.80	2	0.0500	0.08	0.275	0.0	0.00	0.0000	4604	0.00E+00
W126	10	TOR	0.073	0.106	0.96	1.20	2672	0.50	0.450	2800	1.90E-03	Irregular	1.80	2	0.0500	0.08	0.275	0.0	0.00	0.0000	2565	0.00E+00

Table G.3: Dataset for pipeline covers (continued).

	Test		Hydraulic conditions								Stones				Structure			Damage				
Number	Orig nr	Dataset	H_s	$H_{1\%}$	T_m	T_p	N	h	h_c	ρ_s	D_{n50}	shape	Δ	m_0	z_c	B_c	B	S	S^*	z_d	Duration	A_e
-	-	-	[m]	[m]	[s]	[s]	[-]	[m]	[m]	[kg/m³]	[m]	[-]	[-]	[-]	[m]	[m]	[m]	[-]	[-]	[m]	[s]	[m²]
W127	11	TOR	0.098	0.140	1.11	1.39	2872	0.50	0.450	2800	1.90E-03	Irregular	1.80	2	0.0500	0.08	0.275	0.0	0.00	0.0000	3188	0.00E+00
W128	12	TOR	0.106	0.151	1.21	1.51	2982	0.50	0.450	2800	1.90E-03	Irregular	1.80	2	0.0500	0.08	0.275	0.0	0.00	0.0000	3608	0.00E+00
W129	13	TOR	0.072	0.105	1.06	1.33	3115	0.50	0.450	2800	1.90E-03	Irregular	1.80	2	0.0500	0.08	0.275	0.0	0.00	0.0000	3302	0.00E+00
W130	14	TOR	0.080	0.116	1.21	1.51	3224	0.50	0.450	2800	1.90E-03	Irregular	1.80	2	0.0500	0.08	0.275	0.0	0.00	0.0000	3901	0.00E+00
W131	15	TOR	0.103	0.147	1.36	1.70	3262	0.50	0.450	2800	1.90E-03	Irregular	1.80	2	0.0500	0.08	0.275	34.7	0.88	0.0000	4436	1.25E-04
W132	1	TOR	0.075	0.109	0.96	1.20	2741	0.50	0.450	2800	3.30E-03	Irregular	1.80	3	0.0500	0.08	0.375	0.0	0.00	0.0000	2631	0.00E+00
W133	2	TOR	0.090	0.129	1.09	1.36	2858	0.50	0.450	2800	3.30E-03	Irregular	1.80	3	0.0500	0.08	0.375	0.0	0.00	0.0000	3115	0.00E+00
W134	3	TOR	0.099	0.142	1.22	1.53	479	0.50	0.450	2800	3.30E-03	Irregular	1.80	3	0.0500	0.08	0.375	0.0	0.00	0.0000	584	0.00E+00
W135	4	TOR	0.073	0.106	1.09	1.36	3142	0.50	0.450	2800	3.30E-03	Irregular	1.80	3	0.0500	0.08	0.375	0.0	0.00	0.0000	3425	0.00E+00
W136	5	TOR	0.077	0.112	1.26	1.58	3191	0.50	0.450	2800	3.30E-03	Irregular	1.80	3	0.0500	0.08	0.375	0.0	0.00	0.0000	4021	0.00E+00
W137	6	TOR	0.102	0.146	1.31	1.64	3530	0.50	0.450	2800	3.30E-03	Irregular	1.80	3	0.0500	0.08	0.375	0.0	0.00	0.0000	4624	0.00E+00
W138	10	TOR	0.075	0.109	0.95	1.19	2717	0.50	0.450	2800	1.90E-03	Irregular	1.80	3	0.0500	0.08	0.375	0.0	0.00	0.0000	2581	0.00E+00
W139	11	TOR	0.097	0.139	1.09	1.36	2921	0.50	0.450	2800	1.90E-03	Irregular	1.80	3	0.0500	0.08	0.375	0.0	0.00	0.0000	3184	0.00E+00
W140	12	TOR	0.104	0.148	1.19	1.49	3029	0.50	0.450	2800	1.90E-03	Irregular	1.80	3	0.0500	0.08	0.375	0.0	0.00	0.0000	3605	0.00E+00
W141	13	TOR	0.072	0.105	1.10	1.38	3013	0.50	0.450	2800	1.90E-03	Irregular	1.80	3	0.0500	0.08	0.375	0.0	0.00	0.0000	3314	0.00E+00
W142	14	TOR	0.078	0.113	1.23	1.54	3168	0.50	0.450	2800	1.90E-03	Irregular	1.80	3	0.0500	0.08	0.375	0.0	0.00	0.0000	3897	0.00E+00
W143	15	TOR	0.102	0.146	1.40	1.75	3169	0.50	0.450	2800	1.90E-03	Irregular	1.80	3	0.0500	0.08	0.375	1.8	0.05	0.0000	4437	6.50E-06
W 144	1A 1	HEU	0.142	0.197	1.58	1.98	1018	0.45	0.358	2679	1.50E-03	Irregular	1.68	3	0.0919	0.15	0.702	1468.3	14.72	0.0775	1612	3.32E-03
W 145	1A 2	HEU	0.142	0.197	1.59	1.98	3048	0.45	0.358	2679	1.50E-03	Irregular	1.68	3	0.0919	0.15	0.702	2878.2	28.85	0.0671	4840	6.51E-03
W 146	1A 3	HEU	0.143	0.198	1.59	1.99	6054	0.45	0.358	2679	1.50E-03	Irregular	1.68	3	0.0919	0.15	0.702	4112.5	41.22	0.1200	9655	9.29E-03
W 147	1A 4	HEU	0.143	0.198	1.60	2.00	10935	0.45	0.358	2679	1.50E-03	Irregular	1.68	3	0.0919	0.15	0.702	5302.0	53.14	0.0525	17473	1.20E-02
W 148	1A2 1	HEU	0.143	0.199	1.60	2.00	4881	0.45	0.358	2679	1.50E-03	Irregular	1.68	3	0.0920	0.15	0.702	3352.6	33.60	0.0623	7815	7.58E-03
W 149	1A2 2	HEU	0.143	0.198	1.59	1.98	9806	0.45	0.358	2679	1.50E-03	Irregular	1.68	3	0.0920	0.15	0.702	4851.2	48.62	0.0532	15568	1.10E-02
W 150	1A2 3	HEU	0.143	0.198	1.60	2.00	14684	0.45	0.358	2679	1.50E-03	Irregular	1.68	3	0.0920	0.15	0.702	5756.8	57.70	0.0486	23440	1.30E-02
W 151	1A2 4	HEU	0.143	0.198	1.60	2.00	19550	0.45	0.358	2679	1.50E-03	Irregular	1.68	3	0.0920	0.15	0.702	6474.6	64.89	0.0447	31315	1.46E-02
W 152	1B 1	HEU	0.142	0.197	1.58	1.98	1018	0.45	0.368	2691	3.39E-03	Irregular	1.69	3	0.0822	0.15	0.643	59.5	1.34	0.0889	1612	6.83E-04
W 153	1B 2	HEU	0.142	0.197	1.59	1.98	3048	0.45	0.368	2691	3.39E-03	Irregular	1.69	3	0.0822	0.15	0.643	88.0	1.99	0.0865	4840	1.01E-03
W 154	1B 3	HEU	0.143	0.198	1.59	1.99	6054	0.45	0.368	2691	3.39E-03	Irregular	1.69	3	0.0822	0.15	0.643	112.6	2.54	0.0952	9655	1.29E-03
W 155	1B 4	HEU	0.143	0.198	1.60	2.00	10935	0.45	0.368	2691	3.39E-03	Irregular	1.69	3	0.0822	0.15	0.643	128.2	2.90	0.0844	17473	1.47E-03
W 156	1B 5	HEU	0.143	0.199	1.60	2.00	15816	0.45	0.368	2691	3.39E-03	Irregular	1.69	3	0.0822	0.15	0.643	130.4	2.95	0.0854	25325	1.50E-03
W 157	1B 6	HEU	0.143	0.198	1.59	1.98	20741	0.45	0.368	2691	3.39E-03	Irregular	1.69	3	0.0822	0.15	0.643	148.7	3.36	0.0834	32928	1.71E-03
W 158	1B 7	HEU	0.143	0.198	1.60	2.00	25619	0.45	0.368	2691	3.39E-03	Irregular	1.69	3	0.0822	0.15	0.643	164.0	3.71	0.0838	40896	1.88E-03
W 159	1B 8	HEU	0.143	0.198	1.60	2.00	30485	0.45	0.368	2691	3.39E-03	Irregular	1.69	3	0.0822	0.15	0.643	147.2	3.33	0.0847	48831	1.69E-03
W 160	1Av2 1	HEU	0.144	0.199	1.60	2.00	1014	0.45	0.366	2679	1.50E-03	Irregular	1.68	3	0.0838	0.15	0.653	1295.0	12.98	0.0761	1625	2.93E-03
W 161	1Av2 2	HEU	0.144	0.200	1.60	2.00	3144	0.45	0.366	2679	1.50E-03	Irregular	1.68	3	0.0838	0.15	0.653	2530.3	25.36	0.0662	5024	5.72E-03
W 162	1Av2 3	HEU	0.144	0.200	1.59	1.99	6050	0.45	0.366	2679	1.50E-03	Irregular	1.68	3	0.0838	0.15	0.653	3713.2	37.22	0.0589	9647	8.39E-03
W 163	1Av2 4	HEU	0.144	0.200	1.59	1.99	10568	0.45	0.366	2679	1.50E-03	Irregular	1.68	3	0.0838	0.15	0.653	4963.2	49.74	0.0524	16850	1.12E-02
W 164	1Av2 5	HEU	0.144	0.200	1.60	2.00	15619	0.45	0.366	2679	1.50E-03	Irregular	1.68	3	0.0838	0.15	0.653	5930.3	59.44	0.0479	25000	1.34E-02
W 165	1Av2 6	HEU	0.144	0.200	1.60	2.00	20682	0.45	0.366	2679	1.50E-03	Irregular	1.68	3	0.0838	0.15	0.653	6713.2	67.28	0.0448	33126	1.52E-02
W 166	1Av2 7	HEU	0.144	0.199	1.60	2.00	25644	0.45	0.366	2679	1.50E-03	Irregular	1.68	3	0.0838	0.15	0.653	7236.9	72.53	0.0420	41107	1.64E-02
W 167	1Av2 8	HEU	0.144	0.200	1.60	2.00	30519	0.45	0.366	2679	1.50E-03	Irregular	1.68	3	0.0838	0.15	0.653	7783.5	78.01	0.0394	48885	1.76E-02
W 168	1Bv2 1	HEU	0.144	0.199	1.60	2.00	1014	0.45	0.365	2691	3.39E-03	Irregular	1.69	3	0.0847	0.15	0.658	70.8	1.60	0.0817	1625	8.13E-04

Table G.4: Measured test results from physical scale model tests (continued).

	Test			Hydraulic conditions							Stones				Structure			Damage				
Number	Orig nr	Dataset	H_s	$H_{1\%}$	T_m	T_p	N	h	h_c	ρ_s	D_{n50}	shape	Δ	m_0	z_c	B_c	B	S	S^*	z_d	Duration	A_e
-	-	-	[m]	[m]	[s]	[s]	[-]	[m]	[m]	[kg/m³]	[m]	[-]	[-]	[-]	[m]	[m]	[m]	[-]	[-]	[m]	[s]	[m²]
W 169	1Bv2 2	HEU	0.144	0.200	1.60	2.00	3144	0.45	0.365	2691	3.39E-03	Irregular	1.69	3	0.0847	0.15	0.658	108.9	2.46	0.0805	5024	1.25E-03
W 170	1Bv2 3	HEU	0.144	0.200	1.59	1.99	6050	0.45	0.365	2691	3.39E-03	Irregular	1.69	3	0.0847	0.15	0.658	152.9	3.46	0.0782	9647	1.76E-03
W 171	1Bv2 4	HEU	0.144	0.200	1.59	1.99	10568	0.45	0.365	2691	3.39E-03	Irregular	1.69	3	0.0847	0.15	0.658	175.0	3.96	0.0763	16850	2.01E-03
W 172	1Bv2 5	HEU	0.144	0.200	1.60	2.00	15619	0.45	0.365	2691	3.39E-03	Irregular	1.69	3	0.0847	0.15	0.658	208.6	4.72	0.0746	25020	2.40E-03
W 173	1Bv2 6	HEU	0.144	0.200	1.60	2.00	20682	0.45	0.365	2691	3.39E-03	Irregular	1.69	3	0.0847	0.15	0.658	229.5	5.19	0.0737	33126	2.64E-03
W 174	1Bv2 7	HEU	0.144	0.199	1.60	2.00	25644	0.45	0.365	2691	3.39E-03	Irregular	1.69	3	0.0847	0.15	0.658	232.2	5.25	0.0734	41107	2.67E-03
W 175	1Bv2 8	HEU	0.144	0.200	1.60	2.00	30519	0.45	0.365	2691	3.39E-03	Irregular	1.69	3	0.0847	0.15	0.658	243.5	5.50	0.0732	48885	2.80E-03
W 176	2A 1	HEU	0.140	0.192	1.61	2.01	995	0.40	0.313	2679	1.50E-03	Irregular	1.68	3	0.0871	0.15	0.672	1527.2	15.31	0.0750	1599	3.45E-03
W 177	2A 2	HEU	0.140	0.192	1.60	2.00	2946	0.40	0.313	2679	1.50E-03	Irregular	1.68	3	0.0871	0.15	0.672	2987.5	29.94	0.0641	4724	6.75E-03
W 178	2A 3	HEU	0.141	0.193	1.61	2.01	5579	0.40	0.313	2679	1.50E-03	Irregular	1.68	3	0.0871	0.15	0.672	4076.9	40.86	0.0569	8989	9.21E-03
W 179	2A 4	HEU	0.141	0.193	1.61	2.01	10432	0.40	0.313	2679	1.50E-03	Irregular	1.68	3	0.0871	0.15	0.672	5592.1	56.05	0.0498	16777	1.26E-02
W 180	2A 5	HEU	0.144	0.198	1.76	2.20	15293	0.40	0.313	2679	1.50E-03	Irregular	1.68	3	0.0871	0.15	0.672	6734.7	67.50	0.0448	26934	1.52E-02
W 181	2A 6	HEU	0.142	0.195	1.61	2.01	20139	0.40	0.313	2679	1.50E-03	Irregular	1.68	3	0.0871	0.15	0.672	7433.9	74.51	0.0416	32438	1.68E-02
W 182	2A 7	HEU	0.141	0.194	1.61	2.01	25005	0.40	0.313	2679	1.50E-03	Irregular	1.68	3	0.0871	0.15	0.672	8015.8	80.34	0.0384	40135	1.81E-02
W 183	2B 1	HEU	0.140	0.192	1.61	2.01	995	0.40	0.312	2691	3.39E-03	Irregular	1.69	3	0.0882	0.15	0.679	119.5	2.70	0.0842	1599	1.37E-03
W 184	2B 2	HEU	0.140	0.192	1.60	2.00	2946	0.40	0.312	2691	3.39E-03	Irregular	1.69	3	0.0882	0.15	0.679	115.8	2.62	0.0848	4724	1.33E-03
W 185	2B 3	HEU	0.141	0.193	1.61	2.01	5579	0.40	0.312	2691	3.39E-03	Irregular	1.69	3	0.0882	0.15	0.679	172.1	3.89	0.0820	8989	1.98E-03
W 186	2B 4	HEU	0.141	0.193	1.61	2.01	10432	0.40	0.312	2691	3.39E-03	Irregular	1.69	3	0.0882	0.15	0.679	281.4	6.36	0.0760	16777	3.23E-03
W 187	2B 5	HEU	0.144	0.198	1.76	2.20	15293	0.40	0.312	2691	3.39E-03	Irregular	1.69	3	0.0882	0.15	0.679	316.8	7.16	0.0754	26934	3.64E-03
W 188	2B 6	HEU	0.142	0.195	1.61	2.01	20139	0.40	0.312	2691	3.39E-03	Irregular	1.69	3	0.0882	0.15	0.679	349.8	7.91	0.0738	32438	4.02E-03
W 189	2B 7	HEU	0.141	0.194	1.61	2.01	25005	0.40	0.312	2691	3.39E-03	Irregular	1.69	3	0.0882	0.15	0.679	351.4	7.94	0.0735	40135	4.04E-03
W 190	2B 8	HEU	0.142	0.195	1.60	2.00	29883	0.40	0.312	2691	3.39E-03	Irregular	1.69	3	0.0882	0.15	0.679	388.5	8.78	0.0718	47883	4.46E-03
W 191	2Av2 1	HEU	0.139	0.191	1.60	2.01	1020	0.40	0.313	2679	1.50E-03	Irregular	1.68	3	0.0873	0.15	0.674	1825.8	18.30	0.0743	1636	4.13E-03
W 192	2Av2 2	HEU	0.139	0.192	1.62	2.02	3088	0.40	0.313	2679	1.50E-03	Irregular	1.68	3	0.0873	0.15	0.674	3449.6	34.57	0.0620	4992	7.80E-03
W 193	2Av2 3	HEU	0.139	0.192	1.60	2.00	5961	0.40	0.313	2679	1.50E-03	Irregular	1.68	3	0.0873	0.15	0.674	4934.9	49.46	0.0540	9554	1.12E-02
W 194	2Av2 4	HEU	0.140	0.192	1.61	2.01	10840	0.40	0.313	2679	1.50E-03	Irregular	1.68	3	0.0873	0.15	0.674	6349.0	63.63	0.0465	17436	1.43E-02
W 195	2Av2 5	HEU	0.140	0.192	1.61	2.02	15646	0.40	0.313	2679	1.50E-03	Irregular	1.68	3	0.0873	0.15	0.674	7254.1	72.70	0.0425	25224	1.64E-02
W 196	2Av2 6	HEU	0.140	0.193	1.62	2.02	17227	0.40	0.313	2679	1.50E-03	Irregular	1.68	3	0.0873	0.15	0.674	7544.4	75.61	0.0411	27883	1.71E-02
W 197	2Bv2 1	HEU	0.139	0.191	1.60	2.01	1020	0.40	0.318	2691	3.39E-03	Irregular	1.69	3	0.0820	0.15	0.642	77.4	1.75	0.0792	1636	8.89E-04
W 198	2Bv2 2	HEU	0.139	0.192	1.62	2.02	3088	0.40	0.318	2691	3.39E-03	Irregular	1.69	3	0.0820	0.15	0.642	181.9	4.11	0.0751	4992	2.09E-03
W 199	2Bv2 3	HEU	0.139	0.192	1.60	2.00	5961	0.40	0.318	2691	3.39E-03	Irregular	1.69	3	0.0820	0.15	0.642	248.4	5.61	0.0714	9554	2.86E-03
W 200	2Bv2 4	HEU	0.140	0.192	1.61	2.01	10840	0.40	0.318	2691	3.39E-03	Irregular	1.69	3	0.0820	0.15	0.642	334.8	7.57	0.0687	17436	3.85E-03
W 201	2Bv2 5	HEU	0.140	0.192	1.61	2.02	15646	0.40	0.318	2691	3.39E-03	Irregular	1.69	3	0.0820	0.15	0.642	379.7	8.58	0.0666	25224	4.36E-03
W 202	2Bv2 6	HEU	0.140	0.193	1.62	2.02	17227	0.40	0.318	2691	3.39E-03	Irregular	1.69	3	0.0820	0.15	0.642	380.8	8.61	0.0671	27883	4.38E-03
W 203	3A 1	HEU	0.172	0.234	1.67	2.09	946	0.45	0.367	2679	1.50E-03	Irregular	1.68	3	0.0831	0.15	0.648	2038.6	20.43	0.0680	1579	4.61E-03
W 204	3A 2	HEU	0.168	0.230	1.71	2.14	2686	0.45	0.367	2679	1.50E-03	Irregular	1.68	3	0.0831	0.15	0.648	3766.3	37.75	0.0569	4591	8.51E-03
W 205	3A 3	HEU	0.164	0.225	1.75	2.19	5411	0.45	0.367	2679	1.50E-03	Irregular	1.68	3	0.0831	0.15	0.648	5194.9	52.07	0.0485	9467	1.17E-02
W 206	3A 4	HEU	0.164	0.225	1.78	2.22	10378	0.45	0.367	2679	1.50E-03	Irregular	1.68	3	0.0831	0.15	0.648	6920.6	69.36	0.0399	18454	1.56E-02
W 207	3A 5	HEU	0.164	0.225	1.78	2.23	15451	0.45	0.367	2679	1.50E-03	Irregular	1.68	3	0.0831	0.15	0.648	8042.7	80.61	0.0356	27518	1.82E-02
W 208	3A2 1	HEU	0.164	0.225	1.78	2.22	5116	0.45	0.372	2679	1.50E-03	Irregular	1.68	3	0.0785	0.15	0.621	4713.4	47.24	0.0744	9094	1.07E-02
W 209	3A2 2	HEU	0.164	0.225	1.78	2.22	10197	0.45	0.372	2679	1.50E-03	Irregular	1.68	3	0.0785	0.15	0.621	7174.6	71.91	0.0415	18126	1.62E-02
W 210	3A2 3	HEU	0.164	0.225	1.78	2.22	15256	0.45	0.372	2679	1.50E-03	Irregular	1.68	3	0.0785	0.15	0.621	8162.2	81.81	0.0366	27119	1.84E-02

Table G.5: Measured test results from physical scale model tests (continued).

	Test			Hydraulic conditions								Stones				Structure						Damage		
Number	Orig nr	Dataset	H_s	$H_{1\%}$	T_m	T_p	N	h	h_c	ρ_s	D_{n50}	shape	Δ	m_0	z_c	B_c	B	S	S^*	z_d	Duration	A_e
-	-	-	[m]	[m]	[s]	[s]	[-]	[m]	[m]	[kg/m³]	[m]	[-]	[-]	[-]	[m]	[m]	[m]	[-]	[-]	[m]	[s]	[m²]
W 211	3B 1	HEU	0.172	0.234	1.67	2.09	946	0.45	0.365	2691	3.39E-03	Irregular	1.69	3	0.0854	0.15	0.662	186.0	4.20	0.0787	1579	2.14E-03
W 212	3B 2	HEU	0.168	0.230	1.71	2.14	2686	0.45	0.365	2691	3.39E-03	Irregular	1.69	3	0.0854	0.15	0.662	246.6	5.57	0.0762	4591	2.83E-03
W 213	3B 3	HEU	0.164	0.225	1.75	2.19	5411	0.45	0.365	2691	3.39E-03	Irregular	1.69	3	0.0854	0.15	0.662	328.5	7.42	0.0730	9467	3.78E-03
W 214	3B 4	HEU	0.164	0.225	1.78	2.22	10378	0.45	0.365	2691	3.39E-03	Irregular	1.69	3	0.0854	0.15	0.662	399.8	9.04	0.0715	18454	4.59E-03
W 215	3B 5	HEU	0.164	0.225	1.78	2.23	15451	0.45	0.365	2691	3.39E-03	Irregular	1.69	3	0.0854	0.15	0.662	465.2	10.51	0.0681	27518	5.35E-03
W 216	3B 6	HEU	0.164	0.225	1.78	2.23	20567	0.45	0.365	2691	3.39E-03	Irregular	1.69	3	0.0854	0.15	0.662	462.1	10.44	0.0684	36630	5.31E-03
W 217	3B 7	HEU	0.164	0.225	1.78	2.22	25648	0.45	0.365	2691	3.39E-03	Irregular	1.69	3	0.0854	0.15	0.662	504.6	11.40	0.0677	45592	5.80E-03
W 218	3B 8	HEU	0.164	0.225	1.78	2.22	30707	0.45	0.365	2691	3.39E-03	Irregular	1.69	3	0.0854	0.15	0.662	536.2	12.12	0.0655	54583	6.16E-03
W 219	4A 1	HEU	0.140	0.194	1.58	1.98	1028	0.45	0.345	2679	1.50E-03	Irregular	1.68	3	0.1055	0.15	0.783	1368.9	13.72	0.0927	1627	3.09E-03
W 220	4A 2	HEU	0.140	0.195	1.59	1.99	3076	0.45	0.345	2679	1.50E-03	Irregular	1.68	3	0.1055	0.15	0.783	2802.3	28.09	0.0822	4891	6.33E-03
W 221	4A 3	HEU	0.141	0.195	1.59	1.99	6128	0.45	0.345	2679	1.50E-03	Irregular	1.68	3	0.1055	0.15	0.783	4354.1	43.64	0.0727	9741	9.84E-03
W 222	4A 4	HEU	0.141	0.195	1.59	1.98	11240	0.45	0.345	2679	1.50E-03	Irregular	1.68	3	0.1055	0.15	0.783	5948.3	59.62	0.0641	17828	1.34E-02
W 223	4A 5	HEU	0.141	0.195	1.59	1.98	16352	0.45	0.345	2679	1.50E-03	Irregular	1.68	3	0.1055	0.15	0.783	7232.2	72.48	0.0580	25937	1.63E-02
W 224	4A 6	HEU	0.141	0.196	1.59	1.98	21459	0.45	0.345	2679	1.50E-03	Irregular	1.68	3	0.1055	0.15	0.783	8098.9	81.17	0.0544	34057	1.83E-02
W 225	4A 7	HEU	0.142	0.197	1.59	1.98	26568	0.45	0.345	2679	1.50E-03	Irregular	1.68	3	0.1055	0.15	0.783	8851.6	88.72	0.0512	42154	2.00E-02
W 226	4B 1	HEU	0.140	0.194	1.58	1.98	1028	0.45	0.316	2691	3.39E-03	Irregular	1.69	3	0.1343	0.15	0.956	178.0	4.02	0.1269	1627	2.05E-03
W 227	4B 2	HEU	0.140	0.195	1.59	1.99	3076	0.45	0.316	2691	3.39E-03	Irregular	1.69	3	0.1343	0.15	0.956	357.9	8.09	0.1180	4891	4.11E-03
W 228	4B 3	HEU	0.141	0.195	1.59	1.99	6128	0.45	0.316	2691	3.39E-03	Irregular	1.69	3	0.1343	0.15	0.956	525.6	11.88	0.1121	9741	6.04E-03
W 229	4B 4	HEU	0.141	0.195	1.59	1.98	11240	0.45	0.316	2691	3.39E-03	Irregular	1.69	3	0.1343	0.15	0.956	688.9	15.57	0.1075	17828	7.92E-03
W 230	4B 5	HEU	0.141	0.195	1.59	1.98	16352	0.45	0.316	2691	3.39E-03	Irregular	1.69	3	0.1343	0.15	0.956	862.6	19.50	0.1029	25937	9.91E-03
W 231	4B 6	HEU	0.141	0.196	1.59	1.98	21459	0.45	0.316	2691	3.39E-03	Irregular	1.69	3	0.1343	0.15	0.956	945.7	21.37	0.1002	34057	1.09E-02
W 232	4B 7	HEU	0.142	0.197	1.59	1.98	26568	0.45	0.316	2691	3.39E-03	Irregular	1.69	3	0.1343	0.15	0.956	1013.6	22.91	0.0982	42154	1.16E-02
W 233	4B 8	HEU	0.142	0.197	1.59	1.98	31703	0.45	0.316	2691	3.39E-03	Irregular	1.69	3	0.1343	0.15	0.956	1099.6	24.85	0.0961	50300	1.26E-02
W 234	5A 1	HEU	0.143	0.198	1.59	1.98	1025	0.45	0.363	2679	1.50E-03	Irregular	1.68	3	0.0872	0.30	0.823	1103.5	5.53	0.0833	1625	2.49E-03
W 235	5A 2	HEU	0.143	0.199	1.59	1.99	3065	0.45	0.363	2679	1.50E-03	Irregular	1.68	3	0.0872	0.30	0.823	2426.7	12.16	0.0758	4877	5.48E-03
W 236	5A 3	HEU	0.143	0.199	1.59	1.99	6073	0.45	0.363	2679	1.50E-03	Irregular	1.68	3	0.0872	0.30	0.823	3766.5	18.87	0.0688	9645	8.51E-03
W 237	5A 4	HEU	0.143	0.198	1.59	1.98	11183	0.45	0.363	2679	1.50E-03	Irregular	1.68	3	0.0872	0.30	0.823	5277.6	26.45	0.0616	17756	1.19E-02
W 238	5A 5	HEU	0.143	0.198	1.59	1.99	16278	0.45	0.363	2679	1.50E-03	Irregular	1.68	3	0.0872	0.30	0.823	6403.9	32.09	0.0563	25931	1.45E-02
W 239	5A 6	HEU	0.143	0.199	1.59	1.99	21828	0.45	0.363	2679	1.50E-03	Irregular	1.68	3	0.0872	0.30	0.823	7329.0	36.73	0.0525	34812	1.66E-02
W 240	5A 7	HEU	0.143	0.199	1.59	1.99	26432	0.45	0.363	2679	1.50E-03	Irregular	1.68	3	0.0872	0.30	0.823	8030.3	40.24	0.0495	42051	1.81E-02
W 241	5A 8	HEU	0.143	0.198	1.60	2.00	31545	0.45	0.363	2679	1.50E-03	Irregular	1.68	3	0.0872	0.30	0.823	8548.6	42.84	0.0478	50417	1.93E-02
W 242	5B 1	HEU	0.143	0.198	1.59	1.98	1025	0.45	0.361	2691	3.39E-03	Irregular	1.69	3	0.0890	0.30	0.834	85.0	0.96	0.0866	1625	9.77E-04
W 243	5B 2	HEU	0.143	0.199	1.59	1.99	3065	0.45	0.361	2691	3.39E-03	Irregular	1.69	3	0.0890	0.30	0.834	134.0	1.51	0.0855	4877	1.54E-03
W 244	5B 3	HEU	0.143	0.199	1.59	1.99	6073	0.45	0.361	2691	3.39E-03	Irregular	1.69	3	0.0890	0.30	0.834	123.3	1.39	0.0864	9645	1.42E-03
W 245	5B 4	HEU	0.143	0.198	1.59	1.98	11183	0.45	0.361	2691	3.39E-03	Irregular	1.69	3	0.0890	0.30	0.834	183.7	2.08	0.0854	17756	2.11E-03
W 246	5B 5	HEU	0.143	0.198	1.59	1.99	16278	0.45	0.361	2691	3.39E-03	Irregular	1.69	3	0.0890	0.30	0.834	183.3	2.07	0.0854	25931	2.11E-03
W 247	5B 6	HEU	0.143	0.199	1.59	1.99	21828	0.45	0.361	2691	3.39E-03	Irregular	1.69	3	0.0890	0.30	0.834	189.2	2.14	0.0854	34812	2.17E-03
W 248	5B 7	HEU	0.143	0.199	1.59	1.99	26432	0.45	0.361	2691	3.39E-03	Irregular	1.69	3	0.0890	0.30	0.834	216.6	2.45	0.0849	42051	2.49E-03
W 249	5B 8	HEU	0.143	0.198	1.60	2.00	31545	0.45	0.361	2691	3.39E-03	Irregular	1.69	3	0.0890	0.30	0.834	261.4	2.95	0.0845	50417	3.00E-03

Table G.6: Measured test results from physical scale model tests (continued).

Test		Hydraulic conditions								Stones		Structure						Damage			
Orig nr	Dataset	H_s	$H_{1\%}$	T_m	T_p	N	h	h_c	ρ_s	D_{n50}	shape	Δ	m_0	z_c	B_c	B	S	S^*	z_d	Duration	A_e
-	-	[m]	[m]	[s]	[s]	[-]	[m]	[m]	[kg/m^3]	[m]	[-]	[-]	[-]	[m]	[m]	[m]	[-]	[-]	[m]	[s]	[m^2]
6B 1	HEU	0.092	0.132	1.25	1.57	1017	0.5	0.415	2691	3.39E-03	Irregular	1.69	3	0.0847	0.15	0.66	13.8	0.3	0.0844	1274	1.59E-04
6B 2	HEU	0.094	0.134	1.25	1.56	6137	0.5	0.415	2691	3.39E-03	Irregular	1.69	3	0.0847	0.15	0.66	26.8	0.6	0.0837	7659	3.08E-04
6B 3	HEU	0.111	0.158	1.34	1.68	11974	0.5	0.415	2691	3.39E-03	Irregular	1.69	3	0.0847	0.15	0.66	38.3	0.9	0.0833	16082	4.40E-04
6B 4	HEU	0.129	0.182	1.45	1.82	17926	0.5	0.415	2691	3.39E-03	Irregular	1.69	3	0.0847	0.15	0.66	74.9	1.7	0.0822	26046	8.60E-04
6B 5	HEU	0.147	0.204	1.57	1.97	23949	0.5	0.415	2691	3.39E-03	Irregular	1.69	3	0.0847	0.15	0.66	126.1	2.9	0.0810	37681	1.45E-03
6B 6	HEU	0.162	0.225	1.67	2.09	29746	0.5	0.415	2691	3.39E-03	Irregular	1.69	3	0.0847	0.15	0.66	213.6	4.8	0.0782	49703	2.46E-03
6B 7	HEU	0.172	0.237	1.73	2.17	35571	0.5	0.415	2691	3.39E-03	Irregular	1.69	3	0.0847	0.15	0.66	387.9	8.8	0.0692	61674	4.46E-03
6B 8	HEU	0.180	0.247	1.82	2.27	41127	0.5	0.415	2691	3.39E-03	Irregular	1.69	3	0.0847	0.15	0.66	503.5	11.4	0.0649	74761	5.79E-03
7B 1	HEU	0.094	0.135	1.25	1.57	6057	0.5	0.415	2691	3.39E-03	Irregular	1.69	3	0.0853	0.15	0.66	41.1	0.9	0.0846	7586	4.72E-04
7B 2	HEU	0.138	0.194	1.51	1.89	13555	0.5	0.415	2691	3.39E-03	Irregular	1.69	3	0.0853	0.15	0.66	115.5	2.6	0.0819	20482	1.33E-03
7B 3	HEU	0.161	0.222	1.66	2.08	16445	0.5	0.415	2691	3.39E-03	Irregular	1.69	3	0.0853	0.15	0.66	117.9	2.7	0.0817	27380	1.35E-03
7B 4	HEU	0.178	0.244	1.76	2.20	19010	0.5	0.415	2691	3.39E-03	Irregular	1.69	3	0.0853	0.15	0.66	148.2	3.3	0.0794	33518	1.70E-03
7Bv2 1	HEU	0.094	0.135	1.25	1.56	5730	0.5	0.415	2691	3.39E-03	Irregular	1.69	3	0.0845	0.15	0.66	25.7	0.6	0.0836	7157	2.95E-04
7Bv2 2	HEU	0.138	0.193	1.51	1.89	11892	0.5	0.415	2691	3.39E-03	Irregular	1.69	3	0.0845	0.15	0.66	87.4	2.0	0.0819	17970	1.00E-03
7Bv2 3	HEU	0.160	0.222	1.66	2.07	14936	0.5	0.415	2691	3.39E-03	Irregular	1.69	3	0.0845	0.15	0.66	101.5	2.3	0.0816	24725	1.17E-03
7Bv2 4	HEU	0.180	0.247	1.82	2.27	17909	0.5	0.415	2691	3.39E-03	Irregular	1.69	3	0.0845	0.15	0.66	128.6	2.9	0.0801	32515	1.48E-03
7Bv2 5	HEU	0.137	0.192	1.50	1.88	23929	0.5	0.415	2691	3.39E-03	Irregular	1.69	3	0.0845	0.15	0.66	131.7	3.0	0.0801	35956	1.51E-03
7Bv2 6	HEU	0.160	0.221	1.67	2.08	26980	0.5	0.415	2691	3.39E-03	Irregular	1.69	3	0.0845	0.15	0.66	124.3	2.8	0.0801	44974	1.43E-03
7Bv2 7	HEU	0.137	0.193	1.51	1.89	32958	0.5	0.415	2691	3.39E-03	Irregular	1.69	3	0.0845	0.15	0.66	133.2	3.0	0.0798	49717	1.53E-03
7Bv2 8	HEU	0.179	0.246	1.81	2.26	35959	0.5	0.415	2691	3.39E-03	Irregular	1.69	3	0.0845	0.15	0.66	170.4	3.9	0.0797	64945	1.96E-03

Table G.7: Measured test results from physical scale model tests for multiple storms.

Appendix H

Measurement errors

In Chapter 3 the initial measurement errors are described and in Paragraph 4.2.3 the precision of the echo-sounder was further described. There are always deviations in the results of physical scale model testing because the measurement devices are not perfect. For every measurement the deviations are quantified except for the echo-sounder. Because of the large footprint the height measurement done by the echo-sounder can have a considerable error. In this appendix this deviation is investigated.

It was concluded the echo-sounder has a footprint which is in 45 cm water depth in the order of 51 mm. An artist impression of the echo-sounder is shown in Figure H.1. The echo-sounder prefers strong echoes and thus strong echoes which are picked up earlier are taken as the height. Because of this, the echo-sounder prefers higher objects with still strong echoes [General Acoustics, 2013]. Together with the footprint, in which the echo-sounder measures the height, an error is present in the height measurements because it prefers the higher objects in the footprint. Five different cases can be distinguished for this shown in Figure H.1. In the first case there is no error present because the height in the footprint is everywhere the same. In the second case a large error is present and is the most extreme case which can be present. The red dotted line in the middle is height where the height measurement should be recorded. However, because a part of the footprint is still on top of the block, the echo-sounder picks up this echo and measures this height (blue dotted line). In case three the surface within the echo-sounder is equal again and no errors are present in the measured profile. In case four a smaller error is present than in case two, but still an error is measured here. In case five the error of case four has reduced again because the slope of the triangle has reduced. From this it can be concluded that in smooth profiles a smaller error is present than in angular profiles.

Because of the footprint of the echo-sounder an error is present in measuring the near-bed profile. Theoretically this would for a square beam be half of the total footprint of the echo-sounder which is 22.5 mm. For a square beam, which is the most extreme case, the real profile has been measured. It can be seen that the profile is over estimated in Figure H.2. On the right side of the square beam approximately 25 mm is measured extra which is not present in reality. On the left side this is approximately 10 mm. General Acoustics mentioned that this over estimation is less when smooth transitions are present which was also seen from Figure H.1.

An indication to quantify the measurement error is to determine the extra damage area A_e which was calculated too much. However, as was seen in Figure H.1 the measurement error is not always the same. At the start of a tests the profile is not smoothed yet and the largest measurement errors are present. This measurement error is present in every height measurement, but gets smaller as more damage occurs. It can be concluded from this that the absolute error is smaller than the measurement error because two errors have to be subtracted from each other. However, this error
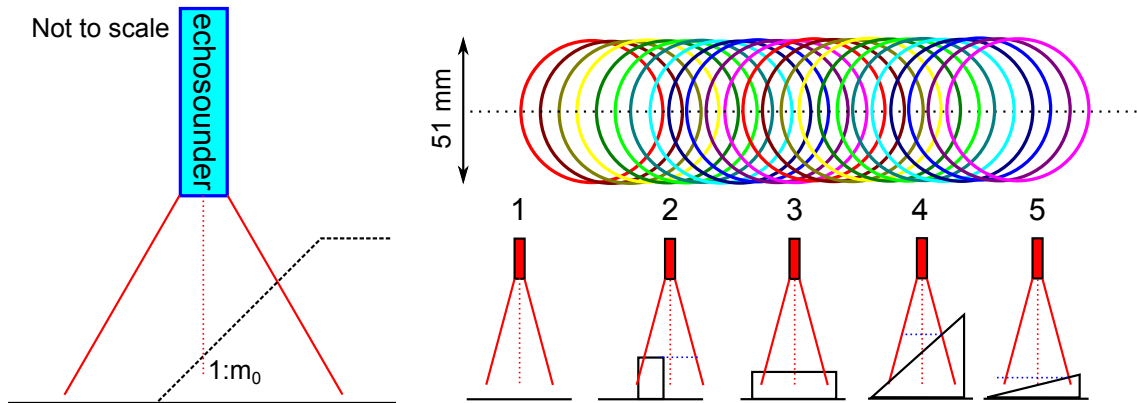
Figure H.1: A not to scale impression of the echo sounder. Left is the echo-sounder measuring a near-bed structure slope. On top are the theoretical footprints of the echo-sounder per measurement with the theoretical line. On the bottom the five different measurements are shown in number 1 to 5.
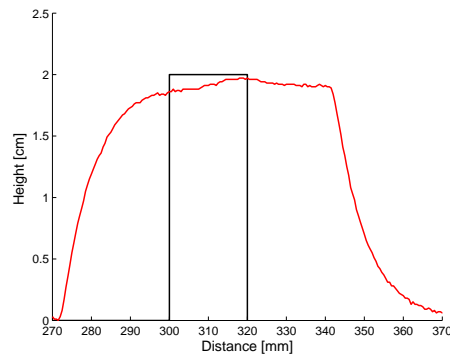
Figure H.2: Square beam measured with echo-sounder.

still has to be quantified because it is expected that this error is not negligible. From Figure H.3 it can be seen that the near-bed structure has been extended on both sides. Clearly can be observed that the measurement error gets smaller when more damage has occurred with the definition of A_e, that the profile has to be below the initial profile. A method to quantify this is error is to calculate the area of the top corners of the near-bed structure. This area is approximated by the height reduction Δz_c multiplied by the extra width that was found from Figure H.2. This approximation can be seen in Figure H.2.
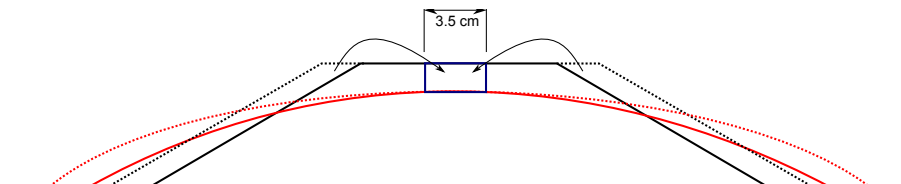
Figure H.3: Extra width measured by the echo-sounder.

By analysing this for each tests in this physical scale model test it resulted that this area was maximal 2% of the total erosion area A_e. This area was on average only 1% of the erosion area from physical scale model tests. This seems rather small for such an error. Because the maximum height of the near-bed structure has been taken in the physical scale model tests to measure the

height reduction, this error is of course small. To get a better indication of the error the erosion area has been divided by the theoretical structure width. In this way an absolute maximum error is obtained because the height reduction cannot be larger than this and the width is of course a little bit more by including the slopes. With this method this surface area was maximal 23% of the total erosion area. With this method the erosion area can maximally be 23% smaller than measured. To get better indications of the real error tests should be done on a known profile in the shape of a near-bed structure in smooth and angular way.

It is also possible the actual erosion area is more with this measurement error. Figure H.4 visualises how this is possible. When the height is lower and because of a bump the total height which is measured is higher less erosion area is calculated. This is visualised by the red dotted lines which are put on the maximum height each time. Because of this it is approximated that the maximal erosion area can be 10% larger than calculated by the height measurements.
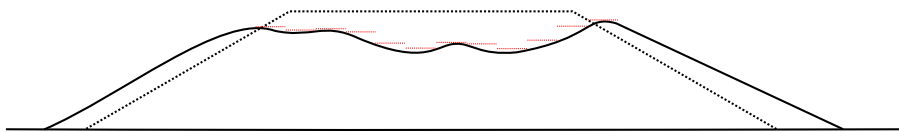
Figure H.4: Extra damage area possible due to measurement errors of the echo-sounder.

Another method to quantify this measurement error is to determine the area of the total profile of the near-bed structure after each height measurement. The profiles on which this calculation is performed are shown in the figures on the left side in Appendix E. Because the measurement error reduces when the profile is smoothed out, this error should reduce as well in a consecutive test. However, it was also observed that stones are removed from the profile which contributes to this error as well. From calculations performed on this it was not observed that when more damage has already occurred the stones removed from the profile became less. In Table H.1 the calculated percentages are shown how much percentage on average per height measurement is lost from the profile for the physical scale model tests. It can be seen that in each tests stones are removed from the profile. This can have a number of causes. The profile can be compacted, stones can be removed from the structure, stones can be moved away and not measured by the echo-sounder or the measurement error of the echo-sounder can cause this. Because of the small percentage that is lost each measurement this error is not taken as representative for the total measurement error of the echo-sounder.

	Average loss	Max loss	Max increase
Test 1A	1.5%	3.5%	0.0%
Test 1B	0.0%	1.2%	1.0%
Test 1Av2	1.5%	2.0%	0.2%
Test 1Bv2	0.3%	2.0%	1.3%
Test 2A	1.7%	3.0%	0.1%
Test 2B	0.8%	3.4%	1.0%
Test 2Av2	1.5%	2.9%	0.4%
Test 2Bv2	0.7%	1.8%	0.4%
Test 3A	4.0%	6.4%	0.0%
Test 3B	0.8%	3.0%	1.0%
Test 4A	1.6%	2.5%	0.0%
Test 4B	0.7%	1.0%	0.0%
Test 5A	1.4%	2.2%	0.0%
Test 5B	0.4%	1.8%	1.0%
Average	1.2%	2.6%	0.5%

Table H.1: Loss or increase percentages of the total profile area from the physical scale model tests.

Appendix I

Statistical tools

This Appendix deals with the statistical tools used in this thesis. In the first section statistical analysis are explained and in the second section the calculation results are treated for formulas which are treated in this thesis.

I.1 Calculating tools

This paragraph is about assessing how good a certain formula represents the data and what are the methods to determine this. This chapter is mainly based on Dekking et al. [2005] and Bendat and Piersol [2011].

To show how much variation or dispersion exists in a dataset, the standard deviation can be used. A standard deviation indicates how much variation exists from the mean or expected value. In this thesis the standard deviation is represented by the Greek letter σ. From for example the physical scale model tests, x is a random variable from a finite dataset of n inputs. From this dataset μ is the average and can be calculated using Equation I.1. The standard deviation given by Equation I.2. The standard deviation squared is called the variance which is often used in statistics. However, the advantage of the standard deviation is that it has the same dimension as the data it is based upon.

$$\mu = \frac{1}{n} \sum_{i=1}^{n} x_i \tag{I.1}$$

$$\sigma = \sqrt{\frac{1}{n} \sum_{i=1}^{n} (x_i - \mu)^2} \tag{I.2}$$

Linear regression Analysis

A linear regression analysis is an approach to model a relationship between a dependent variable and several explanatory variables. The standard form of a linear regression is shown in Equation I.3. Here the parameters a and b are coefficients which can be calculated by the linear regression analysis.

$$y = a + b_1 \cdot x_1 + b_2 \cdot x_2 \tag{I.3}$$

In Matlab the coefficients can be calculated by a linear regression analysis with the use of the Statistical Toolbox [Mathworks, 2013]. Matlab uses the method of least squares for a standard linear regression. Matlab fits a line through the data in the form of I.3, which is called a regression line. In this y are the random realizations which is called the response variable and x the non-random realisations which are called the explanatory variables. The parameters a and b represent the intercept and slope of the regression line.

There are several ways to determine if the model obtained is of a high degree. Matlab gives several factors in order to determine the quality of the fitted model. To determine the quality of the model, use is made of the ANOVA table (ANalysis Of VAriance). In this table Matlab gives the sum of squares, degrees of freedom, mean squares, F-statistic, p-value, lack-of-fit sum and pure error sum of squares. Besides this, also use is made of R^2, adjusted R^2 and the Root Mean Square Error (RMSE). All these coefficients will be explained below.

ANOVA table

An example of the ANOVA table is shown in Table I.1. In this table x is a prediction variable and k is the total amount of predictor variables.

	Sum of Squares	DF	Mean Square	F	p-Value
Total	TSS	$n-1$			
Model	$RegSS$	k	$\frac{RSS}{k}$	$\frac{RegMS}{RMS}$	p-value
Residuals	RSS	$n-k-1$	$\frac{RSS}{n-k-1}$		
	Coefficient	**Standard Err**	**t-Value**	**p-Value**	
x_1	A	$SE(A)$	$\frac{A}{SE(A)}$	p-value	
x_2	B	$SE(B)$	$\frac{B}{SE(B)}$	p-value	

Table I.1: The general version of the ANOVA table for a regression.

The first input of the ANOVA table is the sum of squares. The inputs for the prediction variables x are defined by the regression sum of squares $RegSS$ and can be seen in Equation I.4. In this f_i is the modelled value or predicted value. $RegSS$ is a measure how good the model represents the data. It measures how much variation there is in the model.

$$RegSS = \sum_{i=1}^{n}(f_i - \mu)^2 \tag{I.4}$$

For the residuals the residual sum of squares RSS is given which is shown in Equation I.5. This is a measure of the discrepancy between the estimated model and the data it observes. A relative small RSS means that the model gives a good fit over the data. So far the $RegSS$ and RSS have been treated. In total, this can be written as $RSS + RegSS = TSS$ where TSS is the total sum of squares.

$$RSS = \sum_{i=1}^{n}(x_i - f_i)^2 \tag{I.5}$$

The next column DF, which stands for degrees of freedom, k is the number of predictor variables x. For the model column this is the total number of predictor variables. With the degree of freedom known, the Mean Square and F-statistic column can be calculated. The F-statistic is a way to

analyse if the expected values or variables differ from each other. The F-test is a probability function and from this the p-value can be determined. A p-value will determine the probability that the 0-hypothesis is right. The definition of the 0-hypothesis is that no model is better than the imposed model. A p-value can be given for each parameter, and for the total model. So in summary, the p-value gives us a probability that the imposed model or parameter should be rejected. If the p-value is larger than 0.05 the imposed model should be rejected [Mathworks, 2013].

In the second part of the table per coefficient x the standard error, subsequently a t-value and p-value are shown. The standard error is shown in Equation I.6. In this coefficient σ is the standard deviation of the sample. A t-value is a test if the coefficient divided by the standard error significantly differ from each other. This value should not be close to 0. From the t-test the probability p-value can be calculated. A p-value shows per coefficient a probability if the coefficient should be added to the model or not. If this p-value is larger than 0.05 the imposed parameter should be rejected.

$$SE = \frac{\sigma}{\sqrt{n}} \tag{I.6}$$

The standard error defined in Equation I.6 can be used to determine the confidence interval of the mean from a normally distributed sample. In a normally distributed sample the 5% and 95% confidence bounds can be calculated by $\mu \pm 1.96 \cdot SE$. The normal confidence bounds from an entire distribution can be calculated by $\mu \pm 1.96 \cdot \sigma$ for a normally distributed sample.

The ANNOVA table also gives a lack of fit and a total error. These parameters are given because for other x-parameters, the same measured y-parameter is present in the model. This is statistically impossible and because of this a lack of fit and Pure error can be given. The lack of fit Mean square error can be compared to the Total mean square error. This gives a percentage that the fit of the model is wrong. The Pure error can compared in the same way to the total Mean square error, which should give a very small percentage.

The coefficient of determination R^2

The coefficient R^2 is used in this thesis to denote how good the fit is through the data. It can be seen as how well data points fit a line or curve. R^2 has a scale from 0 to 1 where 1 is a very good fit. R^2 can be calculated with Equation I.7.

$$R^2 = 1 - \frac{RSS}{TSS} = 1 - \frac{\sum\limits_{i=1}^{n}(x_i - f_i)^2}{\sum\limits_{i=1}^{n}(x_i - \mu)^2} \tag{I.7}$$

A indication how good the fit is from R^2 is given by Table I.2 [Bryman and Cramer, 2005 cf. Van den Bos, 2006]

R	R^2	Goodness-of-fit
< 0.19	< 0.039	very low
0.20 - 0.39	0.04 - 0.159	low
0.40 - 0.69	0.16 - 0.489	modest
0.70 - 0.89	0.49 - 0.809	high
> 0.90	> 0.81	very high

Table I.2: Goodness of fit assessment using R^2

With R^2 a first indication will be given if a model fits relatively good or not. An improvement of the R^2 method is that of the adjusted $\bar{R}^2$ method. The adjusted $\bar{R}^2$ method can be calculated using Equation I.8. This method will be used when the number of regression variables k is known.

$$\bar{R}^2 = 1 - (1 - R^2) \cdot \frac{n-1}{n-k-1} \tag{I.8}$$

Root Mean Square Error

The RMSE is method to measure the differences between values predicted by a model and the actual data. The RMSE is scale dependent which means that if the data in the model has a lot of scatter and the data values are really large, the error will be large as well. In a model with a lot of scatter with small data values the RMSE will be smaller. The RMSE should be compared with for instance the mean of the data to see how large the error really is. The RMSE can be calculated using Equation I.9 and is used throughout this thesis.

$$RMSE = \sqrt{\frac{\sum\limits_{i=1}^{n}(x_i - f_i)^2}{n}} = \sqrt{\frac{RSS}{n}} \tag{I.9}$$

Non-linear form

In this thesis non-linear models are used to determine the damage. These models are of the form $y = a \cdot x^b$ where a and b are calculated coefficients. Because the linear regression is obviously linear, the standard equation has to be rewritten. This is done in Equation I.10. With this trick, the linear regression can be done on non-linear models as well. After the regression the obtained coefficients are then translated back to the original model. Because of this trick the y parameters cannot be 0. Because of this values of 0 are filtered out and not included in the linear regression.

$$ln(y) = \ln(a) + b_1 \cdot \ln(x_1) + b_2 \cdot \ln(x_2) \tag{I.10}$$

Because the exponential equation has to be made linear, the RMSE, R^2 and $\bar{R}^2$ can be calculated both on the logarithmic data as the real data. In this thesis the coefficient of determination is calculated from Equation I.10 and from the original form. This is done because the coefficient of determination in its logarithmic form has been used by Van den Bos [2006]. In this way it can be compared for both values of the coefficient of determination. For the RMSE also both values will be calculated. In the thesis however only RMSE from the original form are shown and in the appendix the RMSE for the log function can be seen as well in the ANNOVA tables which is based on the logarithmic form.

Collinearity

By adding more explanatory variables in a linear regression it should be kept in mind that this is a rather dangerous. By adding more variables some parameters might be somehow related to each other which can unrealistically improve the fit. For instance, several parameters can be related to the wave height or the water depth. This phenomenon is called collinearity and must be avoided in the linear regression. In this thesis use is made of a Matlab script by Lau [2013] which is a method after Friendly and Kwan [2009] to determine the collinearity. In Figure I.1 an example is shown how the calculation of the collinearity if visualised. In the first column the condition index is shown which is a first indication of the collinearity. A condition index is the eigenvalue of the variable compared to the sum of the eigenvalues of the other variables. This condition index

can be interpreted using Table I.3. For each prediction variable a row is plotted against again the other prediction variables. Here an example of an economic regression is used where C is the consumption of an amount of money, R the interest rate, dpi the disposable income and $dDPI$ the annual change in disposable income. From this figure it can be seen that the first two rows have a small condition index so no collinearity is present. From the third row a moderate to strong collinearity is found. However, because only the interest rate give a large result no collinearity is present as well. From the last row a high collinearity is found between C, DPI and in less amount with $dDPI$. The number in this plot indicates between which variables a collinearity is present and how strong it is, where 1 is the maximum. These numbers are called the coefficient of variance proportions. Because in this row the Condition index is very large, and large coefficients of variance proportions are found, collinearity is present in this dataset.
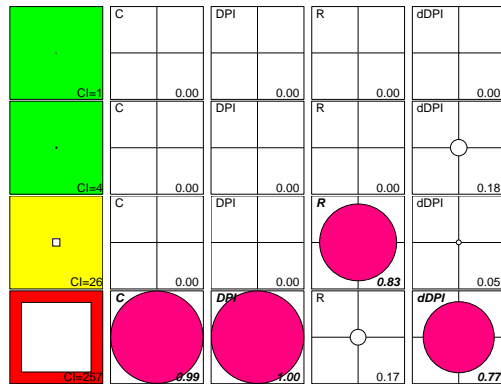
Figure I.1: Example of collinearity visualisation.

Condition index	Degree of collinearity
5 < CI < 10	weak
30 < CI < 100	moderate to strong
CI > 100	severe

Table I.3: Condition index representation taken from Friendly and Kwan [2009].

In this thesis the table plot from Figure I.1 is given in this thesis for our regression as well. As a limitation, the condition index can not be higher than 10. Even when this number is low, it can be seen which parameters depend in a small matter to each other. For more information about collinearity reference is made to Friendly and Kwan [2009].

I.2 Statistics of best-fit equations

In this paragraph the ANOVA table is given for several equations found in this thesis.

For Equation 5.8 below Table I.4 is obtained. In Figure I.2 the collinearity figure from this Equation is shown. From this table it can be seen that the pure error is very low compared to the total and the p-values are sufficient.

$$\frac{S^*}{N^{0.44}} = 0.134 \cdot \theta_{hc1\%}^{2.96} \cdot \left(\frac{B_c}{D_{n50}}\right)^{-0.39} \cdot (m_0 \cdot Kc)^{-1.05} \tag{5.8}$$

Because this table has been calculated using the natural logarithm, the estimate in Table I.4 has to be translated to the real value by the reversed of the natural logarithm.

	SumsQ	DF	MeanSq	F	p-Value
Total	415.8136	226	1.839883		
Model	354.905	3	118.3017	433.129	1.07E-92
Residual	60.90858	223	0.273133		
Lack of fit	58.93701	187	0.315171	5.754874	1.88E-08
Pure error	1.971574	36	0.054766		

	Estimate	SE	t-stat	p-Value
Intercept	-3.93515	0.193421	-20.345	1.23E-52
x1	2.959943	0.106877	27.69484	5.77E-74
x2	-0.3897	0.062744	-6.21102	2.56E-09
x3	-1.04753	0.096177	-10.8916	2.07E-22

Number of observations: 227, Error degrees of freedom: 223
Root Mean Squared Error: 0.523
R-squared: 0.854, Adjusted R-Squared 0.852
F-statistic vs. constant model: 433, p-value = 1.07e-92

Table I.4: ANNOVA table and estimated coefficients Equation 5.8.
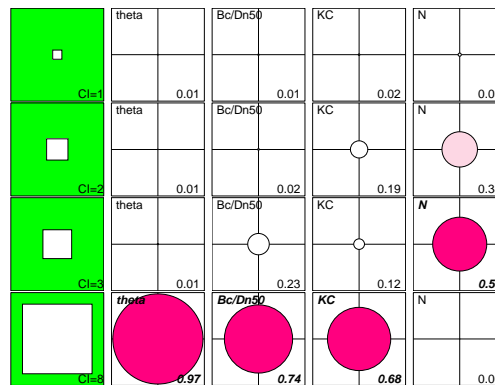
Figure I.2: Collinearity present in Equation 5.8.

For Equation 5.9 the ANNOVA table is shown in Table I.5. In Figure I.3 the collinearity present in this Equation is shown. It can be seen that the pure error is very low compared to the total and the p-values are sufficient.

$$\frac{S^*}{N^{0.37}} = 0.238 \cdot \theta_{hc1\%}^{2.69} \cdot \left(\frac{B_c}{D_{n50}} \right)^{-0.40} \cdot (m_0 \cdot Kc)^{-0.90} \tag{5.9}$$

Because this table has been calculated using the natural logarithm, the estimate in Table I.5 has to be translated to the real value by the reversed of the natural logarithm.

	SumsQ	DF	MeanSq	F	p-Value
Total	194.0567	174	1.115268		
Model	138.1631	3	46.05437	140.8981	5.36E-46
Residual	55.89356	171	0.326863		
Lack of fit	54.51619	135	0.403824	10.55462	2.51E-12
Pure error	1.377373	36	0.03826		
	Estimate	**SE**	**t-stat**	**p-Value**	
Intercept	-3.08992	0.273406	-11.3016	1.91E-22	
x1	2.693193	0.160045	16.82773	4.93E-38	
x2	-0.40301	0.076342	-5.27904	3.92E-07	
x3	-0.89934	0.12152	-7.40076	5.96E-12	

Number of observations: 175, Error degrees of freedom: 171
Root Mean Squared Error: 0.572
R-squared: 0.712, Adjusted R-Squared 0.707
F-statistic vs. constant model: 141, p-value = 5.36e-46

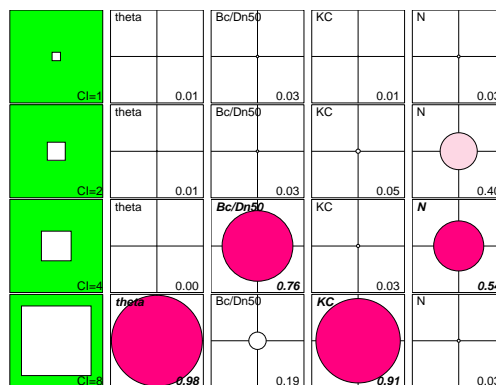**Table I.5:** ANNOVA table and estimated coefficients Equation 5.9.

Figure I.3: Collinearity present in Equation 5.9.

Appendix J

Real case scenario

In this appendix a real 'fictional' situation is compared with the prediction formulas found in this thesis and the formula of Wallast and Van Gent [2002] and Van den Bos [2006]. For this an storm is used with a return period of 10 years to show differences between several formulas. A maximum damage level of $S^* = 2.5$ is defined which Van den Bos reported as the maximum bound of 'initial damage'. For this a minimum median stone size needs to be determined. The hydrodynamical and structural parameters are shown below:

- Hydrodynamic conditions

    - $h = 27$ [m].
    - $H_s = 8.7$ [m].
    - $T_m = 10.7$ [s]. This means a wave steepness s_m of 5.1 [%].
    - $T_p = 13.4$ [s].
    - $N = 2000$. [-]. This is approximately a 6 hour storm.

- Structure parameters

    - $z_c = 1.8$ [m].
    - $B_c = 2$ [m].
    - $m_0 = 3$ [-]. This means the slope of the structure is 1:3.
    - $\Delta = \frac{\rho_s - \rho_w}{\rho_w} = \frac{2650 - 1025}{1025} = 1.59$ [-]. $\rho_s = 2650$ [kg/m^3] is a common density for rock.

The first step is to determine the actual wave conditions present such as the wave-number and orbital velocity. The wave number for the equation of Wallast and Van Gent can be calculated using Equation 2.17. For the formula of Van den Bos and Equation 5.8 and 5.9 the wave-number can be calculated using Equation 2.38. To calculate the wave-number an iteration is always necessary.

$$\frac{2\pi}{T_m} = \sqrt{gk_c \tanh(k_c h_c)} \qquad \text{Local dispersion relation} \qquad (2.17)$$

$$\frac{2\pi}{T_p} = \sqrt{gk_c \tanh(k_c h_c)} \qquad \text{Local dispersion relation} \qquad (2.38)$$

The next step is to calculate the bottom velocity. This bottom velocity is defined for the formula of Van Gent and Wallast as Equation 2.16. For the Equation of Van den Bos and Equation 5.8 and 5.9 first the wave height $H_{1\%}$ needs to be calculated which can be done with Equation 2.39. From this the velocity on the bottom can be calculated using Equation 2.37.

$$\hat{u} = \frac{\pi H_s}{T_m} \frac{1}{\sinh(k_c h_c)} \tag{2.16}$$

$$H_{1\%} = H_s \frac{\sqrt{\frac{1}{2}\ln(100)}}{\sqrt[3]{1 + \dfrac{H_s}{h}}} = H_s \frac{1.52}{\sqrt[3]{1 + \dfrac{H_s}{h}}} \tag{2.39}$$

$$\hat{u}_{hc\,1\%} = \frac{\pi H_{1\%}}{T_p} \frac{1}{\sinh(k_c h_c)} \tag{2.37}$$

All hydrodynamical conditions are now known and the damage predicting equations can be filled in. Because an S^* is known as a requirement, and not S, first a guess on S has to be made. From Chapter 2 it is known that a normal D_{n50} in a near-bed structure is around 0.15 m a first approximation of S can be calculated using Equation 2.41. From here the formula of Wallast and Van Gent and Van den Bos can be filled in. These are shown respectively in Equation 2.30 and 2.35. From these equations the velocity parameter can be determined. From the velocity parameter the median stone diameter D_{n50} can be determined by using Equations 2.31 and 2.36.

$$S^* = S\frac{D_{n50}}{B_c} \tag{2.41}$$

$$\frac{S}{\sqrt{N}} = 0.2\theta_{hc}^3 \tag{2.30}$$

$$\frac{S^*}{N^{0.3}} = 0.048 \cdot (\theta_{hc\,1\%})^{1.6} \cdot m_0^{-0.6} \tag{2.35}$$

$$\theta = \frac{\hat{u_{hc}}^2}{g\Delta D_{n50}} \tag{2.31}$$

$$\theta_{hc\,1\%} = \frac{(\hat{u}_{hc\,1\%})^2}{g\Delta D_{n50}} \tag{2.36}$$

The median stone diameter for the formulas of Wallast and Van Gent and Van den Bos have been determined. For Equation 5.8 and 5.9 an extra step is necessary. Firstly the Keulegan-Carpenter number can be determined with Equation 5.6. To calculate the undistrubed velocity on the bottom u_0 additional calculations with Equation 2.17 and 2.16 need to be performed which should be defined on depth h instead of h_c. From here Equation 5.8 and 5.9 can be filled in. Iterations are necessary because the median stone diameter D_{n50} is present two times in these equations.

$$Kc = \frac{u_0 T_m}{z_c} \tag{5.6}$$

$$\frac{S^*}{N^{0.44}} = \alpha \cdot \theta_{hc1\%}^{2.96} \cdot \left(\frac{B_c}{D_{n50}}\right)^{-0.39} \cdot (m_0 \cdot Kc)^{-1.05} \tag{5.8}$$

$$\frac{S^*}{N^{0.37}} = \alpha \cdot \theta_{hc1\%}^{2.69} \cdot \left(\frac{B_c}{D_{n50}} \right)^{-0.40} \cdot (m_0 \cdot Kc)^{-0.90} \tag{5.9}$$

Now all the median stone diameters D_{n50} are known. However, because this damage level cannot be larger than the S^* defined at the start of this appendix, the D_{n50} with the 95% confidence bound is determined. Because of this there is a high probability that the actual damage is lower than this. For this not the standard confidence bounds described in the literature study of Chapter 2 are used for the formula of Van Gent and Wallast and Van den Bos, but a newly defined confidence bound because more tests have been performed at this stage. For the formula of Van den Bos this was already done in Chapter 5. For the formula of Wallast and Van Gent again a normal distribution is assumed and the distribution of the constant in front of the formula (here 0.2, called parameter A in this thesis) is calculated. The normal distribution can be seen in Figure J.1. An overview is given in Table J.1.
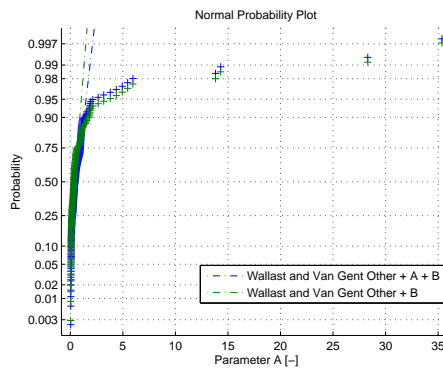
Figure J.1: Normal distribution Wallast and Van Gent [2002] parameter A.

Confidence bounds	5%	50%	95%	σ_α
Equation Wallast and Van Gent [2002]	0.0655	0.20	1.0459	3.7398
Equation Van den Bos [2006]	0.0071	0.048	0.1200	0.0643
Equation 5.8	0.0524	0.1340	0.1962	0.0919
Equation 5.9	0.0908	0.2376	0.3582	0.1397

Table J.1: Confidence bounds and standard deviation for parameter A.

From this the total results can be determined. Note that to determine the S from S^* the results of Equation 5.9 have been used to get a better comparison.

Equation	D_{n50} [m] 50%	D_{n50} [m] 95%
VGW	0.151	0.278
VDB	0.139	0.246
Equation 5.8	0.140	0.163
Equation 5.9	0.150	0.180

Table J.2: Calculated median diameter for several equations.

From Table J.2 it can seen that the formula of Wallast and Van Gent calculates a much higher stone size than the formula of Van den Bos and Equation 5.8 and 5.9. For the 50% confidence bound the formula of Van den Bos calculates the lowest median stone diameter. Because of the larger confidence bound of Van den Bos the 95% confidence bound calculates a much larger stone

size than for Equation 5.8 and 5.9. The velocity parameter in this example is $\theta_{hc} = 1.55$ and $\theta_{hc1\%} = 3.96$. Because of this it is more likely that Equation 5.9 calculates the median stone diameter the closest (See Chapter 6). From here the reduction in height can be calculated using the average between Equation 2.45 and 2.47. The height reduction with Equation 5.9 on the 95% confidence bound is 0.24 m which is the maximum possible height that the structure reduces.

$$\Delta z = \frac{-B_c + \sqrt{B_c^2 + 4m_0 A_e}}{2m_o} \tag{2.45}$$

$$\Delta z = \frac{-(B_c + z_c m_0/2) + \sqrt{(B_c + z_c m_0/2)^2 + 2m_0 A_e}}{m_0} \tag{2.47}$$

From this investigation it can be concluded that with a 95% confidence and a fixed amount of damage Equation 5.8 and 5.9 calculate a much smaller stone size than formulas from Wallast and Van Gent and Van den Bos. Actually this example would mean a totally different standard grading would have to be used. For a $D_{n50} = 0.18$ (15.5 kg) m a standard grading of 5-40 kg [CIRIA, 2007] can be used. For a $D_{n50} = 0.25$ (41.4 kg) at least the standard grading 10-60 kg has to be used. The actual damage because of this grading should be determined after this. This is because a different median diameter can be expected with due to this grading. A follow up on this could be to include multiple storms and determine the damage accordingly.